JSCSEN 76(12)1597–1760(2011)

International Year of CHEMISTRY 2011

Journal of the Serbian Chemical Society

Electronic Version

VOLUME 76

No 12

BELGRADE 2011

Available on line at

www.shd.org.rs/JSCS/

The full search of JSCS is available through

DOAJ DIRECTORY OF OPEN ACCESS JOURNALS

www.doaj.org

Journal of the Serbian Chemical Society
JSCS-info@shd.org.rs • www.shd.org.rs/JSCS

J. Serb. Chem. Soc. Vol. 76, No. 12 (2011)

CONTENTS

Published by the Serbian Chemical Society
Karnegijeva 4/III, 11000 Belgrade, Serbia
Printed by the Faculty of Technology and Metallurgy
Karnegijeva 4, P.O. Box 35-03, 11120 Belgrade, Serbia

Available online at www.shd.org.rs/JSCS

Journal of the Serbian Chemical Society
JSCS-info@shd.org.rs • www.shd.org.rs/JSCS
J. Serb. Chem. Soc. *76* (12) 1597–1606 (2011)
JSCS–4232
UDC 547.783:547.6:544.022:615.28–188
Original scientific paper

Structure–activity relationships of 3-substituted-5,5--diphenylhydantoins as potential antiproliferative and antimicrobial agents

NEMANJA TRIŠOVIĆ[1#], BOJAN BOŽIĆ[1#], ANA OBRADOVIĆ[2], OLGICA STEFANOVIĆ[2], SNEŽANA MARKOVIĆ[2], LJILJANA ČOMIĆ[2], BILJANA BOŽIĆ[3] and GORDANA UŠĆUMLIĆ[1*#]

[1]*Faculty of Technology and Metallurgy, University of Belgrade, Karnegijeva 4, 11000 Belgrade,* [2]*Faculty of Science, University of Kragujevac, Radoja Domanovića 12, 34000 Kragujevac and* [3]*Faculty of Biology, University of Belgrade, Studentski trg 3, 11000 Belgrade, Serbia*

(Received 14 March, revised 2 May 2011)

Abstract: A series of twelve 3-substituted-5,5-diphenylhydantoins was synthesized, including some whose anticonvulsant activities have already been reported in the literature. Their antiproliferative activities against HCT-116 human colon carcinoma cells were evaluated to determine structure–activity relationships. Almost all of the compounds exhibited statistically significant antiproliferative effects at a concentration of 100 μM, while the derivative bearing a benzyl group was active even at lower concentrations. Moreover, their *in vitro* antibacterial activities against *Escherichia coli* ATCC 25922, *Staphylococcus aureus* ATCC 25923 and clinical isolates of *Escherichia coli*, *Proteus mirabilis*, *Pseudomonas aeruginosa*, *Enterococcus faecalis* and *Staphylococcus aureus* were evaluated. Only the 3-isopropyl and 3-benzyl derivatives showed weak antibacterial activities against the Gram-positive bacterium *E. faecalis* and the Gram-negative bacteria *E. coli* ATCC 25922 and *E. coli*.

Keywords: phenytoin derivatives; antiproliferative activity; antimicrobial activity; structure–activity relationship.

INTRODUCTION

The derivatives of hydantoin (imidazolidine-2,4-dione) are well known and clinically widely used in the therapy of epilepsy and cardiac arrhythmias. Phenytoin (5,5-diphenylhydantoin, Dilantin®), one of the oldest anticonvulsants, is very effective in controlling a variety of seizure disorders, while impairing neurological function only slightly, if at all.[1] These effects are due to a selective

* Corresponding author. E-mail: goca@tmf.bg.ac.rs
# Serbian Chemical Society member.
doi: 10.2298/JSC110314143T

block of high frequency neuronal activity. The drug targets the neuronal voltage-sensitive sodium channels (NVSC) to reproduce the normal ion potential and is known to block the release of neurotransmitters, such as serotonin and norepinephrine. At an appropriate level, it inhibits monoamine oxidase activity and tends to alter the membrane potential as well.[2]

After 70 years of phenytoin application, the precise physiological effects of the drug have not been completely determined and it still remains an important subject for new investigations. The drug and its metabolite 5-(4-hydroxyphenyl)-5-phenylhydantoin were reported to possess significant hypolipidemic activity, which is reflected in the reduction of both serum cholesterol and triglyceride levels.[3] Phenytoin did not show inhibitory effect on the growth of a spectrum of microorganisms (*Mycobacterium smegmatis*, *Candida albicans*, *Staphylococcus aureus*, *Pseudomonas aeruginosa* and *Escherichia coli*).[4] Furthermore, a slight increased occurrence of *E. coli* agglutinins was found in patients on long-term phenytoin therapy.[5] In dermatology, the drug has been investigated for the treatment of ulcers, epidermolysis bullosa and different inflammatory conditions.[6]

Hydantoin derivatives are found in many area of medicinal chemistry (serotonin and fibrinogen receptor antagonists,[7] inhibitors of the glycine binding site of the NMDA receptor,[8] antagonists of leukocyte cell adhesion, acting as allosteric inhibitors of the protein–protein interaction[9]). In particular, several reports present interest in cancer research.[10,11] Cancer is one of the most devastating diseases of today. It is manifested as uncontrolled growth of cells and invasion or intrusion into and the destruction of adjacent tissues. Although the progress is evident in diagnosis, surgical techniques, patient care and adjuvant therapies, most of the deaths from cancer are due to metastases.[12] Spiromustin, a hydantoin-containing nitrogen mustard, rapidly penetrates the blood-brain barrier and directs drug delivery to brain tumors.[13] Carmi *et al.*[14,15] demonstrated that 5--benzylidenehydantoins could function as bioisosters of 4-anilinoquinazolines, which are epidermal growth factor receptor (EGFR) tyrosine kinase inhibitors approved for the treatment of lung cancer. They suggested that the presence of an aromatic unit at position C5 is an important structural feature for interactions with molecular targets. Recently, Ananda Kumar and co-workers investigated the antiproliferative effect of certain diazaspiro bicyclo hydantoin derivatives against human leukemia K562 and CEM cells.[16,17] They reported that the cytotoxic activities of compounds bearing a substituent at the N3 position increase in the order alkene > ester > ether. A similar conclusion was reached in a comparative study of the cytostatic activities of L- and D-amino acid derivatives of hydroxyurea and hydantoins. The best antitumor activities were achieved with lipophilic compounds having cycloalkyl, phenyl and benzhydryl substituents.[18]

A deeper understanding of the SARs and modeling of new derivatives with potential antitumor activity can be facilitated by accumulation of detailed struc-

tural and pharmacological data. In this context, a set of twelve phenytoin derivatives bearing different alkyl (methyl, ethyl, *n*-propyl, isopropyl, *n*-butyl, isobutyl and benzyl), alkenyl (allyl), ether (ethoxymethyl, benzyloxymethyl), ester (acetoxymethyl) and alkanoyl (benzoyl) substituents at the N3 position was synthesized (Table I). The antiproliferative activity was evaluated against the HCT--116 human colon carcinoma cell line. These structural modifications of the phenytoin molecule led to several derivatives exhibiting different degrees of anticonvulsant activity (Table I). Poupaert *et al*.[20] observed that the anti-electroshock activity was decreased when the hydantoin ring was N-methylated. The 3-alkoxymethyl derivatives were reported to be active against electrically as well as chemically induced seizures.[19,22] On the other hand, 3-(acetoxymethyl)-5,5-diphenylhydantoin resembled the parent compound showing good activity against maximal electroshock seizures, but was inactive against pentylenetetrazole.[23] In previous papers,[24,25] the hypothesis that the ability to form hydrogen bonds plays the determining role in the anticonvulsant action of these compounds was confirmed.

TABLE I. Structures and anticonvulsant potencies of the investigated compounds

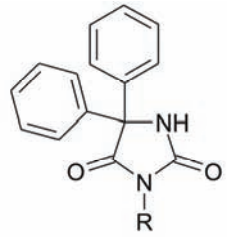

Compound	R	ED_{50}[a] / mg kg^{-1}
1	H	≈7.5[19]
2	CH_3	39.6[20]
3	C_2H_5	–
4	*n*-C_3H_7	–
5	*i*-C_3H_7	–
6	*n*-C_4H_9	–
7	*i*-C_4H_9	–
8	$C_6H_5CH_2$	>200[19]
9	CH_2=$CHCH_2$	30.4[21]
10	$C_2H_5OCH_2$	–
11	$C_6H_5CH_2OCH_2$	>25[22]
12	$CH_3C(=O)OCH_2$	<12.5[19]
13	C_6H_5CO	–

[a]The effective dose required to protect mice against spasms induced by the maximum electric shock (MES)

Certain derivatives of hydantoin, which contained aromatic or heterocyclic substituents at the nitrogen, were reported to exhibit antimicrobial effects.[26]

Hence, the *in vitro* antimicrobial activities of the investigated compounds were additionally evaluated against *E. coli* ATCC 25922, *S. aureus* ATCC 25923 and clinical isolates of *E. coli*, *Proteus mirabilis*, *P. aeruginosa*, *Enterococcus faecalis* and *S. aureus*.

RESULTS AND DISCUSSION

Antiproliferative screening

The investigation of the antiproliferative activities of the phenytoin derivatives on the HCT-116 cell line at a concentration of 100 μM showed that almost all of the compounds, except **2**, **3** and **10**, exhibited statistically significant antiproliferative effects, as is shown in Fig. 1. Furthermore, **8** at concentrations of 0.01, 0.1, 1, 10 and 100 μM showed significant antiproliferative effects (Fig. 2), while compound **9** demonstrated a statistically significant antiproliferative effect at a concentration of 10 μM. Interestingly, valproate (valproic acid) manifested a similar dose-dependent inhibition of proliferation of gastrointestinal neuroendocrine[27] and carcinoid cancer cells.[28] Valproic acid is a simple branched-chain fatty acid, the anticonvulsant efficacy of which is comparable to that of phenytoin.[29] The other compounds showed no significant inhibition of HCT-116 proliferation at lower concentrations.

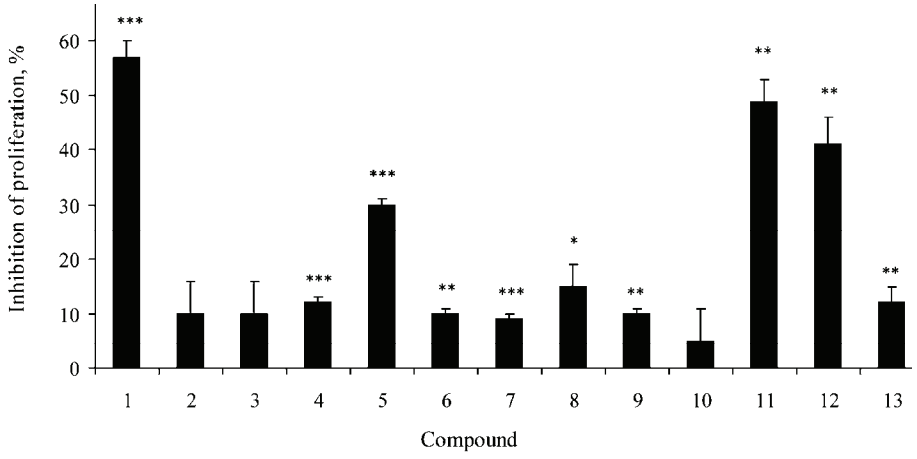

Fig. 1. The antiproliferative effect of 3-substituted-5,5-diphenylhydantoins on the HCT-116 cell line. The cells were treated with a 100 μM concentration of the drugs during a 24 h exposure. The antiproliferative effect was measured by the MTT assay. The results are expressed as the means ± *SD* from cells cultured in triplicate (*$p < 0.05$, **$p < 0.01$, ***$p < 0.001$, compound *vs.* the control).

N-Alkylation of the phenytoin molecule resulted in a diminished ability to form hydrogen bonds and also a decreased antiproliferative activity of compounds **2**–**7** at a concentration of 100 μM. A net stepwise increase in the size of

the alkyl substituent resulted in a slight decrease in the potencies of the compounds with the exception of the isopropyl group. Furthermore, compounds **11** and **12**, potent anticonvulsants, manifested a cytotoxic activity to the cancer cells similar to that of the parent compound **1**. The unexpected activity of compound **8** in low concentrations implies that the relative activity of these compounds is not determined only by the physico–chemical properties of the substituent at the N3 position. It might only be assumed that compounds bearing a benzyl unit (**8** and **11**) are well located in the molecular target, while the derivative with a rigid benzoyl group (**13**) is not well tolerated.

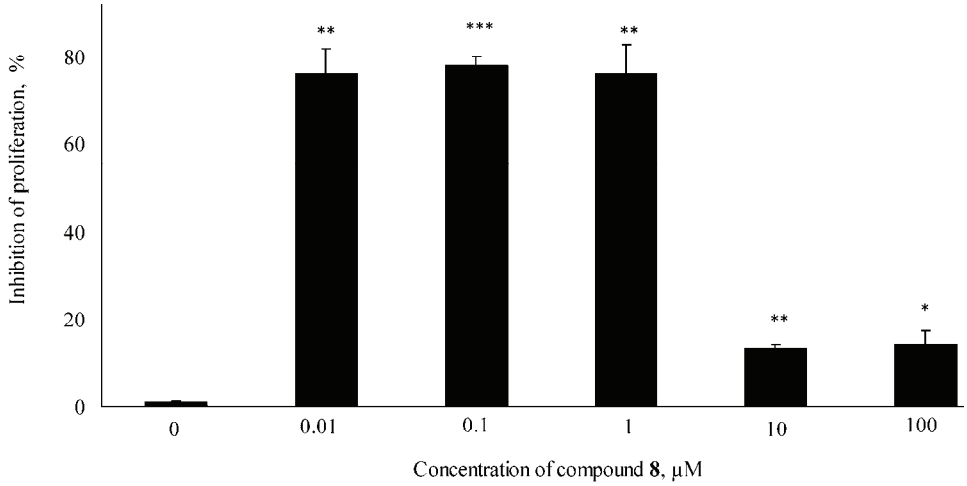

Fig. 2. The antiproliferative effect of **8** on HCT-116 cell line. The cells were treated with various concentrations of drugs during a 24 h exposure. The antiproliferative effect was measured by the MTT assay. The results are expressed as the means ± SD from cells cultured in triplicate. (*p < 0.05, **p < 0.01, ***p < 0.001, different concentrations *vs.* control).

Antibacterial screening

The investigated phenytoin derivatives were additionally screened for their *in vitro* antibacterial activities against three Gram-positive and four Gram-negative bacteria using the well-diffusion method[30] and the microdilution method with resazurin.[31] Overnight cultures of standard strains of *E. coli* ATCC 25922, *S. aureus* ATCC 25923 and clinical isolates of *E. coli*, *P. mirabilis*, *P. aeruginosa*, *E. faecalis* and *S. aureus* were used for the preparation of the bacterial suspensions. The *in vitro* antibacterial activities of the new compounds against both Gram-positive and Gram-negative bacteria are listed in Table II. Among the tested compounds, only **5** and **8** showed significant antibacterial activity against the Gram-positive bacterium *E. faecalis* and the Gram-negative bacteria *E. coli* ATCC 25922 and *E. coli* (clinical isolate). The active compounds showed the best effects against *E. coli.*

TABLE II. Antibacterial activity of the tested 3-alkyl-5,5-diphenylhydantoins

Compds.	*E. coli* ATCC 25922			*E. coli*			*P. mirabilis*			*P. aeruginosa*		
	IZ[a]	*MIC*[b]	*MBC*[c]	*IZ*	*MIC*	*MBC*	*IZ*	*MIC*	*MBC*	*IZ*	*MIC*	*MBC*
1–**4**	/	>10^3	>10^3	–	>10^3	>10^3	–	>10^3	>10^3	–	>10^3	>10^3
5	21.25±1.50	250	>500	23.00±0.00	125	125						
6 and **7**	–	>10^3	>10^3		>10^3	>10^3						
8	20.05±2.28	500	>500	20.50±0.71	250	250						
9–**13**	–	>10^3	>10^3		>10^3	>10^3						

	E. faecalis			*S. aureus* ATCC 25923			*S. aureus*		
	IZ[a]	*MIC*[b]	*MBC*[c]	*IZ*	*MIC*	*MBC*	*IZ*	*MIC*	*MBC*
1–**4**	–	>10^3	>10^3	–	>10^3	>10^3	–	>10^3	>10^3
5	21.00±0.00	250	500						
6 and **7**	–	>10^3	>10^3						
8	18.75±1.50	500	500						
9–**13**	–	>10^3	>10^3						

[a]Inhibition zone, mm; [b]minimum inhibitory concentration, μM; [c]minimum bactericidal concentration, μM

Compound **8** demonstrated weak antibacterial activity as an additional biological effect. Compound **5**, which was shown to be an exception from the group of 3-alkyl substituted derivatives, exhibited a similar effect. Since cytochrome P450 enzymes are responsible for the metabolism of an ever-expanding array of drugs, Suzuki and co-workers[32] tested, among others, the inhibitor potencies of **5** and **8** against recombinant CYP2C19 and CYP2C9 to probe their interactions with their active sites. Metabolic profiling and homology modeling studies suggested that the 3-benzyl substituted derivative was preferentially bound in the active site of CYP2C19 with its C5 phenyl group oriented towards the active oxygen and the benzyl group bound within a lipophilic pocket of the receptor. We are of the opinion that these structural features might be responsible for the biological activity of compound **8**. Several examples from the literature indicate that a benzyl group attached to the nitrogen atom is a promising pharmacophore for antiproliferative activity to be exhibited.[33–35] Since the molecular basis of the biological activity of **8** remains to be determined, further experiments aimed at defining the modes of actions are currently in progress.

EXPERIMENTAL

Chemistry

The methods for the preparations of the investigated compounds are presented in Scheme 1. In the synthesis of **2**–**9**, commercially obtained 5,5-diphenylhydantoin (**1**, Fluka) was alkylated at the N3 position using the corresponding alkyl halide in K_2CO_3/dimethylformamide.[32] The alkoxymethyl substituent was introduced by the reaction of phenytoin sodium salt (**15**) in dimethylformamide with the appropriate chloromethyl alkyl ether (**10** and **11**).[19] The process for preparing **15** was described in the literature.[36] 3-Acetoxymethyl-5,5-diphenylhydantoin (**12**) was prepared by the reaction of 3-(hydroxymethyl)-5,5-diphenylhydantoin and acetic anhydride, and 3-(hydroxymethyl)-5,5-diphenylhydantoin (**14**) was initially synthesized

by the addition of **1** to formaldehyde in the presence of sodium hydroxide in ethanol.[23] 3-Benzoyl-5,5-diphenylhydantoin (**13**) was synthesized in the reaction of phenytoin sodium salt and benzoyl chloride in dry benzene.[37] The structures of the compounds were determined by their melting points, and IR, ^{1}H- and ^{13}C-NMR spectra, which were in agreement with literature data. The ^{1}H- and ^{13}C-NMR spectral measurements were performed on a Bruker AC 250 spectrometer at 250 MHz for the ^{1}H-NMR and 62.89 MHz for the ^{13}C-NMR spectra. FT-IR spectra were recorded on a Bomem MB 100 spectrophotometer. The spectra were recorded at room temperature in DMSO-d_6. The chemical shifts are expressed in ppm values referenced to TMS (δ_H = 0 ppm) in ^{1}H-NMR spectra, and the residual solvent signal (δ_C = 39.5 ppm,) in the ^{13}C-NMR spectra. Elemental analysis was realized using an Elemental Vario EL III micro-analyzer. The yield and chemical characterization of the newly synthesized compound **7** are given here.

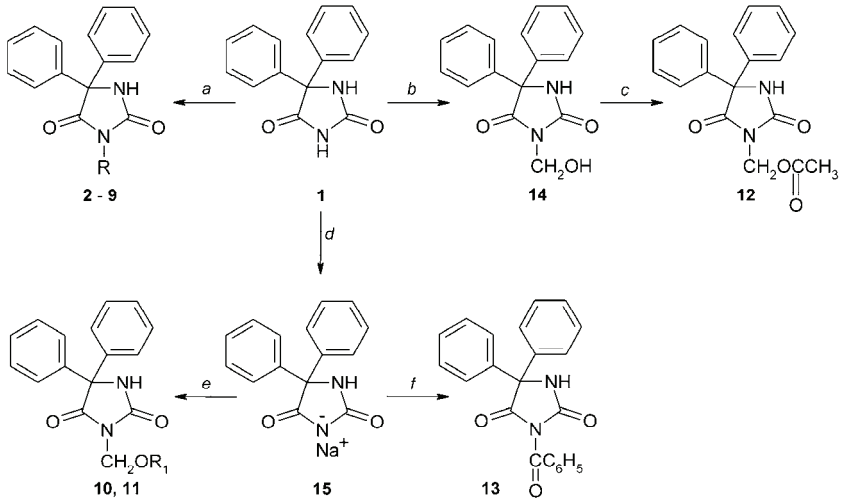

Scheme 1. Synthesis of the investigated derivatives of phenytoin (**1**). Reagents and conditions: a) alkyl halide (1.1 eq.), K_2CO_3, DMF, r. t., 24 h; b) formalin, NaOH, EtOH, r. t., 30 min; c) Ac_2O, r. t. 24 h; d) NaOH, benzene, reflux, 6 h; e) chlormethyl alkyl ether (1.1 eq.), DMF, r. t., 24 h; f) benzoyl chloride, benzene, reflux, 6 h.

Characterization

3-Isobutyl-5,5-diphenylhydantoin (7). White crystalline solid; yield 72 %; mp: 119–122 °C; Anal. Calcd. for $C_{19}H_{20}N_2O_2$: C, 74.00; H, 9.08; N, 6.54 %. Found C 74.08, H, 9.10, N 6.57 %. IR (KBr, cm^{-1}): 3293 (N–H), 1705, 1775 (C=O). ^{1}H-NMR (200 MHz, DMSO-d_6, δ / / ppm): 9.66 (1H, *s*, NH), 7.26–7.44 (10H, *m*, 2Ph–H), 3.25–3.29 (2H, *m*, CH_2–N), 1.89–2.03 (1H, *m*, C**H**–CH_2N), 0.78 (6H, *d*, *J* = 7.0 Hz, 2CH_3). ^{13}C-NMR (50 MHz, DMSO-d_6, δ / / ppm): 173.60 (C4), 155.85 (C2), 140.03 (Ph–C), 128.81 (Ph–CH), 128.37 (Ph–CH), 126.82 (Ph–CH), 69.22 (C5), 45.40 (CH_2–N), 27.12 (CH), 19.91 (CH_3).

In vitro *antiproliferative screening*

The antiproliferative potential of the investigated phenytoin derivatives was determined using the MTT [3-(4,5-dimethylthiazol-2-yl)-2,5-diphenyltetrazolium bromide] assay for the HCT-116 human colon cancer cell line. The relative antiproliferative potency is expressed as

the percentage of proliferation inhibition of the control HCT cells cultured without compounds in the cell cultivation medium. The HCT-116 cells were maintained in Dulbecco-modified Eagle medium (DMEM) supplemented with 10 % fetal bovine serum. The cells were grown in 75 ml culture bottles supplied with 12 ml DMEM, and after a few passages, the cells were seeded in a 96-well plate. The cells were cultured in a humidified atmosphere of 5 % CO_2 at 37 °C. The HCT-116 cells were treated with 0.01, 0.1, 1, 10 and 100 μM concentrations of the investigated compounds for 24 h. Untreated cells served as the control. After 24 h of treatment, the cell proliferation was determined by the MTT assay. This test is based on the color reaction of mitochondrial dehydrogenase from living cells with MTT. Briefly, 10 ml of MTT solution (5 mg ml^{-1}) was added to each well after 24 h of culture and the cultures were incubated for an additional 3 h at 37 °C. The produced formazan was dissolved by overnight incubation in SDS–HCl (10 % SDS (sodium dodecyl sulfate) in 0.01 M HCl) and absorbance was measured at the dual wavelengths of 570/650 nm with an ELISA 96-well plate reader. The percentage of viable cells was calculated as the ratio between the absorbance at each dose of the compounds and the absorbance of the untreated control×100.

In vitro *antibacterial screening*

An overnight culture of standard strains of *E. coli* ATCC 25922, *S. aureus* ATCC 25923 and clinical isolates of *E. coli*, *P. mirabilis*, *P. aeruginosa*, *E. faecalis* and *S. aureus* were used for the preparation of bacterial suspensions. The turbidity of the initial bacterial suspensions was adjusted by comparing with a 0.5 McFarland standard and then diluted 1:100 in sterile 0.85 % saline.

Antibacterial assay was realized by the well-diffusion method[30] and the microdilution method with resazurin.[31] The diffusion method is a qualitative test which allows the classification of microorganisms as susceptible or resistant to the test substance according to diameter of the zone of inhibition. Petri plates with Mueller–Hinton agar were inoculated with adequate bacterial suspensions. The surface of the media was allowed to dry for 3–5 min at room temperature. Subsequently, wells (7 mm) were made in the plate with a sterile metal cylinder, which were filled with 100 μl of solutions of the tested compounds; concentration of 1000 μM. The antibacterial activity was evaluated by measuring the diameters of the zones of inhibition. All tests were performed in triplicate and the results are expressed as mean ± standard deviation. A negative control was prepared with the same solvent used to dissolve the tested substances (5 % DMSO) to ensure that the solvent had no effect on bacterial growth. Each test also included a growth control and a sterility control. The minimum inhibitory concentration (*MIC*) and the minimum bactericidal concentration (*MBC*) were determined using the microdilution plate method. Two-fold, serial dilutions of the tested compounds were performed in Mueller-Hinton broth. The obtained concentration range was from 1000 to 7.81 μM. The diluted bacterial suspensions (10 μl) were added to each well to give a final concentration of 5×10^5 CFU mL^{-1}. Finally, 10 μl resazurin indicator solution was added. Resazurin is an oxidation–reduction indicator used for the evaluation of microbial growth. It is a blue non-fluorescent dye that becomes pink and fluorescent when reduced to resorufin by the oxidoreductases within viable cells. The inoculated plates were incubated at 37 °C for 24 h. The *MIC* is defined as the lowest concentration of a tested substance that prevented the resazurin color change from blue to pink. Each test included a growth control and a sterility control. All tests were performed in triplicate and the *MIC* values were constant. The *MBC* was determined by plating 10 μl of samples from wells where no indicator color change was recorded onto nutrient agar medium. At the end of the incubation period, the lowest concentration with no visible growth was defined as the *MBC*.

CONCLUSIONS

In summary, an evaluation of 3-substituted-5,5-diphenylhydantoins as potential antiproliferative and antimicrobial agents was reported. The trend of the changes in the biological effects produced by substituents at position N3 was studied. Compound **8** showed significant antiproliferative activity even in low concentrations. In addition, it exhibited weak antibacterial activity. Since the molecular basis of its biological activity remains to be determined, further experiments aimed at defining the modes of its actions are currently in progress.

Acknowledgements. The authors acknowledge the financial support of the Ministry of Education and Science of the Republic of Serbia (Project 172013).

ИЗВОД

УТИЦАЈ СТРУКТУРЕ НА АНТИПРОЛИФЕРАТИВНУ И АНТИБАКТЕРИЈСКУ АКТИВНОСТ 3-СУПСТИТУИСАНИХ-5,5-ДИФЕНИЛХИДАНТОИНА

НЕМАЊА ТРИШОВИЋ[1], БОЈАН БОЖИЋ[1], АНА ОБРАДОВИЋ[2], ОЛГИЦА СТЕФАНОВИЋ[2], СНЕЖАНА МАРКОВИЋ[2], ЉИЉАНА ЧОМИЋ[2], БИЉАНА БОЖИЋ[3] и ГОРДАНА УШЋУМЛИЋ[1]

[1]*Технолошко–металуршки факултет, Универзитет у Београду, Карнегијева 4, 11000 Београд,* [2]*Природно–математички факултет, Универзитет у Крагујевцу, Радоја Домановића 12, 34000 Крагујевац и* [3]*Биолошки факултет, Универзитет у Београду, Студентски трг 3, 11000 Београд*

Синтетисана је серија од дванаест 3-супституисаних-5,5-дифенилхидантоина, која обухвата неке од деривата чије су антиконвулзивне активности познате у литератури. Одређена је њихова антипролиферативна активност према ћелијској линији хуманог карцинома колона, како би се утврдио утицај структуре на активност. Скоро сва једињења испољавају антипролиферативан ефекат у концентрацији од 100 μM, док је дериват са бензил групом активан и у нижим концентрацијама. Додатно је одређена и антибактеријска активност проучаваних једињења према *Escherichia coli* ATCC 25922, *Staphylococcus aureus* ATCC 25923 и клиничким изолатима *Escherichia coli*, *Proteus mirabilis*, *Pseudomonas aeruginosa*, *Enterococcus faecalis* и *Staphylococcus aureus*. 3-Изопропил и 3-бензил деривати показују слабу активност према грам-позитивној бактерији *E. faecalis* и грам-негативним бактеријама *E. coli* ATCC 25922 и *E. coli*.

(Примљено 14. марта, ревидирано 2. маја 2011)

REFERENCES

1. Y. Yaari, M. E. Selzer, J. H. Pincus, *Ann. Neurol.* **20** (1986) 171
2. K. Kikuchi, C. I. McCormick, E. A. Neuwelt, *J. Neurosurg.* **61** (1984) 1085
3. J. H. Maguire, A. R. Murthy, I. H. Hall, *Eur. J. Pharm.* **117** (1985) 135
4. N. Esiobu, N. Hoosein, *Anton. Leeuw. Int. J. G.* **83** (2003) 63
5. P. Andersen, L. Mosekailde, T. Hjort *Clin. Exp. Immunol.* **45** (1981) 137
6. N. Scheinfeld, *Dermatol. Online J.* **9** (2003) 6
7. G. P. Moloney, G. R. Martin, N. Mathews, A. Milne, H. Hobbs, S. Dosworth, P. Y. Sang, C. Knight, M. Williams, M. Maxwell, R. Glen, *J. Med. Chem.* **42** (1999) 2504
8. M. Jansen, H. Potschka, C. Brandt, W. Löscher, G. Dannhardt, *J. Med. Chem.* **46** (2003) 64

9. K. Last-Barney, W. Davidson, M. Cardozo, L. L. Frye, C. A. Grygon, J. L. Hopkins, D. D. Jeanfavre, S. Pav, C. Qian, J. M. Stevenson, L. Tong, R. Zindell, T. A. Kelly, *J. Am. Chem. Soc.* **123** (2001) 5643
10. N. R. Penthala, T. R. Yerramreddy, P. A. Crooks, *Bioorg. Med. Chem. Lett.* **21** (2011) 1411
11. D. Lesuisse, J. Mauger, C. Nemecek, S. Maignan, J. Boiziau, G. Harlow, A. Hittinger, S. Ruf, H. Strobel, A. Nair, K. Ritter, J.-L. Malleron, A. Dagallier, Y. El-Ahmad, J.-P. Guilloteau, H. Guizani, H. Bouchard, C. Venot, *Bioorg. Med. Chem. Lett.* **21** (2011) 2224
12. I. Fidler, *J. Semin. Cancer Biol.* **12** (2002) 89
13. D. D. Shoemaker, P. J. O'Dwyer, S. Marsoni, J. Plowman, J. P. Davignon, R. D. Davis, *Invest. New Drugs* **1** (1983) 303
14. C. Carmi, A. Cavazzoni, V. Zuliani, A. Lodola, F. Bordi, P. V. Plazzi, M. Mor, *Bioorg. Med. Chem. Lett.* **16** (2006) 4021
15. A. Cavazzoni, R. R. Alfieri, C. Carmi, V. Zuliani, M. Galetti, C. Fumarola, R. Frazzi, M. Bonelli, F. Bordi, A. Lodola, M. Mor, P. G. Petronini, *Mol. Cancer Ther.* **7** (2008) 361
16. C. S. Ananda Kumar, C. V. Kavitha, K. Vinaya, S. B. Benaka Prasad, N. R. Thimmegoweda, S. Chandrappa, S. C. Raghavan, K. S. Rangappa, *Invest. New. Drugs* **27** (2009) 327
17. C. V. Kavitha, N. Mridula, C. S. Ananda Kumar, C. Bibha, K. Muniyappa, K. S. Rangappa, S. C. Raghavan, *Biochem. Pharmacol.* **77** (2009) 348
18. N. Opačić, M. Barbarić, B. Zorc, M. Cetina, A. Nagl, D. Frković, M. Kralj, K. Pavelić, J. Balzarini, G. Andrei, R. Snoeck, E. De Clercq, S. Ralić-Malić, M. Mintas, *J. Med. Chem.* **48** (2005) 475
19. J. A. Vida, M. H. O'Dea, C. M. Samour, *J. Med. Chem.* **18** (1975) 383
20. J. H. Poupaert, D. Vandervorst, P. Guiot, M. M. M. Moustafa, P. Dumont, *J. Med. Chem.* **27** (1984) 76
21. F. Sandberg, *Acta Physiol. Scand.* **24** (1951) 149
22. C. M. Samour, J. Reinhard, J. A, Vida, *J. Med. Chem.* **14** (1971) 187
23. J. A. Vida, W. R. Wilber, *J. Med. Chem.* **14** (1971) 190
24. N. Banjac, G. Uščumlić, N. Valentić, D. Mijin, *J. Solution Chem.* **36** (2007) 869
25. N. Divjak, N. Banjac, N. Valentić, G. Uščumlić, *J. Serb. Chem. Soc.* **74** (2009) 1195
26. E. Szymańska, K. Kieć-Kononowicz, A. Białecka, A. Kasprowicz, *Farmaco* **57** (2002) 39
27. V. Baradari, A. Huether, M. Höpfner, D. Schuppan, H. Scherübl, *Endocr.-Relat. Cancer* **13** (2006) 1237
28. D. Y. Greenblatt, A. M. Vaccaro, R. Jaskula-Sztul, L. Ning, M. Haymart, M. Kunnimalaiyaan, H. Chen, *Oncologist* **12** (2007) 942
29. E. Perucca, *CNS Drugs* **16** (2002) 695
30. C. Perez, M. Paul, P. Bazerque, *Acta Bio. Med. Exp.* **15** (1990) 113
31. S. D. Sarker, L. Nahar, Y. Kumarasamy, *Methods* **42** (2007) 321
32. H. Suzuki, M. B. Kneller, D. A. Rock, J. P. Jones, W. F. Trager, A. E. Rettie, *Arch. Biochem. Biophys.* **429** (2004) 1
33. L. J. Marton, A. E. Pegg, *Annu. Rev. Pharmacol.* **35** (1995) 55
34. C. Gao, Y. Jiang, C. Tan, X. Zu, H. Liu, D. Cao, *Bioorg. Med. Chem.* **16** (2008) 8670
35. G. T. Elliott, W. A. Nagle, K. F. Kelly, D. McCollough, R. L. Bona, E. R. Burns, *J. Med. Chem.* **32** (1989) 1039
36. R. Gulaboski, A. Galland, G. Bouchard, K. Caban, A. Kretschmer, P.-A. Carrupt, Z. Stojek, H. H. Girault, F. Scholz, *J. Phys. Chem., B* **108** (2004) 4565
37. L. P. Kulev, A. A. Shesterova, *Zhch. Obszh. Khim.* **31** (1961) 1378.

Journal of the Serbian Chemical Society
JSCS-info@shd.org.rs • www.shd.org.rs/JSCS
J. Serb. Chem. Soc. 76 (12) 1607–1615 (2011)
JSCS–4233
UDC 547.532–326+66.095.13:66–911.4+544.478
Original scientific paper

Novel Brønsted-acidic ionic liquids based on benzothiazolium cations as catalysts for esterification reactions

XIAN SI ZHOU, JIA BING LIU, WEN FENG LUO, YI WEN ZHANG and HANG SONG*

School of Chemical Engineering, Sichuan University, Chengdu 610065, P. R. China

(Received 2 January, revised 18 March 2011)

Abstract: Three novel Brønsted-acidic ionic liquids based on benzothiazolium cations were prepared, which served as catalysts for the synthesis of benzoic esters. All three gave good yields of the target esters in esterification reactions. Moreover, they combine the advantages of both homogeneous and heterogeneous solid catalysts in esterification reactions, which enabled them to serve as homogeneous catalysts to catalyze the reactions and be conveniently recovered by simple filtration after the reactions. They could be reused several times without noticeable decrease in efficiency.

Keywords: benzoic esters; benzothiazolium salts; catalyst; esterification; ionic liquid.

INTRODUCTION

Aromatic esters are important intermediates in the chemical and pharmaceutical industries and are usually prepared in acid-catalyzed esterification reactions of alcohols with benzoic acids.[1] Inorganic acid catalysts such as H_2SO_4 and H_3PO_4, resins, supported mineral acids, heteropolyacids and zeolites have been used for esterifications.[2–6] Although high yields could be achieved, the employment of these catalysts has some obvious drawbacks, such as the usage of organic solvents and difficultly in the recycling of the catalysts. Thus, it is necessary to develop new types of catalysts with environmentally friendly, reusable and highly efficient characteristics.

Ionic liquids (ILs), also known as molten salts or room temperature ionic liquids, have gained increasing attentions in the context of green synthesis in recent years. Owing to their negligible volatility, excellent thermal stability and structure variety, ILs are considered as environmentally benign media and catalysts for organic synthesis.[7-10] Fisher esterification in acidic ILs was verified to be an environmentally efficient procedure for the synthesis of various esters and

* Corresponding author. E-mail: hangsong@scu.edu.cn
doi: 10.2298/JSC110102144Z

had many advantages over reactions catalyzed by conventional liquid or solid acids. In recent years, parallel to the rapid development of ILs, their applications in esterification have been extensively studied. For example, catalytic amounts of Brønsted-acidic ionic liquids promoted esterification, microwave-accelerated esterification in Brønsted-acidic ionic liquids and ultrasound-assisted esterification in Brønsted-acidic ionic liquids have been reported.[11–13] These method can reduce the reaction time, reaction temperature or diminish the consumption of ILs, but the isolation of ILs from the reaction mixture was not satisfactorily solved, due to the requirement of relatively complicated separation operations. Although polystyrene (PS)-supported ionic liquid catalysts can be recycled easily by filtration, they cannot serve as homogeneous catalysts to promote reactions.[14] Davis[15] and Wang *et al.*[16,17] investigated Brønsted acidic ILs in some esterification reactions and removed the ILs by simple filtration after the reaction. The employed ILs were not conventional ILs due to their high melting points (some above 100 °C) and their solubility in the reaction mixture could be varied greatly with small-scale changes in temperature. Hence, they could serve as homogeneous catalysts to catalyze efficiently reactions at higher temperatures or as heterogeneous solid catalysts to simplify the isolation of ILs by filtration at lower temperatures. They combined the advantages of both homogeneous and heterogeneous solid catalysts. Nonetheless, the reports were still not completely satisfactory, especially for highly efficient syntheses of benzoic esters. As a result, it is very meaningful to develop new ILs as catalysts for more specific reactions.

Over the last two decades, pyridinium or *N*-methylimidazolium ionic liquids have been widely reported and applied to many organic reactions. However, research on the synthesis and applications of benzothiazolium-containing ILs was lacking until the year of 2010 when Munawar *et al.* first reported the synthesis and characterization of a series of benzothiazolium-containing ILs.[18] Thus, there is an urgent need for research into new ionic liquids. Prompted by these findings and due to our interest in the synthesis of new ILs based on benzothiazolium cations with the above-mentioned properties, in this paper we wish to complement the research findings of Munawar by reporting three novel ILs based on benzothiazolium cations (Scheme 1) and their catalytic activity for the synthesis of benzoic esters as novel catalysts (compound **1c** was described as protonated benzothiazole in previous literature).[19]

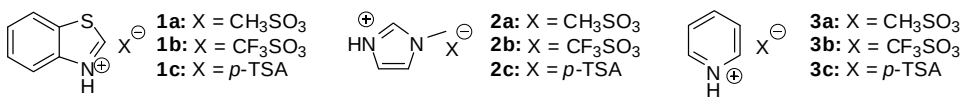

Scheme 1. Structures of the ionic liquids used in this study.

EXPERIMENTAL

Chemicals and instruments

All chemicals (AR) were commercially available and used without further purification. The melting points were determined on an XRC-1 melting point apparatus (Sichuan University Instrument Factory, P. R. China). The ^{1}H- and ^{13}C-nuclear magnetic resonance (NMR) spectra were recorded on an AV-400 spectrometer (Bruker Corporation, Germany) in DMSO-d_6 with tetramethylsilane (TMS) as an internal standard. The electrospray ionization mass spectrometry (ESI-MS) spectra were recorded on a ZQ 4000 mass spectrometer (Waters Corporation, USA). The UV–Vis spectra were recorded on a UV-2450 spectrophotometer (Shimadzu, Japan) in methanol. The concentrations of the products were determined by high performance liquid chromatography (HPLC) using an LC-20AT HPLC instrument (Shimadzu, Japan) with a C18 column (3.9 mm×150 mm, 5 μm) using an internal standard.

Preparation of the ionic liquids

The ionic liquids with *N*-methylimidazolium or pyridinium cations, **2a**–**c** and **3a**–**c** (Scheme 1), were synthesized according to literature procedures.[20-24] The preparation of the novel benzothiazolinm cations-based ionic liquids (ILs **1a**–**c**) was as follows: benzothiazole (100 mmol) was placed in a round-bottom flask equipped with a magnetic stirrer and dissolved in 50 mL ethanol.. The solution was cooled to 0-5 °C in an ice bath and 20 mL of an ethanolic solution of methanesulfonic acid (trifluoromethanesulfonic acid or *p*-toluenesulfonic acid) (110 mmol) was added dropwise way over a period of 0.5 h. The reaction mixture was stirred for a further 4 h at room temperature. The ethanol was removed under vacuum affording crude IL as a white solid, which was washed with diethyl ether (3×10 mL). The crude ionic liquid was purified by recrystallization from hot ethanol to give colorless flake crystals in quantitative yield. The ILs were dried at 80 °C under high vacuum for 12 h and then characterized by ^{1}H-NMR, ^{13}C-NMR and ESI-mass spectroscopy.

Procedure for the esterification reactions

A typical procedure for the esterification reactions is as follows. Benzoic acid (50 mmol, 6.1 g), *n*-butanol (150 mmol, 11.1 g) and IL **1a** (25 mmol, 5.8 g) were added to a 50 mL round-bottom flask equipped with a reflux condenser. The mixture was magnetically stirred for 8 h in an oil bath at 110 °C. After the reaction, the reaction mixture was cooled to room temperature whereby a liquid-solid system formed and then the ionic liquid **1a** precipitated. The IL was collected by filtration and reused after removal of water under vacuum at 80 °C for 4–5 h. The filtrate containing the target ester was analyzed by HPLC. When there was no phase separation of the reaction mixture, the following procedure was employed for ester isolation. The reaction mixture was diluted with water (10 mL) and extracted with diethyl ether (3×10 mL). The combined ether extracts were dried over anhydrous $MgSO_4$, and then analyzed by HPLC.

UV–Vis acidity determination

The Brønsted acidity of the ILs was evaluated by determination of the Hammett acidity function using UV–Vis spectroscopy. In the present case, the ILs and the indicator 4-nitroaniline were dissolved in methanol at concentrations of 20 and 0.1 mmol L^{-1}, respectively.

RESULTS AND DISCUSSION

*Spectral data of the novel ILs **1a–c***

*Benzothiazolium methanesulfonate (**1a**)*. Yield: 95 %, m.p. 105–107 °C. ^{1}H--NMR (400 MHz, DMSO-d_6, δ / ppm): 2.62 (3H, *s*), 7.53 (1H, *t*, *J* = 7.2 Hz), 7.59 (1H, *t*, *J* = 7.2 Hz), 8.14 (1H, *d*, *J* = 8 Hz), 8.21 (1H, *d*, *J* = 8 Hz), 9.49 (1H, *s*). ^{13}C-NMR (100 MHz, DMSO-d_6, δ / ppm): 39.58, 122.53, 122.76, 125.53, 126.25, 133.40, 152.42, 156.38. ESI-MS (*m*/*z* (+)): 137.2, (*m*/*z* (–)): 95.0.

*Benzothiazolium trifluoromethanesulfonate (**1b**)*. Yield: 90 %; m.p. 128–130 °C. ^{1}H-NMR (400 MHz, DMSO-d_6, δ / ppm): 7.54 (1H, *t*, *J* = 7.2 Hz), 7.60 (1H, *t*, *J* = 7.2 Hz), 8.14 (1H, *d*, *J* = 8 Hz), 8.22 (1H, *d*, *J* = 8 Hz), 9.49 (1H, *s*). ^{13}C--NMR (100 MHz, DMSO-d_6, δ / ppm): 119.05, 122.53, 122.74, 125.55, 126.27, 133.39, 152.36, 156.38. ESI-MS (*m*/*z* (+)): 136.4, (*m*/*z* (–)): 148.9.

*Benzothiazolium p-toluenesulfonate (**1c**)*. Yield: 95 %, m.p. 120–122 °C. ^{1}H--NMR (400 MHz, DMSO-d_6, δ / ppm): 2.31 (3H, *s*), 7.19 (2H, *d*, *J* = 8 Hz), 7.52 (1H, *t*, *J* = 7.2 Hz), 7.56 (2H, *d*, *J* = 8.0 Hz), 7.59 (1H, *t*, *J* = 7.2 Hz), 8.13 (1H, *d*, *J* = 8.0 Hz), 8.21 (1H, *d*, *J* = 8.0 Hz), 9.52 (1H, *s*). ^{13}C-NMR (100 MHz, DMSO-d_6, δ / ppm): 20.75, 122.57, 122.69, 125.50, 125.57, 126.31, 128.34, 128.34, 133.38, 138.54, 138.54, 144.26, 152.23, 156.54; ESI-MS (*m*/*z* (+)): 136.8, (*m*/*z* (–)): 170.9.

Acidities of the novel ILs

An efficient approach to evaluate the acidity of a Brønsted acidic ionic liquid is the Hammett method.[25] Hammett acidity function (H_0) is usually determined by UV–Vis spectrophotometry, wherein a basic indicator is used to trap the dissociated proton.[26] With increasing acidity of the acidic ionic liquid, the concentration of the unprotonated form of the basic indicator decreases, whereas the protonated form of the indicator could not be observed because of its small absorbance and its location; so the $[I]/[IH^+]$ ratio could be determined from the measured absorbance differences after addition of Brønsted acidic ionic liquid, and then the Hammett acidity function could be calculated from the following equation:[27,28]

$$H_0 = pK(I)_{aq} + \log ([I]/[IH^+])$$

where $pK(I)_{aq}$ is the pK_a value of the indicator, $[I]$ and $[IH^+]$ are, respectively, the molar concentrations of the unprotonated and protonated forms of the indicator.[29]

The results obtained are shown in Fig 1. The absorbance of the unprotonated form of the indicator with three ionic liquids decreased as follows: benzothiazolium *p*-toluenesulfonate (**1c**) > benzothiazolium methanesulfonate (**1a**) > benzothiazolium trifluoromethanesulfonate (**1b**). The Hammett function was calculated and the obtained values are listed in Table I. It is clearly shown that the acidity order of the novel ILs is benzothiazolium trifluoromethanesulfonate (**1b**) > benzothiazolium methanesulfonate (**1a**) > benzothiazolium *p*-toluenesulfonate (**1c**).

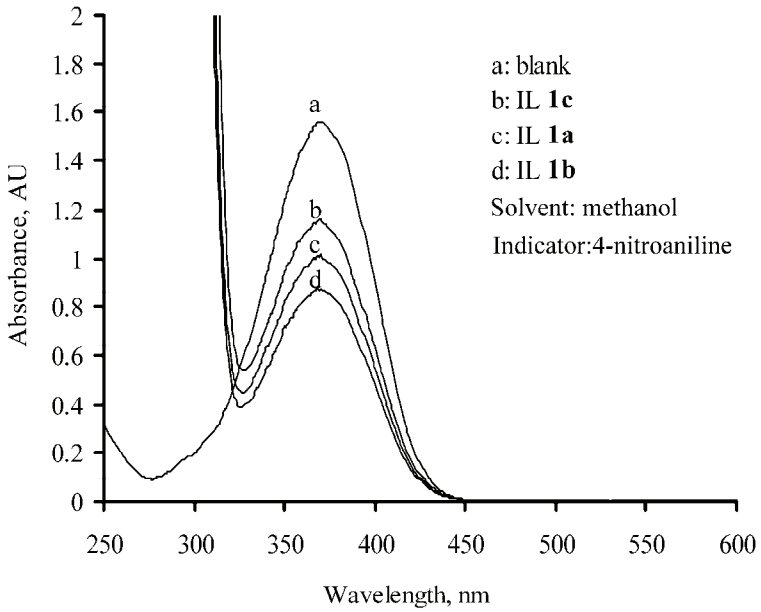

Fig. 1. Absorption spectra of 4-nitroaniline with the novel ionic liquids (20 mmol/L) in methanol.

TABLE I. Calculation and comparison of the Hammett acidity functions (H_0) of the novel ILs in methanol ($H_0 = pK(I)_{aq} + \log([I]/[IH^+])$; indicator: 4-nitroaniline ($pK_a = 0.99$)

Ionic liquid	Absorbance	[I] / %	$[IH^+]$ / %	H_0
Blank	1.5568	100	0	–
1a	1.0159	65.26	34.74	1.26
1b	0.8776	56.37	43.63	1.10
1c	1.1602	74.52	25.47	1.46

Esterification of benzoic acid by n*-butanol using various ILs*

The esterification of benzoic acid and *n*-butanol was chosen as a model reaction. The reaction was initially performed without a catalyst. The result (Table II, entry 1) showed that the esterification reaction was not realized and no product was obtained. This indicated that a catalyst for this reaction could be necessary. The catalytic performance of the ILs **1a**–**c** for the esterification of benzoic acid by *n*-butanol was investigated (Table II, entries 2–4). The ILs showed good catalytic activity and the ester yields were 93.9, 97.3 and 77.4 %, respectively. It was found that the catalytic activities of the acidic ILs in the esterification were in excellent agreement with their acidity order. ILs **1a** and **1c** formed a heterogeneous system (Fig. 2) while IL **1b** formed a homogeneous system after completion of the reaction and cooling down to room temperature. As a result, IL **1a** or **1c** could be easily separated from the reaction mixture by simple filtration. In order

to further compare the novel ILs with other pyridinium or *N*-methylimidazolium ionic liquids, six ILs (Scheme 1, **2a**–**c** and **3a**–**c**), reported in the literature, were used as catalysts for the model reaction (Table II, entries 5–10). As is shown (Table II, entries 5–7), when the reaction was promoted by *N*-methylimidazolium ILs (**2a**–**c**), benzoic acid could hardly react with *n*-butanol, only a trace of product was obtained, and the homogeneous reaction system made these ILs difficult to recover. Moreover, the ester yields were much lower (25.1–35.2 %) when pyridinium ILs (**3a**–**c**) (Table II, entries 8–10) were employed as catalysts than when benzothiazolium-based ILs were used. Taking the product yield of the reaction and the operational simplicity into consideration, benzothiazolium methanesulfonate (IL **1a**) may be preferential for the synthesis of benzoic esters.

TABLE II. Comparison of various ILs in the esterification of benzoic acid by *n*-butanol. Reaction conditions: benzoic acid, 50 mmol; *n*-butanol, 150 mmol; catalyst, 25 mmol; 110 °C for 8 h

Entry	Catalyst	IL precipitated or not (Y/N)[a]	Yield[b], %
1	Without catalyst	–	0
2	**1a**	Y	93.9
3	**1b**	N	97.3
4	**1c**	Y	77.4
5	**2a**	N	6.1
6	**2b**	N	3.7
7	**2c**	N	Trace
8	**3a**	Y	33.8
9	**3b**	Y	35.2
10	**3c**	N	25.1

[a]When the reaction mixture was cooled to room temperature; [b]yields based on benzoic acid

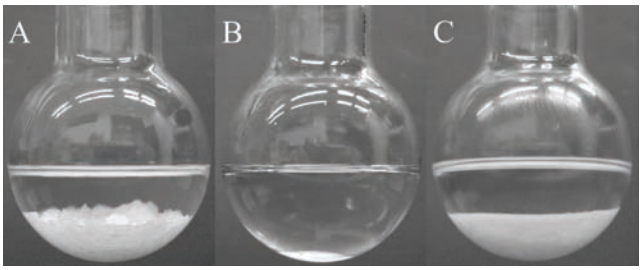

Fig. 2. Photographs of the esterification of benzoic acid with *n*-butanol over IL **1a**. A) Heterogeneous system before reaction. The benzoic acid dissolved in *n*-butanol and the IL **1a** was at the bottom. B) Homogeneous mixture during the reaction. C) Heterogeneous system after completion of the reaction and the system had been cooled to room temperature, the IL has precipitated.

*Various esterification reactions in IL **1a***

For evaluating the catalytic ability of IL **1a**, benzoic acids and several single alcohols were tried as reactants. The results of the experiments are summarized

in Table III. As is shown, under optimal conditions, the catalyst enabled good yields of all the target esters except *t*-butyl benzoate (no product was obtained, entry 8 in Table III). Yields of 70.3–97.3 % were obtained, which demonstrated that IL **1a** is an efficient catalyst for the esterification of benzoic acid with single alcohols. The reaction phenomena varied with the solubility of the catalyst in the reactants. When benzoic acid reacted with ethanol, *n*-propanol, *i*-propanol, *n*-butanol, *i*-butanol, *s*-butanol, *t*-butanol (Table III, entries 2–8), the IL dissolved in the homogeneous reaction mixture at working temperature and then the reaction medium switched from a homogeneous system to liquid–solid biphasic system when the reaction was completed and the system cooled to room temperature (Fig. 2). However, with methanol (Table III, entry 1), the esterification systems were homogeneous throughout the process. A proper explanation to this is that the solubility of the IL in alcohols varies with the polarity of the different alcohols and it decreases with decreasing alcohol polarity. The solubility of IL **1a** in the strongly polar methanol was high. However, IL **1a** has a much lower solubility in the less polar solvents (*i.e.*, ethanol, *n*-propanol, *i*-propanol, *n*-butanol, *i*-butanol, *s*-butanol and *t*-butanol) and is immiscible with the product ester at room temperature; thus, a liquid–solid biphasic system could be formed. Hence, IL **1a** could be removed by simple filtration and recycled; thus, it combines the advantages of both homogeneous catalysts and heterogeneous solid catalysts.

TABLE III. Results of the esterifications of benzoic acid (A) with various aliphatic alcohols (B) in IL **1a**. Reaction conditions: benzoic acid, 50 mmol

Entry	Alcohol	t / °C	τ / h	n_A:n_B:n_{IL}	IL precipitated or Not (Y/N)[a]	Yield[c], %
1	Methanol	120	8	1:4:1	N	97.9
2	Ethanol	110	6	1:4:1.5	Y	97.3
3	*n*-Propanol	110	8	1:4:1	Y	96.1
4	*i*-Propanol	110	8	1:4:1	Y	70.3
5	*n*-Butanol	110	8	1:3:0.5	Y	93.9
6	*i*-Butanol	120	8	1:3:0.5	Y	90.3
7	*s*-Butanol	120	11	1:3:0.5	Y	72.6
8	*t*-Butanol	120	12	1:3:0.5	Y	Trace

[a]When the reaction mixture was cooled to room temperature; [b]yields based on benzoic acid

*Reusability of the ionic liquid **1a***

To investigate the reusability of IL **1a**, a recycling experiment was performed. After the reaction of benzoic acid (50 mmol, 6.1 g), *n*-butanol (150 mmol, 11.1 g) and IL **1a** (25 mmol, 5.8 g) at 110°C for 8 h, the reaction mixture was cooled down to room temperature and IL **1a** was recovered by filtration. After treatment under vacuum at 80 °C for 4–5 h, IL **1a** was directly reused for the next run. The results (Table IV) showed that IL **1a** could be conveniently reused several times to catalyze the reaction in high product yields. The observed

slight decrease in the ester yield with the increase in reuse run may mostly be due to catalyst loss during filtration. In spite of this, the reuse performance of IL **1a** was excellent and 91.1 % yield was retained after three recycles. This indicates that the ionic liquid is recyclable and stable for these reactions.

TABLE IV. Reusability of IL **1a** in the esterification of benzoic acid by *n*-butanol. Reaction conditions: benzoic acid, 50 mmol; *n*-butanol, 150 mmol; catalyst, 25 mmol; 110°C for 8 h

Entry	Run	Yield[a], %
1	Fresh catalyst	93.9
2	1st cycle	93.1
3	2nd cycle	92.0
4	3rd cycle	91.1

[a]Yields based on benzoic acid

CONCLUSIONS

In summary, three novel acidic ionic liquids were successfully synthesized and used as highly efficient catalysts for esterification reactions. The catalytic procedure could produce a series of benzoic esters in high yield under mild reaction conditions. They combined the advantages of both homogeneous and heterogeneous solid catalysts in that they could be recycled by simple filtration and reused at least three times without obvious activity loss. Thus, a new, simple, efficient and eco-friendly method has been developed to synthesize a series of benzoic esters using these novel ILs.

ИЗВОД

НОВЕ ЈОНСКЕ ТЕЧНОСТИ ТИПА БРЕНСТЕД–ЛОРИЈЕВЕ КИСЕЛИНЕ СА БЕНЗОТИАЗОЛИЈУМ КАТЈОНОМ КАО КАТАЛИЗАТОРИ У РЕАКЦИЈАМА ЕСТЕРИФИКАЦИЈЕ

XIAN SI ZHOU, JIA BING LIU, WEN FENG LUO, YI WEN ZHANG и HANG SONG

School of Chemical Engineering, Sichuan University, Chengdu 610065, P. R. China

Синтетисане су три нове Бренстед–Лоријеве киселине као јонске течности, које су употребљене као катализатори у синтези естара бензоеве киселине. Сва три катализатора омогућавају високе приносе у реакцијама естерификације. Осим тога, катализатори имају предности и хомогених и хетерогених катализатора у реакцијама естерификације, што омогућава да се користе као хомогени катализатори током реакције и касније изоловање филтрацијом током обраде реакција и поновно коришћење. Могу бити поново коришћене више пута без запаженог губитка ефикасности.

(Примљено 2. јануара, ревидирано 18. марта 2011)

REFERENCES

1. X. Li, W. Eli, G. Li, *Catal. Commun.* **9** (2008) 2264
2. P. M. Ki-Arvela, T. Salmi, M. Sundell, K. Ekman, R. Peltonen, J. Lehtonen, *Appl. Catal., A* **184** (1999) 25

3. A. Heidekum, M. A. Harmer, W. F. Hoelderich, *J. Catal.* **181** (1999) 217
4. J. Dijs, H. L. F. van Ochten, C. A. vanWalree, J. W. Geus, L. W. Jenneskens, *J. Mol. Catal., A* **188** (2002) 209
5. I. V. Kozhevnikov, *Chem. Rev.* **98** (1998) 171
6. R. A. Sheldon, R. S. Downing, *Appl. Catal., A* **189** (1999) 163
7. J. S. Wilkes, *J. Mol. Catal., A* **214** (2004) 11
8. T. Welton, *Chem. Rev.* **99** (1999) 2071
9. K. N. Marsh, J. A. Boxall, R. Lichtenthaler, *Fluid Phase Equilib.* **219** (2004) 93
10. A. Zare, A. Hasaninejad, A. Parhami, A. R. Moosavi-Zare, F. Khedri, Z. Parsaee, M. Abdolalipoor-Saretoli, M. Khedri, M. Roshankar, H. Deisi, *J. Serb. Chem. Soc.* **75** (2010) 1315
11. Y. Zhao, J. Long, F. Deng, X. Liu, Z. Li, C. Xia, J. Peng, *Catal. Commun.* **10** (2009) 732
12. H. Shi, W. Zhu, H. Li, H. Liu, M. Zhang, Y. Yan, Z. Wang, *Catal. Commun.* **11** (2010) 588
13. X. Li, Q. Lin, L. Ma, *Ultrason. Sonochem.* **17** (2010) 752
14. Z. Xu, H. Wan, J. Miao, M. Han, C. Yang, G. Guan, *J. Mol. Catal. A: Chem.* **332** (2010) 152
15. A. C. Cole, J. L. Jensen, I. Ntai, K. L. T. Tran, K. J. Weaver, D. C. Forbes, J. H. Davis, *J. Am. Chem. Soc.* **124** (2002) 5962
16. Y. Leng, J. Wang, D. R. Zhu, X. Q. Ren, H. Q. Ge, L. Shen, *Angew. Chem. Int. Ed.* **47** (2008) 1
17. W. H. Zhang, Y. Leng, D. R. Zhu, Y. J. Wu, J. Wang, *Catal. Commun.* **11** (2009) 151
18. S. Nadeem, M. A. Munawar, S. Ahmad, M. Smiglak, D. M. Drab, K. I. Malik, R. Amjad, C. M. Ashraf, R. D. Rogers, *ARKIVOC* **7** (2010) 19
19. B. P. Branchaud, Y. L. Choi, *J. Org. Chem.* **53** (1988) 4638
20. G. Y. Zhao, T. Jiang, H. X. Gao, B. X. Han, J. Huang, D. H. Sun, *Green Chem.* **6** (2004) 75
21. A. C. Chaskar, S. R. Bhandari, A. B. Patil, O. P. Sharma, S. Mayeker, *Synth. Commun.* **39** (2009) 366
22. Y. Y. Du, F. L. Tian, *Synth. Commun.* **35** (2005) 2703
23. P. A. Ganeshpure, J. Das, *React. Kinet. Catal. Lett.* **92** (2007) 69
24. F. Freeman, D. S. H. L. Kim, *J. Org. Chem.* **57** (1992) 1722
25. H. B. Xing, T. Wang, Z. H. Zhou, Y. Y. Dai, *J. Mol. Catal., A* **264** (2007) 53
26. C. Thomazeau, H. Bourbigou, S. Luts, B. Gillber, *J. Am. Chem. Soc.* **125** (2003) 5264
27. X. M. Liu, M. Liu, X. W. Guo, J. X. Zhou, *Catal. Commun.* **9** (2008) 1
28. Y. Y. Wang, D. Jiang, L. Y. Dai, *Catal. Commun.* **9** (2008) 2475
29. G. B. Cheng, X. L. Duan, X. F. Qi, C. X. Lu, *Catal. Commun.* **10** (2008) 201.

Journal of the Serbian Chemical Society
JSCS-info@shd.org.rs • www.shd.org.rs/JSCS
J. Serb. Chem. Soc. 76 (12) 1617–1626 (2011)
JSCS–4234
UDC 547.72+547.831:615.281–188:615.276–188
Original scientific paper

Synthesis of quinoline-attached furan-2(3*H*)-ones having anti-inflammatory and antibacterial properties with reduced gastro-intestinal toxicity and lipid peroxidation

MOHAMMAD M. ALAM[1]*, DEBA PRIYA SARKAR[1], ASIF HUSAIN[1], AKRANTH MARELLA[1], MOHAMMAD SHAQUIQUZZAMAN[1], MYMOONA AKHTER[1], MOHAMMAD SHAHARYAR[1], OZAIR ALAM[1] and FAIZUL AZAM[2]

[1]*Department of Pharmaceutical Chemistry, Faculty of Pharmacy, Jamia Hamdard (Hamdard University), New Delhi-110 062, India and* [2]*Department of Medicinal Chemistry, Faculty of Pharmacy, Seventh of October University, P. O. Box 2247, Misurata, Libya*

(Received 31 January, revised 4 May 2011)

Abstract: A series of 5-aryl-3-[(2-chloroquinolin-3-yl)methylene] furan-2(3*H*)-ones (**3a**–**p**) were synthesized. The required 3-(substituted benzoyl)propionic acids **2a**–**d** were prepared under Friedel–Crafts acylation reaction conditions. The substituted 2-chloroquinoline-3-carboxaldehydes **1a**–**d** were synthesized by reaction of substituted phenylethanone oxime with phosphorus oxychloride in presence of dimethylformamide using the Vilsmeier–Haack reaction method. These compounds were screened for their anti-inflammatory and antibacterial activities along with their ulcerogenic and lipid peroxidation potentials. The compounds that showed significant anti-inflammatory activity were further screened for their analgesic activity. The compounds were less toxic in terms of ulcerogenicity as compared to a standard, which was also supported by lipid peroxidation studies. The antibacterial activities were performed against *Staphylococcus aureus* and *Escherichia coli*. Compounds **3f**, **3n** and **3o** showed significant activity against both *S. aureus* and *E. coli* having an minimum inhibitory concentration (*MIC*) value of 6.25 μg mL^{-1}.

Keywords: furanone; quinoline; anti-inflammatory; analgesic; antibacterial activity.

INTRODUCTION

Inflammation occurs due to the biosynthesis of pro-inflammatory prostaglandins from arachidonic acid by the action of the enzyme cyclooxygenase (COX). In the human system, COX occurs in two isoforms, *viz.* COX-1 and COX-2.[1] Constitutive, COX-1 is responsible for housekeeping functions while inducible

* Corresponding author. E-mail: drmmalam@gmail.com
doi: 10.2298/JSC110131142A

COX-2 is released during tissue injury, which causes the overproduction of prostaglandins.[2] Overexpressive COX-2 is also responsible for colon cancer.

Drugs used for treating the signs and symptoms of inflammation are referred to as NSAIDs. However the traditional non-steroidal anti-inflamatory drugs (NSAIDs), in addition to suppressing the effects of pathological COX also interfere with the housekeeping functions of the cyclo-oxygenase enzyme, which results in gastrointestinal tract (GIT) irritation, bleeding and ulceration.[3] This explains why the search for novel anti-inflammatory agent is necessary and hence, the need to develop and screen agents which would specifically inhibit the action of COX-2. However, this selective COX-2 inhibition has adverse cardiovascular effects.[4] Thus, there is a continuous need for the development of compounds with a safe analgesic and anti-inflammatory profile.

Quinoline and its derivatives are an important class of pharmaceutical agents known to occur in several natural compounds and found to possess anti-inflammatory[5] and analgesic[6] activity in addition to other pharmacological activities.[7–10] Similarly, furanone and its derivatives have been reported to have anti-inflammatory,[11,12] cardiotonic,[13] analgesic[12,14] and COX-2 inhibition[15,16] activities in addition to antioxidant,[17] cytotoxic,[18] antifungal,[11,12,14,19] antibacterial[11,12,14,20] and antiviral[21] activities.

Previously, the anti-inflammatory activities of a number of 3-arylidene-5--(substituted phenyl)-2(3*H*)-furanones were studied and the results were encouraging.[11,12,14,22,23] In view of these observations and as a part of an ongoing research program on development of newer anti-inflammatory and analgesic agents, the synthesis and pharmacological activities of a series of 2(3*H*)-furanones fused with the quinoline moiety are reported herein.

RESULTS AND DISCUSSION

Chemistry

Sixteen new compounds **3a**–**p** were synthesized as outlined in Scheme 1. The required 3-(substituted benzoyl)propionic acids **2a**–**d** were prepared by reacting different substituted benzenes with succinic anhydride in presence of anhydrous aluminium chloride followed by acylation under Friedel–Crafts reaction conditions.[14,22,24] The substituted 2-chloroquinoline-3-carboxaldehydes **1a**–**d** were synthesized by reacting substituted phenylethanone oxime with phosphorus oxychloride in presence of dimethyl formamide using the Vilsmeier–Haack reaction method.[25,26]

5-Aryl-3-[(2-chloroquinolin-3-yl)methylene] furan-2(3*H*)-ones **3a**–**p** were synthesized by condensing different aromatic aldehydes (**1a**–**d**) with a 3-(substituted benzoyl)propionic acids (**2a**–**d**) in presence of triethylamine and acetic anhydride under anhydrous conditions following a modified Perkin reaction.[14,22] Calculations of δ-values using incremental parameters for the hydrogen (semi-

cyclic double bond) suggested the (*E*)-configuration. All the synthesized compounds were characterized by spectroscopic data, *i.e.*, IR, ^{1}H-NMR, ^{13}C-NMR and mass, and elemental analysis. The results are given in the supplementary material to this paper.

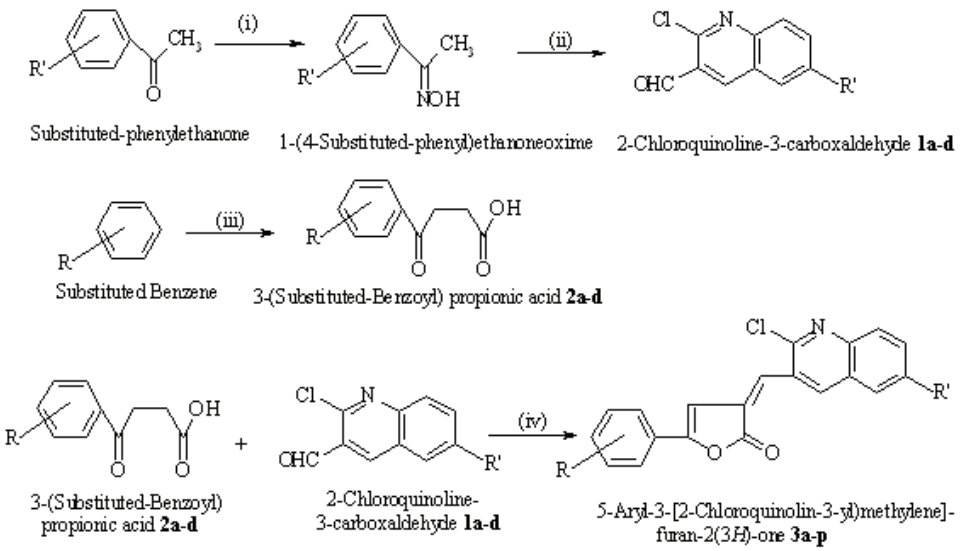

3a: R=H, R'=H; **3b**: R=H, R'=Cl; **3c**: R=H, R'=OCH_3; **3d**: R=H, R'=CH_3
3e: R=4-CH_3, R'=H; **3f**: R=4-CH_3, R'=Cl; **3g**: R=4-CH_3, R'=OCH_3; **3h**: R=4-CH_3, R'=CH_3
3i: R=$(CH_3)_{2,4}$, R'=H; **3j**: R=$(CH_3)_{2,4}$, R'=Cl; **3k**: R=$(CH_3)_{2,4}$, R'=OCH_3; **3l**: R=$(CH_3)_{2,4}$, R'=CH_3
3m: R=4-Br, R'=H; **3n**: R=4-Br, R'=Cl; **3o**: R=4-Br, R'=OCH_3; **3p**: R=4-Br, R'=CH_3

Scheme 1. The reaction scheme for the synthesis of compounds **3a**–**p** (i – hydroxylamine hydrochloride and sodium acetate; ii – dimethylformamide and $POCl_3$; iii – anhydrous $AlCl_3$ and succinic anhydride; iv – acetic anhydride and triethylamine).

In general, the infrared spectral data of the furanones **3a**–**p** revealed bands at 1790–1740 cm^{-1} (lactone C=O), 1610–1560 cm^{-1} (ArC=C), 1070–1060 cm^{-1} (ArC–N) and 827–806 cm^{-1} (ArC–H). In the ^{1}H-NMR spectra, all the compounds showed two singlets of one proton each at around δ 6.6 and 8.2 ppm, which could be assigned to the ring β-H and the olefinic hydrogen of the arylidene substituent. Other peaks were observed at the appropriate positions. Some points could be made regarding the fragmentation pattern observed in the electron impact mass spectrum. The 5-aryl-3-[(2-chloroquinolin-3-yl)methylene] furan-2(3*H*)-ones **3a**–**p** gave an M^+ and M+2 (isotopic peak, due to presence of chlorine) peak of reasonable intensities.

Biological evaluation

Anti-inflammatory activity. The *in vivo* anti-inflammatory activity of the synthesized compounds **3a**–**p** was evaluated by the carrageenan-induced rat paw edema method.[27] Ibuprofen was used as the standard drug for comparison (Table I).The anti-inflammatory activity test showed that 5-(4-bromophenyl)-3-[(2--chloro-6-methoxyquinolin-3-yl)methylene] furan-2(3*H*)-one (**3o**) exhibited the maximum anti-inflammatory activity (68.9 % inhibition) in addition to 5-(4-bromophenyl)-3-[(2,6-dichloroquinolin-3-yl)methylene] furan-2(3*H*)-one (**3n**), 5-(4-methylphenyl)-3-[(2-chloro-6-methoxyquinolin-3-yl)methylene] furan-2(3*H*)-one (**3g**) and 5-(4-bromophenyl)-3-[(2-chloro-6-methylquinolin-3-yl)methylene] furan-2(3*H*)-one (**3p**), showing 59.03, 56.62 and 53.01 % inhibition, respectively. The results are presented in Table I.

TABLE I. Anti-inflammatory and analgesic activity along with the ulcerogenic and lipid peroxidation effect of the synthesized compounds **3a**–**p**

Compound	% Inhibition ± *SEM*[a]		Severity index[b]	Lipid peroxidation[c] nmol MDA mg^{-1} protein	Analgesic activity (writhing test)[b]	
	After 2 h	After 3 h			No. of writhes per 30 min	Protection %
Control	–	–	0.00±0.00	0.24±0.002[b]	83±1.31	–
Ibuprofen	67.7±2.05	80.8±2.60	0.83±0.36	0.73±0.001[a]	29±1.15	65.06
3a	9.5±1.79	16.0±1.81	0.4±0.10	0.39±0.005[ab]	–	–
3b	18.6±3.16	23.4±2.87	0.3±0.12	0.40±0.005[ab]		
3c	16.4±1.72	22.8±0.42	0.33±0.12	0.35±0.001[ab]	–	–
3d	18.8±2.83	29.7±3.39	0.5±0.27	0.39±0.007[ab]	–	–
3e	26.6±4.34	36.0±3.22	0.52±0.36	0.54±0.001[ab]	–	–
3f	28±2.74	50.4±1.73	0.41±0.1	0.40±0.002[ab]	–	–
3g	34.1±4.16	53.8±1.38	0.16±0.12	0.36±0.014[ab]	36±1.89	56.62
3h	44.9±5.22	50.0±2.28	0.41±0.1	0.41±0.002[ab]	–	–
3i	10.4±3.86	19.9±3.06	0.46±0.4	0.55±0.001[ab]	–	–
3j	33.7±2.61	39.7±2.80	0.5±0.27	0.42±0.001[ab]	–	–
3k	21.5±4.01	36.6±3.51	0.48±0.36	0.53±0.017[ab]	–	–
3l	20±1.97	37.0±3.27	0.5±0.27	0.49±0.001[ab]	–	–
3m	26.6±3.98	34.5±3.54	0.43±0.36	0.58±0.001[ab]	–	–
3n	38.2±1.97	56.3±3.49	0.16±0.12	0.29±0.001[ab]	34±1.24	59.03
3o	48.6±3.69	68.9±3.07	0.25±0.12	0.38±0.002[ab]	33±1.31	60.24
3p	42.4±1.79	52.0±2.42	0.2±0.12	0.33±0.006[ab]	39±1.94	53.01

[a]Relative to the standard (ibuprofen) and data were analyzed by one-way ANOVA followed by the Tukey test for $n = 6$; [b]relative to their respective control and the data were analyzed by one-way ANOVA followed by the Tukey test for $n = 6$; [c]lipid peroxidation activity is expressed as nmoles of MDA mg^{-1} protein. "±" indicates the minimum and maximum variation in the average values. "–" indicates not tested

Based on the above observations, the following structure–activity relationship can be concluded:

i) presence of an electronegative group on phenyl moiety of the furanone ring increases the anti-inflammatory activity as compared to that of an electropositive group;

ii) an increase in number of electropositive groups on the phenyl moiety of the furanone ring further decreases the activity;

iii) the presence of a methoxy group on the quinoline nucleus showed maximum activity;

iv) replacement of the methoxy group by a methyl group decreases the activity.

All the synthesized compounds were further tested for their ulcerogenic and lipid peroxidation effects. The test compounds (**3o**, **3n, 3g** and **3p**) that exhibited an above 65 % ibuprofen edema inhibition were further evaluated for their analgesic activity.

Analgesic activity. The analgesic activity was evaluated by the acetic acid-induced writhing test.[28] The results indicated that compounds **3o** and **3n** showed 60.24 and 59.03 % activity, respectively, which were comparable to that of the standard ibuprofen (65.06 %). Compounds **3g** and **3p** also showed good analgesic activity (Table I).

Acute ulcerogenesis. The synthesized compounds were screened for their ulcerogenic activity by the Cioli *et al.* method.[29] Compounds **3o** and **3n** showed a severity index of 0.25±0.12 and 0.16±0.12, respectively, which were much lower as compared to that of ibuprofen (0.83±0.36). The results indicated that the compounds were less toxic in terms of ulcerogenicity as compared to standard, which was also supported by lipid peroxidation studies (Table I).

Lipid peroxidation. All the compounds screened for ulcerogenic activity were also analyzed for lipid peroxidation by the Ohkawa *et al*. method.[30] The lipid peroxidation was measured as nmoles of malondialdehyde (MDA) mg^{-1} of protein. Ibuprofen exhibited high lipid peroxidation 0.73±0.001 whereas control group showed 0.24±0.002. It was found that all the furanone derivatives fused with quinoline ring showed less ulcerogenic activity along with reduced lipid peroxidation (Table I).

Antibacterial activity. All the compounds tested for antimicrobial activity showed inhibition of growth. Compounds **3f**, **3n** and **3o** showed significant activity against both *Staphylococcus aureus* and *Escherichia coli* with a minimum inhibitory concentration (*MIC*) value of 6.25 μg mL^{-1} (Table II). Of the sixteen new compounds, two compounds, **3i** and **3j** were found to be more active against *S. aureus* with an *MIC* value of 6.25 μg mL^{-1}. Analyses of the results indicated that:

i) the presence of a chloro group on the quinoline nucleus induced selectivity of the furanone towards inhibition of *S. aureus*;

ii) the presence of an electropositive group on the phenyl moiety of the furanone ring induced inhibition of *S. aureus*. However, an electronegative group favoured inhibition of *E. coli*.

TABLE II. Antibacterial activity, *MIC* / μg mL^{-1}, results of the 2(3*H*)-furanones (the studies were performed in triplicate)

Compound	*S. aureus*	*E. coli*
Nitrofurazone	12.5±0.0	6.25±0.0
3a	133.37±16.67	167.67±33.34
3b	50±0.0	50±0.0
3c	133±33.34	50±0.0
3d	133±33.34	166±33.34
3e	25±0.0	50±0.0
3f	6.25±0.0	6.25±0.0
3g	12.5±0.0	25±0.0
3h	25±0.0	50±0.0
3i	6.25±0.0	12.5±0.0
3j	6.25±0.0	12.5±0.0
3k	25±0.0	50±0.0
3l	12.5±0.0	25±0.0
3m	12.5±0.0	12.5±0.0
3n	6.25±0.0	6.25±0.0
3o	6.25±0.0	6.25±0.0
3p	12.5±0.0	25±0.0

EXPERIMENTAL

Chemistry

Chemicals were purchased from Merck and Sigma-Aldrich as synthesis grade and were used without further purification. Melting points were determined by the open tube capillary method and are uncorrected. The purity of the compounds was checked by thin layer chromatography (TLC) on silica gel G plates (Merck No. 5544) using toluene:ethyl acetate:formic acid (5:4:1) as the solvent system and the spots were located either under ultraviolet light or through exposure to iodine vapour. The IR spectra were measured as potassium bromide pellets using a Perkin-Elmer 1725X spectrophotometer. The ^{1}H-NMR spectra were recorded on Bruker spectrospin DPX-300 MHz in $CDCl_3$ with tetramethylsilane (TMS) as an internal standard; chemical shifts (δ) are reported in parts per million (ppm) downfield from TMS. Mass spectra were recorded at 70 eV on a Jeol JMS-D 300 instrument fitted with a JMS 2000 data system. Spectral data are consistent with the assigned structures. Elemental analyses were performed on a Perkin-Elmer model 240 analyzer (C, H, N) and were found within the range of ± 0.4 % of the theoretical values.

General procedure for the synthesis of 1-(4-substituted phenyl)ethanone oximes

The 1-(4-substituted phenyl)ethanone oximes were synthesized from different substituted acetophenones (0.1 mol), hydroxylamine hydrochloride (0.12 mol) and sodium acetate (0.12 mol) using the method reported by Cohn *et al.*[25]

*General procedure for the synthesis of the 2-chloroquinolin-3-carboxaldehydes **1a–d***

To dimethylformaldehyde (0.15 mol) cooled to 0 °C, freshly distilled phosphorous oxychloride (0.35 mol) was added dropwise under stirring, then the respective oxime (0.05 mol) was added portion-wise. The reaction mixture was heated at 60 °C for 16 h. It was then poured into ice water (300 mL) and stirred for 30 min. The 2-chloroquinoline-3-carboxaldehyde was filtered and recrystallized from ethyl acetate.[25,26]

*General procedure for the synthesis of 3-(substituted benzoyl)propionic acids **2a–d***

The 3-(substituted benzoyl)propionic acids were synthesized according to a previously reported method[14,22,24] using dry substituted-benzene (50 mL) under anhydrous conditions in presence of anhydrous aluminium chloride (0.15 mol) and succinic anhydride (0.1 mol). The obtained product was crystallized from aqueous ethanol to give a colourless compound that gave effervescence with sodium bicarbonate.

*General procedure for the synthesis of 3-[(2-chloroquinolin-3-yl)methylene]-5-(substituted phenyl) furan-2(3*H*)-ones **3a–p***

Each compound **2a–d** (3 mmol) and each compound **1a–d** (equimolar, 3 mmol) were fused together in presence of acetic anhydride (5–8 drops) in a round-bottom flask for half an hour. To this fused mixture, triethylamine (2 drops) was added and the heating on a heating mantle was continued for a further 15 min. After the completion of reaction, the obtained solid mass was crystallized from methanol and gave the desired products.

Biological evaluation

Animals. The Wistar rats and albino mice used in the present study were housed and kept in accordance with the Hamdard University Animal Care Unit, which applies the guidelines and rules laid down by the Committee for the Purpose of Control and Supervision of Experiments on Animals (CPCSEA), Ministry of Social Justice and Empowerment, Government of India. Wistar rats and albino mice of either sex (Hamdard University, Animal House, New Delhi, India), weighing 180–200 g (12 weeks) and 22–25 g (8 weeks), respectively, were used. The animals were housed in groups of six and acclimatized to ambient conditions for at least 2 days before the experiments. Food and water were freely available up to the time of the experiments. The food was withdrawn on the day before the experiment, but free access to water was allowed.

Anti-inflammatory activity. The synthesized compounds were evaluated for their anti-inflammatory activity using the carrageenan-induced paw edema method of Winter *et al*.[27] The animals were randomly divided into groups of six. Group I was kept as control, and received only 0.5 % carboxymethyl cellulose (CMC) solution. Group II was kept as the standard and received ibuprofen. Carrageenan solution (0.1 % in sterile 0.9 % NaCl solution) in a volume of 0.1 mL was injected subcutaneously into the sub-plantar region of the right hind paw of each rat, 30 min after the administration of the test compounds (20 mg kg^{-1} *p.o.*) and the standard drugs. The paw volume was measured by saline displacement shown on the screen of digital plethysmometer (Ugo Basile) at 2 and 3 h after carrageenan injection. The edema volume in the control group (V_c) and edema volume in the groups treated with test compounds (V_t) was measured and the percentage inhibition of edema was calculated using the formula:

$$\text{Anti-inflammatory activity (\% inhibition)} = 100((V_c - V_t) / V_c)$$

where V_c is the paw volume of the control group and V_t is the paw volume of the test group.

Analgesic activity. The compounds which showed anti-inflammatory activity above 75 % of the ibuprofen inhibition were screened for analgesic activity. The determination of the

analgesic activity was realized by the acetic acid-induced writhing method.[28] Mice were divided into groups with six in each. Group I was taken as the control and received CMC suspension only, group II received the reference drug ibuprofen and the other groups were treated with the test drugs (20 mg kg^{-1}) suspended in 1.0 % CMC orally. A 1 % aqueous acetic acid solution (0.1 mL) was used as writhing-inducing agent. The acetic acid solution was injected intraperitoneally 3 h after the treatment with the reference and test drugs to the various groups, respectively, and writhings were noted for 10–15 min after acetic acid administration.

Acute ulcerogenesis. Acute ulcerogenesis test was performed according to the method of Cioli *et al*.[29] Wistar rats were divided into different groups consisting of six animals in each group. Ulcerogenic activity was evaluated after *p.o.* administration of test compounds or ibuprofen at a dose of 60 mg kg^{-1}. The control rats received *p.o.* administration of the vehicle (suspension of 1 % carboxymethyl cellulose). Food but not water was removed 24 h before administration of the test compounds. After drug treatment, the rats were fed with a normal diet for 17 h and then sacrificed. The stomach was removed and opened along the greater curvature, washed with distilled water and cleaned gently by dipping in normal saline. The mucosal damage was examined by means of a magnifying glass and compared with that after ibuprofen administration. For each stomach, the mucosal damage was assessed according to the following scoring system: 0.5: redness, 1.0: spot ulcers, 1.5: hemorrhagic streaks, 2.0: ulcers > 3 but < 5, 3.0: ulcers > 5.

The mean score of each treated group minus the mean score of the control group was regarded as the severity index of gastric mucosal damage.

Lipid peroxidation. Lipid peroxidation in the gastric mucosa was determined according to the method of Ohkawa *et al*.[30] After screening for ulcerogenic activity, the gastric mucosa was scraped with two glass slides and 10 % of that tissue was homogenized at 10,000 rpm in 1.8 mL of 1.15 % ice-cold KCl solution. 1 mL of suspension medium was taken from the supernatant, 0.5 mL of 30 % trichloroacetic acid (TCA) followed by 0.5 mL of 0.8 % thiobarbituric acid (TBA) reagent were added to it. The tubes were covered with aluminium foil and kept in a shaking water bath for 30 min at 80 °C. After 30 min, the tubes were taken out and kept in ice-cold water for 10 min. These were then centrifuged at 3000 rpm for 15 min. The absorbance of the supernatant was read at 540 nm at room temperature against the blank on a UV spectrophotometer.

The standard curve used for estimating the concentration of MDA was prepared by using 1,1,3,3-tetraethoxypropane. The results are presented as nmol MDA mg^{-1} of protein.

Antibacterial activity. The antibacterial studies were performed on the synthesized compounds against the microorganisms *S. aureus* and *E. coli* in meat peptone agar medium at a concentration of 100 μg ml^{-1}. Compounds inhibiting growth of one or more of the microorganisms were further tested for their *MIC* value. The test was performed according to the turbidity method[31] using nitrofurazone as the standard.

SUPPLEMENTARY MATERIAL

Analytical and spectral data of synthesized compounds are available electronically from http://www.shd.org.rs/JSCS/, or from the corresponding author on request.

Acknowledgements. We are thankful to Mrs. Shaukat Shah, ex-in-charge of the animal house, Jamia Hamdard, for providing the animals for the pharmacological studies and Prof. P. K. Pillai, Head, Department of Microbiology, Majeedia Hospital, for helping in performing the antibacterial activity tests.

ИЗВОД

СИНТЕЗА ХИНОЛИН-ВЕЗАНИХ ФУРАН-2(3*H*)-ОНА КОЈИ ИМАЈУ АНТИИНФЛАМАТОРНА И АНТИБАКТЕРИЈСКА СВОЈСТВА УЗ СМАЊЕНУ ГАСТРОИНТЕСТИНАЛНУ ТОКСИЧНОСТ И ЛИПИДНУ ПЕРОКСИДАЦИЈУ

MOHAMMAD M. ALAM[1], DEBA PRIYA SARKAR[1], ASIF HUSAIN[1], AKRANTH MARELLA[1], MOHAMMAD SHAQUIQUZZAMAN[1], MYMOONA AKHTER[1], MOHAMMAD SHAHARYAR[1], OZAIR ALAM[1] и FAIZUL AZAM[2]

[1]Department of Pharmaceutical Chemistry, Faculty of Pharmacy, Jamia Hamdard (Hamdard University), New Delhi-110 062, India и [2]Department of Medicinal Chemistry, Faculty of Pharmacy, Seventh of October University, P. O. Box 2247, Misurata, Libya

Синтетисана је серија 5-арил-3-[(2-хлорохинолин-3-ил)метилен] фуран-2(3*H*)-она (**3a**–**p**). Потребне 3-(супституент-бензоил)-пропионске киселине **2a**–**d** су добијене Friedel–Crafts--овом реакцијом ациловања. Супституисани 2-хлорохинолин-3-карбалдехиди **1a**–**d** су синтетисани у реакцији супституисаних фенилетанон-оксима са фосфор-оксихлоридом, у присуству диметил-формамида, применом Vilsmeier–Haack-овог реакционог метода. За ова једињења је утврђивана антиинфламаторна, антибактеријска и улцерогена активност, као и способност да изазову липидну пероксидацију. Једињења која су показала значајну антиинфламаторну активност даље су испитивана као аналгетици. Једињења су испољила мању токсичност у поређењу са стандардним препаратима, у погледу улцерогености и липидне пероксидације. Антибактеријска активност је тестирана спрам *S. aureus* и *E. coli*. Једињења **3f**, **3n** и **3o** су показала значајну активност спрам обе бактерије, уз минималну инхибиторну концентрацију од 6,25 μg mL^{-1}.

(Примљено 31. јануара, ревидирано 4. маја 2011)

REFERENCES

1. J. R. Vane, J. A. Mitchell, I. Appleton, A. Tomilison, D. Bishop-Bailey, J. Crontall, D. A. Willoughby, *Proc. Natl. Acad. Sci.* **91** (1994) 2046
2. A. Hosada, Y. Ozaki, A. Kashimada, M. Mutoh, K. Wakabayashi, K. Mizuno, E. Nomura, H. Taniguchi, *Bioorg. Med. Chem.* **10** (2002) 1189
3. M. Allison, A. Homatson, C. Torrance, F. Lee, R. Russell, *N. Eng. J. Med.* **327** (1992) 749
4. J. M. Dogne, C. T. Supuhan, D. Pratico, *J. Med. Chem.* **48** (2005) 2251
5. Y. Chen, J. Chen, C. Lu, C. Tzeng, H. Tsao, J. Wang, *Bioorg. Med. Chem.* **11** (2003) 3921
6. M. Kidwai, N. Negi, *Monatsh. Chem.* **128** (1997) 85
7. B. P. Nandeshmanappa, D. B. A. Kumar, H. S. B. Naik, K. M. Mahadevan, *J. Sulfur Chem.* **26** (2006) 373
8. H. G. Jin, X. Y. Sun, K. Y. Chai, H. R. Pino, Z. S. Quan, *Bioorg. Med. Chem.* **14** (2006) 6868
9. J. Ghosh, V. Swarup, A. Saxena, S. Das, A. Hazra, P. Paira, S. Banerjee, N. B. Mondal, A. Basu, *Int. J. Antimicrob. Agents* **32** (2008) 349
10. Z. Cai, W. Zhon, L. Sun, *Bioorg. Med. Chem.* **15** (2007) 7809
11. M. S. Y. Khan, A. Husain, *Pharmazie* **57** (2002) 448
12. A. Husain, M. S. Y. Khan, S. M. Hasan, M. M. Alam, *Eur. J. Med. Chem.* **40** (2005) 1394
13. L. Leite, D. Jansone, M. Veveris, H. Cirule, Y. Popelis, G. Melikyan, A. Avetisyan, E. Lukevics, *Eur. J. Med. Chem.* **34** (1999) 859

14. a) A. Husain, M. M. Alam, N. Siddiqui, *J. Serb. Chem. Soc.* **74** (2008) 103; b) M. M. Alam, A. Husain, S. M. Hasan, Suruchi, T. Anwer, *Eur. J. Med. Chem.* **44** (2009) 2636
15. W. C. Black, C. Brideau, C. Chan, S. Charleson, W. Cromlish, R. Gordon, E. L. Grimm, G. Hughes, S. Leger, C. Lii, D. Riendeau, M. Therien, Z. Wang, L. Xu, P. Prasit, *Bioorg. Med. Chem. Lett.* **13** (2003) 1195
16. A. Zarghi, P. N. Praveen Rao, E. E. Knaus, *Bioorg. Med. Chem.* **15** (2007) 1056
17. F. Bailly, C. Queffelec, G. Mdemba, J. Mouscadet, N. Pommery, J. Pommery, J. Henichart, P. Cotelle, *Eur. J. Med. Chem.* **43** (2008) 1222
18. A. Albrecht, J. F. Koszuk, J. Modranka, M. Rozalski, U. Krajewska, A. Janecka, K. Studzian, T. Janecki, *Bioorg. Med. Chem.* **16** (2008) 4872
19. L. A. Vale-Silva, V. Buchta, D. Vokurkova, M. Pour, *Bioorg. Med. Chem. Lett.* **16** (2006) 2492
20. E. Lattmann, S. Dunn, S. Niamsanit, N. Sattayasai, *Bioorg. Med. Chem. Lett.* **15** (2005) 919
21. A. I. Hashem, A. S. Youssef, K. A. Kandeel, W. S. Abou-Elmagd, *Eur. J. Med. Chem.* **42** (2007) 934
22. A. Husain, M. M. Alam, M. S. Zaman, M. V. Ismail, *Int. J. Chem. Sci.* **6** (2008) 1535
23. A. Husain, S. M. Hasan, S. Lal, M. M. Alam, *Indian J. Pharm. Sci.* (2006) 536
24. a) A. Husain, M. Ajmal, *Acta Pharma.* **59** (2009) 223; b) M. S. Y. Khan, A. Husain, S. Sharma, *Indian J. Chem., B* **41** (2002) 2160
25. O. M. Cohn, B. Narine, B. Tarnowski, *J. Chem. Soc. Perkin Trans. 1* (1981) 1520
26. A. Srivastava, R. M. Singh, *Indian J. Chem., B* **44** (2005) 1868
27. C. A. Winter, E. A. Risley, G. W. Nuss, *Proc. Soc. Exp. Biol.* **111** (1962) 544.
28. E. Seigmund, R. Cadmus, G. Lu, *Proc. Soc. Exp. Biol.* **95** (1957) 729
29. V. Cioli, S. Putzolu, V. Rossi, P. Sorza Barcellona, C. Corradino, *Toxicol. Appl. Pharmacol.* **50** (1979) 283
30. H. Ohkawa, N. Ohishi, K. Yagi, *Anal. Biochem.* **95** (1979) 351
31. *Medical Microbiology, Vol. 2*, R. Cruickshank, J. P. Dugid, D. P. Marmion, R. H. A. Swain, Eds., Churchill, London, 1975.

Journal of the Serbian Chemical Society
JSCS@tmf.bg.ac.rs • www.shd.org.rs/JSCS
J. Serb. Chem. Soc. 76 (12) S1–S5 (2011) *Supplementary material*

SUPPLEMENTARY MATERIAL TO

Synthesis of quinoline-attached furan-2(3*H*)-ones having anti-inflammatory and antibacterial properties with reduced gastro-intestinal toxicity and lipid peroxidation

MOHAMMAD M. ALAM[1]*, DEBA PRIYA SARKAR[1], ASIF HUSAIN[1], AKRANTH MARELLA[1], MOHAMMAD SHAQUIQUZZAMAN[1], MYMOONA AKHTER[1], MOHAMMAD SHAHARYAR[1], OZAIR ALAM[1] and FAIZUL AZAM[2]

[1]*Department of Pharmaceutical Chemistry, Faculty of Pharmacy, Jamia Hamdard (Hamdard University), New Delhi-110 062, India and* [2]*Department of Medicinal Chemistry, Faculty of Pharmacy, Seventh of October University, P. O. Box 2247, Misurata, Libya*

J. Serb. Chem. Soc. 76 (12) (2011) 1617–1626

ANALYTICAL AND SPECTRAL DATA OF THE SYNTHESIZED COMPOUNDS

The splitting pattern abbreviations for the NMR signals are as follows: *s*, singlet; *d*, doublet; *dd*, double doublet; *t*, triplet; *q*, quartet; *m*, multiplet.

*3-[(2-Chloroquinolin-3-yl)methylene]-5-phenyl furan-2(3*H*)-one (**3a**).* Yield: 52 %; R_f 0.72; m.p. 136 °C; Anal. Calcd. for $C_{20}H_{12}ClNO_2$: C, 71.97; H, 3.62; N, 4.20 %. Found: C, 71.93; H, 3.61; N, 4.21 %; IR (KBr, cm^{-1}): 1740 (lactone C=O), 1560 (ArC=C), 1070 (ArC–N), 864 (ArC–H); ^{1}H-NMR (400 MHz, $CDCl_3$, δ / ppm): 6.84 (1H, *s*, *β*H), 7.22–7.28 (5H, *m*, H-2,3,4,5,6, phenyl ring), 7.43 (2H, *m*, H-5,7, quinoline ring), 7.68 (1H, *t*, *J* = 7.3 Hz, H-6, quinoline ring), 7.92 (1H, *m*, H-8, quinoline ring), 8.28 (1H, *s*, H-4, quinoline ring), 8.38 (1H, *s*, olefinic H); ^{13}C-NMR (100 MHz, $CDCl_3$, δ / ppm): 98.86, 125.67, 126.89, 127.60, 127.91, 128.06, 128.10, 128.60, 128.84, 129.04, 129.18, 131.22, 131.85, 138.00, 147.44, 150.44, 158.98, 168.07; MS (*m*/*z*): 334 (M^+), 336 (M+2).

*3-[(2,6-Dichloroquinolin-3-yl)methylene]-5-phenyl furan-2(3*H*)-one (**3b**).* Yield: 56 %; R_f: 0.74; m.p. 184 °C; Anal. Calcd. for $C_{20}H_{11}Cl_2NO_2$: C, 65.24 ; H, 3.01; N, 3.80 %. Found: C, 65.12; H, 3.02; N, 3.81 %; IR (KBr, cm^{-1}): 1740 (lactone C=O), 1562 (ArC=C), 1068 (ArC–N), 822 (ArC–H); ^{1}H-NMR (400 MHz, $CDCl_3$, δ / ppm): 6.60 (1H, *s*, *β*H), 7.26–7.34 (5H, m, H-2,3,4,5,6, phenyl ring), 7.62 (1H, *d*, *J* = 1.9 Hz, H-5, quinoline ring), 7.68 (1H, *dd*, *J* = 8.6, 1.9Hz, H-7, quinoline ring), 7.80 (1H, *d*, *J* = 8.5 Hz, H-8, quinoline ring), 7.94 (1H, *s*, H-4, quinoline ring), 8.24 (1H, *s*, olefinic H); ^{13}C-NMR (100 MHz, $CDCl_3$, δ / / ppm): 99.04, 124.91, 125.18, 126.73, 127.81, 128.91, 129.11, 130.72, 131.95,

* Corresponding author. E-mail: drmmalam@gmail.com

132.13, 132.64, 133.96, 138.12, 147.67, 150.61, 158.93, 168.13; MS (*m*/*z*): 368 (M^+), 370 (M+2).

*3-[(2-Chloro-6-methoxyquinolin-3-yl)methylene]-5-phenyl furan-2(3*H*)-one (**3c**)*. Yield: 64 %; R_f: 0.82; m.p. 154 °C; Anal. Calcd. for $C_{21}H_{14}ClNO_3$: C, 69.33 ; H, 3.88; N, 3.85 %. Found: C, 69.58; H, 3.87; N, 3.86 %; IR (KBr, cm^{-1}): 1740 (lactone C=O), 1562 (ArC=C), 1066 (ArC–N), 816 (ArC–H); ^{1}H-NMR (400 MHz, $CDCl_3$, δ / ppm): 3.86 (3H, *s*, OCH_3), 6.62 (1H, *s*, *β*H), 7.20–7.26 (5H, *m*, H-2,3,4,5,6, phenyl ring), 7.54 (1H, *d*, *J* = 1.8 Hz, H-5, quinoline ring), 7.60 (1H, *dd*, *J* = 8.0, 1.8 Hz, H-7, quinoline ring), 7.72 (1H, *d*, *J* = 8.0 Hz, H-8, quinoline ring), 7.92 (1H, *s*, H-4, quinoline ring), 8.02 (1H, *s*, olefinic H); ^{13}C--NMR (100 MHz, $CDCl_3$, δ / ppm): 55.56, 98.93, 112.11, 123.73, 124.85, 125.19, 126.45, 128.87, 129.23, 129.46, 130.61, 132.17, 132.52, 138.04, 146.44, 150.31, 158.28, 167.95; MS (*m*/*z*): 364 (M^+), 366 (M+2).

*3-[(2-Chloro-6-methylquinolin-3-yl)methylene]-5-phenyl furan-2(3*H*)-one (**3d**)*. Yield: 64 %; R_f: 0.80; m.p. 176 °C; Anal. Calcd. for $C_{21}H_{14}ClNO_2$: C, 72.52 ; H, 4.06; N, 4.03 %. Found: C, 72.53; H, 4.07; N, 4.01 %; IR (KBr, cm^{-1}): 1740 (lactone C=O), 1558 (ArC=C), 1062 (ArC–N), 810 (ArC–H); ^{1}H-NMR (400 MHz, $CDCl_3$, δ / ppm): 2.15 (3H, *s*, CH_3), 6.88 (1H, *s*, *β*H), 7.18–7.25 (5H, *m*, H-2,3,4,5,6, phenyl ring), 7.49 (1H, *d*, *J* = 1.6 Hz, H-5, quinoline ring), 7.56 (1H, *dd*, *J* = 7.8, 1.6 Hz, H-7, quinoline ring), 7.84 (1H, *d*, *J* = 7.8 Hz, H-8, quinoline ring), 8.26 (1H, *s*, H-4, quinoline ring), 8.34 (1H, *s*, olefinic H). ^{13}C-NMR (100 MHz, $CDCl_3$, δ / ppm): 21.06, 100.16, 124.96, 125.10, 125.27, 128.15, 128.90, 129.29, 129.52, 131.48, 131.83, 132.39, 134.12, 136.75, 137.84, 145.95, 150.21, 158.09, 167.83; MS (*m*/*z*): 348 (M^+), 350 (M+2).

*3-[(2-Chloroquinolin-3-yl)methylene]-5-(4-methylphenyl) furan-2(3*H*)-one (**3e**)*. Yield: 34 %; R_f: 0.89; m.p. 204 °C; Anal. Calcd. for $C_{21}H_{14}ClNO_2$: C, 72.52 ; H, 4.06; N, 4.03 %. Found: C, 72.33; H, 4.05; N, 4.03 %; IR (KBr, cm^{-1}): 1742 (lactone C=O), 1562 (ArC=C), 1066 (ArC–N), 812 (ArC–H); ^{1}H-NMR (400 MHz, $CDCl_3$, δ / ppm): 2.18 (3H, *s*, CH_3), 6.84 (1H, *s*, *β*H), 7.20 (2H, *d*, *J* = = 8.3 Hz, H-3,5, phenyl ring), 7.39 (2H, *d*, *J* = 8.2 Hz, H-2,6, phenyl ring), 7.46 (2H, *m*, H-5,7, quinoline ring), 7.70 (2H, *m*, H-6,8, quinoline ring), 8.18 (1H, *s*, H-4, quinoline ring), 8.38 (1H, *s*, olefinic H). ^{13}C-NMR (100 MHz, $CDCl_3$, δ / / ppm): 21.14, 100.21, 124.13, 125.44, 127.68, 128.04, 128.83, 128.96, 128.99, 129.14, 129.48, 129.54, 131.39, 131.74, 137.77, 147.04, 150.38, 158.49, 167.84; MS (*m*/*z*): 348 (M^+), 350 (M+2).

*3-[(2,6-Dichloroquinolin-3-yl)methylene]-5-(4-methylphenyl) furan-2(3*H*)-one (**3f**)*. Yield: 32 %; R_f: 0.9; m.p. 264 °C; Anal. Calcd. for $C_{21}H_{13}Cl_2NO_2$: C, 65.99 ; H, 3.43; N, 3.66 %. Found: C, 65.88; H, 3.42; N, 3.64 %; IR (KBr, cm^{-1}): 1744 (lactone C=O), 1562 (ArC=C), 1064 (ArC–N), 822 (ArC–H); ^{1}H-NMR NMR (400 MHz, $CDCl_3$, δ / ppm): 2.22 (3H, *s*, CH_3), 6.77 (1H, *s*, *β*H), 7.25 (2H, *d*, *J* = 8.0 Hz, H-3,5, phenyl ring), 7.49 (2H, *d*, *J* = 8.0 Hz, H-2,6, phenyl ring),

7.58 (1H, *d*, *J* = 2.1 Hz, H-5, quinoline ring), 7.64 (1H, *dd*, *J* = 8.6, 2.1 Hz, H-7, quinoline ring), 7.84 (1H, *d*, *J* = 8.6 Hz, H-8, quinoline ring), 8.02 (1H, *s*, H-4, quinoline ring), 8.34 (1H, *s*, olefinic H). ^{13}C-NMR (100 MHz, $CDCl_3$, δ / ppm): 21.18, 100.31, 124.54, 125.32, 126.16, 128.13, 128.96, 129.18, 129.56, 131.34, 132.06, 132.19, 132.73, 133.00, 137.84, 146.98, 150.42, 158.61, 167.93; MS (*m*/*z*): 382 (M^+), 384 (M+2).

*3-[(2-Chloro-6-methoxyquinolin-3-yl)methylene]-5-(4-methylphenyl) furan--2(3*H*)-one (**3g**)*. Yield: 48 %; R_f: 0.82; m.p. 242 °C; Anal. Calcd. for $C_{22}H_{16}ClNO_3$: C, 69.94 ; H, 4.27; N, 3.71 %. Found: C, 70.12; H, 4.28; N, 3.72 %; IR (KBr, cm^{-1}): 1796 (lactone C=C), 1557 (ArC=C), 1060 (ArC–N), 817 (ArC–H); ^{1}H-NMR (400 MHz, $CDCl_3$, δ / ppm): 2.16 (3H, *s*, CH_3), 3.87 (3H, *s*, OCH_3), 6.85 (1H, *s*, *β*H), 7.21 (2H, *d*, *J* = 8.2 Hz, H-3,5, phenyl ring), 7.38 (2H, *d*, *J* = 8.1 Hz, H-2,6, phenyl ring), 7.32 (1H, *d*, *J* = 1.8 Hz, H-5, quinoline ring), 7.68 (1H, *s*, H-4, quinoline ring), 7.81 (1H, *d*, *J* = 8.1 Hz, H-7, quinoline ring), 8.26 (1H, *s*, olefinic H). ^{13}C-NMR (100 MHz, $CDCl_3$, δ / ppm): 21.16, 55.62, 100.24, 111.65, 123.78, 124.61, 126.08, 126.49, 128.90, 129.12, 129.64, 130.72, 132.18, 132.48, 138.11, 146.53, 150.18, 158.45, 167.74; MS (*m*/*z*): 378 (M^+), 380 (M+2).

*3-[(2-Chloro-6-methylquinolin-3-yl)methylene]-5-(4-methylphenyl) furan--2(3*H*)-one (**3h**)*. Yield: 48 %; R_f: 0.81; m.p. 190 °C; Anal. Calcd. for $C_{22}H_{16}ClNO_2$: C, 73.03; H, 4.46; N, 3.87 %. Found: C, 72.95; H, 4.45; N, 3.85 %; IR (KBr, cm^{-1}): 1795 (lactone C=O), 1558 (ArC=C), 1062 (ArC–N), 820 (ArC–H); ^{1}H-NMR (400 MHz, $CDCl_3$, δ / ppm): 2.24 and 2.26 (6H, *s*, 2×CH_3), 6.63 (1H, *s*, *β*H), 7.28 (2H, *d*, *J* = 8 Hz, H-3,5, phenyl ring), 7.42 (2H, *d*, *J* = 8.1 Hz, H-2,6, phenyl ring), 7.53 (1H, *d*, *J* = 1.6 Hz, H-5, quinoline ring), 7.59 (1H, *dd*, *J* = 8.4, 1.6 Hz, H-7, quinoline ring), 7.74 (1H, *d*, *J* = 8.4 Hz, H-8, quinoline ring), 7.88 (1H, *s*, H-4, quinoline ring), 8.27 (1H, *s*, olefinic H). ^{13}C-NMR (100 MHz, $CDCl_3$, δ / ppm): 21.11, 21.29, 100.08, 124.32, 125.33, 125.74, 128.24, 129.06, 129.14, 129.62, 131.57, 131.90, 132.58, 134.18, 136.94, 137.78, 146.11, 150.05, 158.14, 167.90; MS (*m*/*z*): 362 (M^+), 364 (M+2).

*3-[(2-Chloroquinolin-3-yl)methylene]-5-(2,4-dimethylphenyl) furan-2(3*H*)-one (**3i**)*. Yield: 36 %; R_f: 0.92; m.p. 138 °C; Anal. Calcd. for $C_{22}H_{16}ClNO_2$: C, 73.03; H, 4.46; N, 3.87 %. Found: C, 73.18; H, 4.45; N, 3.86 %; IR (KBr, cm^{-1}): 1741 (lactone C=O), 1560 (ArC=C), 1064 (ArC–N), 824 (ArC–H); ^{1}H-NMR (400 MHz, $CDCl_3$, δ / ppm): 2.18 and 2.22 (6H, *s*, 2 x CH_3), 6.61 (1H, *s*, *β*H), 7.11–7.18 (3H, *m*, H-3,5,6, phenyl ring), 7.42–7.76 (5H, *m*, H-4,5,6,7,8, quinoline ring), 8.25 (1H, *s*, olefinic H). ^{13}C-NMR (100 MHz, $CDCl_3$, δ / ppm): 21.42, 22.19, 102.20, 124.43, 126.90, 127.19, 127.89, 128.00, 128.29, 128.57, 128.67, 129.13, 131.78, 132.64, 137.01, 137.95, 141.24, 147.34, 150.44, 159.55, 167.94; MS (*m*/*z*): 362 (M^+), 364 (M+2).

*3-[(2,6-Dichloroquinolin-3-yl)methylene]-5-(2,4-dimethylphenyl) furan--2(3*H*)-one (**3j**)*. Yield: 42 %; R_f: 0.87; m.p. 184 °C; Anal. Calcd. for $C_{22}H_{15}Cl_2NO_2$: C, 66.68 ; H, 3.82; N, 3.53 %. Found: C, 66.72; H, 3.80; N, 3.54 %; IR (KBr, cm^{-1}): 1742 (lactone C=O), 1562 (ArC=C), 1062 (ArC–N), 821 (ArC–H); ^{1}H-NMR (400 MHz, $CDCl_3$, δ / ppm): 2.28 and 2.32 (6H, *s*, 2 x CH_3), 6.60 (1H, *s*, *β*H), 7.06 (1H, *d*, *J* = 1.5 Hz, H-3, phenyl ring), 7.14 (1H, *dd*, *J* = = 7.2, 1.5 Hz, H-5, phenyl ring), 7.32 (1H, *d*, *J* = 7.2 Hz, H-6, phenyl ring), 7.56 (1H, *d*, *J* = 1.7 Hz, H-5, quinoline ring), 7.62 (1H, *dd*, J = 7.4, 1.7 Hz, H-7, quinoline ring), 7.80 (1H, *d*, *J* = 7.4 Hz, H-8, quinoline ring), 8.10 (1H, *s*, H-4, quinoline ring), 8.28 (1H, *s*, olefinic H). ^{13}C-NMR (100 MHz, $CDCl_3$, δ / ppm): 21.49, 22.21, 102.34, 124.56, 126.97, 127.25, 127.98, 128.21, 128.69, 130.81, 131.54, 131.85, 132.73, 133.65, 137.18, 138.11, 141.33, 147.62, 150.73, 159.87, 168.05; MS (*m*/*z*): 396 (M^+), 398 (M+2).

*3-[(2-Chloro-6-methoxyquinolin-3-yl)methylene]-5-(2,4-dimethylphenyl) furan-2(3*H*)-one (**3k**)*. Yield: 36 %; R_f: 0.92; m.p. 200 °C; Anal. Calcd. for $C_{23}H_{18}ClNO_3$: C, 70.50; H, 4.63; N, 3.57 %. Found: C, 70.66; H, 4.62; N, 3.58 %; IR (KBr, cm^{-1}): 1756 (lactone C=O), 1612 (ArC=C), 1060 (ArC–N), 818 (ArC–H); ^{1}H-NMR (400 MHz, $CDCl_3$, δ / ppm): 2.28 and 2.34 (6H, *s*, 2×CH_3), 3.98 (3H, *s*, OCH_3), 6.62 (1H, *s*, *β*H), 6.96 (1H, *d*, *J* = 1.6 Hz, H-3, phenyl ring), 7.11 (1H, *dd*, *J* = 7.2, 1.6 Hz, H-5, phenyl ring), 7.26 (1H, *d*, *J* = 7.2 Hz, H-6, phenyl ring), 7.34 (1H, *d*, *J* = 1.8 Hz, H-5, quinoline ring), 7.52 (1H, *dd*, *J* = 7.7, 1.8 Hz, H-7, quinoline ring), 7.64 (1H, *d*, *J* = 7.6 Hz, H-8, quinoline ring), 7.72 (1H, *s*, H-4, quinoline ring), 8.26 (1H, *s*, olefinic H). ^{13}C-NMR (100 MHz, $CDCl_3$, δ / ppm): 21.45, 22.11, 103.04, 111.59, 124.16, 126.33, 127.02, 127.19, 129.56, 131.83, 131.92, 132.08, 133.14, 137.09, 137.67, 142.11, 146.43, 150.76, 158.93, 159.46, 167.71; MS (*m*/*z*): 392 (M^+), 394 (M+2).

*3-[(2-Chloro-6-methylquinolin-3-yl)methylene]-5-(2,4-dimethylphenyl) furan-2(3*H*)-one (**3l**)*. Yield: 32 %; R_f: 0.91; m.p. 174 °C; Anal. Calcd. for $C_{23}H_{18}ClNO_2$: C, 73.50; H, 4.83; N, 3.73 %. Found: C, 73.53; H, 4.82; N, 3.72 %; IR (KBr, cm^{-1}): 1755 (lactone C=O), 1610 (ArC=C), 1068 (ArC–N), 824 (ArC–H); ^{1}H-NMR: 2.20, 2.24 and 2.30 (9H, *s*, 3×CH_3), 6.60 (1H, *s*, *β*H), 7.15––7.22 (3H, *m*, H-3,5,6, phenyl ring), 7.48 (1H, *d*, *J* = 1.7 Hz, H-5, quinoline ring), 7.56 (1H, *dd*, *J* = 7.8, 1.7 Hz, H-7, quinoline ring), 7.68 (1H, *d*, *J* = 7.7 Hz, H-8, quinoline ring), 7.78 (1H, *s*, H-4, quinoline ring), 8.28 (1H, *s*, olefinic H). ^{13}C-NMR (100 MHz, $CDCl_3$, δ / ppm): 20.98, 21.31, 21.84, 101.63, 124.11, 124.38, 126.93, 128.12, 129.16, 130.92, 131.12, 131.65, 132.78, 132.94, 137.16, 137.91, 138.11, 141.69, 146.21, 150.39, 158.64, 167.84; MS (*m*/*z*): 376 (M^+), 378 (M+2).

*5-(4-Bromophenyl)3-[(2-chloroquinolin-3-yl)methylene] furan-2(3*H*)-one (**3m**)*. Yield: 30 %; R_f: 0.85; m.p. 216 °C; Anal. Calcd. for $C_{20}H_{11}BrClNO_2$: C, 58.21 ; H, 2.69; N, 3.39 %. Found: C, 58.38; H, 2.70; N, 3.38 %; IR (KBr, cm^{-1}): 1748

(lactone C=O), 1612 (ArC=C), 1062 (ArC–N), 826 (ArC–H); ^{1}H-NMR (400 MHz, $CDCl_3$, δ / ppm): 6.71 (1H, *s*, *β*H), 7.36 (2H, *d*, *J* = 8.8 Hz, H-3,5, phenyl ring), 7.48 (2H, *d*, *J* = 8.7 Hz, H-2,6, phenyl ring), 7.58–7.68 (4H, *m*, H-5,6,7,8, quinoline ring), 8.08 (1H, *s*, H-4, quinoline ring), 8.16 (1H, *s*, olefinic H). ^{13}C--NMR (100 MHz, $CDCl_3$, δ / ppm): 99.34, 125.66, 126.55, 126.65, 126.88, 127.02, 127.95, 128.04, 128.66, 129.94, 131.95, 132.36, 138.02, 147.51, 150.37, 158.04, 167.66; MS (*m*/*z*): 413 (M^+), 415 (M+2).

*5-(4-Bromophenyl)-3-[(2,6-dichloroquinolin-3-yl)methylene] furan-2(3*H*)-one (**3n**)*. Yield: 32 %; R_f: 0.86; m.p. 156 °C; Anal. Calcd. for $C_{20}H_{10}BrCl_2NO_2$: C, 53.73; H, 2.25; N, 3.13 %. Found: C, 53.62; H, 2.23; N, 3.12 %; IR (KBr, cm^{-1}): 1750 (lactone C=O), 1580 (ArC=C), 1060 (ArC–N), 818 (ArC–H); ^{1}H-NMR (400 MHz, $CDCl_3$, δ / ppm): 6.60 (1H, *s*, *β*H), 7.35–7.66 (7H, *m*, H-5,7,8 of quinoline ring merged with H-2,3,5,6 of phenyl ring), 8.04 (1H, *s*, H-4, quinoline ring), 8.21 (1H, *s*, olefinic H). ^{13}C-NMR (100 MHz, $CDCl_3$, δ / ppm): 100.12, 125.69, 126.43, 126.63, 127.09, 128.14, 128.26, 128.48, 130.06, 131.88, 132.29, 134.39, 138.14, 146.53, 150.84, 158.13, 167.74; MS (*m*/*z*): 447 (M^+), 449 (M+2).

*5-(4-Bromophenyl)-3-[(2-chloro-6-methoxyquinolin-3-yl)methylene] furan--2(3*H*)-one (**3o**)*. Yield: 38 %; R_f: 0.89; m.p. 264 °C; Anal. Calcd. for $C_{21}H_{13}BrClNO_3$: C, 56.98; H, 2.96; N, 3.16 %. Found: C, 56.83; H, 2.97; N, 3.17 %; IR (KBr, cm^{-1}): 1748 (lactone C=O), 1612 (ArC=C), 1064 (ArC–N), 812 (ArC–H); ^{1}H-NMR (400 MHz, $CDCl_3$, δ / ppm): 3.78 (1H, *s*, OCH_3), 6.64 (1H, *s*, *β*H), 7.34-7.58 (7H, *m*, H-5,7,8 of quinoline ring merged with H-2,3,5,6 of phenyl ring), 7.94 (1H, *s*, H-4, quinoline ring), 8.08 (1H, *s*, olefinic H). ^{13}C--NMR (100 MHz, $CDCl_3$, δ / ppm): 55.68, 99.14, 111.36, 124.52, 124.89, 125.38, 126.48, 126.51, 127.14, 128.19, 131.75, 133.43, 136.31, 144.46, 149.35, 158.06, 160.08, 167.68; MS (*m*/*z*): 443 (M^+), 445 (M+2).

*5-(4-Bromophenyl)-3-[(2-chloro-6-methylquinolin-3-yl)methylene] furan--2(3*H*)-one (**3p**)*. Yield: 42 %; R_f: 0.83; m.p. 174 °C; Anal. Calcd. for $C_{21}H_{13}BrClNO_2$: C, 59.11 ; H, 3.07; N, 3.28 %. Found: C, 58.96; H, 3.08; N, 3.29 %; IR (KBr, cm^{-1}): 1748 (lactone C=O), 1602 (ArC=C), 1066 (ArC–N), 810 (ArC–H); ^{1}H-NMR (400 MHz, $CDCl_3$, δ / ppm): 2.20 (1H, *s*, CH_3), 6.60 (1H, *s*, *β*H), 7.34 (2H, *d*, *J* = 8.6 Hz, H-3,5, phenyl ring), 7.44 (2H, *d*, *J* = 8.6 Hz, H-2,6, phenyl ring), 7.50 (1H, *d*, *J* = 1.9 Hz, H-5, quinoline ring), 7.60 (1H, *dd*, *J* = 8.3, 1.9 Hz, H-7, quinoline ring), 7.78 (1H, *d*, *J* = 8.4 Hz, H-8, quinoline ring), 7.96 (1H, *s*, H-4, quinoline ring), 8.21 (1H, *s*, olefinic H). ^{13}C-NMR (100 MHz, $CDCl_3$, δ / ppm): 20.93, 99.44, 125.18, 125.21, 126.32, 126.72, 127.19, 127.98, 128.27, 131.76, 131.84, 131.93, 136.53, 138.19, 146.12, 148.49, 158.19, 167.70; MS (*m*/*z*): 427 (M^+), 429 (M+2).

Journal of the Serbian Chemical Society
JSCS-info@shd.org.rs • www.shd.org.rs/JSCS
J. Serb. Chem. Soc. *76* (12) 1627–1637 (2011)
JSCS–4235
UDC 634.4:665.52/.54:54.062+54.02
Original scientific paper

Chemical composition of the essential oils of *Citrus sinensis* cv. *Valencia* and a quantitative structure–retention relationship study for the prediction of retention indices by multiple linear regression

PARVIZ ABEROOMAND AZAR[1], MEHDI NEKOEI[1]*, KAMBIZ LARIJANI[1] and SAKINEH BAHRAMINASAB[2]

[1]*Department of Chemistry, Science and Research Branch, Islamic Azad University, Tehran and* [2]*Department of Chemistry, Shahrood branch, Islamic Azad University, Shahrood, Iran*

(Received 18 December 2010, revised 27 February 2011)

Abstract: The chemical composition of the volatile fraction obtained by head-space solid phase microextraction (HS–SPME), single drop microextraction (SDME) and the essential oil obtained by cold-press from the peels of *C. sinensis* cv. *Valencia* were analyzed employing gas chromatography–flame ionization detector (GC–FID) and gas chromatography–mass spectrometry (GC––MS). The main components were limonene (61.34, 68.27 and 90.50 %), myrcene (17.55, 12.35 and 2.50 %), sabinene (6.50, 7.62 and 0.5 %) and α-pinene (0, 6.65 and 1.4 %) respectively obtained by HS–SPME, SDME and cold--press. Then a quantitative structure–retention relationship (QSRR) study for the prediction of retention indices (*RI*) of the compounds was developed by application of structural descriptors and the multiple linear regression (MLR) method. Principal components analysis was used to select the training set. A simple model with low standard errors and high correlation coefficients was obtained. The results illustrated that linear techniques such as MLR combined with a successful variable selection procedure are capable of generating an efficient QSRR model for prediction of the retention indices of different compounds. This model, with high statistical significance (R^2_{train} = 0.983, R^2_{test} = = 0.970, Q^2_{LOO} = 0.962, Q^2_{LGO} = 0.936, *REP*(%) = 3.00), could be used adequately for the prediction and description of the retention indices of the volatile compounds.

Keywords: *Citrus sinensis* cv. *Valencia*; volatile constituents; HS–SPME; SDME; QSRR.

INTRODUCTION

The genus *Citrus* (Rutaceae) is represented in Iran by the species *C. sinensis*, *C. medica*, *C. limon*, *C. nobelis*, *C. aurantifolia* and *C. aurantium*. Citrus fruits

* Corresponding author. E-mail: m_nekoei1356@yahoo.com
doi: 10.2298/JSC101218141A

are the most common subtropical crops in the world. There is a great amount of variation among citrus species and cultivars as a result of frequent bud mutation, interspecific and intergeneric hybridization, apomixis and a long history of cultivation. In Iran, there are many citrus variants the phylogeny of which remains unknown.[1] The essential oils of *Citrus* are placed within the glands in the outer layer of the fruit skin. This oil is composed of many constituents, including monoterpenes, sesquiterpenes, alcohols, esters and aldehydes. The most valuable oils are those of orange and lemon. Cold-press peel oils are generally in use in many food, confectionary, drug, cosmetic and flavoring products.[2] Several studies were performed on the composition of the essential oils from leaves and peel of *C. sinensis* and its hybrids and on their biological activities, such as antifungal, antioxidant and antiaflatoxigenic.[3–10] Although *C. sinensis* (orange) is one of the most important horticulture products of Iran, a literature survey revealed that there are no reports of an adequate comparative study of the volatile constituents of *C. sinensis* from Iran in which a variety of extraction techniques were employed. Conventional sampling methods for the extraction of *Citrus* essential oil in previous studies were mainly cold-press and hydro-distillation (HD). The cold--press method is mainly used for *Citrus* fruit peel. However, both volatile and non volatile compounds are simultaneously extracted by cold-press and their separation would be inevitable. HD usually requires large amount of samples, long time (several hours), and high energy. Moreover, many unstable aroma volatiles may be thermally decomposed and degraded during thermal extraction or distillation.[11]

Recently, many kinds of extraction techniques, such as single-drop micro extraction (SDME)[12–14] and solid-phase microextraction (SPME),[15–18] have been developed. The SDME technique involves extraction of analytes from a mixture into a microdrop of an organic solvent suspended from to the tip of a microsyringe. After extraction, the microdrop is retracted back into the microsyringe and injected into a GC–MS instrument for analysis. The SPME technique is performed using a fused silica fiber that is coated with different stationary phases and is characterized by its high sensitivity to volatile natural compounds. These methods are rapid, simple and inexpensive sample preparation techniques for the extraction and pre-concentration of volatile compounds. Generally, the use of SDME and SPME to extract analytes from a matrix is mainly performed by direct immersion (DI) and headspace (HS). Especially, HS–SPME is considered as a good choice for sample preparation in fragrance and aroma analyses.[19]

The Kovatz retention indices is the key tool for identification of diverse natural compounds present in a volatile oil separated by a variety of isolation techniques. The search for quantitative relationships between molecular structure and retention indices is a basic task in chemistry. Quantitative structure–retention relationship (QSRR) analysis is now a well-established and highly respected te-

chnique to correlate diverse simple and complex physico-chemical properties of a compound with its molecular structure, through a variety of descriptors. The basic strategy of QSRR analysis is to find optimum quantitative relationships, which can then be used for the prediction of the properties from molecular structures. Once a reliable relation has been obtained, it is possible to use it to predict that same property for other structures not yet measured or even not yet prepared.

QSRR for retention indices have been reported for different types of organic compounds.[20–28] The application of these techniques usually requires variable selection for building well-fitted models. In this work, the elimination selection––stepwise regression (ES–SWR) variable selection method was employed. The proposed methodology was validated using several strategies: cross-validation, external validation using division of the entire data set into training and test sets and *Y*-randomization. The aim of this work was the investigation of the chemical composition of *C. sinensis* cv. *Valencia* volatile compounds and also the construction an accurate quantitative relationship between the molecular structure and the retention indices by the stepwise-multiple linear regression (MLR) method.

EXPERIMENTAL

Plant material

The fruits of *C. sinensis* cv. *Valencia* were collected from Ramsar, Province of Mazandaran, Iran, in January 2008. The material plant was identified and a voucher specimen was deposited at the Herbarium of the *Citrus* Research Institute of Ramsar, Mazandaran, Iran.

Isolation of the essential oil

The essential oil of *C. sinensis* cv. *Valencia* was extracted by cold-press. The volatile constituents were extracted by HS–SPME and HS–SDME. Accordingly, 1.5 g of the peel of *C. sinensis* was placed in a 20 ml vial with screw caps and PTFE/silicone septa. The vial was immersed in a controlled water bath at 70 °C for 30 min. A 100 μm polydimethylsiloxane (PDMS) fiber (Supelco, USA) was used to extract the compounds which evaporated to headspace of the vial (15 min). The analytes were thermally desorbed for 3 min at 250 °C in a splitless GC injector. The equilibration temperature and time were 50 °C and 30 min, respectively. SDME extraction was performed using 2 μl hexadecane (Merck, Germany) as the extraction solvent. The temperature and time conditions were similar to the SPME conditions.

Analysis of the volatile compounds

Gas chromatography analysis. Analytical GC was performed on HP-6890 GC system (Hewlett-Packard, USA) equipped with a flame ionization detector (FID) and a HP-5 capillary fused silica column (30 m×0.25 mm ID, film thickness: 0.25 μm). The oven temperature was held at 60 °C for 3 min then programmed at rate of 6 °C min^{-1} to 250 °C and held isothermally for 3 min. The carrier gas was nitrogen at a flow rate of 1 ml min^{-1}; the split/splitless injector temperature was 250 °C.

Gas chromatography–mass spectrometry analysis. The GC–MS analyses were performed on a HP-6890 gas chromatograph (Hewlett-Packard, USA) coupled to an HP-5973 quadrupole mass spectrometer (Hewlett-Packard, USA). The analytes were separated on a HP-5MS capillary column (30 m×0.25 mm with a phase thickness of 0.25 μm). The split/splitless injector temperature was set at 250 °C and the temperature program was 60 °C for 3 min, 6 °C min^{-1}

ramp rate to 250 °C and held constant for 3 min. The carrier gas was helium (99.999 %) at a 1 ml min^{-1} flow rate. In the SPME analysis, splitless injection (3 min) was used at 250 °C. The mass spectrometer was operated in the electron-impact mode (EI) at 70 eV.

Qualitative and quantitative analysis of the compounds

The compounds in each sample were identified by comparison of their mass spectral pattern and their linear retention indices based on a homologous series of even normal alkanes (C_8–C_{24}) with those of authentic references[29] and the Wiley 257 mass spectra database. The percentage of each compound was calculated from peak area obtained by FID.

QSRR study

Calculation of molecular descriptors. Molecular descriptors are defined as numerical characteristics associated with chemical structures. A molecular descriptor is the final result of a logic and mathematical procedure which transforms chemical information encoded within a symbolic representation of a molecule into a useful number, which is applied to correlate physical properties. The Dragon software (Milano Chemometrics and QSAR Research Group, Milan, Italy) was used to calculate the descriptors in this study and a total of 1481 molecular descriptors were calculated for each molecule. Since the values of many descriptors are related to the bond lengths and bond angles *etc*., the chemical structure of every molecule must be optimized before calculation of its molecular descriptors. For this reason, the chemical structures of the 25 studied molecules were drawn with Hyperchem software (version 7.0 Hypercube, Alberta, Canada) and saved with the HIN extension. To optimize the geometry of these molecules, the AM1 geometrical optimization was applied. After optimization of the chemical structures of all compounds, the molecular descriptors were calculated using Dragon. A wide variety of descriptors have been reported in the literature, having been used in QSRR analyses.[30-35]

Stepwise multiple linear regression. As described in the introduction section, the ES–SWR algorithm[30] was used to select the most appropriate descriptors. ES–SWR is a popular stepwise technique that combines forward selection (FS–SWR) and backward elimination (BE–SWR). It is essentially a forward selection approach, but at each step it considers the possibility of deleting a variable as in the backward elimination approach, provided that the number of model variables is greater than two.

Model validation. The stability and robustness of the proposed MLR model was illustrated using the following evaluation techniques: leave-one-out (LOO) and leave-group-out (LGO) cross-validation procedures, validation through an external test set and *Y*-randomization.

Cross-validation is a popular technique used to explore the reliability of statistical models. Based on this technique, a number of modified data sets are created by deleting in each case one or a small group (leave-group-out) of objects. For each data set, an input–output model is developed, based on the utilized modeling technique. The model is evaluated by measuring its accuracy in the prediction of the responses of the remaining data stands that were not utilized in the development of the model.[36]

The *Y*-randomization technique ensures the robustness of a QSRR model. The dependent variable vector (*RI*) is randomly shuffled and a new QSRR model is developed using the original independent variable matrix. The new QSRR models (after several repetitions) are expected to have low R^2 and Q^2 values. If this is not the case, then an acceptable QSRR model cannot be obtained for the specific modeling method and data.

RESULTS AND DISCUSSION

Chemical composition of the essential oil

The volatile components of fruit peel of *C. sinensis* cv. *Valencia* that were isolated by SPME, SDME and cold- press are listed in Table I. Thirteen compounds (representing 99.77 %), ten compounds (representing 98.46 %) and fourteen compounds (representing 97.9 %) were experimentally identified, respectively. The oils were rich in monoterpenes: limonene (61.34, 68.27 and 90.5 %), as the major component, followed by myrcene (17.55, 12.35 and 2.50 %); sabinene (6.50, 7.62 and 0.5 %); α-pinene (0.0, 6.65 and 1.4 %) in the oils obtained by the SPME, SDME and cold-press methods, respectively.

TABLE I. Chemical composition of the essential oil of *C. sinensis* cv. *Valencia* isolated by the SPME, SDME and cold-press methods and the corresponding observed and predicted *RI* values by SW–MLR for the training and test set

Compound		SPME, %	SDME, %	Cold-press, %	*RI* (Exp.)	*RI*[a] (Pred.)	*E*[b] / %
1a	Octane	8.37	0.1	–	800	816.12	2.01
2a	4-Methylthiazole	–	0.14	–	819	856.29	4.55
3b	*n*-Nonane	–	–	0.2	900	953.18	5.90
4a	α-Pinene	–	6.65	1.4	939	932.38	–0.70
5a	Sabinene	6.50	7.62	0.5	975	1010.11	3.60
6b	Myrcene	17.55	12.35	2.5	991	1047.60	5.71
7a	*n*-Octanal	–	0.19	0.8	999	1001.93	0.29
8a	α-Phellandrene	–	0.33	–	1003	1033.04	2.99
9a	*iso*-Sylvesteren	1.14	–	–	1009	1016.00	0.69
10b	Limonene	61.34	68.27	90.5	1029	1040.46	1.01
11a	*E*-β-Ocimene	–	0.5	0.1	1050	1025.95	–2.28
12a	γ-Terpinene	0.5	–	0.2	1060	1053.73	–0.59
13b	Terpinolene	–	–	–	1089	1046.97	–3.85
14a	Linalool	1.84	–	0.8	1097	1089.45	–0.68
15a	α-Thujene	–	2.31	–	1114	1067.35	–4.18
16b	*trans*-Limonene oxide	0.18	–	–	1142	1160.10	1.58
17a	Citronellal	0.29	–	0.2	1153	1146.40	–0.57
18a	Decanal	1.40	–	–	1202	1158.00	–3.65
19b	β-Elemene	0.08	–	0.1	1391	1382.56	–0.60
20a	Tetradecane	–	–	0.2	1400	1360.02	–2.85
21a	β-Caryophyllene	0.1	–	–	1419	1419.46	0.03
22a	*trans*-Uurola-3,5-diene	–	–	–	1454	1461.25	0.49
23b	Valencene	0.48	–	–	1496	1493.75	–0.15
24a	Pentadecane	–	–	0.2	1500	1559.54	3.96
25a	Hexadecane	–	–	0.2	1600	1600.16	0.00
Total		99.77	98.46	97.9			

[a]Predicted by SW–MLR method; [b]relative error

Comparison of the chemical profile with similar reports

An investigation in China revealed that limonene was observed as the dominant constituent (77.49 %) in the peel oil of sweet orange, followed by myrcene (6.27 %), α-farnesene (3.64 %) and γ-terpinene (3.34 %).[4] The main compounds in *C. sinensis* from Uganda and Rwanda were limonene (87.9 and 92.5 %), myrcene (2.4 and 2.0 %), α-pinene (0.5 and 2.4 %) and linalool (1.2 and 0.9 %).[5] Limonene (90.16 and 77.34 %) was the main compound in fresh and dried pericarps of *C. sinensis* in China. Monoterpene hydrocarbons were the most abundant fraction in the oils of three Kenyan *C. sinensis* varieties, *i.e.*, Salustiana (96.9 %), Valencia (94.5 %) and Washington navel (92.7 %) oils. In each oil, limonene, α-pinene, sabinene and α-terpinene were the major compounds.[9] The oil of Italian *Citrus sinensis* (L.) Osbeck cv. *Maltese* was characterized by limonene (92.6 %) as the major constituent.[10]

QSRR results

Principal components analysis (PCA) was performed with the calculated structure descriptors for the whole data set to detect the homogeneities in the data set and to show the spatial location of the samples to assist the separation of the data into training and test sets. The PCA results showed that two principal components (PC1 and PC2) described 69.67 % of the overall variables, as follows: PC1 47.40 % and PC2 22.27 %. As almost all the variables can be accounted for by the first two PCs, their score plot is a reliable representation of the spatial distribution of the points for the data set. The plot of PC1 against PC2 (Fig. 1) displays the distribution of the compounds over the space of the first two principal components.

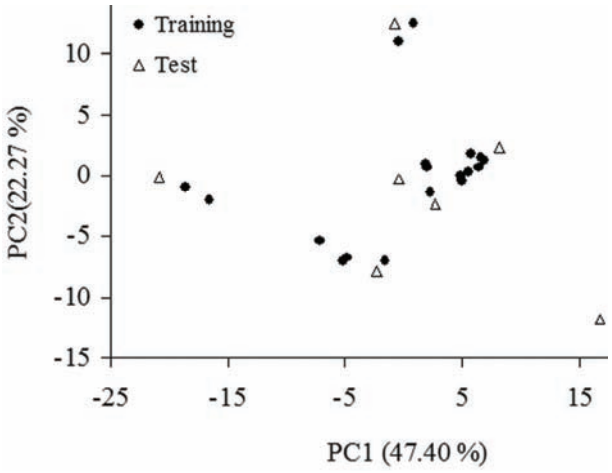

Fig. 1. Principal components analysis of the training and test sets.

According to the results of PCA, all the data were divided into a training set of 18 compounds to develop the models and a test set of 7 compounds to evaluate the models based on two rules:

1. the range of the *RI* values of both the training set and the test set should be covered from the lowest to the highest;

2. the points corresponding to the training set in the PCA plot should not be outside the main clusters. The two sets are listed in Table I.

After analysis of the division of the data set into the training and the test sets, MLR analysis was performed to derive the best QSRR model. The MLR technique was performed on the molecules of the training set given in Table I. After regression analysis, a few suitable models were obtained among which the best model was selected and presented in Eq. (1). A small number of molecular descriptors were used to establish the QSRR model. Additional validation was performed on the external data set (test set) consisting of 7 essential oil compounds. MLR analysis provided a useful equation that could be used to predict the *RI* of an essential oil compound based on these parameters. The result of this study was the development of a new linear QSRR model containing 4 variables. The best equation obtained for the *RI* of the essential oil compounds is:

$$RI = 758.10 + 5.23(Mor01m) - 155.64(Gu) - 895.46(Mor30v) - 246.37(Mor29u) \quad (1)$$

$$N_{training} = 18;\ R^2_{training} = 0.983;\ RMSE_{training}=27.801;\ \%REP = 3.00;$$
$$Q^2_{LOO} = 0.962;\ Q^2_{LGO} = 0.936,\ R^2_{test} = 0.970;\ RMSE_{test} = 34.505$$

In Eq. (1), N is the number of compounds in the training set, R^2 is the squared correlation coefficient, Q^2_{LOO}; Q^2_{LGO} are the squared cross-validation coefficients for LOO and LGO, respectively, *REP* is the relative error of prediction and *RMSE* is the root mean square error of prediction.

From Eq. (1), it can be concluded that the three of most significant descriptors according to the ES–SWR algorithm are 3D-MoRSE descriptors. Furthermore, the other one belongs to the WHIM descriptors. A brief explanation of the descriptors that were selected is given below.

Three-dimensional MoRSE descriptors are derived from infrared spectra simulation using a generalized scattering function.[30] The three descriptors, appearing in the model are *Mor01m*, *Mor30v* and *Mor29u*. *Mor01m* was proposed as signal 01 / weighted by atomic mass, which relates to the mass of the molecule. *Mor30v* was proposed as signal 30 / weighted by atomic van der Waals volumes, which relates to atomic van der Waals volumes. *Mor29u* was proposed as signal 29 / unweighted.

Mor01m displays a positive sign, which indicates that the atomic mass of a molecule is directly related to its retention index. *Mor30v* and *Mor29u* display a

negative sign which indicates that the volume of a molecule is inversely related to the retention index.

Gu (*G* total symmetry index / unweighted) is the fourth descriptor appearing in the model. It is one of the WHIM descriptors, which are based on the statistical indices calculated on the projections of atoms along the principal axes. The algorithm consists of performing a principal components analysis on the centered Cartesian coordinates of a molecule using a weighted covariance matrix obtained from different weighing schemes for the atoms. Directional WHIM symmetry descriptors are related to the number of central symmetric atoms (along the m^{th} component), the number of asymmetric atoms and the total number of atoms in the molecule. *Gu* displays a negative sign, which indicates that the retention index is inversely related to the *Gu* descriptor.

From the above discussion, it was concluded that the atomic masses and atomic van der Waals volumes are the main independent factors contributing to the retention index of the components of the studied essential oils.

As can be seen from the correlation matrix (Table II), there was no significant correlation between the selected descriptors.

TABLE II. Correlation matrix for the seven selected descriptors

	Mor01m	*Gu*	*Mor30v*	*Mor29u*
Mor01m	1			
Gu	0.285	1		
Mor30v	0.208	–0.411	1	
Mor29u	–0.694	–0.026	–0.625	1

Equation (1) was used to predict the *RI* for the test set. The data set and the corresponding experimental and predicted *RI* values of all the molecules studied in this work are summarized in Table I. A plot of the values predicted by the SW–MLR against the experimental values of the retention indices of the training and test sets is shown in Fig. 2.

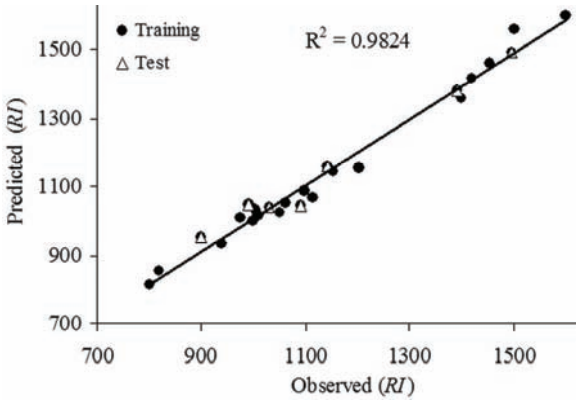

Fig. 2. The *RI* values predicted by MLR modeling *vs.* the experimental *RI* values.

The residuals (observed *RI* – predicted *RI*) *vs*. the observed *RI* value, obtained by the SW–MLR modeling, are shown in Fig. 3. The distribution of the residuals on both sides of the zero line indicates that there is no systematic error in the SW–MLR model.

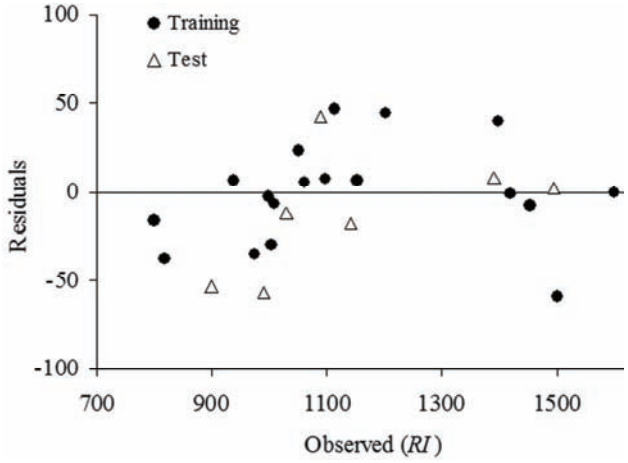

Fig. 3. Plot of the residuals against the experimental values of the retention indices.

The results illustrated once more that the linear MLR technique combined with a successful variable selection procedure is adequate to generate an efficient QSRR model for predicting the *RI* values of essential oil components.

For a more exhaustive testing of the predictive power of the model, validation of the model was also performed using the LOO and the LGO cross-validation techniques on the training set of compounds. For the LOO cross-validation, a data point is removed from the set, and the model is recalculated. The predicted *RI* for that point is then compared with its actual value. This is repeated until each data point has been omitted once. For LGO, 20 % of the data points are removed from the dataset and the model was refitted; the predicted values for those points were then compared with the experimental values. Again, this is repeated until each data point has been omitted once. The results produced by the LOO (Q^2_{LOO} = 0.962) and the LGO (Q^2_{LGO} = 0.936) cross-validation tests illustrated the quality of the obtained model.

The model was further validated by applying *Y*-randomization. Several random shuffles of the *Y* vector (*RI*) were performed and the low R^2 and Q^2 values that were obtained showed that the good results in the original model use were not due to a chance correlation or structural dependency of the training set. The results of the *Y*-randomization test are presented in Table III.

The proposed method, due to the high predictive ability and simplicity could be a useful aid to the costly and time consuming experiments for determining the *RI* values of the components of essential oils.

TABLE III. R^2 and Q^2 values after several *Y*-randomization tests

Iteration	R^2	Q^2
1	0.082	0.230
2	0.104	0.075
3	0.332	0.061
4	0.072	0.123
5	0.073	0.135
6	0.305	0.044
7	0.182	0.001
8	0.142	0.023
9	0.168	0.009
10	0.241	0.026

CONCLUSIONS

This paper deals with the characterization of the volatile oils obtained from the peels of *C. sinensis* cv. *Valencia* by the HS–SPME, SDME and cold-press methods. In the all identified oils, monoterpenes dominated over non-terpenes and sesquiterpenes. The QSRR method using stepwise-MLR analysis employed to develop a model for predicting the retention indices of the components of essential oils. The developed QSRR model with simply calculated molecular descriptors could be employed to estimate the retention index for new compounds, even in the absence of standard candidates.

ИЗВОД

ХЕМИЈСКИ САСТАВ ЕТАРСКОГ УЉА *Citrus sinensis* cv. *Valencia* И QSRR АНАЛИЗА У ПРОЦЕНИ РЕТЕНЦИОНИХ ИНДЕКСА ПРИМЕНОМ МЕТОДЕ ВИШЕСТРУКЕ ЛИНЕАРНЕ РЕГРЕСИЈЕ

PARVIZ ABEROOMAND AZAR, MEHDI NEKOEI , KAMBIZ LARIJANI и AZAM VAFAEI

Department of Chemistry, Faculty of Basic Sciences, Science and Research Branch, Islamic Azad University, Tehran, Iran

Хемијски састав испарљивих фракција добијених микроекстракцијом у чврстој фази (HS–SPME), микроекстракцијом из капи (SDME), као и састав етарског уља добијеног хладним цеђењем из *C. sinensis* cv. *Valencia* је испитан методама GC–FID и GC–MS. Главни састојци су били лимонен (61,34, 68,27 и 90,50 %), мирцен (17,55, 12,35 и 2,50 %), сабинен (6,50, 7,62 и 0,50 %) и α-пинен (0,00, 6,65 и 1,40 %). QSRR испитивање за процену ретенционих индекса једињења (*RI*) је развијено користећи методу вишеструке линеарне регресије (MLR). Анализа главних састојака је коришћена у избору модела са ниском стандардном грешком и високим коефицијентом корелације. Резултати су показали да линеарне технике, као што је MLR, у комбинацији са успешним избором променљиве могу успоставити ефикасан QSRR модел за предвиђање *RI* различитих једињења. Овај модел се, са високом статистичком значајношћу (R^2_{train} = 0,983, R^2_{test} = 0,970, Q^2_{LOO} = 0,962, Q^2_{LGO} = 0,936, *REP*(%) = = 3,00), може користити за успешно предвиђање и описивање ретенционих индекса испарљивих супстанци.

(Примљено 18. децембра 2010, ревидирано 27. фебруара 2011)

REFERENCES

1. V. Mozaffarian, *A dictionary of Iranian plants names*, Farhang Mo'aser Publishers, Tehran, Iran, 1998
2. S. Nagy, P. Shaw, M. Veldhuis, *Citrus Sci. Technol.* **2** (1977) 290
3. P. Singh, R. Shukla, B. Prakash, A. Kumar, S. Singh, P. K. Mishra, N. K. Dubey, *Food Chem. Toxicol.* **48** (2010) 1734
4. N. G. To, Y. J. Liu, M. L. Zhang, *Int. J. Food Sci. Technol.* **44** (2009) 1281
5. S. M. Njoroge, N. T. Phi, M. Sawamura, *J. Essential Oil Bearing Plants* **12** (2009) 26
6. M. Viuda-Martos, Y. Ruiz-Navajas, J. Fernández-López, J. Pérez-Álvarez, *Food Control* **19** (2008) 1130
7. C. P. Araújo-Junior, C. A. G. Dacamara, N. C. Ribeiro, C. A. Gomes, M. M. de Moraes, P. S. Botelho, *Nat. Prod. Commun.* **5** (2010) 471
8. N. C. Ribeiro, C. A. G. Dacamara, F. S. Born, H. A. A. Siqueira, *Nat. Prod. Commun.* **5** (2010) 1819
9. S. M. Njoroge, H. Koaze, P.N. Karanja, M. Sawamura, *Flavour Fragr. J.* **20** (2005) 80
10. A. Trozzi, A. Verzera, G. Lamonica, *J. Essent. Oil Res.* **11** (1999) 482
11. A. C. Kimbaris, N. G. Siatis, D. J. Daferera, *Ultrason. Sonochem.* **13** (2006) 54
12. C. H. Deng, Y. Mao, F. L. Hu, X. M. Zhang, *J. Chromatogr., A* **1152** (2007) 193
13. L. Vidal, A. Canals, N. Kalogerakis, E. Psillakis, *J. Chromatogr., A* **1089** (2005) 25
14. D. A. Lambropoulou, E. Psillakis, T. A. Albanis, N. Kalogerakis, *Anal. Chim. Acta* **516** (2004) 205
15. C. H. Deng, X. Q. Xu, N. Yao, N. Li, X. M. Zhang, *Anal. Chim. Acta* **556** (2006) 289
16. Q. Ye, *J. Chromatogr., A* **1213** (2008) 239
17. G. Ouyang, J. Pawliszyn, *Anal. Chim. Acta* **627** (2008) 184
18. N. Li, C. H. Deng, Y. Li, H. Ye, X. M. Zhang, *J. Chromatogr., A* **1133** (2006) 29
19. F. Augusto, A. L. Lopes, C. A. Zini, *Trends Anal. Chem.* **22** (2003) 160
20. C. Ji, Y. Li, L. Su, X. Zhang, X. Chen, *J. Sep. Sci.* **32** (2009) 3967
21. M. H. Fatemi, E. Baher, M. Ghorbanzadeh, *J. Sep. Sci.* **32** (2009) 4133
22. L. Komsta, *Anal. Chim. Acta* **593** (2007) 224
23. B. D. Junkes, R. D. Amboni, R. A. Yunes, V. E. F. Heinzen, *Anal. Chim. Acta* **477** (2003) 29
24. M. Jalali-Heravi, M. H. Fatemi, *J. Chromatogr., A* **915** (2001) 177
25. Z. Garakani-Nejad, M. Karlovits, W. Demuth, T. Stimpfl, W. Vycudilik, M. Jalali-Heravi, K. Varmuza, *J. Chromatogr., A* **1028** (2004) 287
26. J. Acevedo-Martinez, J. C. Escalona-Arranz, A. Villar-Rojas, F. Tellez-Palmero, R. Perez-Roses, L. Gonzalez, R. Carrasco-Velar, *J. Chromatogr., A* **1102** (2006) 238
27. P. Tulasamma, K. S. Reddy, *J. Mol. Graphics Modell.* **25** (2006) 507
28. K. Heberger, T. Kowalska, *Chemom. Intell. Lab. Syst.* **47** (1999) 205
29. R. P. Adams, *Identification of essential oil components by gas chromatography / quadrupole mass spectroscopy*, Allured Publishing Corp., Carol Stream, IL, USA, 2004
30. R. Todeschini, V. Consonni, *Handbook of molecular descriptors*. Wiley-VCH, Weinheim, Germany, 2000
31. L. B. Kier, L. H. Hall, *Molecular Connectivity in Structure–Activity Analysis*, RSP-Wiley, Chichester, UK, 1986
32. E. V. Konstantinova, *J. Chem. Inf. Comp. Sci.* **36** (1997) 54
33. G. Rucker, C. Rucker, *J. Chem. Inf. Comp. Sci.* **33** (1993) 683
34. J. Galvez, R. Garcia, M. T. Salabert, *J. Chem. Inf. Comp. Sci.* **34** (1994) 520
35. P. Broto, G. Moreau, C. Vandicke, *J. Med. Chem.* **19** (1984) 66
36. B. Efron, *J. Am. Stat. Assoc.* **78** (1983) 316.

Journal of the Serbian Chemical Society
JSCS-info@shd.org.rs • www.shd.org.rs/JSCS
J. Serb. Chem. Soc. 76 (12) 1639–1648 (2011)
JSCS–4236
UDC 546.562+542.9+547.571+547.551:537.621
Original scientific paper

Spectral, thermal and magnetic properties of Cu(II) and Ni(II) complexes with Schiff base ligands

BEATA CRISTÓVÃO*

Department of General and Coordination Chemistry, Maria Curie-Sklodowska University, Maria Curie-Sklodowska sq. 2, PL. 20-031 Lublin, Poland

(Received 12 November 2010, revised 7 March 2011)

Abstract: Mononuclear copper(II) and nickel(II) complexes of the formulae [Cu(L^1)] (**1**), [Ni(L^1)] (**2**), [Cu(L^2)] (**3**) and [Cu(L^3)H_2O] (**4**) (where L^1 = *N*,*N*'--ethylenebis(4,6-dimethoxysalicylideanaminato), L^2 = *N*,*N*'-ethylenebis(5-bromosalicylidenaminato) and L^3 = *N*,*N*'-ethylenebis(5-bromo-3-methoxysalicylidenaminato)) were synthesized as microcrystalline powders and characterized by IR spectroscopy, thermal analysis and magnetic measurements. The magnetic susceptibility of the Cu(II) complexes changed with temperature according to the Curie–Weiss law. The complexes **1**, **3** and **4** exhibit magnetic moments of 2.29, 2.20 and 1.88 μ_B, respectively, at 303 K. These values practically do not change with lowering the temperature to 77 K. The nickel(II) complex **2** is diamagnetic.

Keywords: copper(II) complexes; Schiff base; magnetic properties.

INTRODUCTION

The interest in the synthesis and characterization of transition metal complexes containing Schiff bases lies in their biological and catalytic activity in many reactions. The transition metal complexes having oxygen and nitrogen donor Schiff bases possess unusual configuration, structural lability and are sensitive to the molecular environment. The environment around the metal center, such as coordination geometry, number of coordinated ligands and their donor group, is a key factor for a metalloprotein to perform specific physiological functions.[1–10] Schiff bases offer opportunities for inducing substrate chirality, tuning the metal centered electronic factor, enhancing solubility and either performing homogenous or heterogeneous catalyses. Salicylaldimine metal complexes constitute a family of one of the most important systems due to the number of applications in catalysis and biomimetic chemistry. These compounds can be used as

* E-mail: beata.cristovao@poczta.umcs.lublin.pl
doi: 10.2298/JSC101112140C

components for the assembly of supramolecular architectures, displaying interesting structures and properties.[11–14]

N,*N*'-Ethylenebis(4,6-dimethoxysalicylideneiminato)copper(II) (**1**), *N*,*N*'--ethylenebis(4,6-dimethoxysalicylideneaminato)nickel(II) (**2**), *N*,*N*'-ethylenebis-(5-bromosalicylideneaminato)copper(II) (**3**) and aqua(*N*,*N*'-ethylenebis(5-bromo--3-methoxysalicylideneaminato)copper(II) (**4**) have hitherto not been obtained in powder form. However in the literature there are papers only about their synthesis and crystal structure determination,[15–18] but there is no the information on their various properties. Therefore, the aim of this work was to obtain complexes of Cu(II) and Ni(II) with the Schiff base ligands as microcrystalline powder and to examine some of their physicochemical properties, including thermal stability in air during heating to 973 K, IR spectral characterization and magnetic behavior in the temperature range of 76–303 K.

EXPERIMENTAL

Materials

All chemicals and solvents used for the syntheses were of commercially available reagent grade and were used without further purification.

Synthesis of the Schiff bases

All the Schiff base ligands (H_2L^1 = $C_{20}H_{24}N_2O_6$, H_2L^2 = $C_{16}H_{14}Br_2N_2O_2$, H_2L^3 = = $C_{18}H_{18}Br_2N_2O_4$) were prepared by known methods[19–21] by the 2:1 condensation of 4,6--dimethoxysalicylaldehyde, 5-bromosalicylaldehyde or 5-bromo-3-methoxysalicylaldehyde, respectively, and ethylenediamine in methanol. The Schiff bases were separated as yellow needles and were recrystallized twice from methanol. The compounds were stable at room temperature and were characterized by IR spectroscopy and elemental analysis. Anal. Calcd. for $C_{20}H_{24}N_2O_6$ (H_2L^1): C, 61.86; H, 6.19; N, 7.22 %. Found: C, 61.80; H, 6.10; N, 7.12 %. Anal. Calcd. for $C_{16}H_{14}Br_2N_2O_2$ (H_2L^2): C, 45.07; H, 3.29; N, 6.57 %. Found: C, 45.12; H, 3.10; N, 6.45 %. Anal. Calcd. for $C_{18}H_{18}Br_2N_2O_4$ (H_2L^3): C, 44.46; H, 3.71; N, 5.76 %. Found: C, 44.36; H, 3.61; N, 5.69 %.

Synthesis of the complexes

Complexes **1**, **3** and **4** were obtained by the treatment of copper(II) nitrate trihydrate (1.0 mmol) with H_2L^1, H_2L^2 and H_2L^3 (1.0 mmol), respectively in methanolic solution under reflux. For preparation of the complex **2**, nickel(II) nitrate hexahydrate and H_2L^1 were used. The reaction mixtures were cooled and the resulting precipitates were filtered off, washed with diethyl ether and dried.

Methods and apparatus applied

The contents of carbon, hydrogen and nitrogen in the analyzed compounds were determined by elemental analysis using a CHN 2400 Perkin Elmer analyzer.

The contents of copper and nickel were established using an ED–XRF spectrophotometer (Canberra-Packard).

Single-crystal diffraction data for compounds **1**–**4** were measured at room temperature in the ω mode on a Oxford Diffraction Xcalibur CCD diffractometer using graphite-monochromated MoK_α radiation (λ = 0.71073 Å).

The infrared spectra of the complexes were recorded in the range of 4000–400 cm^{-1} using an M-80 spectrophotometer (Carl Zeiss, Jena, Germany). Samples for IR spectroscopy measurements were prepared as KBr discs.

The thermal stability and decomposition of the complexes were studied in air using a Setsys 16/18 (Setaram) TG/DTA/DSC instrument. The experiments were performed under a dynamic air atmosphere (flow rate 17 mL min^{-1}) in the temperature range of 297–973 K at a heating rate of 5 K min^{-1}. The initial mass of the samples (mg) used for the measurements were following: **1** – 7.33; **2** – 7.24; **3** – 7.44; **4** – 7.25. The samples were heated in Al_2O_3 crucibles.

The X-ray diffraction patterns of the final product of thermal decomposition were taken on a HZG-4 (Carl Zeiss, Jena) diffractometer using Ni filtered CuK_α radiation. The measurements were performed in the 2θ range 4–80° by means of the Bragg–Brentano method.

The magnetic susceptibility values of the compounds were determined by the Gouy method in the temperature range of 76–303 K. The calibrant employed was $Hg[Co(SCN)_4]$ for which a magnetic susceptibility of 1.644×10^{-5} cm^3 g^{-1} was taken. Correction for diamagnetism of the constituent atoms was calculated using Pascal's constants.[22] The effective magnetic moment values, μ_{eff} , were calculated from the equation:

$$\mu_{eff} = 2.83\ (\chi_M T)^{1/2}$$

where χ_M is the magnetic susceptibility and T is the absolute temperature.

RESULTS AND DISCUSSION

The elemental analyses (C, H, N and M) data and the IR spectra analysis of the Schiff base complexes, (Tables I and II, respectively) showed that they may be represented by the formulae $[CuC_{20}H_{22}N_2O_6]$ (**1**), $[NiC_{20}H_{22}N_2O_6]$ (**2**), $[CuC_{16}H_{12}Br_2N_2O_2]$ (**3**) and $[Cu(C_{18}H_{16}Br_2N_2O_4)H_2O]$ (**4**). The structures of **1**–**4** were also confirmed by single crystal X-ray diffraction. The unit cell parameters of **1** ($P2_1/c$, a = 7.5548(2) Å, b = 15.8484(4) Å, c = 15.7716(4) Å, α = 90°, β = 91.013(3)°, γ = 90° and V = 1888.1(1) $Å^3$) and **2** ($P2_1/c$, a = 7.5342(3) Å, b = = 15.7566(5) Å, c = 15.8626(6)Å, α = 90°, β = 91.187(4)°, γ = 90° and V = = 1882.7(1) $Å^3$) are similar to those reported earlier by Assey *et al.*[15,16] Compound **1** is isostructural with **2**.[15,16] In addition, the unit cell parameters of **3** (P-1, a = 8.3372(9) Å, b = 9.6880(11) Å, c = 11.0308(12) Å, α = 115.259(11)°, β = = 92.689(9)°, γ = 101.732(9)° and V = 779.9(2)$Å^3$) resemble those described by

TABLE I. Elemental analysis data of the Schiff base complexes

Complex	Color	Calcd. (Found), %			
		C	H	N	M
$[CuC_{20}H_{22}N_2O_6]$ (**1**)	Brown	53.39	4.89	6.23	14.14
		(53.29)	(4.62)	(6.10)	(13.94)
$[NiC_{20}H_{22}N_2O_6]$ (**2**)	Green	53.98	4.95	5.40	13.20
		(53.65)	(4.72)	(5.11)	(13.00)
$[CuC_{16}H_{12}Br_2N_2O_2]$ (**3**)	Brown	39.40	2.46	5.75	13.04
		(39.14)	(2.17)	(5.44)	(12.76)
$[Cu(C_{18}H_{16}Br_2N_2O_4)H_2O]$ (**4**)	Green	38.21	3.18	4.95	11.24
		(38.04)	(3.04)	(4.82)	(11.12)

Xie *et al.*[17] The unit cell parameters of **4** (*Pnma*, a = 8.7379(3) Å, b = 27.9612(9) Å, c = 7.9779(3) Å, $\alpha = \beta = \gamma = 90°$ and V = 1949.2(1)Å^3) are similar to those reported by Xie.[18] These metal complexes are soluble in polar organic solvents, such as MeOH, $CHCl_3$, DMF and EtOH, but less soluble in non-polar solvents, such as hexane, heptane and toluene.

TABLE II. IR spectral data of the Schiff base ligands and their metal complexes (cm^{-1})

Compound		ν(O–H)	ν(C=N)	ν(C–O)	ν(M–N)	ν(M–O)
$C_{20}H_{24}N_2O_6$	H_2L^1	3424	1624	1276	–	–
$C_{16}H_{14}Br_2N_2O_2$	H_2L^2	3416	1636	1216	–	–
$C_{18}H_{18}Br_2N_2O_4$	H_2L^3	3440	1628	1252	–	–
$[CuC_{20}H_{22}N_2O_6]$	**1**	–	1608	1232	555	400
$[NiC_{20}H_{22}N_2O_6]$	**2**	–	1604	1236	548	436
$[CuC_{16}H_{12}Br_2N_2O_2]$	**3**	–	1632	1176	544	448
$[Cu(C_{18}H_{16}Br_2N_2O_4)H_2O]$	**4**	3448	1624	1240	564	464

Infrared spectra

The infrared spectra of the free Schiff base ligands H_2L^1, H_2L^2 and H_2L^3 (Table II) showed a strong band in the region of 1624–1636 cm^{-1} which is characteristic of the azomethine (C=N) group. In addition to this characteristic (C=N) absorption, these ligands also exhibit broad medium bands with a maximum around 3440 cm^{-1}, which can be assigned to phenolic (O–H) group vibrations. According to the literature,[23–30] the participation of the nitrogen atom of the Schiff base ligands in the coordination sphere should reduce the bond order in the C=N group due to the strong donation of electron density toward the metal ion, and result in a decrease in the C=N stretching frequency. In the IR spectra of the Schiff base complexes (Table II), the band due to ν(C=N) showed a negative shift and appeared at 1632–1604 cm^{-1}, indicating coordination of the azomethine nitrogen to copper and nickel metals, respectively.[8,9,23–30] A strong band observed at 1216–1276 cm^{-1} in the free Schiff bases is assigned to the phenolic C–O stretching vibration. On complexation, this band is shifted to the lower frequency range of 1240–1176 cm^{-1}, indicating coordination through the phenolic oxygen.[9,29] This was further supported by the disappearance of the broad ν(OH) band around 3400 cm^{-1} in the complexes, indicating deprotonation of the phenolic proton prior to coordination. That the azomethine nitrogen and the phenolic oxygen are involved in complexation with the metal ion is also clearly evident from the appearance of the new medium intensity bands at 548–564 and 400–460 cm^{-1} in the spectra, assignable to ν(M–N) and ν(M–O).[9,30–32] The bands at 3440 and 3448 cm^{-1} in the spectra of the H_2L^3 ligand and analyzed complex **4**, respectively, have a similar position but their shapes are different. In the spectra of **4**, this intense broad absorption band confirms the presence of water molecules.[30]

Thermal analysis

The thermal properties of complexes **1**–**4** were investigated by thermogravimetric (TG) analysis, differential thermogravimetric (DTG) analysis and differential thermal analysis (DTA). The recorded TG/DTG and DTA curves of three copper(II) Schiff base complexes in an air atmosphere are presented in Figs. 1–3. It can be seen that the TG curves of **1** (Fig. 1) and **3** (Fig. 2) show no mass loss up to 573 and 563 K, respectively, indicating the absence of water molecules and other adsorbed solvent molecules in the coordination sphere. As the temperature

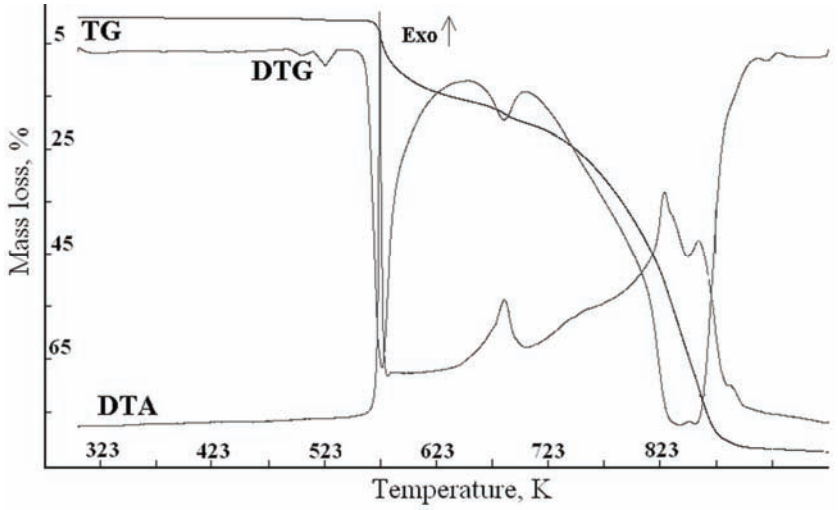

Fig. 1. TG, DTG and DTA curves of $[CuC_{20}H_{22}N_2O_6]$ (**1**).

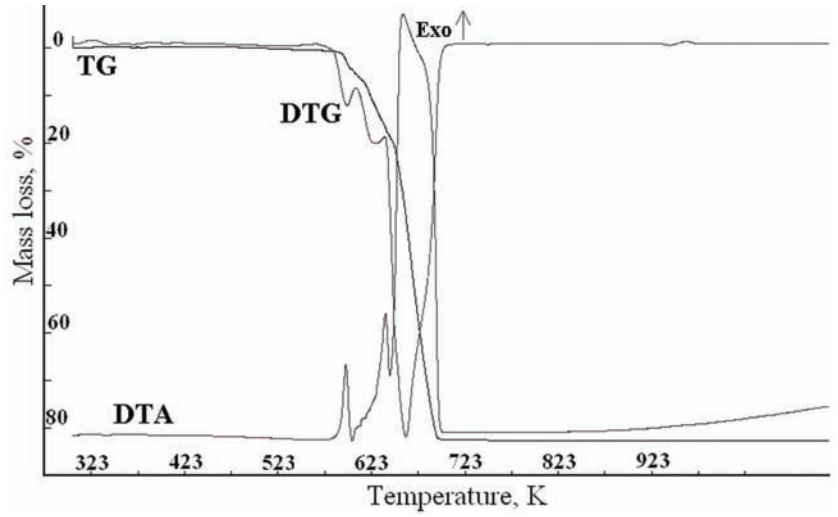

Fig. 2. TG, DTG and DTA curves of $[CuC_{16}H_{12}Br_2N_2O_2]$ (**3**).

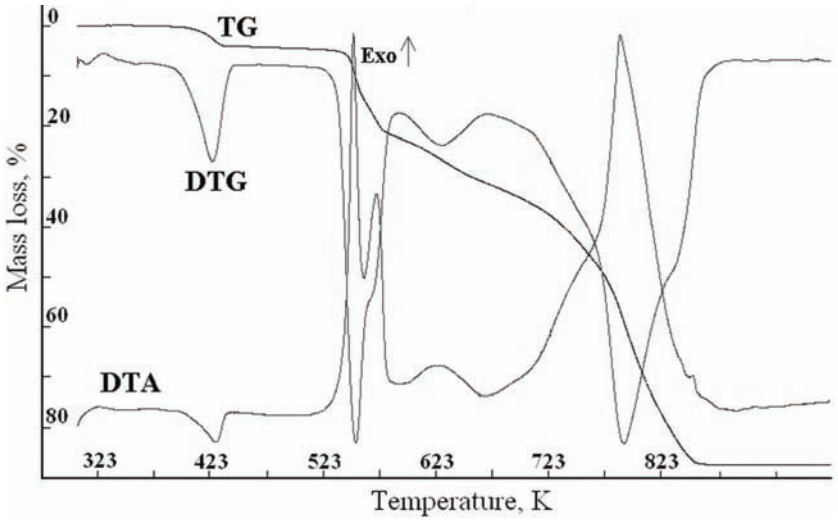

Fig. 3. TG, DTG and DTA curves of $[Cu(C_{18}H_{16}Br_2N_2O_4)H_2O]$ (**4**).

was increased, the TG/DTG curves of the copper(II) complexes exhibit a sharp mass loss in the temperature ranges of 578–703 K (**1**) and 563–948 K (**3**), which are accompanied with sharp exothermic peaks in the DTA curves at 656 (**1**), 573 (**3**) and 825 K (**3**) that may be due to the decomposition of the ligand molecule. The complex **2** (nickel (II)) similar to **1**, displays a one-step decomposition. This step shows drastic mass loss within a wide temperature range of 573–713 K with a DTG peak at 673 K, also giving rise to a sharp exothermic peak at 678 K in the DTA curve. This process can be interpreted as decomposition of the ligand molecules. The thermal decomposition of complex **4** occurred in two steps (Fig. 3), giving one endothermic and two exothermic DTA peaks. The first step displays a gradual mass loss of 3.90 % within the temperature range of 413–433 K with a DTG peak at 423 K, which may be attributed to the loss of the one water molecule (calcd. 3.20 %). The recorded DTA curve reveals an endothermic peak at 426 K. The water elimination process occurs at a high temperature. This may indicate the coordination of the water molecules.[23] The anhydrous complex is stable up to 536 K. The next decomposition steps of **4** also exhibit a gradual loss of mass within the temperature range of 536–858 K with DTG peaks at 505 and 788 K. They are probably connected with the decomposition of the Schiff base ligand. Combustion of the organic ligand is accompanied by strong exo-effect peaks seen on the DTA curves with maximums at 547 and 783 K.

The complexes decompose to the respective oxides: CuO (in the case of **1**, **3**, and **4**) and NiO (in the case of **2**).[32] The mass losses calculated from the TG curves are in the range of 87.20–82.50 % (the theoretical values are 86.00–82.30

%). The compositions of the final products were calculated from the TG curves and experimentally verified by their X-ray diffraction patterns and IR spectra.

According to the beginning temperature of the decomposition of the Schiff base complexes, the following order of thermal stability may be proposed:

$$[Cu(L^1)]\ (\mathbf{1}) > [Ni(L^1)]\ (\mathbf{2}) > [Cu(L^2)]\ (\mathbf{3}) > [Cu(L^3)H_2O]\ (\mathbf{4})$$

Magnetic properties

The magnetic behavior of the title compounds was studied in the temperature range 77–300 K (Table III). The magnetic susceptibility of the Cu(II) complexes changed with temperature according to the Curie–Weiss law. The magnetic properties of **1** in the form of an χ_M *vs.* *T* plot (χ_M is the molar magnetic susceptibility) is shown in Fig. 4. The observed effective moment of complexes **1** and **3** (having square-planar geometry[15,17]) at 76 K is 2.12 μ_B, while that at room temperature is 2.20 μ_B. The copper(II) ion ($3d^9$) has one unpaired electron in the 3d shell, therefore its compounds were considered to have magnetic moments close to the spin-only value, 1.73μ_B but due to spin orbit coupling, higher values are often observed.[29,33–35] The magnetic moment values calculated for **4** are in the range of 1.85–1.88 μ_B. The environment around the copper in **4** is square-pyramidal.[18] The magnetic moments of the copper(II) complexes were treated by

TABLE III. The magnetic data of the Cu(II) complexes with Schiff bases

T / K	$[Cu(C_{20}H_{22}N_2O_6)]$ (**1**)		$[Cu(C_{16}H_{12}Br_2N_2O_2)]$ (**3**)		$[Cu(C_{18}H_{16}Br_2N_2O_4)(H_2O)]$ (**4**)	
	$\chi_M \times 10^6$ $cm^3 \cdot mol^{-1}$	μ_{eff} μ_B	$\chi_M \times 10^6$ $cm^3 \cdot mol^{-1}$	μ_{eff} μ_B	$\chi_M \times 10^6$ $cm^3 \cdot mol^{-1}$	μ_{eff} μ_B
76	7697	2.16	7353	2.12	426166	1.85
123	4475	2.10	4622	2.13	411570	1.82
133	4088	2.09	4236	2.12	412301	1.82
143	3851	2.10	3904	2.11	410964	1.81
153	3501	2.07	3636	2.11	415280	1.82
163	3464	2.13	3422	2.11	412067	1.82
173	3289	2.13	3208	2.11	416636	1.83
183	3152	2.15	3026	2.11	416376	1.83
193	3039	2.17	2897	2.12	421158	1.84
203	2927	2.18	2758	2.12	420026	1.83
213	2840	2.20	2597	2.10	419467	1.83
223	2740	2.21	2426	2.08	422846	1.84
233	2640	2.22	2351	2.09	423211	1.84
243	2552	2.23	2287	2.11	426829	1.85
253	2465	2.23	2169	2.10	429249	1.85
263	2402	2.25	2201	2.15	430473	1.86
273	2402	2.27	2083	2.11	429744	1.86
283	2278	2.27	2040	2.13	433092	1.86
293	2253	2.30	1944	2.12	436703	1.87
303	2165	2.29	1987	2.20	441532	1.88

Boudreaux. According to Boudreaux, in complexes having a square pyramidal configuration, the five-fold degenerate 3d level of Cu(II) is split by a ligand field of C_{4v} symmetry into four components. The $d_{x^2-y^2}$, d_{z^2} and d_{xy} levels are non degenerate, while (d_{xz}, d_{yz}) levels are four-fold degenerate, including spin. The spin-orbit interaction splits this level into two components, each of which is further split into two sublevels by the external magnetic field. Boudreaux calculated theoretically the magnetic moment of square-pyramidal copper(II) complexes to be 2.11–2.21 μ_B at room temperature.[36,37] These values are slightly higher than those obtained during the experimental measurements (1.88 μ_B). The nickel(II) complex **2** (having a square planar geometry [16]) is diamagnetic.[2,4,23,33,38]

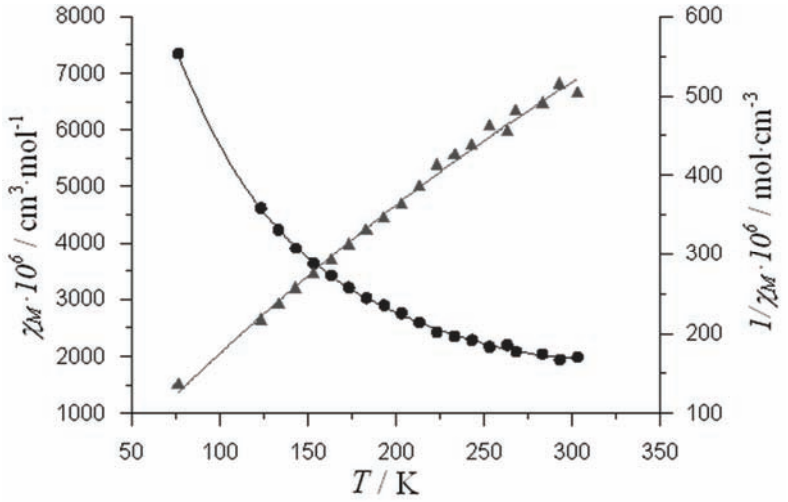

Fig. 4. Dependence between the magnetic susceptibility values *vs.* temperature for $[CuC_{20}H_{22}N_2O_6]$ (**1**).

CONCLUSIONS

The analytical data showed the presence of one metal ion per Schiff base ligand molecule and suggested a mononuclear structure for the Cu(II) and Ni(II) complexes obtained as microcrystalline powder. The complexes **1**, **2** and **3** are anhydrous compounds, whereas **4** contains one molecule of coordinated water, which is lost at 413–433 K. The TG and DTG data of the copper(II) complexes revealed that their decomposition patterns are different. The complexes **1**–**3** exhibit only a one-step decomposition, whereas a two-stage decomposition was observed in the case of complex **4**. The final products of complex decomposition were identified as CuO and NiO, respectively. The susceptibilities of all compounds closely follow the Curie law, but the magnetic moments of **1** and **3** are

slightly larger than that of **4**. This may indicate that the orbital contribution in **1** and **3** is higher than in **4**.

И З В О Д

СПЕКТРАЛНА, ТЕРМАЛНА И МАГНЕТНА СВОЈСТВА КОМПЛЕКСА БАКРА(II) И НИКЛА(II) СА ШИФОВИМ БАЗАМА КАО ЛИГАНДИМА

BEATA CRISTÓVÃO

Department of General and Coordination Chemistry, Maria Curie-Sklodowska University, Maria Curie-Sklodowska sq.2, PL. 20-031 Lublin, Poland

Синтетизовани су мононуклеарни комплекси бакра(II) и никла(II) опште формуле $[Cu(L^1)]$ (**1**), $[Ni(L^1)]$ (**2**), $[Cu(L^2)]$ (**3**) и $[Cu(L^3)H_2O]$ (**4**) (где је L^1 = *N*,*N*'-етиленбис(4,6-диметоксисалицилиденаминато), L^2 = *N*,*N*'-етиленбис(5-бромосалицилиденаминато), L^3 = *N*,*N*'-етиленбис(5-бромо-3-метоксисалицилиденаминато)). Комплекси су кристалисали у облику монокристалног праха и за њихову карактеризацију употребљени су IR спектроскопија, термална анализа и магнетна мерења. Магнетна сусцептибилност бакар(II) комплекса се мења са температуром у складу са Кири–Вајсовим (*Curie–Weiss*) законом. Магнетни моменти (μ_B) испитиваних комплекса на 303 K су: 2.29 (**1**), 2.20 (**3**) и 1.88 (**4**). Свака од наведених вредности се не мења са снижавањем температуре на 77 K. Комплекс никла(II) (**2**) је дијамагнетичан.

(Примљено 12. новембра 2010, ревидирано 7. марта 2011)

REFERENCES

1. R. Karmakar, C. R. Choudhury, D. L. Hughes, G. P. A. Yap. M. Salah el Fallah, C. Desplanches, J.-P. Sutter, S. Mitra, *Inorg. Chim. Acta* **359** (2006) 1184
2. A. Bottcher, H. Elias, E. G. Jager, H. Langfelderova, M. Mazur, L. Muller, H. Paulus, P. Pelikan, M. Rudolph, M. Valko, *Inorg. Chem.* **32** (1993) 4131
3. D. E. Fenton, *Biocoordination Chemistry*, 1st ed., Oxford University Press, Oxford, 1995
4. J. Manonmani, R. Thirumuruhan, M. Kandaswamy, V. Narayanan, S. Shanmuga Sundara Raj, M. N. Ponnuswamy, G. Shanmugam, H. K. Fun, *Polyhedron* **20** (2001) 3039
5. A. Puglisi, G. Tabbi, G. Vecchio, *J. Inorg. Biochem.* **98** (2004) 969
6. V. Daier, H. Biava, C. Palopoli, S. Shova, J.-P. Tuchagues, S. Signorella, *J. Inorg. Biochem.* **98** (2004) 1806
7. A. Trujillo, M. Fuentealba, D. Carillo, C. Manzur, I. Ledoux-Rak, J.-R. Hamon, J.-Y. Saillard, *Inorg. Chem.* **49** (2010) 2750
8. G. B. Roy, *Inorg. Chim. Acta* **362** (2009) 1709
9. K. Naresh Kumar, R. Ramesh, *Spetrochim. Acta, A* **60** (2004) 2913
10. R. Klement, F. Stock, H. Ellias, H. Paulus, P. Pelikan, M. Valko, M. Mazur, *Polyhedron* **18** (1999) 3617
11. W. Radecka-Paryzek, W. I. Pośpieszna-Markiewicz, M. Kubicki, *Inorg. Chim. Acta* **306** (2007) 488
12. M. Nayak, R. Koner, H.-H. Lin, U. Florke, H.-H. Wei, S. Mohanta, *Inorg. Chem.* **45** (2009) 10764
13. S. Nastase, F. Tuna, C. Maxim, C. A. Muryn, N. Avarvari, R. E. P. Winpenny, M. Andruh, *Cryst. Growth Des.* **7** (2007) 1825

14. M. R. Bermejo, A. Castineiras, J. C. Garcia-Monteagudo, M. Rey, A. Sousa, M. Watkinson, C. A. McAuliffe, R. G. Pritchard, R. L. Beddoes, *J. Chem. Soc., Dalton Trans.* (1996) 2935
15. G. Assey, R. J. Butcher, Y. Gultneh, *Acta Cryst., E* **66** (2010) m653
16. G. Assey, R. J. Butcher, Y. Gultneh, *Acta Cryst., E* **66** (2010) m620
17. Q.-F. Xie, Y.-M. Chen, M.-L. Huang, *Acta Cryst., E* **65** (2009) m903
18. H. Xie, *Acta Cryst., E* **65** (2009) m1577
19. T. Fukuda, F. Sakamoto, M. Sato, Y. Nakano, X. S. Tan, Y. Fujii, *Chem. Commun.* (1998) 1391
20. D. Das, C. P. Cheng, *J. Chem. Soc., Dalton Trans.* (2000) 1081
21. M. Harihran, F. L. Urbach, *Inorg. Chem.* **8** (1969) 556
22. E. König, *Magnetic Properties of Coordination and Organometallic Transition Metal Compounds*, Springer Verlag, Berlin, 1966
23. K. Krishnankutty, P. Sayudevi, M. B. Ummathur *J. Serb. Chem. Soc.* **72** (2007) 1075
24. K. Mitra, S. Biswas, C. R. Lucas, B. Adhikary, *Inorg. Chim. Acta* **359** (2006) 1997
25. G. Kumar, D. Kumar, C. P. Singh, A. Kumar, V. B. Rana, *J. Serb. Chem. Soc.* **75** (2010) 629
26. G. Rajendran, C. S. Amritha, R. J. Anto, V. T. Cheriyan, *J. Serb. Chem. Soc.* **75** (2010) 749
27. O. Pouralimardan, A. Chamayou, C. Janiak, H. Hosseini-Monfared, *Inorg. Chim. Acta* **360** (2007) 1599
28. M. Imran, L. Mitu, S. Latif, Z. Mahmood, I. Naimat, S. S. Zaman, S. Fatima, *J. Serb. Chem. Soc.* **75** (2010) 1075
29. G. G. Mohamed, C. M. Sharaby, *Spetrochim. Acta* A **66** (2007) 949
30. K. Nakamoto, *Infrared and Raman Spectra of Inorganic and Coordination Compounds*, Wiley, Toronto, Canada, 1997
31. R. C. Maurya, P. Patel, S. Rajput, *Synth. React. Inorg. Met.-Org. Chem.* **23** (2003) 81
32. M. Sönmeza, M. Ekercib *J. Serb. Chem. Soc.* **72** (2007) 259
33. V. Katović, L. T. Taylor, D. H. Busch, *Inorg. Chem.* **10** (1971) 458
34. L. V. Ababei, A. Kriza, C. Andronescu, A. M. Musuc, *J. Serb. Chem. Soc.* **76** (2011) 1103
35. N. R. S. Kumar, M. Nethiji, K. C. Patil, *Polyhedron* **10** (1991) 365
36. E. A. Boudreaux, *Trans. Faraday Soc.* **59** (1963) 1055
37. L. Sacconi, M. Ciampolini, U. Campigli, *Inorg. Chem.* **4** (1965**)** 407
38. L. T. Taylor, W. M. Coleman, *J. Am. Chem. Soc.* **92** (1970) 1449.

Journal of the Serbian Chemical Society
JSCS-info@shd.org.rs • www.shd.org.rs/JSCS
J. Serb. Chem. Soc. *76* (12) 1649–1660 (2011)
JSCS–4237
UDC 547.854+548.121:541.12.011/.017
Original scientific paper

The role of Duschinsky rotation in intersystem crossing: a case study of uracil

MIHAJLO ETINSKI*#

Faculty of Physical Chemistry, University of Belgrade, Studentski trg 12–16, P. O. Box 47, 11158 Belgrade, Serbia

(Received 13 July 2011)

Abstract: The intersystem crossing rate for the transition between the lowest excited singlet and triplet electronic states of uracil was studied by means of *ab initio* methods. The rate was evaluated using the time-dependent approach based on the correlation function and its two approximations: the second-order cumulant expansion and the short-time approximation. The normal modes of the singlet and triplet states are related by the Duschinsky transformation, *i.e.*, by rotation and translation. It was found that for singlet–triplet adiabatic energy gaps below 6000 cm^{-1}, the inclusion of the Duschinsky rotation is necessary for quantitative results. Above energy gaps of 6000 cm^{-1}, the rates obtained with and without the Duschinsky rotation are similar. The cumulant expansion approximates well the correlation function. The short-time approximation, although crude, can be used as the first estimate of the rate.

Keywords: uracil; excited states; intersystem crossing.

INTRODUCTION

Absorption of ultraviolet light creates excited electronic states in molecules. These states will eventually decay to the ground electronic state through radiative or non-radiative processes.[1–3] Non-radiative processes can be observed indirectly as they modify the spectra and rates of photochemical reactions. If a non-radiative transition is between electronic states of the same spin multiplicity, then the process is an internal conversion (IC), otherwise it is an intersystem crossing (ISC). Transitions between states with different spin multiplicities are formally forbidden in non-relativistic quantum theory. In order to treat these transitions, spin–orbit coupling must be taken into account.

Uracil is pyrimidine nucleobasis that is involved in the formation of nucleic acids. Its excited states properties are intriguing because although to a large ex-

* E-mail: etinski@ffh.bg.ac.rs
# Serbian Chemical Society member.
doi: 2298/JSC110713147E

tent they are photostable, ultrafast time-resolved experiments showed that electronic relaxation from the initially excited $^1\pi\pi^*$ state proceeds in multiple steps.[4–6] Much is known about the relaxation of the singlet excited states of uracil but knowledge of the dynamics of its triplet states are still limited. Although the triplet state has a low quantum yield, it is of interest when excited-state nucleic acids chemistry is considered. Triplet excited states usually have much longer lifetimes than singlet states and their reactivity is also higher.

Nanosecond pump–probe experiments with low-pressure molecular beams revealed that uracil and its methylated compounds, after initial photoexcitation to the S_2 ($\pi\pi^*$) state, were captured in the dark electronic state that lived several tens to hundreds of nanoseconds.[7–10] Based on quantum-chemical calculations, Marian and coworkers argued that this state is the lowest triplet state T_1 ($^3\pi\pi^*$).[11] They proposed two mechanisms for the formation of the triplet: (a) a non-radiative transition from the intermediate singlet S_1 ($n\pi^*$) state to the lowest triplet state, (b) a transition from the initially populated S_2 state to the second triplet state T_2 ($n\pi^*$) followed by internal conversion to the lowest triplet T_1 state. Due to the experimental findings that there is a fast depletion of the initially excited state to the ground electronic state and the S_1 state, Marian and coworkers suggested that T_1 state is populated by ISC process from the intermediate singlet S_1 state.

In the condensed phase, the S_1 and T_1 states are populated during electronic relaxation from the initially excited S_2 state.[12,14] The quantum yield of the triplet state depends on the solvent and it ranges from 0.02 in water up to 0.54 in ethyl acetate for 1-cyclohexyluracil[12] and 1.00 for 6-azauracil.[13]

The rate of the ISC is determined by the properties of the chromophore, such as spin–orbit and vibronic couplings. For rigid molecules in the body-fixed rotating molecular coordinate system, the electronic potential energy in the vicinity of the minimum can be diagonalized by introducing normal-mode coordinates $\{Q_i\}$. Electronic transitions are usually followed by a change in normal modes. Normal modes of the final state could be displaced and rotated relative to the normal modes of the initial state. The transformation that relates two sets of the normal modes is called the Duschinsky transformation.[15]

Usually, non-totally symmetric modes or modes with very small displacements are ignored in electronic relaxation rate calculations. This is justified when the normal modes of the electronic states are neither mixed nor distorted. In this case, non-totally symmetric modes have zero Franck–Condon (FC) integrals. Even when there is a distortion, it is possible to ignore their contribution to the rate. Sando *et al.*[16] showed that when the Duschinsky rotation is present, non-totally symmetric modes cannot be ignored in the calculation of the electron transfer rate, particularly when their number is large. They argued that in real

molecules, low-frequency modes could mix with high-frequency modes so that their net contribution to the rate increases.

The goal of this work was to establish to what extent the rotation of the normal modes is important for the quantitative evaluation of the $S_1 \rightarrow T_1$ ISC rate in uracil. By comparing the rates obtained with and without the Duschinsky rotation, the importance of the various approximations for the evaluation of the ISC rate will be established.

The paper is organized as follows: in the next section, the manner in which ISC rates can be calculated using the correlation function approach and its approximations is explained. Then, details of the rate calculations are presented. In the subsequent section, this method is applied to the calculation of the intersystem crossing rates for uracil and the results are discussed. Finally, conclusions are given.

The correlation function method

ISC rates are calculated using truncation of the time dependent perturbation expansion, *i.e.*, the Golden rule approximation. This is justified because all atoms in uracil are light so that spin–orbit coupling $\hat{H}_{\mathrm{SO}}$ could be treated as a perturbation. As zero-order states, pure spin Born–Oppenheimer states $\left|S_{\mathrm{a}},\{v_{\mathrm{aj}}\}\right\rangle$ and $\left|T_{\mathrm{b}}^{\alpha},\{v_{\mathrm{bk}}\}\right\rangle$ were used. Here S_{a} is a singlet electronic state and T_{b}^{α} is an α fine-structure component of a triplet electronic state. $\{v_{\mathrm{aj}}\}$ and $\{v_{\mathrm{bk}}\}$ are vibrational states related to the S_{a} and T_{b}^{α} states. In this work, potential surfaces are approximated by a harmonic potential. The normal modes of the triplet $\{Q_{\mathrm{T_i}}\}$ and singlet $\{Q_{\mathrm{S_i}}\}$ electronic states are related through the Duschinsky transformation:[15]

$$Q_{\mathrm{T}_i} = \sum_j J_{ij} Q_{\mathrm{S}_j} + D_i \tag{1}$$

where J is the Duschinsky rotation matrix and D is the displacement vector. The Duschinsky matrix represents to what extent normal modes of the triplet electronic state are mixed based on the normal modes of the singlet electronic state. The displacement vector presents the displacement of the triplet potential surface in respect to that of the singlet.

The rate from the initially populated vibronic state $\left|S_{\mathrm{a}},\{v_{\mathrm{aj}}\}\right\rangle$ to the triplet vibronic states $\left|T_{\mathrm{b}}^{\alpha},\{v_{\mathrm{bk}}\}\right\rangle$, assuming the statistical limit (high density of the final states), is given by the Golden Rule Formula:

$$k_{\mathrm{ISC}} = 2\pi \sum_k \left|\left\langle S_{\mathrm{a}},\{v_{\mathrm{aj}}\}\right| \hat{H}_{\mathrm{SO}} \left|T_{\mathrm{b}}^{\alpha},\{v_{\mathrm{bk}}\}\right\rangle\right|^2 \delta(E_{\mathrm{aj}} - E_{\mathrm{bk}}) \tag{2}$$

Spin–orbit matrix elements are generally a function of normal mode coordinates. They can be expanded using the Taylor expansion:

$$\left\langle S_{\mathrm{a}},\{v_{\mathrm{aj}}\}\left|\hat{H}_{\mathrm{SO}}\right|T_{\mathrm{b}}^{\alpha},\{v_{\mathrm{bk}}\}\right\rangle=\left\langle v_{\mathrm{aj}}\left|\left\langle S_{\mathrm{a}}\left|\hat{H}_{\mathrm{SO}}\right|T_{\mathrm{b}}^{\alpha}\right\rangle\right|_{Q_0}\left|v_{\mathrm{bk}}\right\rangle+\right.$$
$$\left.+\left\langle v_{\mathrm{aj}}\left|\sum_i\frac{\partial\left\langle S_{\mathrm{a}}\left|\hat{H}_{\mathrm{SO}}\right|T_{\mathrm{b}}^{\alpha}\right\rangle}{\partial Q_{\mathrm{i}}}\right|_{Q_0}Q_{\mathrm{i}}\left|v_{\mathrm{bk}}\right\rangle+\ldots\right.\right. \tag{3}$$

Keeping only the first term represents the Condon approximation and contributes to the direct spin–orbit coupling. The second and higher order terms represent the Herzberg–Teller expansion and they contribute to the vibronic spin–orbit coupling. It is assumed that a spin–orbit matrix element is expanded at an optimized geometry of the initial (singlet) electronic state. In this work, only the direct spin–orbit coupling will be considered. This is justified when the spin––orbit matrix element is large.

Assuming only a direct spin–orbit coupling, the ISC rate from the initial vibronic level, is given by:

$$k_{\mathrm{ISC}}=2\pi\left|\left\langle S_{\mathrm{a}}\left|\hat{H}_{\mathrm{SO}}\right|T_{\mathrm{b}}^{\alpha}\right\rangle\right|^2\sum_k\left|\left\langle v_{\mathrm{aj}}\left|v_{\mathrm{bk}}\right\rangle\right|^2\delta(E_{\mathrm{aj}}-E_{\mathrm{bk}})\right. \tag{4}$$

In this case, the calculation of the rate is reduced to the calculation of the electronic part $\left|\left\langle S_{\mathrm{a}}\left|\hat{H}_{\mathrm{SO}}\right|T_{\mathrm{b}}^{\alpha}\right\rangle\right|$ and the vibrational part, *i.e.*, the Franck–Condon integrals $\left\langle v_{\mathrm{aj}}\left|v_{\mathrm{bk}}\right\rangle\right.$.

Recently, Marian and coworkers developed a new method for the calculation of ISC rates using a time-dependent approach.[17] It is based on a transformation of expression (4) into the Heisenberg picture. Instead of the evaluation of an enormously large number of the Franck–Condon integrals, the method evaluates the correlation function. The rate is then obtained by performing an integration of the correlation function. If the initial state is the lowest vibronic state of the singlet manifold, then:

$$k_{\mathrm{ISC}}^{\mathrm{corr}}=\left|\left\langle S_{\mathrm{a}}\left|\hat{H}_{\mathrm{SO}}\right|T_{\mathrm{b}}^{\alpha}\right\rangle\right|^2\int_{-\infty}^{\infty}F_{\mathrm{corr}}(t)\,\mathrm{d}t \tag{5}$$

where

$$F_{\mathrm{corr}}(t)=2^{N/2}\sqrt{\frac{\det(\mathbf{S}_{\mathrm{T}}^{-1}\mathbf{\Omega}_{\mathrm{S}}\mathbf{\Omega}_{\mathrm{T}})}{\det(J^{\mathrm{T}}\mathbf{\Omega}_{\mathrm{T}}\mathbf{B}_{\mathrm{T}}J+\mathbf{\Omega}_{\mathrm{S}})\det(J^{\mathrm{T}}\mathbf{\Omega}_{\mathrm{T}}\mathbf{B}_{\mathrm{T}}^{-1}J+\mathbf{\Omega}_{\mathrm{S}})}}\times$$
$$\times\exp\{D^{\mathrm{T}}[\mathbf{\Omega}_{\mathrm{T}}\mathbf{B}_{\mathrm{T}}J(J^{\mathrm{T}}\mathbf{\Omega}_{\mathrm{T}}\mathbf{B}_{\mathrm{T}}J+\mathbf{\Omega}_{\mathrm{S}})^{-1}J\mathbf{\Omega}_{\mathrm{T}}\mathbf{B}_{\mathrm{T}}-\mathbf{\Omega}_{\mathrm{T}}\mathbf{B}_{\mathrm{T}}]\mathbf{D}\}\times \tag{6}$$
$$\times\mathrm{e}^{it(\Delta E_{\mathrm{ST}}+1/2Tr\mathbf{\Omega}_{\mathrm{S}})}$$

and $\mathbf{\Omega}$, $\mathbf{S}$ and $\mathbf{B}$ are diagonal matrices with elements $(\mathbf{\Omega})_{\mathrm{ii}}=\omega_{\mathrm{i}}$, $(\mathbf{S})_{\mathrm{ii}}=\sinh(i\omega_{\mathrm{i}}t)$, $(\mathbf{B})_{\mathrm{ii}}=\tanh(i\omega_{\mathrm{i}}t/2)$, ω_{i} is a normal mode frequency, indexes S and T label normal modes of the singlet and triplet electronic states, respectively, and superscript T

indicates the transposition of a matrix. ΔE_{ST} is the adiabatic energy between singlet and triplet electronic states.

In order to ease the calculations of the correlation function, two approximations were derived.[17] The first approximation is based on the cumulant expansion. The expression obtained using the second-order cumulant expansion of the correlation function is:

$$k_{ISC}^{cum} = \left|\left\langle S_a \left| \hat{H}_{SO} \right| T_b^{\alpha} \right\rangle\right|^2 \int_{-\infty}^{\infty} F_{cum}(t)dt = \left|\left\langle S_a \left| \hat{H}_{SO} \right| T_b^{\alpha} \right\rangle\right|^2 \int_{-\infty}^{\infty} \exp(-i\kappa_1 - \kappa_2)dt \quad (7)$$

where the first and the second cumulants are:

$$\kappa_1 = (\frac{1}{4}\sum_i \frac{M_{ii}}{\omega_{S_i}} + C - \Delta E_{ST})t \quad (8)$$

$$\kappa_2 = \frac{1}{8}\sum_{i,j} \frac{M_{ij}^2}{\omega_{S_i}\omega_{S_j}} \{\frac{-it}{\omega_{S_i} + \omega_{S_j}} + \frac{1-\exp[-it(\omega_{S_i} + \omega_{S_j})]}{(\omega_{S_i} + \omega_{S_j})^2}\} + \frac{1}{2}\sum_i \frac{A_i^2}{\omega_{S_i}} [\frac{-it}{\omega_{S_i}} + \frac{1-\exp(-it\omega_{S_i})}{\omega_{S_i}^2}] \quad (9)$$

Values of the matrix $\mathbf{M}$, vector $\mathbf{A}$ and scalar C are: $\mathbf{M} = \mathbf{J}^T\boldsymbol{\Omega}_T^2\mathbf{J} - \boldsymbol{\Omega}_S^2$, $\mathbf{A} = \mathbf{J}^T\boldsymbol{\Omega}_T^2\mathbf{D}$ and $C = \frac{1}{2}\mathbf{D}^T\boldsymbol{\Omega}_T^2\mathbf{D}$. There is a particular simple expression for the rate if the first and second cumulants are expanded up to the second order in time.[17] This gives the short-time approximation:

$$k_{ISC}^{ST} = \left|\left\langle S_a \left| \hat{H}_{SO} \right| T_b^{\alpha} \right\rangle\right|^2 \sqrt{\frac{\pi}{\frac{1}{16}\sum_{i,j}\frac{M_{ij}^2}{\omega_{S_i}\omega_{S_j}} + \frac{1}{4}\sum_i \frac{A_i^2}{\omega_{S_i}}}} \times \exp(-\frac{(\frac{1}{4}\sum_i \frac{M_{ii}}{\omega_{S_i}} + C - \Delta E_{ST})^2}{\frac{1}{4}\sum_{i,j}\frac{M_{ij}^2}{\omega_{S_i}\omega_{S_j}} + \sum_i \frac{A_i^2}{\omega_{S_i}}}) \quad (11)$$

This expression does not require integration for its evaluation. The first test results showed that both the cumulant and short-time approximation gave results that were similar to the complete correlation function results.[17]

The calculation of the correlation function and its cumulant expansion involves only matrix multiplication, matrix inversion and calculation of a determinant. They have odd imaginary parts and even real parts. Due to this, the evaluation of the rate is reduced to the calculation of the correlation function or its cumulant expansion in a real positive time interval. The input parameters

required for the calculation of the ISC rate are normal mode frequencies of the initial and final states, their displacements, the Duschinsky matrix, the electronic adiabatic energy gap and spin-orbit matrix element.

DETAILS OF THE INTERSYSTEM CROSSING RATE CALCULATIONS

In this work, the electronic structure data obtained in the work of Marian and co-workers[11] for uracil and its methylated compounds was used. They optimized the S_1 ($^1n\pi^*$) and T_1 ($^3\pi\pi^*$) excited states using the coupled-cluster with approximative doubles (CC2) method. This method represents an approximation of the coupled-cluster singles and doubles (CCSD) method, in which the singles equations are retained in the original form and the doubles equations are truncated to first order in the fluctuating potential.[18] The basis set was Dunning's cc-pVDZ basis set (C, N, O, 9s4p1d/3s2p1d; H, 4s1p/2s1p).[19,20] The excited state geometries were optimized without symmetry constraints. The molecular geometry of the S_1 state was planar while the T_1 state was non-planar. Since there is a large difference in the S_1 and T_1 molecular geometries, the parameters from the Duschinsky relation, the displacement and mixing of the normal modes are large. The normal mode frequencies and displacements of the S_1 and T_1 states of uracil are presented in Table I. There are several low-frequency modes that are highly displaced. The Duschinsky matrix for the transition between the S_1 and T_1 states of uracil is shown in Fig. 1. Almost all normal modes of the triplet states have more than one component in the basis of the singlet state normal modes. The mixing of the normal modes is particularly large for the low-frequency modes and the two highest frequency modes that represent N–H oscillation. In addition, some high-frequency modes are mixed with low-frequency modes.

TABLE I. Frequencies of the normal modes of the S_1 ($n\pi^*$) and T_1 ($\pi\pi^*$) electronic states of uracil and displacements of the T_1 normal modes in dimensionless harmonic oscillator coordinates

S_1 ω_i / cm^{-1}	T_1 ω_i / cm^{-1}	Displacement	S_1 ω_i / cm^{-1}	T_1 ω_i / cm^{-1}	Displacement
35.53	126.58	–2.57	970.84	959.28	–1.37
157.82	158.63	–0.31	1012.93	1014.62	1.11
287.76	228.99	–2.80	1105.30	1144.59	–0.36
302.49	367.48	–2.38	1150.37	1226.78	0.49
311.36	460.53	–0.13	1276.78	1353.70	–0.08
341.19	480.02	0.46	1306.92	1361.40	–1.23
472.37	497.58	–0.72	1405.45	1378.63	0.43
503.72	530.57	0.33	1427.08	1404.59	0.03
533.69	554.60	1.06	1451.08	1456.93	0.21
550.11	640.72	0.81	1631.67	1609.53	–2.84
593.22	683.30	0.97	1777.20	1769.36	–0.24
690.71	697.63	–0.49	3256.56	3240.67	–0.50
718.40	727.41	–0.18	3276.26	3255.20	0.90
742.69	762.45	–0.61	3626.67	3599.49	0.09
910.20	938.30	–1.38	3630.50	3599.67	–0.04

The adiabatic energy gap between the S_1 and T_1 electronic states of uracil obtained at the CC2/cc-pVDZ level is 5150 cm^{-1}. Spin–orbit matrix elements were calculated[11] using the SPOCK program based on the DFT/MRCI electronic structure method.[21] SPOCK employs a

one-center mean-field approximation of the Breit–Pauli Hamiltonian.[22] SOME were calculated at the S_1 optimized minimum. The sum of the squares of all spin–orbit matrix elements between the S_1 state and all fine-structure components of the T_1 state is 2391 cm^{-2}. All rates that will be presented in this work are the sum of the three rates from the S_1 state and the three fine-structure components of the T_1 state.

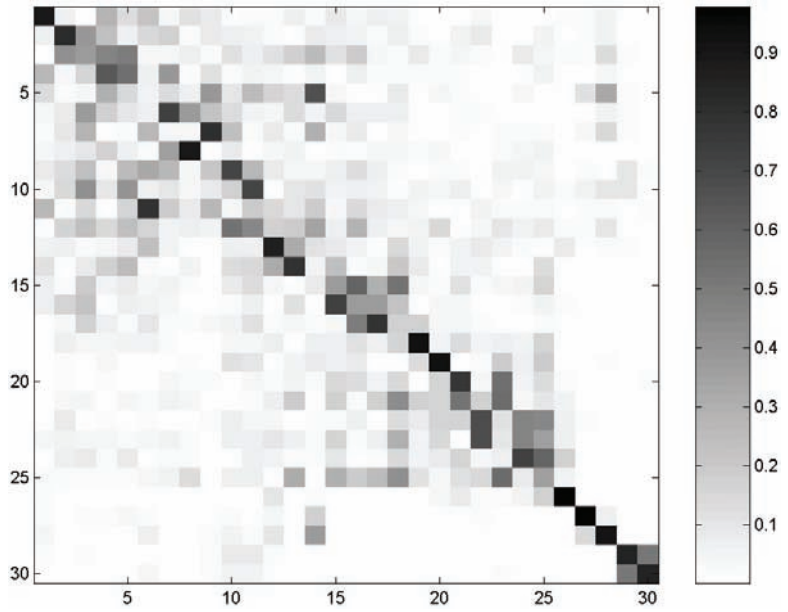

Fig. 1. The Duschinsky matrix related to the transition between the S_1 and T_1 states of uracil. In order to visualize the normal mode mixing, absolute values of the matrix elements are shown.

All normal modes are included in the rate calculations. The correlation function was calculated for the first 10 fs using 100 points. It was found that the rate is very robust to the density of points required for the integration of the correlation function.

RESULTS

The time dependence of the correlation function F_{corr} and its second-order cumulant expansion F_{cum} when the Duschinsky rotation is excluded and included are shown in Figs. 2 and 3, respectively. The adiabatic energy gap for the calculation was 5150 cm^{-1}. The correlation function and its cumulant expansion practically overlap in Fig. 2. The plotted functions perform one oscillation and then decay to zero. After 10 fs, their values are practically zero. The second-order cumulant expansion approximates the correlation function very well. Comparing the correlation function when the Duschinsky rotation is excluded and included, one finds that the amplitude of the correlation function oscillation in the first case is larger than in the second. The rates obtained using the correlation function and its second-order cumulant expansion are 6.66×10^9 and 6.64×10^9 s^{-1}, when the

Duschinsky rotation is excluded and 1.53×10^{10} and 2.60×10^{10} s^{-1}, when the Duschinsky rotation is included. The rates obtained using the short-time approximations are 1.47×10^{10} and 2.73×10^{10}, respectively. There is an order of magnitude higher rate when the Duschinsky rotation is included. Only the short-time approximation gives the same order of magnitude in both cases. In the absence of the Duschinsky rotation, the correlation function method gives the same result as the approximate cumulant expansion, as can be deduced from Fig. 2. This is an encouraging result because it is easier to calculate the cumalant expansion than the correlation function. When the Duschinsky rotation is present, the cumulant approximation gives a slightly higher value than the exact correlation function. Although the short-time approximation is a simple approximation, it gives reasonable results. Marian and coworkers [11] calculated the $S_1\rightarrow T_1$ ISC rate for uracil using the time-independent method, *i.e.*, they explicitly summed the Franck–Condon factors. As the number of the Franck–Condon factors was enormous, they limited the number of quanta in the triplet state normal modes to five per mode. This limitation decreased the number of the final vibronic levels. Using the same adiabatic energy gap, spin–orbit matrix elements and the Duschinsky rotation, they obtained 0.93×10^{10} s^{-1} for the rate value. This value is the lower limit for the true value due to the limitations concerning the accessible number of the final state vibronic levels. The present rates obtained with the Duschinsky rotation are in accordance with the result obtained by the time-independent method.

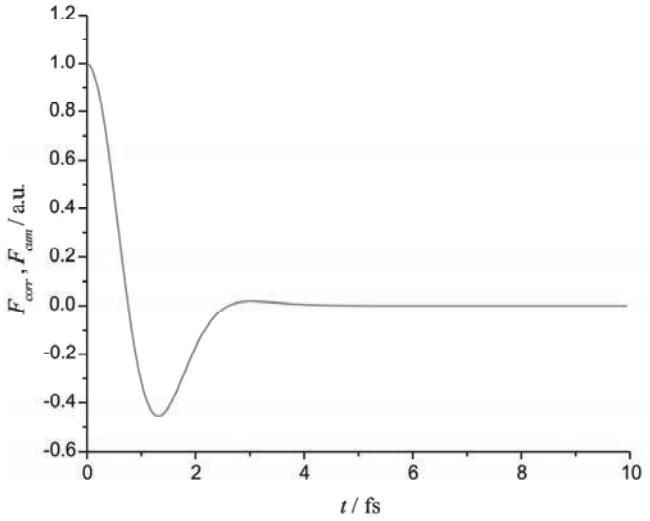

Fig. 2. Time dependence of the correlation function F_{corr} (black) and the second–order cumulant expansion F_{cum} (gray) – overlapped. The Duschinsky rotation was excluded and the adiabatic energy gap was 5150 cm^{-1}.

Solvation can modify adiabatic energy gaps. Etinski and Marian[23] found that hydration could significantly shift electronic excited states. They found that the $S_1(n\pi^*)$ state was blue-shifted by 0.56 eV and that the $S_2(\pi\pi^*)$ state was red-

shifted by 0.19 eV. Due to this, it is of importance to examine in what manner the adiabatic energy gap modifies the ISC rate. The rate constants calculated using the three methods: the correlation function, the second-order cumulant expansion and the short-time approximation for various adiabatic energy gaps are contained in Table II. The rate obtained without the Duschinsky rotation is one to three orders of magnitude smaller than the rate obtained with the Duschinsky rotation for energy gaps below 6000 cm^{-1}. For larger energy gaps, the inclusion of the Duschinsky rotation does not significantly contribute to the rate values. The least sensitive to the adiabatic energy gap change is the short-time approximation. It gives rather good results when the Duschinsky rotation is included.

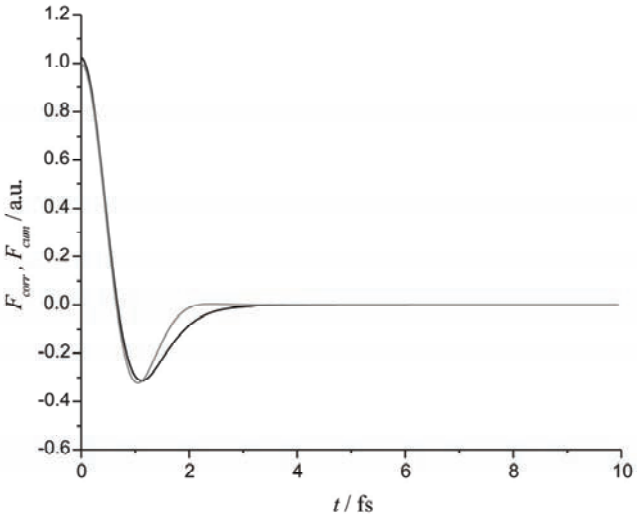

Fig. 3. Time dependence of the correlation function F_{corr} (black) and the second-order cumulant expansion F_{cum} (gray). The Duschinsky rotation was included and the adiabatic energy gap was 5150 cm^{-1}.

TABLE II. The intersystem crossing rates calculated by the three methods: the correlation function (k_{corr}), the second-order cumulant expansion (k_{cum}) and the short-time approximation (k_{st}) for different adiabatic energy gaps

ΔE / cm^{-1}	Without the Duschinsky rotation			With the Duschinsky rotation		
	k_{corr} / 10^8 s^{-1}	k_{cum} / 10^8 s^{-1}	k_{st} / 10^{10} s^{-1}	k_{corr} / 10^9 s^{-1}	k_{cum} / 10^{10} s^{-1}	k_{st} / 10^{10} s^{-1}
1000	0.0483	0.0808	0.124	0.102	0.535	0.716
2000	0.810	0.912	0.241	0.684	0.823	1.02
3000	5.03	5.20	0.449	2.48	1.23	1.43
4000	19.7	19.9	0.799	6.52	1.77	1.96
5000	57.8	57.6	1.36	13.8	2.48	2.62
6000	137	136	2.21	25.2	3.36	3.43
7000	276	275	3.44	40.7	4.44	4.40
8000	487	485	5.11	59.9	5.69	5.53
9000	770	769	7.26	81.6	7.10	6.79
10000	1110	1110	9.86	104	8.61	8.17

According to the simple rule, called the energy gap law,[24] it is generally assumed that the rate of a non-radiative transition between two electronic states becomes larger if the energy difference between the states decreases. This simple rule is limited to non-displaced potential energy surfaces. In the present case, where the potential surfaces are strongly displaced, the rate increases with increasing energy gap. When the Duschinsky rotation is excluded in the rate calculation, the increase of the rate is five orders of magnitude for energy gaps from 1000 to 10000 cm^{-1}. On the other hand, it increases only three orders of magnitude when the Duschinsky rotation is present. This is due to fact that the Duschinsky rotation mixes many modes so that the Franck–Condon factors become less sensitive to an energy gap change.

CONCLUSIONS

We have studied The $S_1 \rightarrow T_1$ intersystem crossing rate in uracil was studied using the time-dependent approach. Three different rate equations were used. The first uses an exact correlation function and the second and third are approximations. The first approximation is the second-order cumulant expansion of the correlation function. The second approximation is an expansion of the cumulant formula up to the second order in time. This is the short-time approximation.

Since the normal modes of the singlet and triplet potential energy surfaces are different, the Duschinsky transformation between the normal modes was introduced. It relates the normal modes of the singlet and triplet states by translation and rotation.

It was found that the time-dependent approach gave similar rates as they were obtained using the time-independent approach. Furthermore, the issue of the necessity to include the Duschinsky rotation of the normal modes was examined. It was found that for adiabatic energy gaps larger than 6000 cm^{-1}, there was a good agreement between the rates obtained with and without the Duschinsky rotation. In addition, for these adiabatic energy gaps, the rates obtained using the cumulant expression and the correlation function, when the Duschinsky mixing was excluded, were practically the same. As it is easier to calculate the cumulant expansion than the complete correlation function, this result looks promising for the application of this method to molecules with a large number of normal modes. For energy gaps below 6000 cm^{-1}, it is necessary to include the Duschinsky mixing in order to obtain qualitatively the rate. Although crude, the short-time approximation is easy to calculate and it can serve as a first estimate of the rate.

Acknowledgements. The author acknowledges Professors M. Perić (Belgrade), C. M. Marian (Duesseldorf) and J. Tatchen (Dusseldorf) for helpful discussions and the Ministry of Science and Technological Development of Serbia for the financial support (Contract No. 172040).

ИЗВОД

УЛОГА РОТАЦИЈЕ ДУШИНСКОГ У ИНТЕРСИСТЕМСКИМ ПРЕЛАЗИМА: СТУДИЈА О УРАЦИЛУ

МИХАЈЛО ЕТИНСКИ

Факултет за физичку хемију, Универзитет у Београду, Студентски трг 12–16, п. пр. 47, 11158 Београд

Константа брзине интерсистемских прелаза између најнижег побуђеног синглетног и триплетног електронског стања урацила је проучавана помоћу *ab initio* метода. Константа брзине је израчуната користећи временски зависан прилаз заснован на корелационој функцији и њеним двема апроксимацијама: кумулантном развоју другог реда и апроксимацији кратког времена. Нормални модови синглетног и триплетног стања су повезани трансформацијом Душинског, тј. помоћу ротације и транслације. Нађено је да је за синглетно–триплетне адијабатске енергетске процепе испод 6000 cm^{-1} укључивање ротације Душинског неопходно за добијање квантитативних резултата. Изнад 6000 cm^{-1}, константе брзине добијене са ротацијом Душинског и без ње су сличне. Кумулатни развој добро апроксимира корелациону функцију. Апроксимација кратког времена, иако груба, може се користити као прва процена константе брзине.

(Примљено 13. јула 2011)

REFERENCES

1. M. Klessinger, J. Michl, *Excited States and Photochemistry of Organic Molecules*, VCH Publishers, New York, 1995
2. N. J. Turro, V. Ramamurthy, J. C. Scaiano, *Principles of Molecular Photochemistry*, University Science Books, Sausalito, CA, USA, 2009
3. W. Domcke, D. R. Yarkony, H. Köppel, *Conical Intersections: Electronic Structure, Dynamics and Spectroscopy*, World Scientific, Singapore, 2004
4. C. E. Crespo-Hernández, B. Cohen, P. M. Hare, B. Kohler, *Chem. Rev*. **104** (2004) 1977
5. C. T. Middleton, K. de La Harpe, C. Su, Y. K. Law, C. E. Crespo-Hernández, B. Kohler, *Annu. Rev. Phys. Chem.* **60** (2009) 217
6. B. Kohler, *J. Phys. Chem. Lett.* **1** (2010) 2047
7. Y. He, C. Wu, W. Kong, *J. Phys. Chem., A* **107** (2003) 5143
8. Y. He, C. Wu, W. Kong, *J. Phys. Chem., A* **108** (2004) 943
9. M. Busker, M. Nispel, T. Häber, K. Kleinermanns, M. Etinski, T. Fleig, *Chem. Phys. Chem*. **9** (2008) 1570
10. J. González-Vázquez, L. González, E. Samoylova, T. Schultz, *Phys. Chem. Chem. Phys*. **11** (2009) 3927
11. M. Etinski, T. Fleig, C. M. Marian, *J. Phys. Chem., A* **113** (2009) 11809
12. P. M. Hare, C. E. Crespo-Hernández, B. Kohler, *J. Phys. Chem., B* **110** (2006) 18641
13. M. Etinski, C. M. Marian. *Phys. Chem. Chem. Phys*. **12** (2010) 15665
14. P. M. Hare, C. E. Crespo-Hernández, B. Kohler, *Proc. Nat. Acad. Sci. U.S.A.* **104** (2007) 435
15. F. Duschinsky, *Acta Physicochim. USSR* **7** (1937) 551
16. G. M. Sando, K. G. Spears, J. T. Hupp, P. T. Ruhoff, *J. Phys. Chem., A* **105** (2001) 5317
17. M. Etinski, J. Tatchen, C. M. Marian, *J. Chem. Phys*. **134** (2011) 154105
18. O. Christiansen, H. Koch, P. Jørgensen, *Chem. Phys. Lett*. **243** (1995) 409
19. T. H. Dunning, *J. Chem. Phys*. **90** (1989) 1007

20. R. A. Kendall, T. H. J. Dunning, R. J. Harrison, *J. Chem. Phys.* **96** (1992) 6796
21. M. Kleinschmidt, J. Tatchen, C. M. Marian. *J. Comp. Chem.* **23** (2002) 824
22. B. A. Hess, C. M. Marian, U. Wahlgren, O. Gropen, *Chem. Phys. Lett.* **251** (1996) 365
23. M. Etinski, C. M. Marian. *Phys. Chem. Chem. Phys.* **12** (2010) 4915
24. R. Englman, J. Jortner, *Mol. Phys.* **18** (1970) 145.

Journal of the Serbian Chemical Society
JSCS-info@shd.org.rs • www.shd.org.rs/JSCS
J. Serb. Chem. Soc. 76 (12) 1661–1671 (2011)
JSCS–4238
UDC 546.46'72–31+665.652.7:54–32.004.12+54–36.004.12
Original scientific paper

Mg–Fe-mixed oxides derived from layered double hydroxides: a study of the surface properties

MILICA S. HADNAĐEV-KOSTIĆ[1*#], TATJANA J. VULIĆ[1#], RADMILA P. MARINKOVIĆ-NEDUČIN[1#], ALEKSANDAR D. NIKOLIĆ[2] and BRANISLAV JOVIĆ[2]

[1]*Faculty of Technology, University of Novi Sad, Bul. Cara Lazara 1, 21000 Novi Sad and* [2]*Faculty of Science, University of Novi Sad, Serbia*

(Received 29 April, revised 1 June 2011)

Abstract: The influence of surface properties on the selectivity of the synthesized catalysts was studied, considering that their selectivity towards particular hydrocarbons is crucial for their overall activity in the chosen Fischer–Tropsch reaction. Magnesium- and iron-containing layered double hydroxides (LDH), with the general formula: $[Mg_{1-x}Fe_x(OH)_2](CO_3)_{x/2}\cdot mH_2O$, $x = n(Fe)/(n(Mg)+n(Fe))$, synthesized with different Mg/Fe ratio and their thermally derived mixed oxides were investigated. Magnesium was chosen because of its basic properties, whereas iron was selected due to its well-known high Fischer-Tropsch activity, redox properties and the ability to form specific active sites in the layered LDH structure required for catalytic application. The thermally less stable multiphase system (synthesized outside the optimal single LDH phase range with additional Fe-phase), having a lower content of surface acid and base active sites, a lower surface area and smaller fraction of smaller mesopores, showed higher selectivity in the Fischer-Tropsch reaction. The results of this study imply that the metastability of derived multiphase oxides structure has a greater influence on the formation of specific catalyst surface sites than other investigated surface properties.

Keywords: Mg–Fe-LDHs; hydrotalcite; acid–base properties; Fischer–Tropsch reaction; selectivity.

INTRODUCTION

The Fischer–Tropsch (FT) reaction is an alternative route for converting syngas and entails the production of hydrocarbons in the presence of various metal-based catalysts. This reaction has been commercially used for many years and is still attracting much attention as a means of producing transportation fuels from coal, natural gas and biogas.[1–3] Iron-based catalysts are particularly used in the

* Corresponding author. E-mail: hadnadjev@tf.uns.ac.rs
# Serbian Chemical Society member.
doi: 10.2298/JSC110429149H

FT reaction due to their high activity and selectivity in syngas conversion with low H_2/CO ratios. Previous work on iron FT reaction catalyst focused on the improvement of the performances of Fe catalysts by various metal promoters.[3,4] This paper presents a study of the surface properties and catalytic performance of Mg–Fe-mixed oxides derived from layered double hydroxides (LDHs), synthesized within and outside the optimal range for attaining an LDH single phase. The possibility to vary the nature and content of M(II) and M(III) metals, the synthesis parameters and methods, enabling the design of LDH properties taking into consideration their future application, made these materials the subject of numerous investigations, especially in the field of environmental research. The LDH structure consists of positively charged layers compensated with anions positioned in the interlayers.[5] The layered structure collapses during thermal treatment leading to the formation of non-stoichiometric mixed oxides with a developed surface area, and specific acid–base and redox properties.[6] Mg–Fe-LDHs described by the formula $[Mg_{1-x}Fe_x(OH)_2](CO_3)_{x/2}\cdot mH_2O$, where x = Fe/[Mg+Fe] were studied. Magnesium was chosen as the M(II) ion because of its basic properties and the ability to enhance the selectivity towards FT products of iron catalysts.[4] In addition, according to the literature, mixed oxides obtained by thermal decomposition of LDHs can promote base-catalyzed reactions, particularly when the anions arranged in the interlayers are CO_3^{2-} anions, due to their important role in the basic properties of LDH structures.[7] Besides its well-known high FT activity, iron was selected as the active M(III) ion due to its redox properties and the ability to form specific active sites in the layered structure required for catalytic application.[8] The acid–base properties in correlation to other physico-chemical properties of the LDHs and their derived mixed oxides were examined. For the detection of the acid properties, pyridine adsorption was selected since, according to the literature,[9] pyridine molecules are excellent for the differentiation between Brønsted and Lewis acid sites on the surfaces of catalysts, as well as for ranking the strength and coordination of Lewis acid sites. The presence and nature of the base-active sites on the surface of the calcined samples were detected by phenol adsorption.

The focal point of this study was to investigate the influence of surface properties on the selectivity of the synthesized samples considering that their selectivity towards particular hydrocarbons is crucial for their overall activity in the FT reaction. The selectivity of the derived Mg–Fe-mixed oxides in the FT reaction was studied in correlation with different catalyst properties obtained by Mg––Fe-LDH synthesis within and outside the optimal range for a LDH single phase, especially with their textural properties, surface composition and morphology.

EXPERIMENTAL

Layered double hydroxides were synthesized by the low supersaturation coprecipitation method at a constant pH (9.6–9.9). Aqueous solution of $Mg(NO_3)_2\cdot 6H_2O$ and $Fe(NO_3)_3\cdot 9H_2O$

were continuously dropwise mixed (4 cm^3 min^{-1}) at a constant pH that was maintained by the simultaneous addition of Na_2CO_3 and NaOH solution.[10] The metal content was varied and two different values of x were chosen, one being $x = 0.3$, inside the optimal range for single LDH phase synthesis ($0.2 \leq x \geq 0.33$) and the other exceeding this range with $x = 0.7$. The samples were denoted according to their starting composition: sample 0.7Mg–0.3Fe ($x = 0.3$) and sample 0.3Mg–0.7Fe ($x = 0.7$). The LDHs were calcined at 500 °C for 5 h in air. Scanning electron microscopy (SEM) was used to analyze the morphology of the LDHs and derived mixed oxides and electron dispersive spectroscopy (EDS) for chemical analysis of the surface (JEOL, JSM-460 LV instrument). The acceleration voltage was 20 kV, with the working distance of 10 mm. Textural characterization of calcined samples (denoted K-), reduced samples (denoted H-) and samples after FT reaction (denoted TR-) was realized by low-temperature nitrogen sorption at –196 °C using Micromeritics ASAP 2010 instrument. The IUPAC classification of pores and the Barret, Joyner and Halend (BJH) method for the pore size distribution were used for the textural analyses. Thermal analysis, thermogravimetry (TG) and differential thermal analysis (DTA), of synthesized samples was performed using a Baehr STA503 instrument (BAEHR, Huellhorst, Germany) in the temperature range from room temperature to 1000 °C, at a heating rate of 5 °C min^{-1} under a static air atmosphere. The acid–base surface properties of the samples were investigated by detecting the amount of pyridine and phenol adsorbed on the surface of the samples using Fourier transform infrared (FTIR) analysis. The surface acidity of the samples was analyzed by the adsorption of pyridine on the sample surfaces. The calcined samples were degassed under a vacuum atmosphere (133.3 Pa) at room temperature for 30 min prior to the adsorption of pyridine. The pyridine was chemisorbed on the surface of the samples at room temperature under the vacuum atmosphere for 7 h. The surface base properties were analyzed by the adsorption of phenol on the sample surfaces. The same procedure was used for the adsorption, the only difference being the phenol chemisorption time was 24 h. The FTIR spectra of the previously adsorbed pyridine or phenol on the surface of the calcined samples were recorded in the range of 4000––400 cm^{-1} with a 2 cm^{-1} resolution on a Thermo Nicolet Nexus 670 FTIR spectrophotometer. Prior to the FTIR analysis, physically adsorbed pyridine or phenol was removed from the calcined samples under vacuum.[11] Selectivity tests were performed in a tubular quartz reactor in which the chosen catalysts were loaded. The entire reactor system was placed inside a temperature-regulated furnace. All the catalysts were *in situ* activated, prior to the FT investigation, at 350 °C for 2 h by the reduction treatment with pure hydrogen flow of 20 ml/min. After the reduction of the samples, the gas flow of reactants H_2 and CO having ratio of H_2:CO = 1:1 was adjusted and regulated by mass flow controllers. The FT reaction temperature was either 350 °C, 375 °C or 400°C. After passing through the reactor system, aliquots of the reaction mixture were taken with the syringe and analyzed. The reaction products were separated on a 30 m long PONA GC-capillary column and analyzed by gas chromatography using an HP 5890 Series II instrument equipped with thermal conductivity (TC) and flame ionization (FI) detectors. The selectivity (S) of catalysts was calculated using the following formula:

$$S = 100 \frac{F_x nC_x A_x}{\sum \left(F_{\text{product}} nC_{\text{product}} A_{\text{product}} \right)} \left[\% \right]$$

where S – selectivity, F – detector response factor, x – desired product, nC – number of C atoms in the product and A – value of the surface under the peak.

RESULTS AND DISCUSSION

Characteristic X-ray diffraction patterns for LDH were detected in both samples, LDH being the only crystalline phase in the $x = 0.3$ sample, whereas in the $x = 0.7$ sample, an additional goethite, FeO(OH), phase was also observed as published elsewhere.[10]

In order to determine the temperature leading to thermal decomposition of the LDHs, as well as to the formation and thermal stability of the mixed oxides, thermal analysis (TG-DTA) was performed. The mass loss and the corresponding endothermic/exothermic transitions of the synthesized Mg–Fe-LDH samples were simultaneously monitored. Two distinct transitions were observed on the TG–DTA curves of both samples (Fig. 1). The first endothermic transition in the temperature range from 90 to 200 °C accompanied by a mass loss is related to the dehydration of the samples, removal of the interlayer water and physically adsorbed water. The second endothermic transition, also accompanied by a mass loss, occurring in the temperature range from 300 to 400 °C, was assigned to dehydroxylation and decarbonation reactions. At higher temperatures (≈500 °C), broad endothermic peaks without mass loss were detected, probably due to spinel formation and Mg oxides. These findings are in good agreement with the literature.[12–14] Since in both samples the second endothermic transition was detected at temperatures lower than 500 °C, it was concluded that this temperature is sufficient for completion of the formation of mixed oxides and was selected as the calcination temperature. A comparison between the starting temperatures of spinel formation at ≈650 °C, corresponding to the beginning of the third endothermic peak in the sample 0.7Mg–0.3Fe, and at ≈550 °C for the sample 0.3Fe––0.7Mg suggests the formation of a mixed oxide phase in the single LDH phase sample 0.7Mg–0.3Fe which is more thermally stable at higher temperatures.

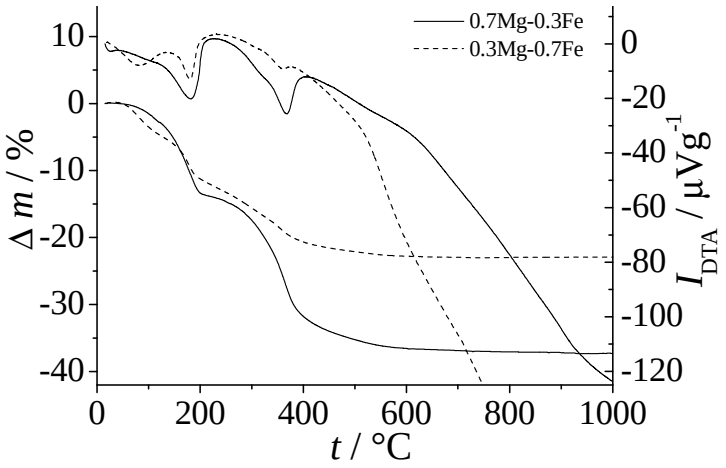

Fig. 1. TG–DTA Profiles of 0.7Mg–0.3Fe-LDH and 0.3Mg–0.7Fe-LDH.

For qualitative and quantitative analysis (EDS), Fig. 2, two locations for each synthesized sample (LDH-0.7Mg–0.3Fe and LDH-0.3Fe–0.7Mg) were used for the generation of EDS spectra. The provided elemental information revealed that the Mg and Fe contents on the surface of the samples are in good agreement with the targeted Mg/Fe ratios (sample 0.7Mg–0.3Fe: 70 mol % Mg and 30 mol % Fe, sample 0.3Mg–0.7Fe: 30 mol% Mg and 70 mol % Fe), confirming the successful synthesis of both samples. The pore size distributions of synthesized samples after calcination (K-0.7Mg–0.3Fe and K-0.3Mg–0.7Fe) and after the reduction treatment (H-0.7Mg–0.3Fe and H-0.3Mg–0.7Fe) are shown in Fig. 3. The multimodal pores size distribution of the K-0.7Mg–0.3Fe sample showed a small fraction of smaller mesopores ($d_p \approx 3$ nm) and a broad region with mesopores of 10 to 90 nm in diameter, having a maximum at 15 nm and a "shoulder" at 50 nm, indicating a significant fraction of mesopores. On the contrary, the K--0.3Mg–0.7Fe sample showed a region with mesopores from 20 to 70 nm having a maximum at 40 nm and smaller mesopores were not detected, Fig, 3a. These results are in good agreement with those of a previous study,[10] in which it was found that the presence of additional phases in a K-0.3Mg–0.7Fe sample negatively influenced the development of surface area (50 m^2 g^{-1} compared to 150 m^2 g^{-1} in a K-0.7Mg–0.3Fe sample), thereby disabling the formation of smaller mesopores and shifting the pore size distribution region to higher values.

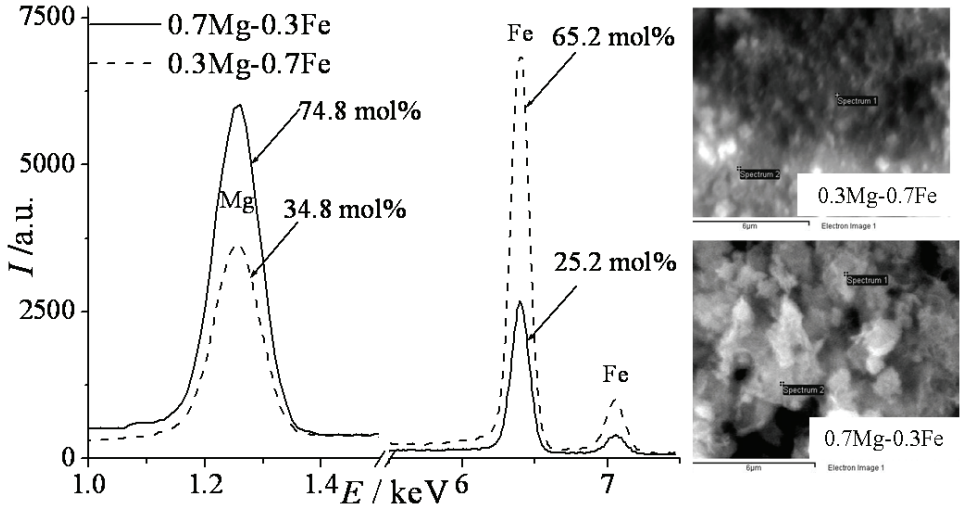

Fig. 2. EDS Analysis of the synthesized samples: 0.3Mg–0.7Fe-LDH and 0.7Mg–0.3Fe-LDH.

The pore size distributions of both calcined samples after the reduction treatment are shown in Fig. 3. It can be observed that after reduction the pore size distribution in both samples had changed. A decrease in a fraction of smaller mesopores and a shift toward higher values for both peak maximum (≈40 nm) and

"shoulder" (60 nm) was observed for the K-0.7Mg–0.3Fe sample, which explains the decrease in surface area (105 m^2 g^{-1}). In the K-0.3Mg–0.7Fe sample, a slight shift in the peak maximum towards mesopores of ≈50 nm diameter and the formation of a small fraction of mesopores with diameter of 3 and 5 nm were detected. The decrease and increase in the mentioned diameter values resulted in an insignificant change in the surface area, from 50 before to 48 m^2 g^{-1} after the reduction.[10] According to the literature, this behavior is explained by the collapse of smaller mesopores in the mixed oxides during the reduction treatment and the formation of mesopores of larger diameters.[4]

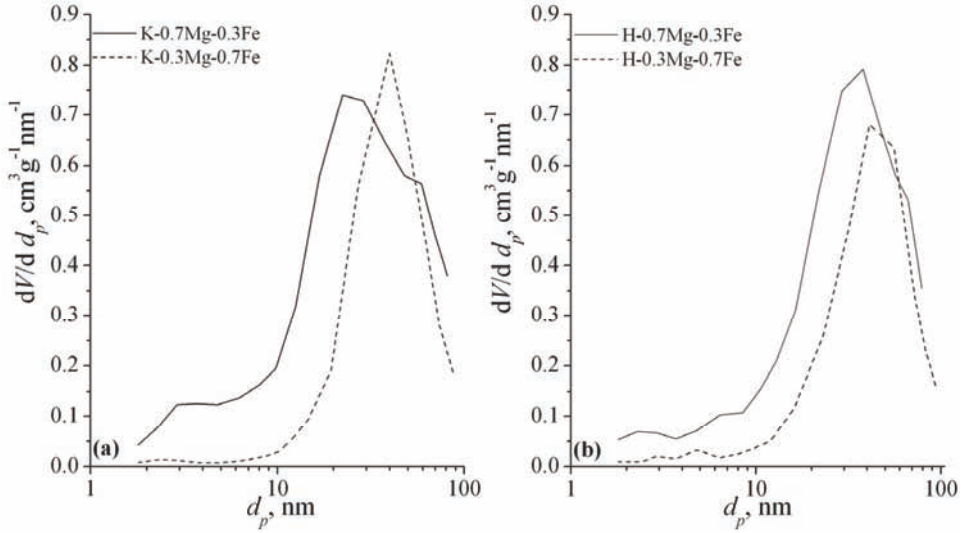

Fig. 3. Pore size distribution of the sample a) after calcination (K-0.7Mg–0.3Fe and K-0.3Mg–0.7Fe) and b) after reduction treatment (H-0.7Mg–0.3Fe and H-0.3Mg–0.7Fe).

The FTIR spectra of the calcined samples and the FTIR spectra of samples after pyridine/phenol adsorption at room temperature in air are presented in Figs. 4 and 5, respectively. Based on the spectra of calcined samples, it can be concluded that all key absorption bands (3455, 2924, 1642 and 1465 cm^{-1}) of the mixed oxides derived from LDH are present with sufficient intensities.[14–16]

The FTIR spectra of the pyridine pre-adsorbed samples are presented in Fig. 5a, in which absorption bands at around 1440 and 1460 cm^{-1} are observed. According to the literature, if an absorption band around 1540 cm^{-1} is detected, this is indicative for pyridinium ions adsorbed on Brønsted acid sites, while bands that appear around 1440 and 1460 cm^{-1} are attributed to coordinatively adsorbed pyridine molecule on Lewis acid sites.[9,17] Therefore, the detected surface acid sites are assigned as Lewis acid sites in both samples. That more intense bands are visible in the spectrum of the K-0.7Mg–0.3Fe-P sample implies a higher num-

ber of acid sites with stronger surface interaction are present on the surface of this sample. The smaller number of acid sites present on the surface of the sample synthesized outside the optimal range for a single phase LDH could be explained by the negative effect of the formation of the additional Fe-phase and smaller fraction of LDH-derived mixed oxide phase.

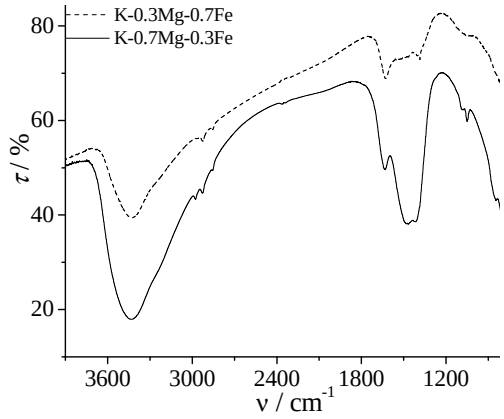

Fig. 4. FTIR Absorption bands of the calcined samples (K-0.7Mg–0.3Fe and K--0.3Mg–0.7Fe).

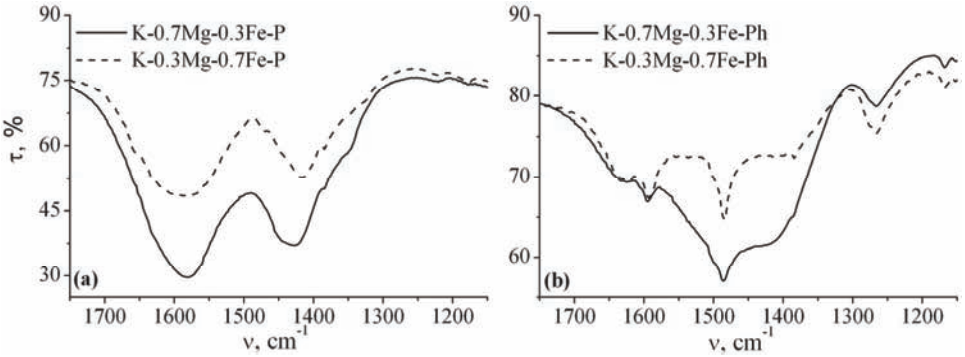

Fig. 5. FTIR Spectra of the calcined samples a) pyridine adsorbed (K-0.7Mg–0.3Fe-P and K-0.3Mg–0.7Fe-P) and b) phenol adsorbed (K-0.7Mg–0.3Fe-Ph and K-0.3Mg–0.7Fe-Ph).

The FTIR analysis of the pre-adsorbed phenol samples (Fig. 5b) showed the presence of absorption bands at around 1604, 1485, 1265 and 1170 cm^{-1} in both samples, assigned to base active sites.[18] According to the literature reference, phenol molecules chemisorbed on base active sites on sample surfaces generate the most intense FTIR absorption bands of their functional groups at wave numbers intervals ranging from 1605–1594, 1485–1475, 1260–1224 and 1180–1170 cm^{-1}. In the spectrum of the sample K-0.7Mg–0.3Fe-Ph with a higher Mg content, more intense peaks related to the adsorbed phenol were detected, indicating a larger number of base active sites on its surface compared to the K-0.3Mg–––0.7Fe-Ph sample. This significant decrease in the number of base active sites on

the K-0.3Mg–0.7Fe-Ph sample surface could be explained by the smaller amount of Mg, the additional Fe-phase and smaller fraction of the LDH-derived mixed oxide phase.

These results support the hypothesis that the FT selectivity should be higher on the K-0.7Mg–0.3Fe-Ph sample due to the higher content of base active sites and the ability of the Mg oxide phase to enhance the selectivity towards FT products of iron catalysts.[4]

The selectivity of all samples at different reaction temperatures (350, 375 and 400 °C) with an H_2:CO ratio of 1:1 are presented in Fig. 6. The sample with the highest Mg content (0.7Mg–0.3Fe), having a larger number of base sites compared to the other sample (0.3Mg–0.7Fe) exhibited lower selectivity at all three reaction temperatures. Comparing the selectivity of samples towards C_4- and C_5-compounds after 100 min of the FT reaction, the sample 0.7Mg–0.3Fe showed low selectivity towards C_4-compounds, while selectivity towards C_5-compounds was not detected despite the variation of the reaction temperature. This low selectivity could be explained by its stable structure, disabling high catalytic performance, observed and published elsewhere.[10] The sample synthesized outside the optimal range and with the highest Fe content showed selectivity towards both C_4- and C_5-compounds after 100 min of FT reaction at all reaction temperatures. Therefore, although the K-0.7Mg–0.3Fe sample, synthesized within the optimal range for single phase LDH, has a larger number of base active sites on the surface, the K-0.3Mg–0.7Fe sample showed higher selectivity, Fig. 6, at all three FT reaction temperatures, implying that other surface properties also have a great impact on catalytic selectivity in the chosen reaction.

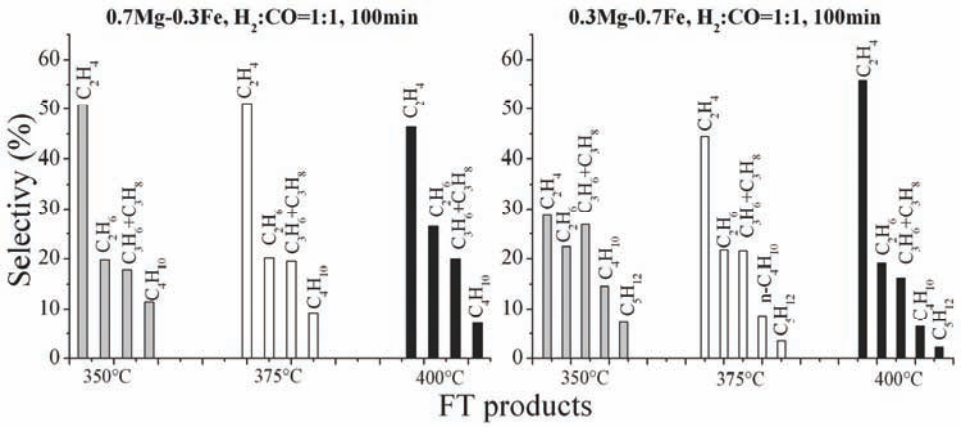

Fig. 6. Selectivity of calcined samples after the reduction process at different FT reaction temperatures after 100 min of the reaction.

The results of textural analysis of both reduced samples before and after the FT reactions at different temperatures are presented in Figs. 7 and 8. The surface area of the reduced H-0.7Mg–0.3Fe sample had not changed significantly after the FT reaction at 350 °C, being also the temperature for the reduction treatment. With increasing FT reaction temperature, the surface area increased, as well as the amount of both larger mesopores (30–40 nm) and the amount of smaller mesopores (2–3 nm), Fig. 8a. This could be explained by the "prolonged" calcinations, evolution of the remaining, trapped carbonates and by the influence of the formed FT products. The increase in surface area, together with better acid––base properties, did not have positive effects on the selectivity in the FT reaction.

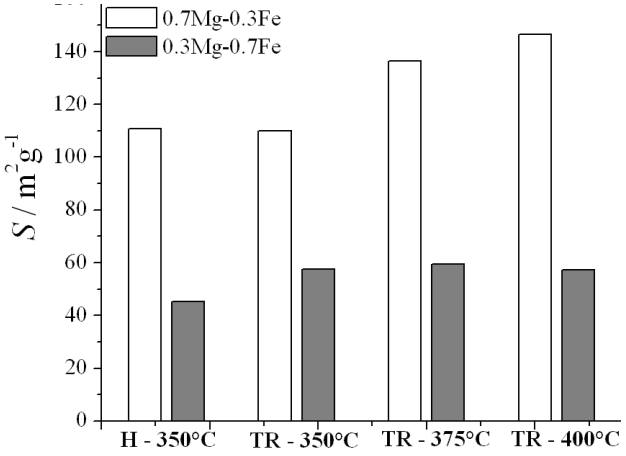

Fig. 7. Surface areas of the reduced, calcined samples before (H – 350 °C) and after FT reactions at different temperatures (TR – 350 °C, TR – 375 °C, TR – 400 °C).

In the sample 0.3Mg–0.7Fe, the surface area slightly increased during the FT reaction, but did not change significantly with change in the reaction temperature, although a small change in the pore size distribution was observed. With increasing reaction temperature, the fraction of larger mesopores in range from 35 to 45 nm decreased with the simultaneous increase in fraction of smaller mesopores in range from 2 to 4 nm (Fig. 8b), resulting in no significant change in the values of surface area (Fig. 7). It should be noted that TG/DTA analysis revealed that the formation of the spinel phase commenced at lower temperatures (≈550 °C) in the sample 0.3Mg–0.7Fe, indicating a less stable structure compared to the 0.7Mg–0.3Fe sample (≈650 °C). Although having a smaller surface area and smaller number of acid–base sites, the 0.3Mg–0.7Fe sample showed higher selectivity towards the desired products in the FT reaction. This is probably due to its metastable structure of a non-stoichiometric mixed oxide, which has a greater influence on the formation of active sites on the catalyst surface than the other investigated surface properties.

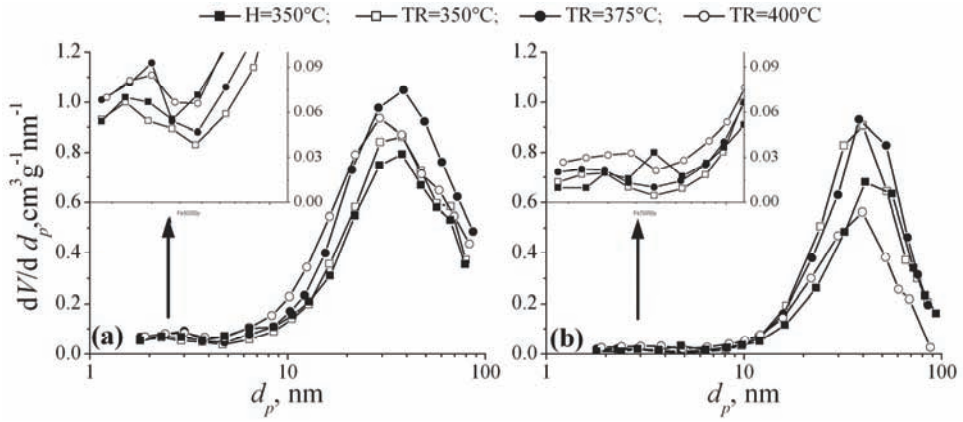

Fig 8. Pore size distribution of samples a) 0.7Mg–0.3Fe and b) 0.3Mg–0.7Fe after the reduction treatment and after FT reactions at different temperatures.

CONCLUSIONS

The characterization of the Mg–Fe-LDH samples confirmed their successful synthesis having an Mg–Fe content in good agreement with desired Mg/Fe ratio set before the synthesis. The properties of the mixed oxides obtained by thermal treatment and their surface properties were highly influenced by the Mg/Fe ratio. Thermal analysis of the synthesized LDHs revealed the formation of more stable mixed oxides when originating from the single LDH phase sample compared to the sample synthesized outside the optimal range. The metastable multiphase system (LDH and additional Fe-phase) with a lower number of surface acid and base active sites, a lower surface area and a smaller fraction of the smaller mesopores showed a higher selectivity in the FT reaction, implying that the metastability of the derived multiphase oxides structure had a greater influence on the formation of active sites on the catalyst surface than the other investigated surface properties.

Acknowledgment. The financial support received from the Ministry of Education and Science of the Republic of Serbia (Contract No. III 45008) is gratefully acknowledged.

И З В О Д

Mg–Fe МЕШОВИТИ ОКСИДИ ДОБИЈЕНИ РАЗГРАДЊОМ ДВОСТРУКИХ СЛОЈЕВИТИХ ХИДРОКСИДА: ИСПИТИВАЊА СВОЈСТАВА ПОВРШИНЕ

МИЛИЦА С. ХАДНАЂЕВ-КОСТИЋ[1], ТАТЈАНА Ј. ВУЛИЋ[1], РАДМИЛА П. МАРИНКОВИЋ-НЕДУЧИН[1], АЛЕКСАНДАР Д. НИКОЛИЋ[2] и БРАНИСЛАВ ЈОВИЋ[2]

[1]Технолошки факултет, Универзитет у Новом Саду, Бул. цара Лазара 1, 21000 Нови Сад и [2]Природно-математички Факултет, Универзитет у Новом Саду

Утицај својстава површине на селективност синтетисаних катализатора је испитиван узимајући у обзир да је селективност према одређеним угљоводоницима од пресудног значаја за укупну активност у одабраној Фишер–Тропш реакцији. Анализирани су двостуки слојевити

хидроксиди са магнезијумом и гвожђем, опште формуле $[Mg_{1-x}Fe_x(OH)_2](CO_3)_{x/2}\cdot mH_2O$, x = = n(Fe)/(n(Mg)+n(Fe)) синтетисани при различитим Mg/Fe односима, као и мешовити оксиди настали њиховом термичком разградњом. Избор градивних метала за синтезу катализатора заснован је на познатим својствима гвожђа, као што су висока активност у Фишер–Тропш реакцији са редокс карактеристикама, као и могућност формирања специфичних активних центара у слојевитој структури LDH; магнезијум је првенствено одабран услед базних својстава одговарајућег оксида. Термички мање стабилан вишефазни систем (синтетисан ван опсега оптималног за синтезу једнофазних LDH са додатном фазом гвожђа) показује већу селективност у Фишер–Тропш реакцији, и поред евидентно мање киселих и базних центара на површини и слабије развијене специфичне површине, уз смањен удео мањих мезопора. Резултати истраживања указују да метастабилност структуре добијених вишефазних оксида има већи утицај на формирање специфичних површинских центара катализатора него остала испитивана својства површине.

(Примљено 29. априла, ревидирано 1. јуна 2011)

REFERENCES

1. K. Kumabe, T. Sato, K. Matsumoto, Y. Ishida, T. Hasegawa, *Fuel* **89** (2010) 2088
2. H. Xiong, M. Moyo, M. A. M. Motchelaho, L. L. Jewell, N. J. Coville, *Appl. Catal., A* **388** (2010) 168
3. N. Lohitharn, J. G. Goodwin, *J. Catal.* **260** (2008) 7
4. J. Yang, Y. Sun, Y. Tang, Y. Liu, *J. Mol. Catal., A* **245** (2006) 26
5. F. Cavani, F. Trifiro, A. Vaccari, *Catal. Today* **11** (1991) 173
6. A. Vaccari, *Catal. Today* **41** (1998) 53
7. V. R. L. Constantino, T. J. Pinnaviaia, *Inorg. Chem.* **34** (1995) 883
8. M. Hadnadjev, T. Vulic, R. Marinkovic-Neducin, Y. Suchorski, H. Weiss, *Appl. Surf. Sci.* **254** (2008) 4297
9. J. A. Lercher, C. Grundling, G. Eder-Mirth, *Catal. Today* **27** (1996) 353
10. M. Hadnađev-Kostić, T. Vulić, R. Marinković-Nedučin, *J. Serb. Chem. Soc.* **75** (2010) 1
11. X. Lei, F. Zhang, L. Yang, X. Guo, Y. Tian, S. Fu, F. Li, D. Evans, X. Duan, *AlChE J.* **53** (2007) 932
12. Z. Yang, K. Choi, N. Jiang, S. Park, *Bull. Korean Chem. Soc.* **28** (2007) 11
13. W. Yanga, Y. Kima, P. Liub, M. Sahimia, T. Tsotsisa, *Chem. Eng. Sci.* **57** (2002) 2945
14. J. Pérez-Ramırez, G. Mul, F. Kapteijn, J. A. Moulijn, *Appl. Catal., A* **204** (2000) 265
15. D. Carriazo, C. Martin, V. Rives, *Eur. J. Inorg. Chem.* (2006) 4608
16. J. T. Kloprogge, R. L. Frost, *J. Solid State Chem.* **146** (1999) 506
17. F. Prinetto, Z. Li, E. Kemnitz, A. Trunschke, J. Deutsch, H. Lieake, A. Auroux, *J. Catal.* **234** (2005) 119
18. I. Poljanšek, M. Krajnc, *Acta Chim. Slovenica* **52** (2005) 238.

Journal of the Serbian Chemical Society
JSCS-info@shd.org.rs • www.shd.org.rs/JSCS
J. Serb. Chem. Soc. 76 (12) 1673–1685 (2011)
JSCS–4239
UDC 542.913–732:546.92'97'811–44:547.262+66.094.3
Original scientific paper

Microwave synthesis and characterization of Pt and Pt–Rh–Sn electrocatalysts for ethanol oxidation

SANJA STEVANOVIĆ[1*#], DUŠAN TRIPKOVIĆ[2#], DEJAN POLETI[3#], JELENA ROGAN[3#], AMALIJA TRIPKOVIĆ[1#] and VLADISLAVA M. JOVANOVIĆ[1]

[1]*Department of Electrochemistry, ICTM, University of Belgrade, Njegoševa 12, Belgrade, Serbia,* [2]*Materials Science Division, Argonne National Laboratory, Argonne, IL 60439, USA and* [3]*Faculty of Technology and Metallurgy, University of Belgrade, Karnegijeva 4, Belgrade, Serbia*

(Received 5, revised 29 April 2011)

Abstract: Carbon-supported Pt and Pt–Rh–Sn catalysts were synthesized by the microwave-polyol method in ethylene glycol solution and were investigated in the ethanol electro-oxidation reaction. The catalysts were characterized in terms of structure, morphology and composition employing the X-ray diffraction (XRD), scanning tunneling microscopy and energy-dispersive X-ray spectroscopy techniques. The STM analysis indicated rather uniform particles and particle sizes below 2 nm for both catalysts. The XRD analysis of the Pt/C catalyst revealed two phases, one with the main characteristic peaks of the face-centered cubic crystal structure (*fcc*) of platinum and the other related to the graphite-like structure of the carbon support, Vulcan XC-72R. However, in the XRD pattern of the Pt–Rh–Sn/C catalyst, diffraction peaks for Pt, Rh or Sn could not be resolved, indicating extremely low crystallinity. The small particle sizes and homogeneous size distributions of both catalysts could be attributed to the advantages of the microwave-assisted modified polyol process in ethylene glycol solution. The Pt–Rh–Sn/C catalyst was highly active for ethanol oxidation with the onset potential shifted by more than 150 mV to more negative values and with currents nearly 5 times higher in comparison to the Pt/C catalyst. The stability tests of the catalysts, as studied by chronoamperometric experiments, revealed that the Pt–Rh–Sn/C catalyst was evidently less poisoned than the Pt/C catalyst. The increased activity of Pt–Rh–Sn/C in comparison to Pt/C catalyst was most probably promoted by the bi-functional mechanism and the electronic effect of the alloyed metals.

Keywords: Pt–Rh–Sn catalyst; ethanol oxidation; polyol synthesis; microwave irradiation; STM.

* Corresponding author. E-mail: sanjat@tmf.bg.ac.rs
# Serbian Chemical Society member.
doi: 10.2298/JSC110405166S

INTRODUCTION

High surface area carbon-supported Pt and Pt-alloys are widely proposed as promising anode catalysts in direct alcohol fuel cells (DAFCs).[1] Platinum is an excellent catalyst for the adsorption and dissociation of small organic molecules. However, platinum itself is known to be rapidly poisoned by reaction intermediates, such as CO, that are formed by dehydrogenation of the alcohol molecule[2] and limited ability for cleavage of C−C bonds. The most common fuel besides methanol is ethanol, which is less toxic and can be easily produced by fermentation of sugar-containing biomass. The oxidation mechanism of ethanol in acid solution may be summarized in the following schema of parallel reactions:[1]

$$CH_3CH_2OH \rightarrow [CH_3CH_2OH]_{ad} \rightarrow C1_{ad}, C2_{ad} \rightarrow CO_2 \text{ (total oxidation)} \quad (1)$$

$$CH_3CH_2OH \rightarrow [CH_3CH_2OH]_{ad} \rightarrow CH_3CHO \rightarrow CH_3COOH \text{ (partial oxidation)} \quad (2)$$

Differential mass spectrometry (DEMS) and *in situ* infrared spectroscopy (FTIR) determined acetaldehyde (CH_3CHO) and acetic acid (CH_3COOH) as the main products of the oxidation of ethanol in acidic solution, with carbon dioxide (CO_2) appearing at very high positive potentials.[3,4] The efficiency of C−C bond cleavage is the key to enable this reaction to be useful in fuel cell applications and thus, the major challenge is to achieve total oxidation of ethanol to CO_2 at low overpotentials. Efforts in this sense have been focused on the addition of co-catalysts, such as Ru, Rh, W, Pd, Sn, *etc*.[1,5–10] The addition of metals such as Sn or Ru, even though beneficial for the overall electrochemical activity of the catalysts for ethanol oxidation, does not enhance the yield of CO_2, *i.e*., C−C bond breakage.[4,11] On the other hand, the addition of Rh to Pt improves the activation for C−C bond dissociation, but does not enhance the overall electrochemical reaction.[9,10] Thus, a good electrocatalyst for ethanol oxidation should have, besides Pt, both kind of metals that would improve dehydrogenation, C−C bond dissociation and CO–O coupling.[9] Different ternary catalysts have been described in the literature[1] (and references therein), but although PtSn appears to enhance ethanol oxidation better than other bimetallic catalysts and presence of Rh significantly increases C−C bond breakage, there are only a few data on ternary Pt catalyst with Sn and Rh.[12–14] Colmati *et al*.[12] investigated the activity for ethanol oxidation of Pt–Rh–Sn catalysts and found that at potentials higher than 0.45 V *vs*. RHE, the alloy possessed the highest activity for this reaction, while at potentials more negative than 0.45 V, the activity was lower than that of the binary PtSn catalyst. Kowal *et al*.[13] indicated that Pt–Rh–SnO_2 exhibited higher activity than $PtSnO_2$ even at lower potentials. The extent of activity of such catalyst depends strongly on the SnO_2 content.[14]

In general, metal catalytic activity is considerably dependent on the particle shape, size and particle size distribution.[15] A variety of methods can be used for nanocatalyst preparation, such as wet impregnation, sonochemical method, che-

mical reduction of metal precursors, *etc*. In the last decade, Pt or Pt-based nanoclusters with small particle size and narrow size distribution have often been synthesized by the polyol method.[16] This procedure, as most of the other conventional methods, requires longer treatment of metal precursors at a high temperature. To overcome the arduous processes, in recent years, microwave irradiation has been widely used for the preparation of nanomaterials. Compared with conventional preparation methods, microwave synthesis has the advantages of very short heating time and uniform heating of the substance, leading to a small particle size, narrow particle size distribution and high purity. Yu *et al*.[17] suggested that these advantages could be attributed to fast homogenous nucleation and growth of metal particles.

The goal of this work was to examine ethanol oxidation on a carbon-supported Pt–Rh–Sn catalyst synthesized by the microwave-assisted polyol method. This procedure for the preparation of the previously mentioned catalyst, to the best of our knowledge, has not hitherto been described in the literature.

EXPERIMENTAL

Preparation of Pt and Pt–Rh–Sn/C electocatalysts

To prepare Pt–Rh–Sn catalyst, a mixture of 0.5 ml of 0.05 M H_2PtCl_6, 0.5 ml of 0.1 M $SnCl_2$ solution and 0.5 ml 0.05M of $RhCl_3$ was mixed with 25 ml of ethylene glycol (EG) in a 100 ml beaker under magnetic stirring. Then 0.8 M NaOH was added drop wise to adjust the pH to ≈12. The same procedure was used to synthesize the Pt catalyst. In each case, the beaker was placed in the center of a domestic microwave oven and heated 60 s for the Pt and 90 s for Pt–Rh–Sn catalyst at 700 W. After microwave heating, the mixture was uniformly mixed with 20 ml of an aqueous suspension of Vulcan XC-72 carbon (containing 20 mg of carbon in the case of Pt catalyst and 53.5 mg of carbon in the case of Pt–Rh–Sn catalyst) and 150 ml of 2 M H_2SO_4 solution for 3 h under magnetic stirring. The resulting suspension was filtered and the residue was washed with high purity water. The solid product was dried at 160 °C for 3 h under a N_2 atmosphere. The metal loading for both catalysts should have been ≈20 wt. %. Thermogravimetric analysis (TGA) confirmed 19 wt. % for Pt/C, while for Pt–Rh–Sn/C, a lower loading of metal (≈11 wt. %) was found.

Characterization of the Pt/C and Pt–Rh–Sn/C electrocatalysts

Thermogravimetry (TG) and differential thermal analyses (DTA) were performed simultaneously (30–800 °C temperature range) on a SDT Q600 TGA/DSC instrument (TA Instruments). The heating rate was 20 °C min^{-1} and the sample mass was less than 10 mg. The furnace atmosphere consisted of air at a flow rate of 100 cm^3 min^{-1}.

The unsupported Pt and Pt–Rh–Sn nanoparticles were characterized by scanning tunneling microscopy (STM). Samples were prepared by applying a few drops of a diluted colloidal solution of catalyst on a hot HOPG plate. The STM characterizations were realized using a NanoScope III A (Veeco, USA) microscope. The images were obtained in the height mode using a Pt–Ir tip (set-point current, I_t, from 1 to 2 nA, bias voltage, V_b = –300 mV). The mean particle size and size distribution were acquired from several randomly chosen areas of the STM images containing about 50 particles.

X-Ray diffraction (XRD) patterns of the powder catalysts were recorded with an Ital Structure APD2000 X-ray diffractometer in Bragg–Brentano geometry using CuK_α radiation (λ = 0.15418 nm) in the step-scan mode (range: 15−85° 2θ, step-time: 2.50 s, step-width: 0.02°). The program PowderCell [18] was used for phase analysis and calculation of the unit cell parameters.

Microstructural examination was performed by scanning electron microscopy (SEM). An XL 30 environmental scanning microscope with a field emission gun (ESEM–FEG) (manufactured by FEI, The Netherlands) equipped with an energy dispersive X-ray (EDX) spectrometer was used. The samples were inspected using 5, 10 and 20 kV acceleration voltages at magnifications of 20000× and 10000×.

The electrocatalytic activity of the catalysts was investigated by potentiodynamic and chronoamperometric tests using an Autolab potentiostat/galvanostat (ECO Chemie, The Netherlands) and a three-electrode compartment cell at room temperature. The working electrode was a thin layer of Nafion-impregnated Pt/C or Pt–Rh–Sn/C catalyst applied on a glassy carbon disk electrode with a loading of 10 μg cm^{-2} of the catalyst counted on metal content. The thin layer was obtained from a suspension of 2 mg of the Pt–Rh–Sn/C or 1 mg of Pt/C catalyst in a mixture of 1 ml water and 50 μl of 5 % aqueous Nafion solution, prepared in an ultrasonic bath, placed onto the substrate and dried at room temperature. A Pt wire and a saturated calomel electrode (SCE) were used as the counter and reference electrode, respectively. The electrocatalytic activity of the as-prepared Pt/C and Pt–Rh–Sn/C was studied in 0.1 M $HClO_4$ + 0.5 M C_2H_5OH solution. The electrolyte was prepared with high purity water and deaerated with N_2. Ethanol was added to the supporting electrolyte solution while holding the electrode potential at –0.2 V. The potential was then cycled up to 0.3 V, *i.e.*, the potential range of technical interest (E < 0.4 V), at sweep rate of 20 mV s^{-1}. Current–time transient curves were recorded after immersion of the freshly prepared electrode in the solution at –0.2 V for 2 s followed by stepping the potential to 0.2 V and holding the electrode at this potential for 30 min.

RESULTS AND DISCUSSION

Catalysts characterizations

The particle size and surface morphology of the unsupported Pt and Pt–Rh–Sn catalysts were characterized by STM. As observed from the top view of the STM images (Fig. 1), both catalysts had rather uniform particles of small diameter. Most of particles were spherical in shape. Cross section analysis (Fig. 1) confirmed particle sizes of < 1.7 nm for both catalysts (Table I).

The Pt/C and Pt–Rh–Sn/C catalysts were characterized by X-ray powder diffraction analysis. The XRD patterns of the carbon-supported catalysts are shown in Fig. 2. Two phases were identified in the Pt/C pattern, one with the main characteristic peaks of the face-centered cubic crystal structure (*fcc*) of platinum (111, 200, 220 and 311) and the other with a diffraction peak at around 2θ 25° related to the graphite-like structure of the Vulcan XC-72R carbon support. The XRD peaks of the Pt–Rh–Sn/C catalyst were rather broad and diffraction peaks for Pt, Rh and Sn in the catalyst could not be separately resolved, indicating a small metal content and a very low crystallinity or an amorphous form of the catalyst. Since TGA analysis revealed the presence of only 11 wt. % of the metals

in the supported catalyst and the STM analysis showed very small particle size, the low metal fraction and low crystallinity could be the reason for the obtained XRD pattern of the Pt–Rh–Sn/C catalyst. The mean particle size for the Pt/C catalyst calculated by the Scherrer formula[19] was larger than that obtained by STM (Table I), possibly because unsupported catalysts were used for the STM analysis. Still, the agreement can be described as good because the values calculated by the Scherrer formula also account for a very probable lattice stress.

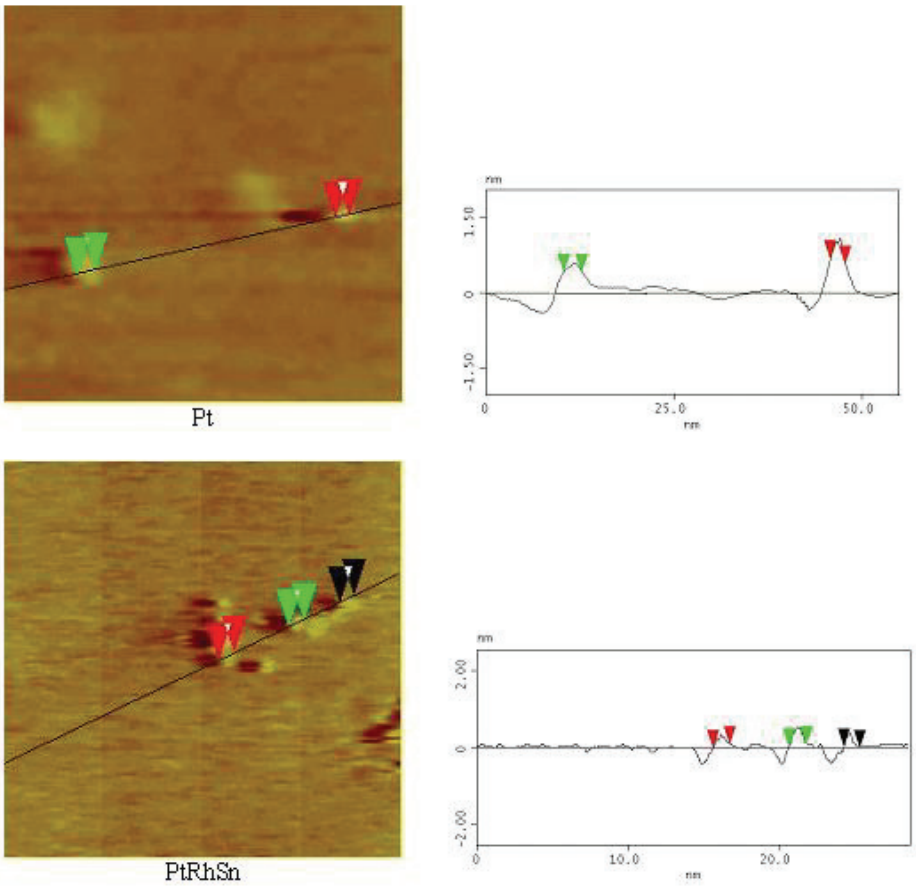

Fig. 1. STM Images and height profiles of the Pt catalyst (50×50 nm^2×4 nm) and Pt–Rh–Sn catalyst (30×30 nm^2×4 nm).

The small particle sizes and homogeneous size distributions of both catalysts could be attributed to the advantages of the microwave-assisted modified polyol process in which ethylene glycol (EG) and hydroxide are used as stabilizers. The metal salts and hydroxide react to form colloidal metal hydroxide particles, which are reduced to metal nanoclusters by EG.[16] In this process, pH value of the

TABLE I. Characteristics of the Pt/C and Pt–Rh–Sn/C catalysts obtained by STM, XRD and EDX analysis

Catalyst	Particle size, nm		Unit cell parameter (XRD), a / nm	Elemental composition (Pt:Rh:Sn), at. %	
	STM	XRD		Nominal	EDX
Pt/C	1.7±0.3	2.5	0.3944		
Pt–Rh–Sn/C	1.2±0.3	–	–	25:25:50	46:32:22

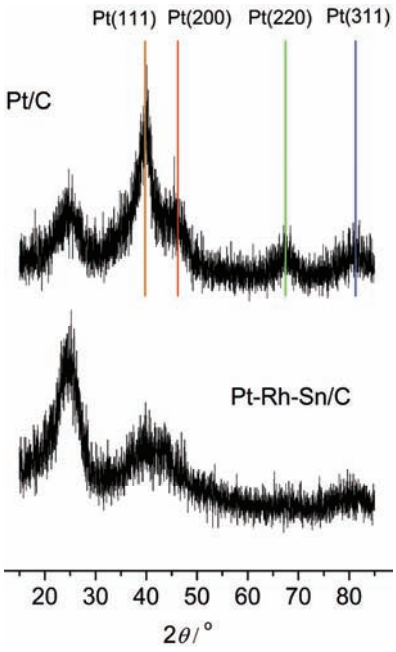

Fig. 2. XRD Patterns of the Pt /C and Pt–Rh–Sn/C catalysts.

solution is very important for obtaining stable metal particles. Hydroxide/metal molar ratio depends on the metal in question and is characteristic of electrostatic stabilization of metal colloids by the adsorbed anions.[16] EG acting as both reaction and dispersion media can efficiently adsorb and stabilize the surface of the particles[20] and favor the production of monodispersed metal particles with good dispersivity.[17] The high viscosity of this compound also helps in preventing agglomeration of the nanoparticles and for this reason, the water content in the reaction solution effects this process as well as the reaction temperature in influencing the particle size and size distribution.[21] Since EG has a large permanent dipole, it is very susceptible to microwave irradiation, which can absorb the energy from the microwave field and the polar reaction solution is heated up to a high temperature instantaneously.[22] Nevertheless, the heating rate of EG dispersion system could be affected by parameters of microwave operation, such as irradiation time, amount of dielectric and additives.[23] The fast and uniform microwave heating reduces the temperature and concentration gradients, thus accele-

rating the reduction of the metal ions and the formation of metallic nuclei.[24–27] In processes with plurality of pathways and activation barriers, according to Rao *et al*.[26], microwaves might promote the pathway with the lowest activation barrier.

EDX Analysis of the Pt–Rh–Sn/C surface composition gave 48 at. % Pt and 32 at. % Rh and 20 at. % Sn for the Pt–Rh–Sn alloy (Table I), which deviates from the nominal composition in the initial mixture (25:25:50).

Bearing in mind the aforesaid, the irradiation time in the microwave heating together with NaOH/metal and EG/water ratios used in the synthesis of both catalyst were probably the reason for the so small particle size obtained, and also for the yield of the metal and the catalyst composition.

Electrochemical performances

Ethanol oxidation was studied at the as-prepared Pt/C and Pt–Rh–Sn/C catalysts. The cyclic voltammogram for Pt–Rh–Sn/C after only two cycles to characterize roughly the surface but to avoid significant dissolution of Rh and Sn is shown in Fig. 3. The cyclic voltammograms for Pt/C are given as steady state and after two cycles for comparison. The steady state CV for Pt/C was similar to those for polycrystalline platinum or other Pt catalysts supported on high surface area carbon, with a well-defined region of hydrogen adsorption/desorption, separated by a double layer from the region of surface oxide formation. These regions were not well-defined at the beginning of cycling since the surface was still not fully reconstructed. The CV for Pt–Rh–Sn/C was similar to the CV for PtRh/C[10]

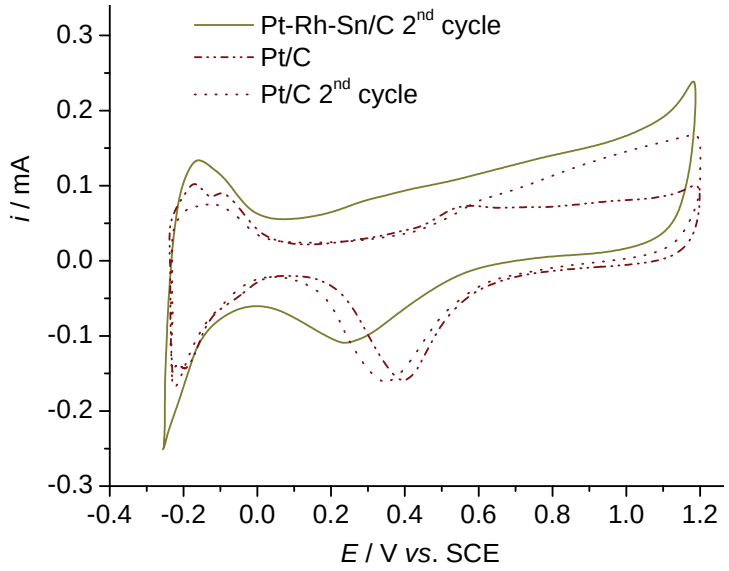

Fig. 3. Basic voltammograms of the Pt/C and Pt–Rh–Sn/C catalysts in 0.1 M $HClO_4$, v = 50 mV s^{-1}.

and is characterized by a large single peak in the hydrogen adsorption/desorption region, which Lima *et al.*[10] associated with adsorption/desorption of hydrogen on the intermetallic phase of PtRh. The shift of the reduction peak for Pt–Rh–Sn/C to more a negative potential value in comparison to Pt/C could be an indication of alloyed Pt and Rh. The larger double layer in the case of Pt–Rh–Sn/C compared to Pt/C was due to the lower metal content (11 mass %) of this catalyst in comparison to Pt/C (20 mass %).

The electrocatalytic activities of the as-prepared catalysts were studied in 0.1 M $HClO_4$ + 0.5 M C_2H_5OH solution and the positive scan voltammetric curves are presented in Fig. 4. The Pt–Rh–Sn/C catalyst was highly active in ethanol oxidation with the onset potential at approximately –0.15 V (shifted by ≈0.15 V towards more negative potentials compared to Pt/C) and rapid kinetics. The hydrogen adsorption/desorption peaks were clearly suppressed because the ethanol adsorption displaced the adsorbed hydrogen from the interface. The current densities, calculated on Pt content, throughout the studied potential region were five times higher for the Pt–Rh–Sn/C catalyst in comparison to the Pt/C catalyst. The stability of the catalysts was studied in chronoamperometric experiments and the results are presented in Fig. 5. The higher initial current density at 0.2 V on the Pt–Rh–Sn/C catalyst in comparison to the Pt/C catalyst is in accordance with the

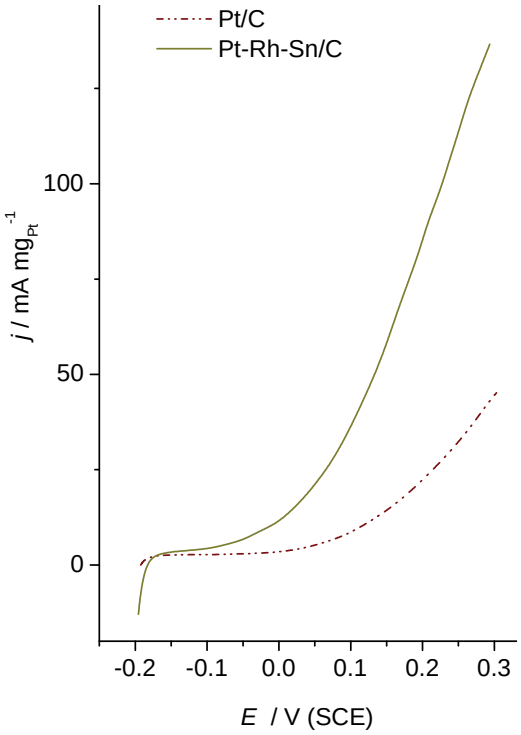

Fig. 4. Potentiodynamic curves for the oxidation of 0.5 M C_2H_5OH at the Pt/C and Pt–Rh–Sn/C catalysts in 0.1 M $HClO_4$, v = 20 mV s^{-1}.

potentiodynamic measurements. The initial current at Pt–Rh–Sn/C stabilizes at a value that was significantly higher than that for the Pt/C catalyst. The Pt–Rh––Sn/C catalyst is evidently more active and less poisoned than the Pt/C catalyst.

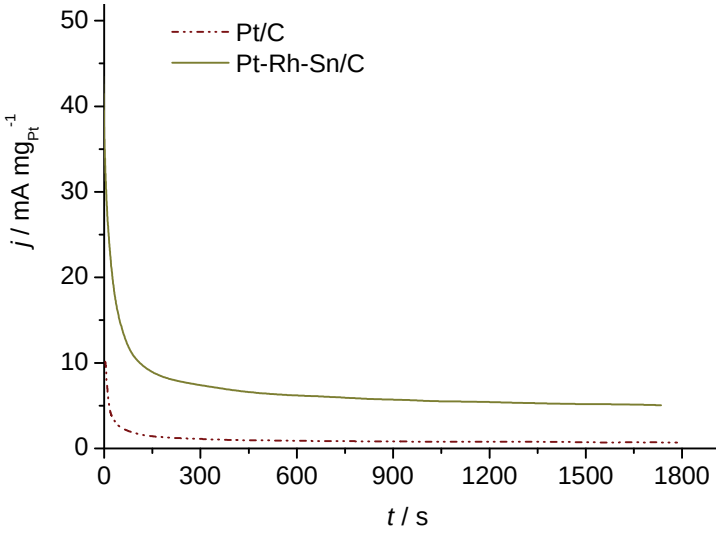

Fig. 5. Chronoamperometric curves for the oxidation of 0.5M C_2H_5OH at 0.2 V at the Pt/C and Pt–Rh–Sn/C catalysts in 0.1 M $HClO_4$.

The better activity for the EOR of the ternary Pt–Rh–Sn catalyst in comparison to Pt/C catalyst must be related to the formation of the ternary alloy. Thus, the presence of Sn and Rh in the catalyst can promote ethanol oxidation by an electronic effect in the Pt-based electrode material affecting the adsorption properties of the surface, making this system less prone to poisoning by organic species than pure Pt. Sn or its oxides can supply surface oxygen-containing species at lower potentials by activation of the interfacial water molecule necessary to complete the oxidation of the adsorbed reaction intermediates leading to carbon dioxide, in the situation that the C−C bond was broken, or to the formation of acetic acid.[12,29] This oxidative removal of CO-like species strongly adsorbed on adjacent Pt active sites proceeds through the so-called bi-functional mechanism. According to density functional theory (DFT) calculations,[14] the role of Rh was to adsorb and stabilize the key intermediate CH_2CH_2O in this route, which leads to the cleavage of C−C bonds. A back donation from the Rh d-band electrons to Pt was proposed. Thus, the presence of Pt could modify the electronic structure of Rh by partially emptying its d-band states enabling its strong bonding to CH_2CH_2O, while the activity of Pt was lowered, thereby preventing the partial oxidation of ethanol on the Pt sites.[14]

In comparison with other Pt–Rh–Sn/C catalysts described in the literature[12–14] in which the atomic fraction of Sn was equal or higher than that of Pt, while the atomic fraction of Rh was much smaller than both Pt and Sn, the presently studied Pt–Rh–Sn/C catalyst with highest fraction of Pt and lowest fraction of Sn exhibited a comparably high activity for ethanol oxidation.

Colmati *et al.*[12] studied ethanol oxidation at Pt–Rh–Sn/C catalysts with molar ratios 1:1:1 and 1:0.3:1, prepared by formic acid oxidation. The ternary catalyst with the lower fraction of Rh was found to have a higher activity, but both the Pt–Rh–Sn/C catalysts exhibited a significantly lower activity in comparison with PtSn/C catalyst at lower potentials (< 0.45 V RHE) and the opposite at higher potential values. The higher activity of PtSn/C was ascribed to the presence of SnO_2 that could supply oxygen-containing species for the oxidative removal of CO and CH_3CO adsorbed on adjacent Pt active sites. The introduction of Rh changes the geometry (Pt−Pt bond distances) and electronic (Pt d-band vacancy) structure of PtSn catalysts, which could improve the adsorption of ethanol and the cleavage of C−C bonds, increasing in this way the activity for ethanol oxidation at higher potentials.[12] For ethanol oxidation, Kowal *et al.*[13] and Li *et al.*[14] used Pt–Rh–SnO_2/C catalysts prepared by the polyol method with conventional heating. XRD Analysis of these catalysts showed the presence of two phases, Pt–Rh alloy and SnO_2. The catalysts were highly active at lower potentials (< 0.5 V RHE). The catalysts were synthesized with different ratios of the components (Pt:Rh:Sn from 3:1:2 to 3:1:6) and the highest activity for ethanol oxidation and capability to split C−C bonds, as revealed by infrared reflection-adsorption spectroscopy (IRRAS), was achieved with Pt–Rh–Sn 3:1:4.[14]

Although XRD analysis of the present catalyst did not give any information except for its very low crystallinity, some reasonable assumptions can be made based on literature data. It can be assumed that, similarly to other Pt–Rh–Sn catalysts, the Pt was alloyed with Rh since, according to the Pt–Rh phase diagram,[29] these two metals form a solid solution at any ratio. XPS and XRD analyses of bimetallic PtSn catalysts prepared by microwave or conventional heating of ethylene glycol solutions of H_2PtCl_6 and $SnCl_2$ salts indicated significant amounts of SnO_2 and rather low degree of alloying.[25,30] Thus, it can be assumed that the Sn in the present Pt–Rh–Sn catalyst existed mainly as SnO_2. Both assumptions mean that the prepared catalyst should be similar to the catalysts obtained by Li *et al.*[14] but with a larger fraction of Rh and a lower fraction of Sn, but still exhibiting a comparable performance. It was shown that the addition of a small quantity of Sn greatly enhanced the electrooxidation of ethanol at low potentials.[28,31] On the other hand, a low amount of Rh added to Pt only slightly improved the CO_2 yield in ethanol oxidation, while the optimum catalyst composition for C−C bond breakage and CO_2 formation was Pt:Rh 1:1 or even better 3:1.[9,10] Hence, the high activity for ethanol oxidation of the present Pt–Rh–Sn/C

catalyst can be explained by a balanced action and well-tuned content of all three components. In addition, the particle size effect cannot be ignored since very small particles of Pt–Rh–Sn/C catalyst contribute to an increase of the active surface area of the catalyst.

CONCLUSIONS

A microwave-assisted polyol method was used to prepare carbon supported Pt and Pt–Rh–Sn nanoparticles with high electrocatalytic activities for the ethanol electrooxidation reaction.

The structural (XRD) and surface characterization (STM) of the catalysts revealed that catalysts with small particles and a rather uniform size distribution were synthesized by this method. This could be attributed to the advantages of the microwave-assisted modified polyol process in ethylene glycol solution.

The electrochemical measurements revealed a high activity of the prepared Pt–Rh–Sn/C catalyst for ethanol oxidation. This catalyst had five times higher oxidation currents and significantly lower reaction onset potential than the Pt/C catalyst. Chronoamperometric measurements confirmed notably less poisoning of the Pt–Rh–Sn/C catalyst than of the Pt/C catalyst. Although with significantly higher fraction of Rh and lower fraction of Sn in comparison to other Pt–Rh–Sn catalysts described in the literature, the catalyst prepared in the present study exhibited a similar shift of onset potential to negative values as well as lower poisoning. The increased activity of Pt–Rh–Sn/C catalyst in comparison to Pt/C catalyst was most probably promoted by the bi-functional mechanism and the electronic effect of the alloyed metals.

Acknowledgements. This work was financially supported by the Ministry of Education and Science of the Republic of Serbia, Contract No. 172060.

И З В О Д

МИКРОТАЛАСНА СИНТЕЗА И КАРАКТЕРИЗАЦИЈА Pt И Pt–Rh–Sn КАТАЛИЗАТОРА ЗА ОКСИДАЦИЈУ ЕТАНОЛА

САЊА СТЕВАНОВИЋ[1], ДУШАН ТРИПКОВИЋ[2], ДЕЈАН ПОЛЕТИ[3], ЈЕЛЕНА РОГАН[3], АМАЛИЈА ТРИПКОВИЋ[1] И ВЛАДИСЛАВА М. ЈОВАНОВИЋ[1]

[1]ИХТМ – Центар за електрохемију, Његошева 12, Београд, [2]Materials Science Division, Argonne National Laboratory, Argonne, IL 60439, USA и [3]Технолошко–металуршки факултет, Универзитет у Београду, Карнегијева 4, Београд

Pt и Pt–Rh–Sn катализатори на угљенику развијене површине су синтетизовани полиол-микроталасним поступком у раствору етиленгликола и испитивани за реакцију елетрохемијске оксидације етанола у киселој средини. Катализатори су окарактерисани структурно, морфолошки и по саставу коришћењем XRD, STM и EDX техника. STM анализа је потврдила да су Pt и Pt–Rh–Sn честице униформне величине и пречника мањег од 2 nm. XRD анализа Pt/C катализатора показала је присуство две фазе, једне са главним карактеристичним пиковима за пљосно-центрирану кубну кристалну структуру платине (111, 200, 220 и 311) и друге са дифракционим пиком на 2θ око 25° карактеристичним за хексагоналну структуру

вулкана XC-72R (угљеничног носача). XRD анализа Pt–Rh–Sn/C катализатора није показала карактеристичне пикове, што је индикација веома мале кристаличности катализатора. Активност катализатора испитивана је потенциодинамичким и хроноамперометријским мерењима. Pt–Rh–Sn/C катализатор је веома активан за оксидацију етанола са почетком реакције на потенцијалима за око 150 mV помереним ка негативнијим вредностима и струјама које су око пет пута веће у поређењу са Pt/C катализатором. Стабилност катализатора испитивана хроноамперометријски показала је да се Pt–Rh–Sn/C катализатор мање troше од Pt/C катализатора. Мала величина и хомогена дистрибуција честица могу се приписати предностима микроталасне синтезе и модификованог полиол поступка у раствору етиленгликола. Већа активност Pt–Rh–Sn/C катализатора у поређењу са Pt/C катализатором последица је би-функционалног механизма и електронског (лиганд) ефекта метала у синтетизованој легури.

(Примљено 5., ревидирано 29. априла 2011)

REFERENCES

1. E. Antolini, *J. Power Sources* **170** (2007) 1
2. A. Lopez-Cudero, J. Solla-Gullon, E. Herrero, A. Aldaz, J. M. Feliu, *J. Electroanal. Chem.* **644** (2010) 117
3. H. Wang, Y. Jusys, R. J. Behm, *J. Power Sources* **154** (2006) 351
4. Q. Wang, G. Q. Sun, L. H. Jiang, Q. Xin, S. G. Sun, Y. X. Jiang, S. P. Chen, Z. Jusys, R. J. Behm, *Phys. Chem. Chem. Phys.* **9** (2007) 2686
5. S. Rousseau, C. Coutanceau, C. Lamy, J. M. Leger, *J. Power Sources* **18** (2006) 158
6. W. Zhou, Z. Zhou, S. Song, W. Li, G. Sun, P. Tsiakaras, Q. Xin, *Appl. Catal., B* 46 (2003) 273
7. W. J. Zhou, S. Q. Song, W. Z. Li, Z. H. Zhou, G. Q. Sun, Q. Xin, S. Douvartzides, P. Tsiakaras, *J. Power Sources* **140** (2005) 50
8. H. Li, G. Sun, L. Cao, L. Jiang, Q. Xin, *Electrochim. Acta* **52** (2007) 6622
9. J. P. I. de Souza, S. L. Queriroz, K. Bergamaski, E. R. Gonzalez, F. C. Nart, *J. Phys. Chem. B* **106** (2002) 9825
10. F. H. Lima, D. Profeti, W. H. Lizcano-Valbuena, E. A. Ticianelli, E. R. Gonzales, *J. Electroanal. Chem.* **617** (2008) 121
11. A. V. Tripković, J. D. Lović, K. Dj. Popović, *J. Serb. Chem. Soc.* **75** (2010) 1559
12. F. Colmati, E. Antolini, E. R. Gonzalez, *J. Alloys Compd.* **456** (2008) 264
13. A. Kowal, S. Lj. Gojković, K. S. Lee, P. Olszewski, Y. E. Sung, *Electrochem. Comm.* **11** (2009) 724
14. M. Li, A. Kowal, K. Sasaki, N. Marinkovic, D. Su, E. Korach, P. Liu, R. R. Adzic, *Electrochim. Acta* **55** (2010) 4331
15. J. Perez, V. A. Paganin, E. Antolini, *J. Electroanal. Chem.* **654** (2011) 108
16. Y. Wang, J. Zhang, X. Wang, J. Ren, B. Zuo, Y. Tang, *Top. Catal.* **35** (2005) 35
17. W. Yu, W. Tu, H. Liu, *Langmuir* **15** (1999) 6
18. W. Kraus, G. Nolze, *PowderCell for Windows*, V.2.4, Federal Institute for Materials Research and Testing, Berlin, Germany, 2000
19. H. P. Klug, L. E. Alexander, *X-Ray diffraction procedures*, 2nd ed., Wiley, New York, 1974, p. 687
20. C. Feldmann, C. Metzmacher. *J. Mater. Chem.* **11** (2001) 2603
21. S. L. Knupp, W. Li, O. Paschos, T. M. Murray, J. Snyder, P. Haldar, *Carbon* **46** (2008) 1276

22. W. X. Tu, H. F. Liu, *Chem. Mater.* **12** (2000) 564
23. S. Song, J. Liu, J. Shi, H. Liu, V. Maragou, Y. Wang, P. Tsiakaras, *Appl. Catal., B* **103** (2011) 223
24. W. Tu, H. Liu, *J. Mater. Chem.* **10** (2000), p. 2207.
25. Z. Liu, B. Guo, L. Hong, T. H. Lim, *Electrochem. Comm.* **8** (2006) 83
26. K. J. Rao, B. Vaidhyanatham, M. Ganguli, P. A. Ramakrishnan, *Chem. Mater.* **11** (1999) 882
27. W. X. Chen, J. Y. Lee, Z. L. Liu, *Chem. Comm.* (2002) 2588
28. F. C. Simoes, D. M. Dos Anjos, F. Vigier, J. M. Leger, F. Hahn, C. Coutanaceau, E. R. Gonyaley, G. Tremiliosi-Filho, A. R. De Andrade, P. Olivi, K. B. Kokoh, *J. Power Sources* **11** (2007) 1567
29. M. Hansen, K. Anderko, *Constitution of binary alloys*, 2nd ed., McGraw-Hill, New York, 1958
30. Z. Liu, L. Hong, S. W. Tay, *Mater. Chem. Phys.* **105** (2007) 222
31. C. Lamy, S. Rousseau, E. M. Belgsir, C. Coutanceau, J. M. Leger, *Electrochim. Acta* **49** (2004) 3901.

Journal of the Serbian Chemical Society
JSCS-info@shd.org.rs • www.shd.org.rs/JSCS
J. Serb. Chem. Soc. 76 (12) 1687–1701 (2011)
JSCS–4240
UDC 546.982'922+543.51:530.145.6
Original scientific paper

Comparison of MALDI-TOF mass spectra of [PdCl(dien)]Cl and $[Ru(en)_2Cl_2]Cl$ acquired with different matrices

BOJANA DAMNJANOVIĆ[1#], BILJANA PETROVIĆ[2#], JASMINA DIMITRIĆ-MARKOVIĆ[3] and MARIJANA PETKOVIĆ[1*#]

[1]*Laboratory of Physical Chemistry, Institute of Nuclear Sciences "Vinča", University of Belgrade, Belgrade,* [2]*Department of Chemistry, Faculty of Science, University of Kragujevac, Kragujevac and* [3]*Faculty of Physical Chemistry, University of Belgrade, Belgrade, Serbia*

(Received 1 February, revised 15 April 2011)

Abstract: In this work, the matrix-assisted laser desorption and ionization time-of-flight (MALDI-TOF) mass spectra of two cationic complexes, *i.e.*, [PdCl(dien)]Cl and $[Ru(en)_2Cl_2]Cl$, acquired under different conditions were analyzed. The spectra were recorded with three matrices with or without trifluoroacetic acid (TFA), *i.e.*, two traditional matrices, *i.e.*, 2,5-dihydroxybenzoic acid and α-cyano-hydroxycinnamic acid, and one flavonoid, quercetin. The spectra acquired with quercetin appeared to be the simplest, whereas in the spectra obtained with other matrices, peaks arising either from the addition of matrix molecules or from the fragmentation products were detectable. Addition of TFA did not complicate the spectra of the Pd(II) and Ru(III) complexes when the traditional matrices were used. On the other hand, the spectra of Pd complex were simpler, whereas the addition of TFA in the case of the Ru complex resulted in a higher number of peaks, some of which could not be identified. Taken together, the results of this study once more emphasize the differences arising in the MALDI-TOF mass spectra of transition metal complexes in dependence on the applied matrix.

Keywords: MALDI-TOF MS; metallo-drugs; matrix; peak assignment.

INTRODUCTION

There are serious scientific efforts aimed at synthesizing new transition metal complexes as potential candidates for antitumor therapeutics but which exhibit fewer toxic effects than the well-established platinum complexes.[1–4] Pd(II) complexes are usually very good model compounds for mechanistic investigations since they exhibit a 10^4 to 10^5 fold higher reactivity than the well-known Pt(II) antitumor complexes, whereby their structural and equilibrium behavior are

* Corresponding author. E-mail: marijanapetkovic@vinca.rs
# Serbian Chemical Society member.
doi: 10.2298/JSC110201145D

rather similar.[5] In addition, a number of Ru(III) complexes showed promising antitumor and antimetastatic activity.[6,7]

Several methods can be used for the analysis and characterization of transition metal complexes, as well as for monitoring their possible interaction with biomolecules; among them, matrix-assisted laser desorption and ionization time-of-flight mass spectrometry (MALDI-TOF MS) seems to be a promising tool, due to its capability of analyzing both transition metal complexes and biomolecules.

Generally, mass spectrometry has been routinely applied for the analysis of metal complexes. For instance, fast atom bombardment (FAB) MS has been applied for the analysis of platinum(II) and platinum(I) dinuclear hybrids.[8] In addition, a combination of various MS ionization methods, such as electron ionization (EI), FAB and MALDI, provides important structural information.[9]

Mild ionization techniques, *i.e.*, those which yield fewer fragmentation products, such as electrospray ionization (ESI) and MALDI,[10] are not only suitable for the analysis of high mass molecules, but have also found their application in the analysis of inorganic compounds. MALDI was used for the characterization of transition metal complexes,[11,12] and for monitoring the interaction of platinum drugs with different molecules, such as poly(ethylene glycol)[13] and polystyrene,[14] as well as with biological systems.[15–17]

Choice of the matrix for the MALDI-TOF MS analysis is an important issue since the matrices used for MALDI-TOF mass spectrometric analysis of transition metals complexes exhibit certain drawbacks, as was recently described.[18–20] On the other hand, flavonoids, when used as matrices for MALDI-TOF MS seem to stabilize Pt, Pd and Ru complexes and enable reproducible and reliable analysis of these compounds.[18,20] This is an advantage over the other more commonly used methods, since in most cases the ligand–metal bond is preserved when flavonoids were used as matrices and little or no fragmentation could be detected. Although being good matrices for transitional metal complexes, flavonoids cannot be used as matrices for MALDI-TOF MS analysis of biomolecules; the application of more "traditional" matrices for this purpose is still required.

The main aim of this work was to analyze the spectra of two cationic complexes ([PdCl(*dien*)]Cl and [Ru(*en*)$_2$Cl$_2$]Cl) obtained with the assistance of traditional matrices (DHB and CHCA) and one selected flavonoid, *i.e.*, quercetin. Moreover, the positive ion MALDI-TOF mass spectra in more acidic environments, *i.e.*, addition of trifluoroacetic acid (TFA) to the matrix solution, which was shown to result in better signals for biomolecules, were also analyzed.[21]

EXPERIMENTAL

Chemicals

Paladium(II) and ruthenium(III) complexes: [Pd(dien)Cl]Cl (diethylenetriamine paladium(II) chloride) (*Mr* = 280.5) and [Ru(en)$_2$Cl$_2$]Cl (dichlorido (ethylenediemine)ru-

thenium(III) chloride) (*Mr* = 327.6) were synthesized as described in the literature.[23,24] Chemical analysis, UV–Vis and ^{1}H-NMR spectral data of these complexes were in good agreement with those obtained in previous preparations. TFA, matrices for MALDI-TOF MS, *i.e.*, 2,5-DHB and α-CHCA, were purchased from Sigma-Aldrich (München, Germany) and were applied without further purification. Quercetin dihydrate (≥ 98 %) was also purchased from Sigma-Aldrich (Munich, Germany) and was used without further purification.

Methods

Preparation of the samples for MALDI-TOF MS. The metal complexes were dissolved in a combination of methanol/physiological solution (0.9 % NaCl) at the following concentrations: [Pd(dien)Cl]Cl, 8.62×10^{-3} M (50 % methanol/50 % physiological solution) and $[Ru(en)_2Cl_2]Cl$, 6.1×10^{-3} M (50 % methanol/50 % physiological solution). The matrices, 2,5-DHB and α-CHCA, were prepared prior to use. The following solutions of the matrices were used: 0.5 M 2,5-DHB in methanol and 5 mM α-CHCA in acetonitrile/water (1:1, v/v). For some experiments, a small amount of TFA (0.1 % final concentration) was added to the matrix solution.

The following approach was used for the application of the sample onto the MALDI target: a small volume (0.5 μL) of the solution of a metal complex was applied onto the sample plate, which was followed by immediate addition of the same volume of a matrix solution (DHB, CHCA or quercetin). The mixture was then left at room temperature to co-crystallize. This approach was shown to result in the best quality of MALDI-TOF mass spectra, as demonstrated in previous studies.[19,21]

MALDI-TOF MS. The MALDI-TOF mass spectra were acquired on a Voyager Biospectrometry DE Pro workstation (Perseptive Biosystems, Framingham, MA, USA). The system utilizes a 20 Hz pulsed nitrogen laser emitting at 337 nm. The spectra were acquired without a low mass gate and under delayed extraction conditions in the reflector mode. All spectra represent the average of 400 single laser shots. The laser intensity was kept sufficiently low to prevent degradation of the flavonoids and to obtain a good signal-to-noise ratio of the analyte.

Theoretical presentation of the mass spectra. Theoretical presentation of the spectra was realized with the assistance of the Selket program, version 1.4, available online.

RESULTS AND DISCUSSION

MALDI-TOF MS has been proven itself to be a useful method for the analysis of biomolecules. The most used matrices for the MALDI-TOF MS analysis of various classes of biomolecules are α-cyano-hydroxycinnamic (CHCA), synapinic acid (SA), and dihydroxybenzoic acid (DHB).[21] Although matrices usually serve as an assistance for the desorption/ionization process, they also yield signals in the mass spectra,[24] which, in certain cases, might overlap with peaks of interest.

Therefore, the first aim in the present study was to assign matrix peaks, in order to make the identification of peaks arising from an analyte more certain. This is particularly important when newly synthesized and not yet fully characterized transition metal complexes, as well as their interaction with various biomolecules, are to be studied by MALDI-TOF MS. In the second part of the work, the MALDI-TOF mass spectra of Pd(II) and Ru(III) complexes were analyzed and differences in the relation to the matrix used are discussed. Finally, the effect

of the laser intensity on the signal intensity of the positive ion mass spectra of the selected complexes in relationship with the chosen matrix is addressed.

LDI-TOF MS of DHB, CHCA and quercetin

Spectra of matrices used in this study are given in Fig. 1: in Figs. 1a and 1b the spectra of DHB are presented without and with TFA, respectively; Figs. 1c and 1d represent the positive ion mode LDI-TOF mass spectra of CHCA, also without and with TFA, respectively; the trace in Fig. 1e is the positive ion mode spectrum of quercetin and for the spectrum given in Fig. 1f, small amount of TFA was added. The identities of the peaks detected in the presented spectra are listed in Table I, and they will not be discussed here in more detail.

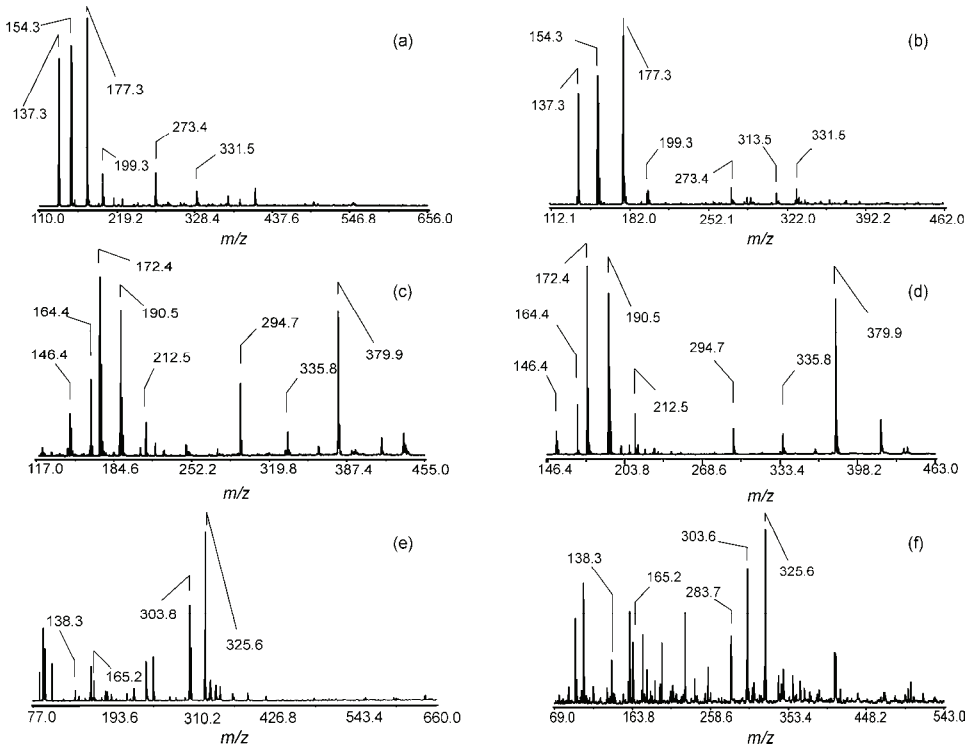

Fig. 1. Positive ion mode LDI-TOF mass spectra of DHB without and with TFA (a and b, respectively), CHCA without and with TFA (c and d, respectively) and quercetin, also recorded without and with TFA (e and f, respectively). Peaks are indicated according to their *m/z* position and their identities are given in Table I.

In agreement with previously published data,[24] the most intense peaks in the positive ion mode LDI-TOF mass spectra of DHB appeared at *m/z* = 137.3, 154.3 and 177.3. These peaks are generated either by the loss of a water molecule followed by addition of a proton, addition of a proton, or addition of a sodium ion

(Figs. 1a and 1b; *cf.* Table I), respectively. After the addition of TFA to the solution of DHB, neither significant differences in quality of mass spectra nor the number of peaks could be detected.

TABLE I. Peaks detected in the positive ion MALDI-TOF mass spectra of the used matrices. The corresponding spectra are given in Fig. 1; "M" corresponds to the molecule; the fragmentation pattern of quercetin is given in the literature[25]

Matrix	*m/z*	Peak assignment
2,5-DHB	137.3	$M - H_2O + H^+$
	154.3	M
	177.3	$M + Na^+$
	199.3	$M - H^+ + 2Na^+$
	273.4	$2M - 2H_2O + H^+$
	313.5	$2M - H_2O + Na^+$
	331.5	$2M + Na^+$
α-CHCA	146.4	$M - CO_2 + H^+$
	164.4	$M - CN + H^+$
	172.4	$M - H_2O + H^+$
	190.5	$M + H^+$
	212.5	$M - H^+ + Na^+$
	294.7	$2M + H^+ - CCNCOOH$
	335.8	Not assigned
	379.9	Not assigned
Q	138.3 and 165.2	$^{0,2}M^{+\#}$
	283.7	$M - H_2O + H^+$
	303.6	$M + H^+$
	325. 6	$M + Na^+$

The addition of TFA to the solution of CHCA did not significantly change the pattern of the LDI-TOF mass spectra of this matrix; neither did it result in an increase in the intensities of the peaks. The most expressed peaks in the spectra of CHCA were detectable at *m/z* = 172.4 ($M - H_2O + H^+$), *m/z* = 190.5 ($M + H^+$) and at *m/z* = 379.9, which has not been assigned so far (Figs. 1c and 1d; *cf.* Table I for peak assignment).

On the other hand, new peaks appeared in the spectra of quercetin after the addition of TFA (Fig. 1e without TFA, Fig. 1f with TFA). The most intense peaks in the spectra of quercetin correspond to the protonated and sodiated adducts of quercetin (peak at *m/z* = 303.8 and at *m/z* = 325.6, respectively). Certain high-intensity peaks could be assigned to possible degradation products of quercetin induced by the laser in the acidic solution, most probably according to pattern given in the footnote to Table I (*cf.* Table I). A number of undefined peaks were also detectable in the spectra of quercetin, irrespective of the presence of TFA, which leads to the assumption that quercetin combined with TFA might not be a good choice for MALDI-TOF MS analysis of transition metal complexes, at

least not under the conditions applied in this study. This finding might seem to be in contradiction to a previous work,[18] in which the addition of TFA did not lead to the fragmentation of quercetin. The possible reason for this might be the difference in the employed solvents: in the previous work, an aqueous suspension of quercetin was used as the matrix, whereas in this work, a methanolic solution of quercetin was preferred in an attempt to increase the miscibility with the methanolic solutions of the transition metal complexes. This difference in the solutions might result in the different behavior of this flavonoid under laser irradiation.

Theoretical presentation of the mass spectra of the Pd(II) and Ru(III) complexes

Each peak in the MALDI-TOF mass spectra actually represents a group of signals resulting from a number of combinations of naturally occurring isotopes. This is particularly expressed when the spectra are acquired in the reflector mode. Such a picture is in the case of transition metals and their complexes is even more complicated, since transition metals have a large number of natural isotopes. Therefore, before considering the experimental spectra, a theoretical presentation of the mass spectra of the used complexes will be briefly described.

Figure 2 represents theoretical presentations of the mass spectra of [Pd(en)Cl]Cl on the left and $[Ru(en)_2Cl_2]Cl$ on the right panel. These spectra are given for the purpose of reference and only a few signals are indicated. Figure 2 is accompanied by Table II, which contains a list of the isotopes of Pd and Ru, with their natural abundances.

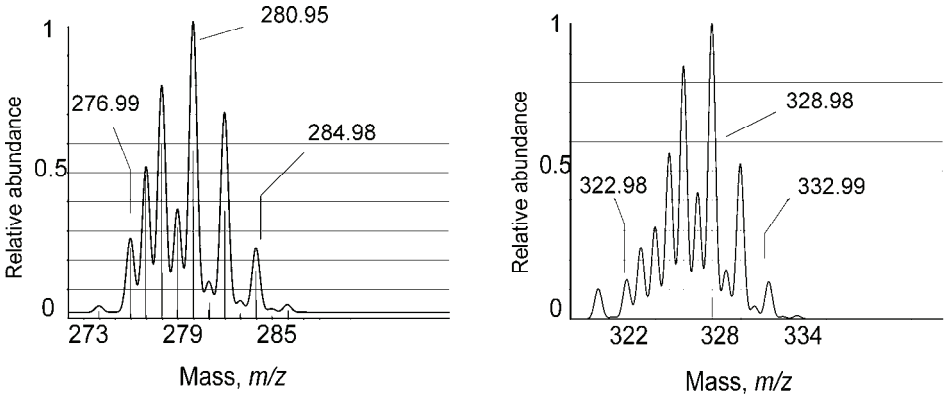

Fig. 2. Theoretical presentation of the mass spectra of Pd(II) (left panel) and Ru(III) complex (graph on the right). The spectra were created using the Selket program.

Pd has 6 naturally occurring isotopes with masses ranging from 101.91 to 109.91, whereas Ru has 7 (from 95.91 to 103.91). The most abundant isotope of Pd is the one with the mass 105.90 and that of Ru has the mass 101.90. It is easy to assume that the spectrum of both transition metal complexes will be even more

complex since a large number of isotope combinations (Pd, or Ru with C, N, H or Cl) are possible: the theoretical spectrum of the Pd complex contains 10 peaks, whereas that of Ru has 12 peaks.

TABLE II. List of isotopes of Pd and Ru and their natural abundance. The data were taken from the Selket program

Metal	Relative molar mass	Probability (abundance)
Pd	101.91	0.0373216245883644
	103.90	0.407610684229784
	104.91	0.817050859860959
	105.90	1
	107.90	0.968166849615807
	109.91	0.428832784485913
Ru	95.91	0.175
	97.91	0.0591772151898734
	98.91	0.401898734177215
	99.90	0.39873417721519
	100.91	0.541139240506329
	101.90	1
	103.91	0.588607594936709

In this study, it was decided to take the most intense peak in each peak group of the MALDI-TOF mass spectra of the Pd and Ru complexes for further discussion.

MALDI-TOF MS Analysis of the [Pd(dien)Cl]Cl complex

The positive ion MALDI-TOF mass spectra of [Pd(*dien*)Cl]Cl are given in Fig. 3: the spectra acquired with the assistance of DHB without and with TFA are given in Figs. 3a and 3b respectively; the spectrum of the same complex with CHCA without TFA is shown in Fig. 3c and in Fig. 3d spectrum acquired after the addition of TFA; the spectra in Figs. 3e and 3f represent the positive ion mode MALDI-TOF mass spectra of the same complex recorded with quercetin as the matrix without and with TFA, respectively. The identity of the peaks arising from the metal complexes analyzed in this study is overviewed in Table III. Since the matrix peaks have been discussed above, they will not be addressed here.

There are two major peaks arising from the Pd(II) complex: at m/z = 209.3 and 246.3. These two peaks are emphasized in the inset in Fig. 1a to demonstrate the complex structure of the experimentally obtained peak group, as described in the theoretical presentation of the spectra of the complexes (*cf.* Fig. 2). The latter peak (at m/z = 246.3) is generated by the elimination of one easy-leaving Cl^- from the complex, which leaves the singly-positively charged species; additional loss of neutral HCl from the complex results in the generation of the ion detectable at the lower m/z ratio. Neither significant changes nor additional peaks were detected in the spectra of this complex acquired with DHB matrix after the addi-

tion of TFA (Figs. 3a and 3b). In a previous work, the peaks arising from the Pd(II) complex were not detectable after addition of TFA to the matrix solution.[19] It seems that the conditions that were previously applied were different and that the concentration of the Pd(II) complex in the previous work was sufficiently high to lead to saturation of the detector. In this work, 10-fold lower concentration of complex was tested, which seemed to result in well detectable peaks.

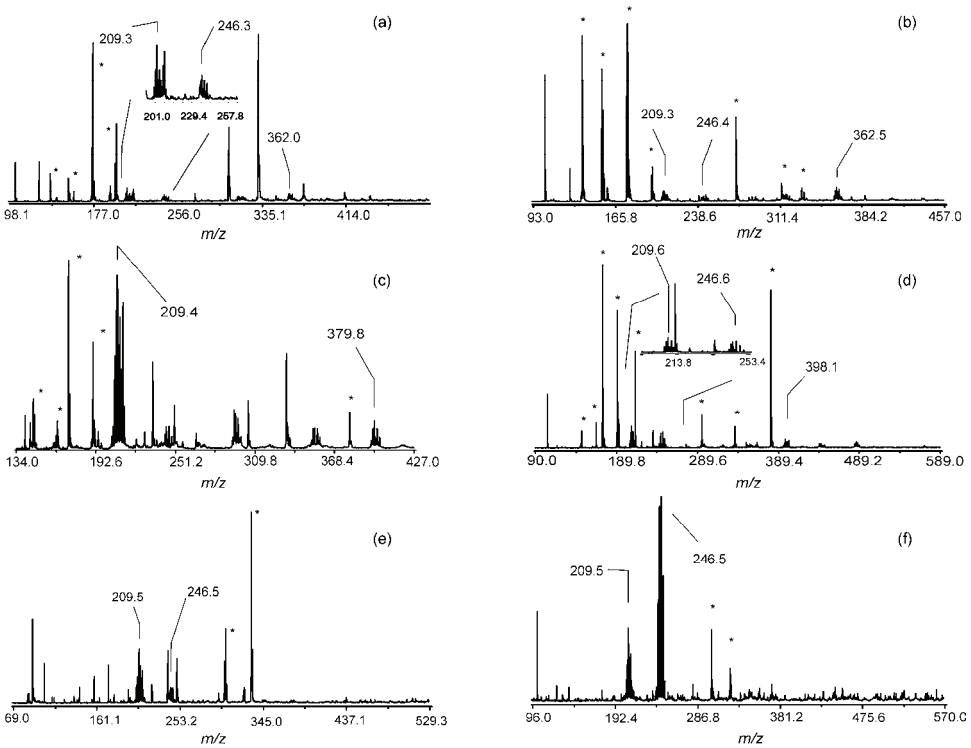

Fig. 3. Positive ion MALDI-TOF mass spectra of the Pd complex acquired with DHB (a and b), CHCA (c and d) and quercetin (e and f). Spectra in a, c and e were acquired without TFA, whereas a small amount of TFA was added to the matrix solutions for the spectra given in b, d and f. The insets in the traces present the expanded mass region from $m/z \approx 200$ up to 260.

When CHCA was used as matrix, only one high-intensity peak arising from the Pd complex at m/z=209.4 was detectable in the MALDI-TOF mass spectra of [Pd(dien)Cl]Cl (Fig. 3c). After the TFA addition, both peaks arising from the complex could be detected, but at much lower intensity compared to the peak obtained without TFA. Similar spectra were obtained also in a previous work and it is important to indicate that this behavior and formation of unusual clusters with the matrix was the motivation to test new matrices for the reliable MALDI-TOF MS analysis of transition metal complexes.

TABLE III. Peaks detected in the positive ion MALDI-TOF mass spectra of the Pd and Ru complexes. The corresponding spectra are given in Figs. 3 and 4; "M" corresponds to the molecule; Q: quercetin

Matrix	*m/z*	Peak assignment
	[Pd(dien)Cl]Cl	
2,5-DHB	209.4	M – HCl – Cl^-
α-CHCA	246.6	M – Cl^-
Q		
Q		
2,5-DHB (TFA)	362.5	M – Cl^- – HCl + 2,5-DHB
α-CHCA	398.1	M + Cl^- – HCl + α-CHCA
	397.8	Not assigned
	$[Ru(en)_2Cl_2]Cl$	
2,5-DHB	193.5	Not assigned
2,5-DHB	292.6	M – Cl^-
α-CHCA		
Q		
2,5-DHB	373.4	M – H^+ + $2Na^+$
2,5-DHB	412.6	n.a.

As will be shown in this section, quercetin with the addition of TFA appeared to be the most suitable matrix for the analysis of [Pd(dien)Cl]Cl. The two peaks arising from the complex were also detected in the spectra acquired with quercetin (Fig. 3e). After the addition of TFA, the intensity of these peaks arising from the Pd(II) complex strongly increased in comparison to the matrix peaks. This might be surprising, since the addition of TFA leads most probably to the fragmentation of quercetin induced by the laser irradiation, as observed in the LDI-TOF mass spectra of quercetin (*cf.* Fig. 1f). On the other hand, it is possible that the amount of quercetin, which is still able to absorb the UV light and to assist desorption and the ionization process of the analyte favored by TFA, is quite sufficient and results in higher peak intensities compared to the spectra obtained without TFA.

MALDI-TOF MS Analysis of $[Ru(en)_2Cl_2]Cl$ complex

The positive ion MALDI-TOF mass spectra of $[Ru(en)_2Cl_2]Cl$ acquired with DHB (Figs. 4a and 4b), CHCA (Figs. 4c and 4d) and quercetin as matrices (Figs. 4e and 4f) are shown in Fig. 4. The spectra in Figs. 4a, 4c and 4e were acquired without TFA, whereas for the spectra presented in other traces given in Fig. 4, a small amount of TFA was added.

A peak arising from the Ru(III) complex is detectable at *m/z* = 292.5 and it is generated by the lost of Cl^- from the complex, resulting in a single positively charged ion. The isotopic peak distribution of this positive ion can be observed in the inset to spectrum in Fig. 4a. There are also other peaks which might arise

from Ru, judging by the characteristic spectra pattern (at *m/z* = 193.5, 373.4 and 412.6, Fig. 4b), but their identity remains so far unknown.

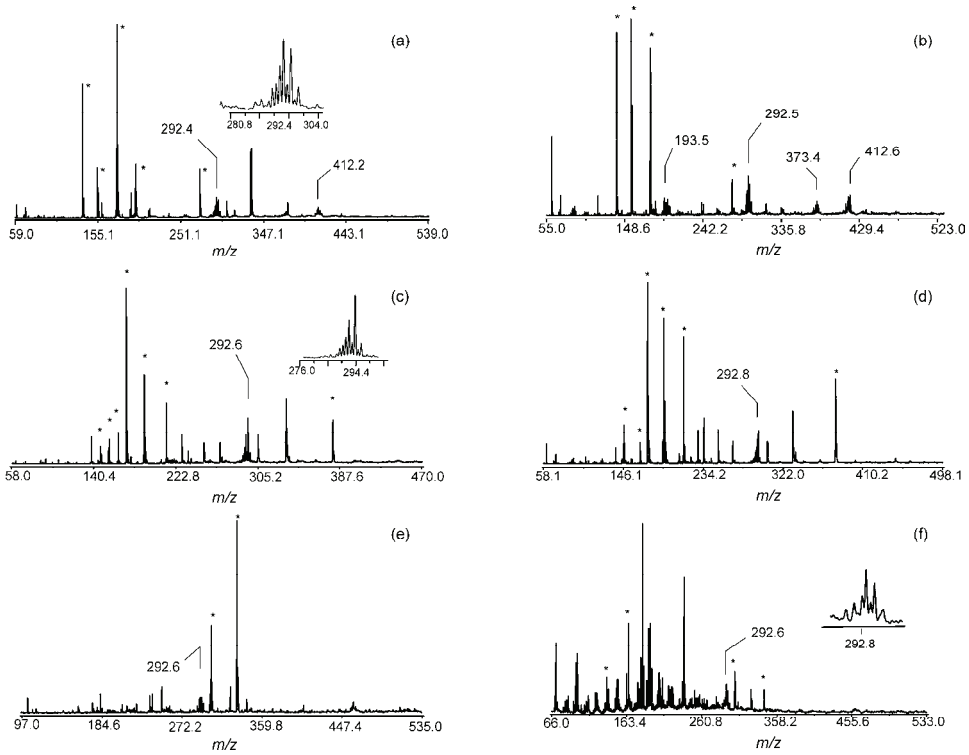

Fig. 4. MALDI-TOF mass spectra of the Ru(III) complex acquired with DHB (a and b), CHCA (c and d) and quercetin (e and f) matrices. The matrix solutions for the spectra in a, c and e were prepared without TFA, whereas for the spectra b, d and f, 0.1 % TFA was added to the matrix solutions. The insets in the figure represent the expanded regions of the *m/z* ratio where characteristic peaks arising from the Ru(III) complex are detected.

Effect of the laser intensity on the S/N *ratio*

In the last part of the experiments, the dependence of the *S*/*N* ratio of peaks arising from the Pd and Ru complexes on the applied laser intensity was tested and the changes in the S/N in relationship with the matrix used and the presence of TFA were compared.

[Pd(dien)Cl]Cl. The dependence of the *S*/*N* ratio of the Pd(II) complex peak at *m/z* = 209.4 on the applied laser intensity when the positive ion MALDI-TOF mass spectra of this transition metal complex were acquired with the assistance of DHB (Fig. 5a), CHCA (Fig. 5b) and quercetin (Fig. 5c) are presented in Fig. 5. For some of the measurements, a small amount TFA was added to the matrix

solution. The laser intensity, expressed in internal, arbitrary units, a.u, was changed gradually and varied from 1500 to 2300 a.u.

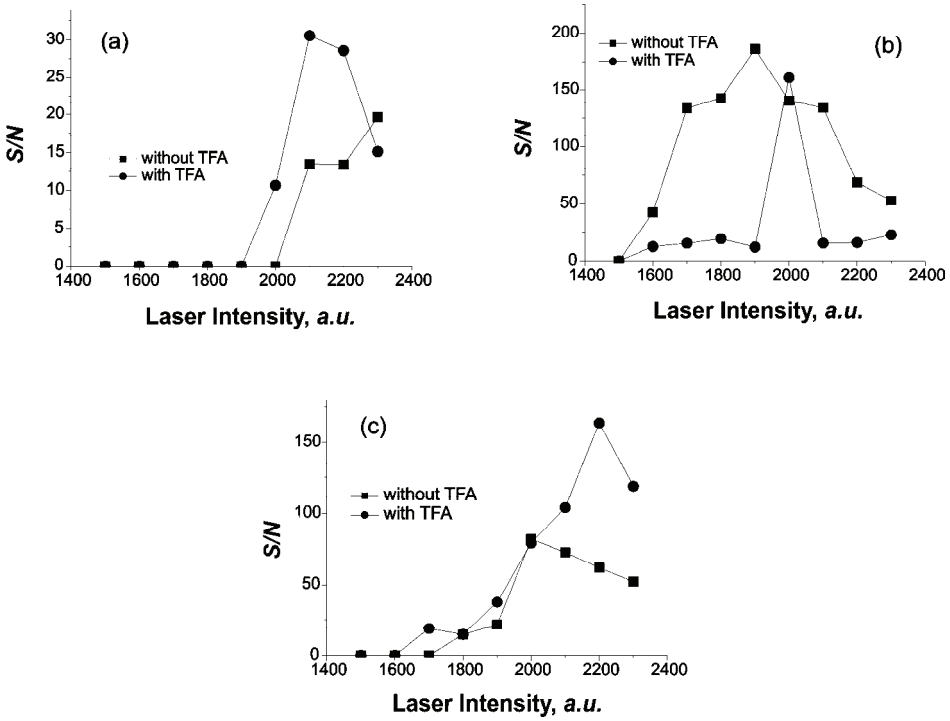

Fig. 5. *S*/*N* ratio of the peak arising from the positive ion MALDI-TOF mass spectra of the Pd(II) complex at *m*/*z* = 209.4 acquired either with DHB (a), CHCA (b) or quercetin (c) as matrices. All the spectra were recorded with or without TFA as indicated in the graphs. The presented results are an average of three independent measurements.

When DHB was used as the matrix, the first signal at *m*/*z* = 209.4 appeared at about 2100 a.u. without TFA and at about 2000 in the presence of TFA. Subsequently, the *S*/*N* ratio of the selected peak increased and reached the maximum already at about 2100 with TFA, whereas in the absence of TFA, this maximum was shifted towards higher laser intensities. Moreover, it seems that the maximum of the *S*/*N* ratio was not reached in the laser intensity range set for testing (Fig. 5a). Unfortunately, due to instrument limitations, a further increase in the laser intensity was not possible.

In the case of the CHCA matrix (Fig. 5b), the palladium peak appeared at much lower laser intensity (already at 1500 a.u.) without TFA, whereas the *S*/*N* ratio for this peak was much lower when TFA was added to the matrix solution. This might be explained by the ionization properties of CHCA: in the presence of

TFA, the ionization of the matrix itself is enhanced, and it might be that the matrix peaks suppressed the peak of interest.

The peak arising from the Pd complex was also detectable with the assistance of quercetin as the matrix (Fig. 5c) and had its maximum intensity at 2000 a.u. in the absence of TFA, whereas its maximum was shifted towards higher laser intensity in the presence of TFA. This might be explained by the increased fragmentation of quercetin induced by the laser in the presence of TFA, which results most probably in a somewhat lower quercetin concentration for the matrix function.

[Ru(en)$_2$Cl$_2$]Cl. In the case of the Ru(III) complex used in this study, the peak at *m/z* = 292.6 was selected for the analysis of the effect of the laser intensity on the *S*/*N* ratio in relationship to the matrix used. The results are shown in Fig. 6; in Fig. 6a DHB was used as the matrix, in Fig. 6b CHCA and in Fig. 6c quercetin was tested.

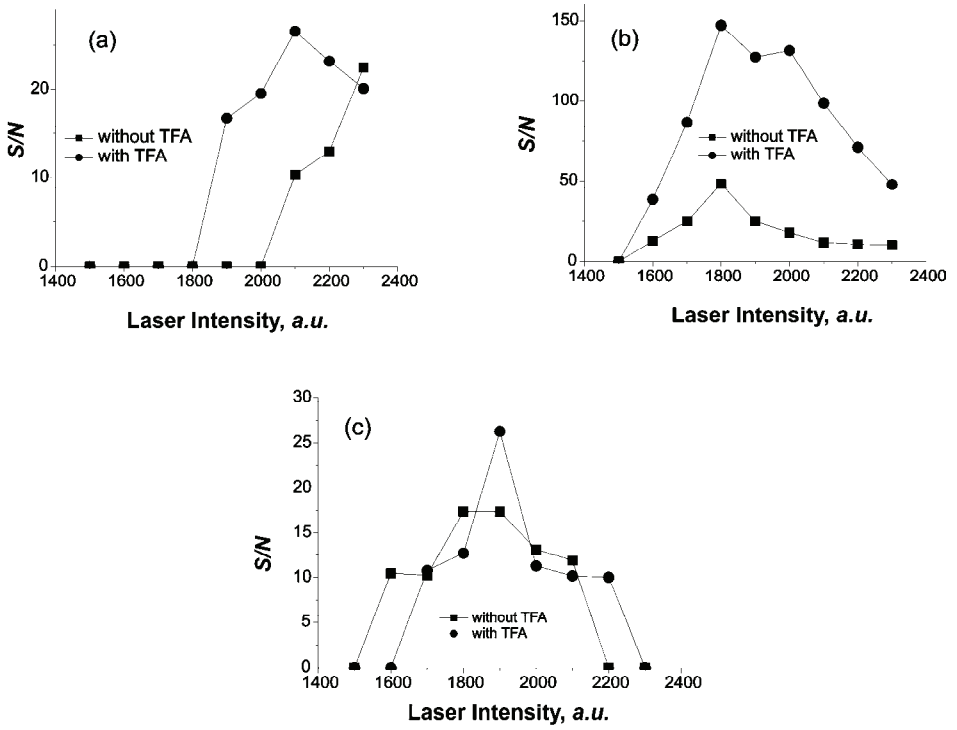

Fig. 6. *S*/*N* ratio of the peak arising from the positive ion MALDI-TOF mass spectra of the Ru(III) complex at *m/z* = 292.6 acquired either with the DHB (a), CHCA (b), or quercetin (c) as matrices. All the spectra were recorded with or without TFA as indicated in the graphs. The presented results are an average of three independent measurements.

In a similar manner to the Pd(II) complex, the addition of TFA to the DHB matrix solution results in a slight shift of the maximum *S*/*N* ratio towards lower applied laser intensities in comparison to DHB without TFA. In the latter case, the maximum *S*/*N* ratio was most probably not achieved, due to instrumental limitations.

When CHCA was used as the matrix, a difference was observed in the pattern of the *S*/*N* ratio of the peak arising from Ru(III) complex compared to that of the Pd(II) complex, thus with addition of TFA, the *S*/*N* ratio was in this case much higher compared to the matrix prepared without TFA (Fig. 6b). The maximum *S*/*N* ratio was achieved at about 1800 a.u., irrespective of the presence of TFA. This different behavior in comparison to the Pd(II) complex might be explained by the detectability of the Ru(III) complex also without matrix[12] (and unpublished observations), which also contributes to the high signal intensity in the presence of the matrix.

When quercetin was used as the matrix for the analysis of the Ru(III) complex, addition of TFA resulted in a shift of the *S*/*N* ratio towards somewhat higher laser intensities required for peak to be detectable in the MALDI-TOF mass spectra of the Ru(III) complex. On the other hand, the maximum *S*/*N* ratio was measured at about 1900 a.u. for both the spectra recorded with and without TFA.

CONCLUSIONS

In summary, matrices used for MALDI-TOF MS analysis of the studied Pd(II) and Ru(III) complexes exhibited differences in their behavior with respect to the quality of the obtained positive ion mode mass spectra. In general, quercetin gave much simpler spectra, resulting in the easy detection and analysis of the complexes. The generation of clusters with DHB and CHCA matrices complicated the spectra of the transition metal complexes, whereas it seems that quercetin stabilized both the Pd(II) and Ru(III) complexes for their detection by MALDI-TOF MS. The addition of TFA to the matrix solution did not significantly affect the quality of the spectra, but affected the intensity of the signals arising from the complexes. Taken together, the results presented in this study once more confirmed the necessity for the establishment of reliable conditions for the analysis of the novel metallo-drugs by MALDI-TOF MS and for potential investigations of their interaction with various classes of biomolecules by this method.

ABBREVIATIONS

CHCA – α-cyano-hydroxycinnamic acid; DHB – 2,5-dihydroxybenzoic acid; ESI – electrospray ionization; FAB – fast atom bombardment; LDI – laser desorption and ionization; MALDI-TOF MS – matrix-assisted laser desorption and ionization time-of-flight mass spectrometry; MS – mass spectrometry; SA – synapinic acid; TFA – trifluoroacetic acid.

Acknowledgment. This work was supported by the Ministry of Education and Science of the Republic of Serbia, grant No. 172011.

И З В О Д

ПОРЕЂЕЊЕ MALDI-TOF МАСЕНИХ СПЕКТАРА [PdCl(dien)]Cl И $[Ru(en)_2Cl_2]Cl$ КОМПЛЕКСА СНИМЉЕНИХ УЗ ПОМОЋ РАЗЛИЧИТИХ МАТРИЦА

БОЈАНА ДАМЊАНОВИЋ[1], БИЉАНА ПЕТРОВИЋ[2], ЈАСМИНА ДИМИТРИЋ-МАРКОВИЋ[3] и МАРИЈАНА ПЕТКОВИЋ[1]

[1]*Лабораторија за физичку хемију, Институт за нуклеарне науке "Винча", Универзитет у Београду, Београд,* [2]*Институт за хемију, Природно–математички факултет, Универзитет у Крагујевцу, Крагујевац и* [3]*Факултет за физичку хемију, Универзитет у Београду, Београд*

У овом раду су испитивани експериментални услови за *matrix-assisted laser desorption and ionization time-of-flight* (MALDI-TOF) масеноспектрометријску детекцију и анализу [PdCl(dien)]Cl и $[RuCl_2(en)]Cl$ комплекса. Спектри ових једињења су снимљени уз помоћ традиционалних матрица – 2,5-дихидроксибензоеве киселине и α-цијанохидроксициметне киселине – и уз помоћ кверцетина. Најједноставнији спектри се добијају уз помоћ кверцетина као матрице, док се са осталим матрицама појављују сигнали који потичу од јона формираних додатком молекула матрице или од производа фрагментације молекула. Додатак трифлуоросирћетне киселине (TFA) не компликује спектра Pd(II) и Ru(III) уколико се користе традиционалне матрице, док су спектри Pd(II) комплекса добијени уз помоћ кверцетина и уз додатак TFA једноставнији за интерпретацију. С друге стране, у MALDI-TOF маселим спектрима Ru(III) комплекса се детектују додатни сигнали након додатка TFA. На крају, у овом раду је показана неопходност проналажења услова за сваку комбинацију узорак/матрица, као и значајне разлике у квалитету, односно у броју сигнала у MALDI-TOF маселим спектрима комплекса прелазних метала када се користе различите матрице за снимање.

(Примљено 1. фебруара, ревидирано 15. априла 2011)

REFERENCES

1. M. Jakupec, M. Galanski, B. Keppler, *Rev. Phys. Biochem. Pharmacol.* **146** (2003) 1
2. M. Galanski, V. Arion, M. Jakupec, B. Keppler, *Curr. Pharm. Design* **9** *(*2003) 2078
3. P. Heffeter, U. Jungwirth, M. Jakupec, C. Hartinger, M. Galanski, L. Elbling, M. Micksche, B. Keppler, W. Berger, *Drug Res. Updates* **11** (2006) 1
4. G. V. Kalayda, S. Fakih, H. Bertram, T. Ludwig, H. Oberleithner, B. Krebs, J. Reedijk, *J. Inorg. Biochem.* **100** (2008) 1332
5. E. Budzisz, U. Keajewska, M. Rozalski, *Polish J. Pharmacol.* **56** (2004) 473
6. E.S. Antonarakis, A. Emadi, *Cancer Chemother. Pharmacol.* **66** (2010)1
7. E. Alessio, G. Mestroni, A. Bergamo, G. Sava, in *Metal Ions in Biological Systems: Metal Complexes in Tumor Diagnosis and as Anticancer Agents*, Vol. 42, A. Sigel, H. Sigel, Eds., CRC Press, New York, 2004, p. 323
8. M. Vaccaro, R. D. Litto, G. Mangiapia, A. M. Carnerup, G. D'Errico, F. Ruffo, L. Paduano, *Chem. Commun.* **11** (2009) 1404
9. G. Banditelli, A. Bandini, G. Minghetti, R. Seraglia, P. Iraldi, *Rapid Commun. Mass Spectrom*. **10** (1996) 1107
10. E. Osei-Twum, L. Litorja Jr., J. Darkwa, L. Maisela, A. Lesimple, O. Mamer, *J. Am. Soc. Mass Spectrom*. **16** (2005) 94

11. A. Mazzaglia, L. Scolaro, D. Garozzo, P. Malvagna, R. Romeo, *J. Organometal. Chem.* **690** (2005) 1978
12. C. Jahier, S. Nlate, *J. Organometal. Chem.* **694** (2009) 637
13. E. M. Peña-Méndez, B. González, P. Lorenzo, A. Romerosa, J. Havel, *Rapid Commun. Mass Spectrom.* **23** (2009) 3831
14. M. J. Deery, K. R. Jennings, C. B. Jasieczek, D. M. Haddleton, A. T. Jackson, H. T. Yates, J. H. Scrivens, *Rapid Commun. Mass Spectrom.* **11** (1997) 57
15. J. Bariyanga, *J. Bioact. Comp. Polym.* **17** (2002) 37
16. F. Gonnet, F. Kocher, J. Blais, G. Bolbach, J. Tabet, J. Chottard, *J. Mass Spectrom*. **31** (1996) 802
17. M. Brindell, S. Elmroth, G. Stochel, *J. Inorg. Biochem.* **98** (2004) 1367
18. J. Turkson, S. Zhang, L. B. Mora, A. Burns, S. Sebti, R. Jove, *J. Biol. Chem.* **280** (2005) 32979
19. M. Petković, A. Vujačić, J. Schiller, Z. Bugarčić, J. Savić, V. Vasić, *Rapid Commun. Mass Spectrom.* **23** (2009) 1467
20. A. Vujačić, Ž. D. Bugarčić, J. Schiller, V. Vasić, M. Petković, *Polyhedron* **28** (2009) 2905
21. M. Petković, B. Petrović, J. Savić, Ž. D. Bugarčić, J. Dimitrić-Marković, T. Momić, V. Vasić, *Int. J. Mass Spectrom.* **29** (2010) 39
22. F. Hillenkamp, J. Peter-Katalinic, *MALDI MS: A Practical Guide to Instrumentation, Methods and Applications*, Wiley-VCH Verlag, Weinheim, Germany, 2007, p. 13
23. L. P. Battaglia, A. B. Corradi, C. G. Palmieri, M. Nardelli, M. E. V. Tani, *Acta Cryst., B* **29** (1973) 762
24. G. Mahal, R. Van Eldik, *Inorg. Chim. Acta* **127** (1987) 203
25. M. Petkovic, J. Schiller, M. Müller, S. Benard, S. Reichl, K. Arnold, J. Arnhold, *Anal. Biochem.* **289** (2001) 202
26. R. March, J. Brodbelt, *J. Mass Spectrom.* **43** (2008) 1581.

Journal of the Serbian Chemical Society
JSCS-info@shd.org.rs • www.shd.org.rs/JSCS
J. Serb. Chem. Soc. 76 (12) 1703–1723 (2011)
JSCS–4241
UDC 678.652+678.84:66.095.26:541.124:543.42:536.5.004.12
Original scientific paper

Influence of the content of hard segments on the properties of novel urethane–siloxane copolymers based on a poly(ε-caprolactone)-*b*-poly(dimethylsiloxane)-*b*--poly(ε-caprolactone) triblock copolymer

MARIJA V. PERGAL[1]*, VESNA V. ANTIĆ[2#], SANJA OSTOJIĆ[3], MILENA MARINOVIĆ-CINCOVIĆ[4] and JASNA DJONLAGIĆ[5#]

[1]*Center of Chemistry, Institute of Chemistry, Technology and Metallurgy, University of Belgrade, Studentski trg 12–16, Belgrade,* [2]*Faculty of Agriculture, University of Belgrade, Nemanjina 6, Belgrade,* [3]*Institute of General and Physical Chemistry, Studentski trg 12–16, Belgrade,* [4]*Vinča Institute of Nuclear Sciences, P. O. Box 522, Belgrade and* [5]*Faculty of Technology and Metallurgy, University of Belgrade, Karnegijeva 4, Belgrade, Serbia*

(Received 7 March, revised 8 April 2011)

Abstract: A series of novel thermoplastic urethane–siloxane copolymers (TPUSs) based on a α,ω-dihydroxy-[poly(ε-caprolactone)-*b*-poly(dimethylsiloxane)-*b*--poly(ε-caprolactone)] (α,ω-dihydroxy-PCL-PDMS-PCL) triblock copolymer, 4,4'-methylenediphenyl diisocyanate (MDI) and 1,4-butanediol (BD) was synthesized. The effects of the content (9–63 mass %) of hard urethane segments and their degree of polymerization on the properties of the segmented TPUSs were investigated. The structure, composition and hard segment degree of polymerization of the hard segments were examined using ^{1}H- and quantitative ^{13}C-NMR spectroscopy. The degree of crystallinity of the synthesized copolymers was determined using wide-angle X-ray scattering (WAXS). The surface properties were evaluated by measuring the water contact angle and water absorption. In the series of the TPUSs, the average degree of polymerization of the hard segments was varied from 1.2 to 14.4 MDI-BD units. It was found that average values from 3.8 to 14.4 MDI-BD units were effective segment lengths for crystallization of hard segments, which resulted in an increase in the degree of microphase separation of the copolymers. Spherulite-like superstructures were observed in copolymer films by scanning electron microscopy (SEM), which are believed to arise from the crystallization of the hard segments and/or PCL segments, depending on the content of the hard segments. The surface of the copolymers became more hydrophobic with increasing weight fraction of PDMS. The synthesized copolymers based on a PCL-PDMS-PCL segment showed good thermal stability, which increased with increasing content of soft

* Corresponding author. E-mail: marijav@chem.bg.ac.rs
# Serbian Chemical Society member.
doi: 10.2298/JSC110307146P

PDMS segments, as was confirmed by the value of the starting temperature of thermal degradation.

Keywords: urethane–siloxane copolymers; polyaddition; hard segment content; quantitative ^{13}C-NMR spectroscopy; thermal properties; X-ray scattering.

INTRODUCTION

Thermoplastic polyurethane elastomers (TPUs) have been used extensively as biomaterials because of their biocompatibility and good mechanical properties. TPUs are multiblock copolymers composed of rigid polyurethane sequences, hard segments (HS) connected *via* flexible soft segments (SS). A variety of aliphatic and aromatic diisocyanates with diol or diamine chain extenders have been employed for hard segment formation in polyurethane materials based on polyether or polyester macrodiols (typically of molecular weight 1000–5000 g mol^{-1}) as the soft segment components.

The favorable physical properties of segmented TPUs are the consequence of microphase separation between the segments. The thermodynamic incompatibility of the hard and soft segments at low temperatures results in phase separation and, consequently, in the formation of a domain structure. It is believed that the hard segments, either glassy or crystalline with a melting temperature (T_m) above ambient temperature, form domains of approximately a few to tens of nanometers in size. These hard domains separate from the soft segments, which are usually formed of either low glass transition temperature (T_g) amorphous or low T_m crystalline segments. Their two-phase microstructure imparts excellent mechanical properties.[1,2] TPUs that are made of crystallizable HS and SS resemble a unique crystalline–crystalline multiblock copolymer, where crystallization of each segment provides nanoscale confinement of the other. The morphology of semicrystalline TPU block copolymers is determined by the following factors: block lengths, chemical composition, the thermodynamic incompatibility between the constituent blocks and crystallization of crystallizable blocks.[3–5]

The introduction of poly(dimethylsiloxane) (PDMS) into a polyurethane chain has the advantage of imparting some of the attractive properties of PDMS to the new polyurethane materials, such as high flexibility, biocompatibility, excellent thermal, oxidative and hydrolytic stability and low surface energy.[6–11] PDMS prepolymer used for the preparation of siloxane–urethane copolymers have number average molecular weight ($\bar{M}_n$) values in the range 1000–5000 g mol^{-1}. Due to substantial difference between the solubility parameters of PDMS and urethane hard segments, materials based on siloxane–urethane copolymers display the presence of microphase morphology. Early attempts of incorporating PDMS into a polyurethane backbone were unsuccessful due to the difficulty in the synthesis of TPUSs with acceptably high molecular weights from a mixture of polar and non-polar components.[12] However, a mixed or special type of polyol

was used in order to increase the compatibility of the reaction mixture and, therefore, to achieve higher molecular weights and better mechanical properties.[13–18]

In the past few years, significant research has been devoted to understand the correlation between microstructure and properties of segmented polyurethanes.[19,20] Maafi *et al.* concluded that the structure of TPUs synthesized by two-step polyaddition method was more regular with narrower HS size distribution compared to the one–step method.[21] Barreiro *et al.* studied the microstructure of poly(ester–urethane)s by experimental determination of the distribution of hard segments length using methods based on the hydrolysis of the polymer and subsequent size exclusion chromatography (SEC) analysis of the hydrolyzed products.[22] However, until now ^{13}C-NMR spectroscopy was used to examine the sequence distribution of hard segments in polyurethane copolymers in only a few research papers.[23,24]

In a previous paper, the optimization of the synthesis of TPUSs with a high PCL-PDMS-PCL content was described.[25] In the present work, a series of novel urethane–siloxane copolymers based on an *α*,*ω*-dihydroxy-PCL-PDMS-PCL) triblock copolymer, 4,4'-methylenediphenyl diisocyanate (MDI) and 1,4-butanediol (BD) was investigated. The triblock prepolymer contained terminal crystallizable poly(*ε*-caprolactone) blocks and a central poly(dimethylsiloxane) block. The combination of the properties of PCL and PDMS makes these block copolymers excellent candidates for employment as surface modifying additives in pharmaceutical and biomaterial applications.[26–28] The content of hard MDI-BD segments in the polymer chains was varied from 9 to 63 mass %. Simultaneously, the length of the hard segments increased with increasing HS content. In this study, an analysis of the microstructure, *i.e.*, the determination of the distribution of hard segments length by quantitative ^{13}C NMR spectroscopy, of urethane––siloxane copolymers is given. Hence, the influences of the content and average degree of the repeating units (MDI-BD) of the hard segments on the thermal, morphological and some physical properties of the synthesized TPUSs are presented in this paper.

EXPERIMENTAL

Materials

α,*ω*-Dihydroxy-(PCL-PDMS-PCL) (supplied by ABCR, Germany, $\bar{M}_n$ = 5700–6900 g mol^{-1}) was dried at room temperature under vacuum for 2 h. The ($\bar{M}_n$) of the *α*,*ω*-dihydroxy--(PCL-PDMS-PCL), determined by ^{1}H-NMR spectroscopy, was 6100 g mol^{-1}. The molecular weights of the central PDMS block and the terminal poly(*ε*-caprolactone) sequences were 2000 and 2050 g mol^{-1}, respectively. 4,4'-Methylenediphenyl diisocyanate (MDI) (supplied by Aldrich), with an isocyanate content of 33.6 wt. %, was used as received. 1,4-Butanediol (BD) (from Aldrich) was purified by vacuum distillation. *N*,*N*-Dimethylacetamide (DMAc) (from Across) was dried over calcium hydride and then distilled under vacuum. The solvent tetrahydrofuran (THF) (supplied by J. T. Baker) was dried over lithium aluminum hydride and

distilled before use. Stannous octanoate ($Sn(Oct)_2$) (purchased from Aldrich) was used as the catalyst without further purification.

Synthesis of polyurethane samples

The thermoplastic polyurethane copolymers were prepared by a two-step catalyzed polymerization in solution, starting from 4,4'-methylenediphenyl diisocyanate, 1,4-butanediol and α,ω-dihydroxy-(PCL-PDMS-PCL). All the copolymers were synthesized in the same manner under the optimal polymerization conditions:[25] the molar ratio of NCO/OH groups was 1.05/1, the amount of the catalyst was 0.15 mol % $Sn(Oct)_2$/α,ω-dihydroxy-(PCL-PDMS-PCL) and a mixture of DMAc/THF (1/1 v/v) was employed as the solvent. As an example, the synthesis of a copolymer with 87 mass % soft segment is described. A four necked round-bottom flask equipped with a mechanical stirrer, an inlet for dry argon, a reflux condenser and a dropping funnel was charged with 18.300 g (3.0 mmol) of α,ω-dihydroxy-(PCL-PDMS-PCL), 1.575 g (6.3 mmol) of 4,4'-methylenediphenyl diisocyanate, 60 mL of DMAc and 60 mL of THF. The flask was heated to 80 °C on a silicone oil bath and the reaction was started by the introduction of 0.29 mL of a solution of stannous octanoate in DMAc/THF (1.8 mg, 4.5×10^{-3} mmol of $Sn(Oct)_2$). The reaction mixture was stirred for 40 min at 80 °C to prepare the NCO--terminated prepolymer. The content of NCO during reaction was determined using the dibutylamine back-titration method.[29] The reaction was stopped when the theoretical NCO content was attained (1.27 mass %).[25] For chain extension, a dilute solution of BD (0.540 g, 6.0 mmol) in DMAc/THF was added dropwise to the prepolymer with the addition of a second portion of MDI (0.785 g, 3.1 mmol) dissolved in DMAc/THF. The reaction was continued at the same temperature for 24 h. The viscous polymer solution was precipitated into methanol/water (1/1 v/v) and the polymer was filtered off and dried to constant weight in a vacuum oven at 40 °C for 3 days. Polyurethane films were prepared from a 10 mass % solution in DMAc and cast onto a Teflon® plate. The solvent was evaporated for 48 h at 40 °C in a force-draft oven. The films were obtained under vacuum at 40 °C for 24 h (0.4–0.5 mm thick) and stored in a desiccator.

Characterization

The NMR experiments were performed on Bruker Avance 500 spectrometer equipped with 5 mm inverse detection *z*-gradient probe. The ^{1}H- and ^{13}C-NMR spectra (at 500.13 and 125.75 MHz, respectively) were measured at 25 °C using DMSO-d_6 as the solvent. Chemical shifts are given on the δ scale relative to the residual DMSO signal. The copolymers were dissolved in DMSO-d_6 at 50 °C at a concentration of 10 % (w/v). The quantitative ^{13}C-NMR spectra were obtained using the gated decoupling method under the following conditions: pulse delay time of 10 s, an acquisition time of 1.10 s, a pulse width of 16.8 μs, a spectral width of 29.8 kHz and the number of scans was between 7000 and 21000.

The viscosities of solutions of the copolymers in DMAc were measured at 25 °C using an Ubbelohde viscometer. The intrinsic viscosities were calculated from these measurements.

Wide angle X-ray scattering (WAXS) was performed using a Diffractometric System APD 2000 diffractometer with CuK_α radiation using a copper anode (tube: 40 kV, 30 mA, λ = = 0.154178 nm). The diffraction patterns were obtained in the Bragg angle range of 5–60°. The scan speed was 0.02 s per step in all measurements. The peaks in diffraction patterns were fitted by the Voigt deconvolution technique, using the Peakfit program, resulting in the areas of peaks. The percent crystallinity was calculated by peak deconvolution and subsequent determination of the relative areas under the amorphous halo and the crystalline peaks of the

X-ray diffraction pattern. The ratio of the area under the crystalline peaks to the total (amorphous + crystalline) area gave the degree of crystallinity.

The thermal stability of the copolymers was determined using TGA Q500 V6.3 Build 189 instrument in the temperature range from 25 to 700 °C, at a heating rate of 10 °C min^{-1}. The TGA scans were recorded under a dynamic nitrogen atmosphere with a gas flow rate of 50 mL min^{-1}. The average weight of the samples was about 10 mg.

The free or "air exposed" and cross-section morphology of the copolymer films was analyzed by field emission scanning electron microscopy (SEM). The samples were adhered to aluminum sample holders and sputter coated with Au to a thickness of *ca.* 5 nm (BAL-TEC SCD 005). The samples were then inserted into a JEOL JSM-6460LV microscope and the microphotographs were obtained at a working distance of *ca.* 14 mm at an acceleration voltage of 20 kV.

Water contact angle (WCA) measurements of the polymer films were realized in a Krüss DSA100 instrument using the sessile drop method. Single drops of distilled water with a volume of 20 μL were deposited on the film surface and the contact angles were measured after 30 s. All measurements were performed in air, at a temperature of 26 °C. The WCA measurements on polymer films were used to evaluate the surface properties and the wettability of the polymers by means of the sorption rate after 10 min (WCA_{10}) of deposition of the water droplet on the film surface. In all cases, at least five measurements were performed and the average contact angle was calculated.

To determine equilibrium water content of the synthesized TPUSs, polymer films were immersed in phosphate buffered saline (PBS, pH 7.4) at 37 °C, for 2.5, 5, 8, 24, 26, 28 and 48 h, respectively. At each time point, the samples were removed and blotted lightly with filter paper to remove excess water. The weight of the hydrated samples was then determined and the water absorption was calculated as follows: $(w - w_0)\times 100/w_0$, where w is the maximum wet weight measured and w_0 is the weight of the dry sample.

RESULTS AND DISCUSSION

A series of novel TPUSs was synthesized using PCL-PDMS-PCL as the soft segment component and MDI and BD as the hard segment components. The chemical structure of the synthesized polyurethanes is shown in Scheme 1. The samples were synthesized by a two-step polyaddition reaction in solution under optimized conditions.[25] In the synthesis of the TPUSs, the PCL blocks served as a compatibilizer between the non-polar PDMS blocks and the polar comonomers, MDI and BD. The TPUSs were synthesized first using an NCO-terminated prepolymer obtained from *α,ω*-dihydroxy-(PCL-PDMS-PCL) with slight excess of MDI and then chain extended with 1,4-butanediol to prepare the final TPUSs. The molar ratio of the *α,ω*-dihydroxy-(PCL-PDMS-PCL), MDI and BD was varied from 1:2:1 to 1:27:26 (Table I). The hard segment content of TPUSs was in the range of 9 to 60 mass %. The yields of the synthesized copolymers after precipitation were in the range of 85–93 % (Table I).

The structure and composition of the TPUSs

The molecular structure of the polyurethanes was investigated by ^{1}H and ^{13}C NMR spectroscopy.

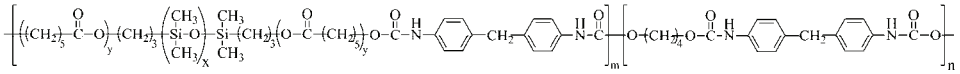

soft segment hard segment

Scheme 1. The chemical structure of the synthesized polyurethane copolymers based on soft PCL-PDMS-PCL and hard MDI-BD segments.

TABLE I. Composition of the reaction mixture and the copolymers, the average degree of polymerization of the hard segments, intrinsic viscosities, yields and degree of crystallinity determined by WAXS of the synthesized TPUSs

Sample	Molar ratio[a]	Fraction of MDI-BD, HS units		L_n (HS)[d]	$[\eta]$	Yield[e]	X_c / %
		mass %[b]	mass %(NMR)[c]		dL g^{-1}	%	(WAXS)
TPUS-9	1:2:1	8.8	8.5	1.2	0.50	87	40
TPUS-13	1:3:2	13.2	15.3	1.7	0.55	85	36
TPUS-17	1:4:3	17.2	17.2	1.9	0.58	88	30
TPUS-21	1:5:4	20.9	19.9	3.8	0.61	90	26
TPUS-30	1:8:7	30.1	29.4	4.0	0.64	91	8[f]; 25[g]
TPUS-40	1:12:11	39.5	38.4	4.7	0.67	91	9[f]; 16[g]
TPUS-50	1:18:17	49.7	48.4	10.2	0.74	93	10[f]; 7[g]
TPUS-60	1:27:26	59.8	62.6	14.4	0.83	92	13[f]; 5[g]

[a]PCL-PDMS-PCL:MDI:BD in the reaction mixture; at a 1.05 molar ratio of NCO/OH groups; [b]predetermined by the composition of the reaction mixtures; cdetermined by ^{1}H-NMR spectroscopy; [d]determined by quantitative ^{13}C-NMR spectroscopy; [e]calculated after precipitation of the copolymers; [f]degree of crystallinity of the MDI-BD segments; [g]degree of crystallinity of the PCL segments

The ^{1}H-NMR spectra of the copolymers showed characteristic signals at chemical shift values: –0.04 ppm of the Si–CH_3 protons; 0.43 ppm of the Si–CH_2 protons; 1.27 ppm of the central CH_2 protons from the ε-caprolactone residues and the central CH_2 protons from the PDMS propylene groups; 1.51 ppm of the internal CH_2 protons from the ε-caprolactone residues; 2.25 ppm of the CH_2–COO protons from the ε-caprolactone residues; 3.96 ppm of the terminal CH_2 protons from the ε-caprolactone residues; 3.77 ppm of the CH_2 protons from the MDI residues; 1.70 and 4.09 ppm of the central and terminal CH_2 protons of the BD residues, respectively; 3.40 ppm of the CH_2–OOC protons from the PDMS propylene groups; 7.08 and 7.34 ppm of the aromatic protons and 8.50 and 9.50 ppm of the –NH urethane protons.

As an example, the ^{1}H-NMR spectrum of TPUS-60 is shown in Fig. 1.

The ^{13}C-NMR spectra showed characteristic signals at the chemical shift values: 0.2 ppm of the $SiCH_3$ carbon; 24.1, 24.9 and 27.8 ppm of the central and internal CH_2 carbons from the ε-caprolactone residues; 60.4 and 63.5 ppm of the terminal CH_2 carbons from the PDMS propylene groups and terminal CH_2 carbons from the ε-caprolactone residues; 33.4 ppm of the **C**H_2–COO carbons from the ε-caprolactone residues; 25.3 and 63.7 ppm of the central and terminal CH_2 carbons from the BD residues; 40.0 ppm of the CH_2 carbon from the MDI resi-

dues; 153.6 and 172.7 ppm of the carbonyl carbons from the urethane and esters groups, respectively; 118.6, 129.1, 135.5 and 137.1 ppm of the aromatic carbons.

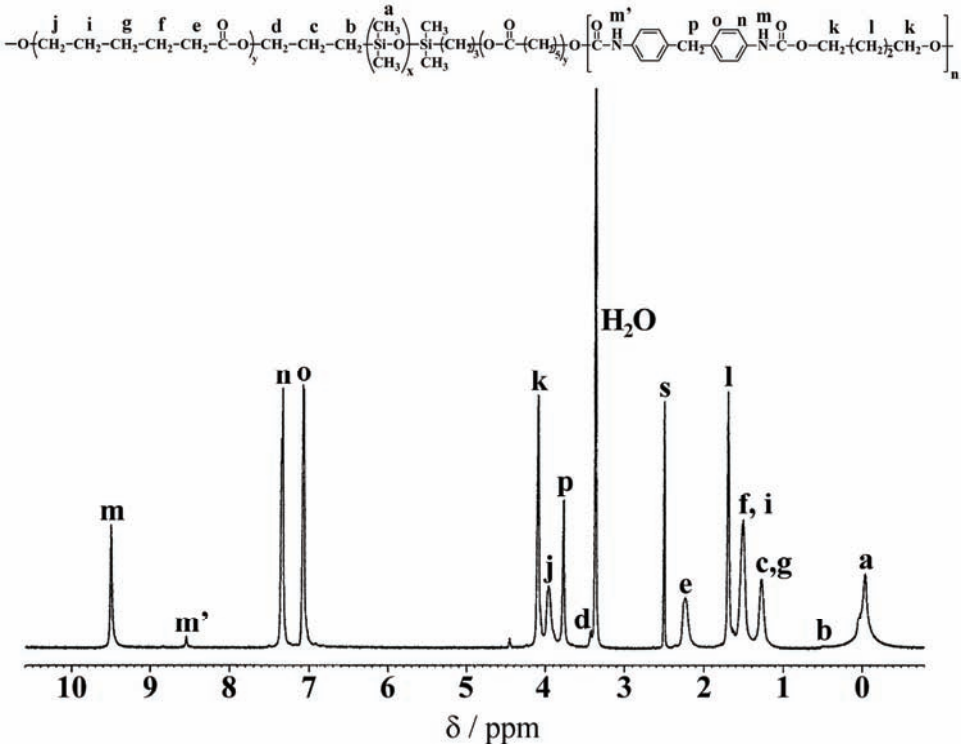

Fig. 1. ^{1}H-NMR Spectrum of the polyurethane copolymer with 40 mass % PCL-PDMS-PCL.

The composition of the polyurethanes, *i.e.*, the content of hard and soft segments, was calculated from the ^{1}H-NMR spectra as the relative intensities of the methyl proton signals arising from the –$SiCH_3$ groups and the aromatic proton signals from the MDI moieties. Thus, the mole and weight fraction of hard and soft segments were calculated, using the formulas:

$$x_{HS} = \frac{\frac{I(\mathrm{Ar-H})}{8}}{\frac{I(\mathrm{SiCH_3})}{6\overline{X}_x + 6} + \frac{I(\mathrm{Ar-H})}{8}} \qquad x_{SS} = 1 - x_{HS}$$

$$w_{HS} = \frac{x_{HS} M_{HS}}{x_{HS} M_{HS} + x_{SS} M_{SS}} \qquad w_{SS} = 1 - w_{HS}$$

where: x_{HS} and x_{SS} are the mole fractions of hard and soft segments, respectively; w_{HS} and w_{SS} are the weight fractions of hard and soft segments, respec-

tively; M_{HS} = 340 g mol^{-1}, the molecular weight of an MDI-BD unit; M_{SS} = = 6350 g mol^{-1}, molecular weight of a PCL-PDMS-PCL segment and $\overline{X}_X$ = = 25.3, the degree of polymerization of the PDMS-block in the prepolymer.

The theoretical and experimental mass % contents of the hard segments of the synthesized copolymers are presented in Table I. These results show that the weight fractions of the hard segments obtained from the ^{1}H-NMR analysis were in the range from 8.5 to 62.6 mass %. The obtained values of the weight fraction of the hard segments were in good agreement with values predetermined from the reaction mixture composition. For all the samples, except for TPUS-60, the disagreement was in the range of experimental error. It could be concluded that the composition of the polyurethanes was in good agreement with those expected from the composition of the feed, except for that of TPUS-60.

The NMR analysis showed that the syntheses of the polyurethane copolymers were successful, resulting in TPUSs with different lengths of the hard segments. The length of the hard segments in copolymer chains is defined as the number of repeating units $(MDI\text{-}BD)_n$ (where n = 1, 2, 3, 4,...) and is designated as L_n(HS). The length of the hard segments, *i.e.*, the average degree of polymerization, L_n (HS), was calculated from the results of quantitative ^{13}C-NMR spectroscopy, which are given in Table I. The ^{13}C-NMR spectra of the non-protonated aromatic region for polyurethane copolymers with different HS content are shown in Fig. 2, from which it could be seen that the peaks of the original symmetrical aromatic carbon atoms contained in MDI split and different signals (**r**, **r'** at 134.9–135.5 ppm and **t**, **t'** at 137.1–137.7 ppm) resulted due to the existence of MDI-BD and MDI-PCL linkages.[23,24] In addition, two signals, one at δ 152.5 and the other at δ 153.4 ppm that are related to –NHCOO– were found, which could be attributed to the –NHCOO– formed by reaction of MDI with 1,4-butanediol and with ε-caprolactone, respectively. The L_n(HS) was calculated from the ratio of the integral of the aromatic carbon signal from the MDI connected to 1,4-butanediol (**r**, Fig. 2) and that of the aromatic carbon signal from the MDI connected to ε-caprolactone (**r'**, Fig. 2). The synthesized TPUSs showed that the average hard segment lengths increased from 1.2 to 14.4 MDI-BD units with increasing HS content. According to the obtained results, ^{13}C-NMR analysis provides a relatively simple and reliable method to determine the microstructure of TPUS copolymers.

The results of the intrinsic viscosity, [η], measurements of the polyurethanes are presented in Table I. The intrinsic viscosities values were between 0.50 and 0.83 dL g^{-1}. Increasing content of hard segments in the copolymer, *i.e.*, a decrease in the flexibility of the copolymer chains, led to an increase of the intrinsic viscosity.

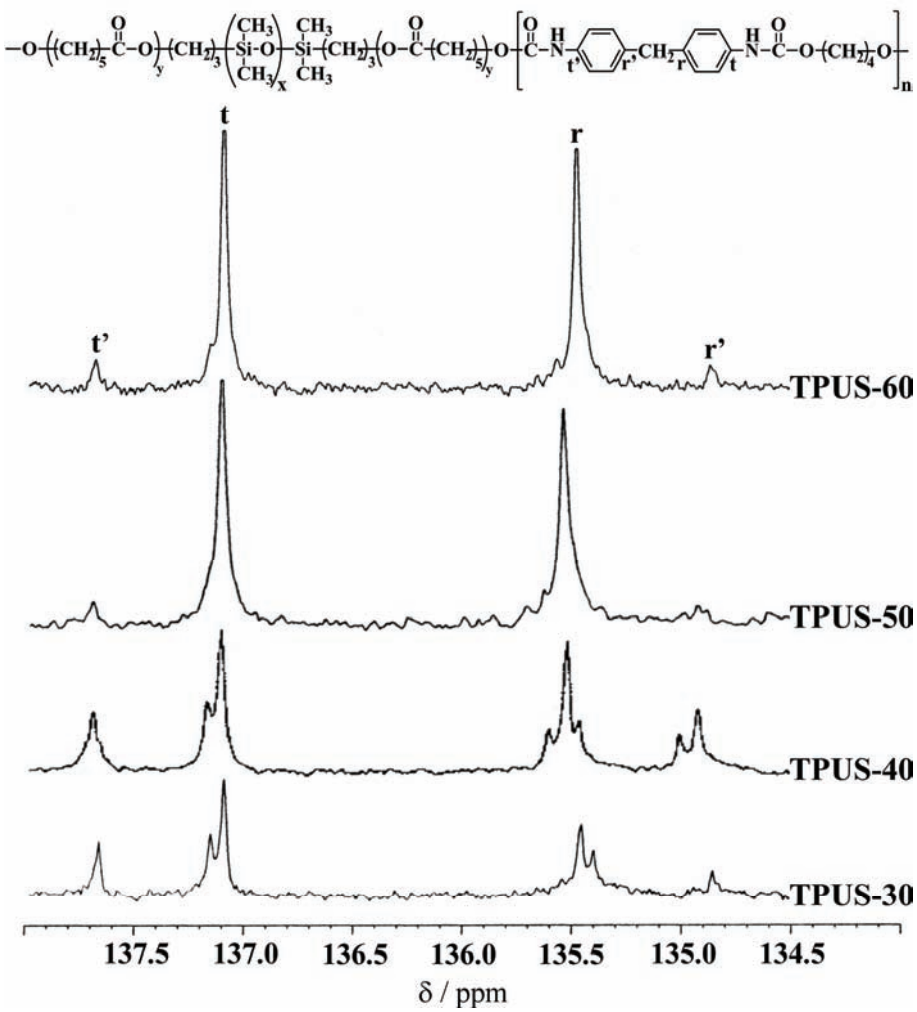

Fig. 2. Comparison of quantitative ^{13}C-NMR spectra of the polyurethane copolymers in the aromatic region showing the splitting for the non-protonated carbons.

Sequence length distribution of the TPUSs

In this study, the hard-segment length distribution in the obtained polyurethane copolymers was analyzed according to the Peebles statistical procedure,[30] assuming that the polyurethanes were formed by polyaddition reaction without side reactions and under stoichiometric conditions, and with the relative reactivity of the MDI groups $\mu = 1$. The calculated hard-segment length distributions are presented as weight and mole fraction distributions. Plots of the two distribution functions for several reaction mixture compositions are shown in Fig. 3.

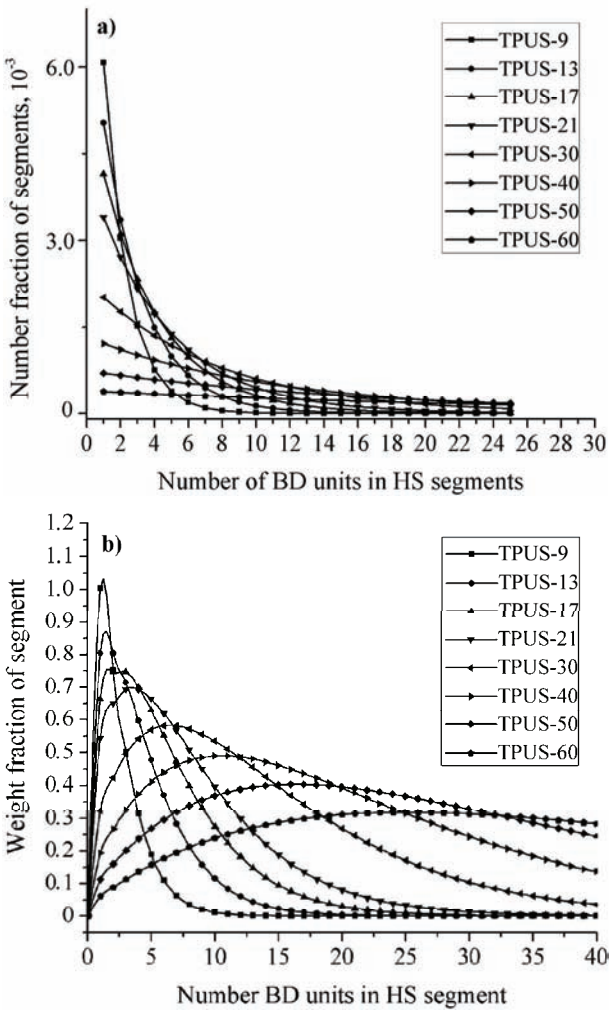

Fig. 3. Number fraction distribution curve (a) and weight fraction distribution curve (b) of the hard segment length for the TPUS copolymers.

The distribution of the sequence lengths, as was previously reported,[30] followed the most probable form:

$$P_i = C_1 (1-p)^2 \, p^{i-1}$$

where P_i is the concentration of sequence lengths that contain exactly i extenders (BD) and i+1 MDI units, C_1 is the initial concentration of BD.

The weight fraction distributions were calculated from the weight fraction of MDI residues containing BD units, (i+1) P_i / A_1, and the weight fraction of the internal diisocyanate units X_1^{int}/A_1, both normalized to the initial concentration of MDI, A_1.

It can be seen that on a number basis there were more lone MDI units than any other HS units regardless of the copolymer composition. The weight fraction distribution shows that the most probable segment length increased from 2 to 26 with increasing hard segment content from 9 to 63 mass %. The average segment length was below 5 for the copolymers with a hard segment content of less than 40 mass %. The content of one MDI unit in the copolymer chains was reduced with increasing hard segment content. In addition, the polydispersity of the HS distribution increased with increasing hard-segment content. Higher contents of hard segments introduce longer sequence lengths into the polymer chains, which would promote microphase separation.

WAXS Analysis of the TPUSs

The information on the crystalline structure of the synthesized copolymers was obtained from WAXS measurements. The diffraction diagrams for the polyurethanes are shown in Fig. 4, from which it can be seen that all the TPUSs displayed three crystalline peaks at 2θ values of 21.31–21.66, 22.06–22.30 and 22.99–23.98°. The X-ray diffraction pattern of the α,ω-dihydroxy-(PCL-PDMS--PCL) prepolymer displayed an amorphous halo from the PDMS block and three peaks at 2θ values of 21.21, 21.85 and 23.56°, which originated from the PCL blocks. For poly(ε-caprolactone), PCL, the presence of only one crystalline system, ortho-rhombic, was reported.[31] Based on the combined X-ray and electron diffraction data, the unit cell of poly(MDI-BD) is triclinic with dimensions a = = 5.33 Å, b = 5.26 Å, c = 38.68 Å, α = 113.6°, β = 116.0°, γ = 94.4°.[32]

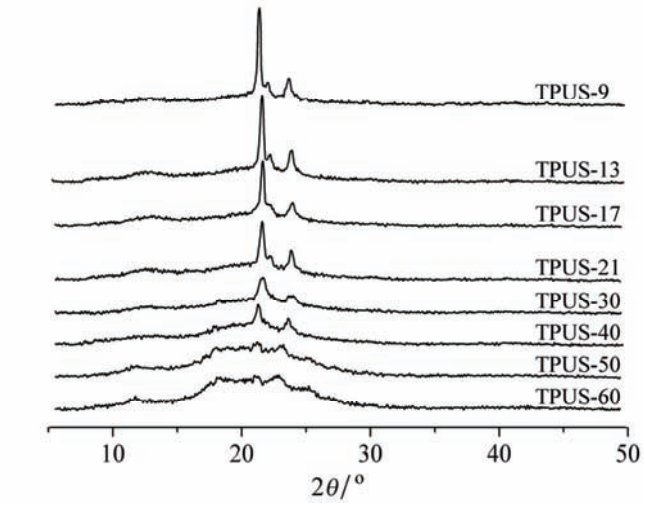

Fig. 4. X-Ray diffraction patterns of the synthesized polyurethane copolymers.

From the X-ray data and the peak positions in the diffractograms of the α,ω--dihydroxy-(PCL-PDMS-PCL) prepolymer and TPUS copolymers, it may be

stated that the soft PCL-PDMS-PCL segments in the TPUSs formed a crystalline structure. This is due to crystallization resulting from the PCL component in the soft segments. The diffractograms of the TPUSs were very similar to the diffractogram of the *α*,*ω*-dihydroxy-(PCL-PDMS-PCL) prepolymer and the main peaks occurred at almost the same 2*θ* values. Shifts in the peaks positions were observed for every copolymer, which could be attributed to deformations of the unit cell due to constraints imposed by the segmented structure and strong hydrogen bonds. In addition, it is visible that with increasing content of hard segments in the polymers, the areas of the crystalline peaks were reduced compared to the peaks from the *α*,*ω*-dihydroxy-(PCL-PDMS-PCL) prepolymer. The X-ray diffraction patterns of the TPUS-30, TPUS-40, TPUS-50 and TPUS-60 samples displayed additional, not very sharp, peaks at 2*θ* 19.39 and 25.24°.[7] These peaks positions were reported in the literature for MDI-BD crystallinity. In all the TPUS diffractograms, an amorphous halo at 2*θ* 12° due to the presence of the PDMS blocks was also observed. The behavior clearly demonstrates that the PDMS blocks formed a completely separated phase in the copolymers at room temperature.

The WAXS analyses confirmed that the hard MDI-BD segments partially contributed to the total degree of crystallinity of the TPUS samples with a hard segment content between 20 and 63 mass %. It can be concluded that the average degree of polymerization from 3.8 to 14.4 MDI-BD units were effective segment lengths for the formation of crystalline hard segments. The degrees of crystallinity, X_c^{WAXS}, of the polyurethanes were in the range from 17 to 40 % (Table I), while the degree of crystallinity of the *α*,*ω*-dihydroxy-(PCL-PDMS-PCL) prepolymer was 57 %. The value of degree of crystallinity of the HS tended to increase with increasing content of the hard segment length while the value of degree of crystallinity of the PCL-segments tended to decrease with increasing content and average degree of polymerization of HS (Fig. 5). The fact that the WAXS degree of crystallinity decreased with increasing weight fraction of MDI-BD hard segments in TPUSs was confirmed by the results of DSC analysis (to be published elsewhere). The total degree of crystallinity for TPUS-60, calculated from the DSC results, was the lowest in the series of copolymers and was around 30 %, from which it can be concluded that the presence of the hard segments probably disturbed the crystal growth of the PCL-segments. The synthesized TPUSs that consisted of crystallizable hard MDI-BD and soft PCL-PDMS-PCL segments were double crystalline copolymers.

A decrease in the crystallinity of segmented polyurethanes was previously reported for copolymers with different segment lengths of PCL,[33,34] but a systematic verification of the influence of the polyurethane hard segment length on the morphology of the PCL-block was not addressed. In a general way, the observed decrease in the degree of crystallinity of the PCL phase with increasing

urethane content in the copolymers can be explained in terms of the restrictions introduced by the covalent linkages and, more importantly, by the presence of strong interchain interactions through hydrogen bonding.[35,36]

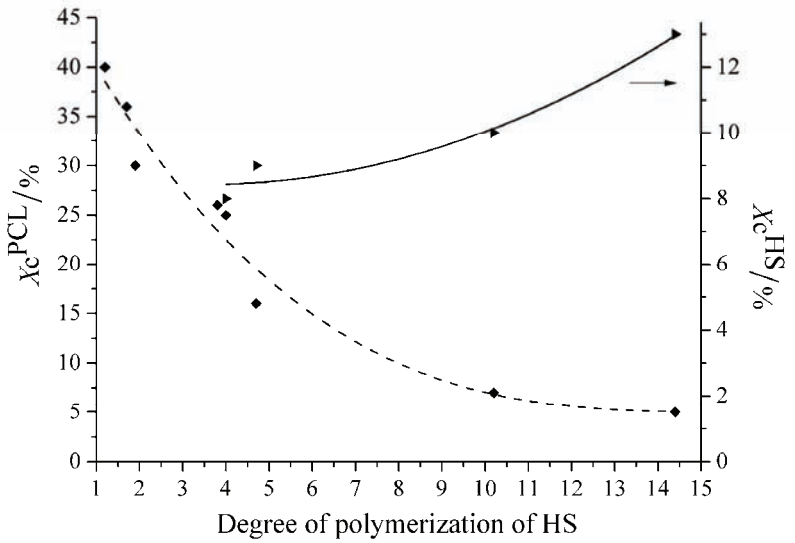

Fig. 5. Change in the degree of crystallinity of the PCL and hard segments determined by WAXS, as a function of the average degree of polymerization, L_n, of the hard segments.

TG analysis of the TPUSs

The thermal stability and degradation behavior of the synthesized polyurethanes were investigated by thermogravimetric analysis under a nitrogen atmosphere. The TG curves for the TPUSs with different contents of hard segments in the integral and differential form are shown in Figs. 6a and 6b, respectively. The characteristic temperatures for weight losses of 5 %, 50 % and 90 % as well as the residual weight at 600 °C are considered. The obtained results are given in Table II. The $T_{5\%}$ value is considered to represent the beginning of degradation.

The degradation of the copolymers commenced between 281 and 316 °C. From these data, it could be concluded that the thermal stability of the synthesized TPUSs depended strongly on the concentration of the urethane groups and decreased with increasing hard segment content in the copolymers. In addition, the temperature of 50 % weight loss in the TPUS series decreased with increasing content of hard segments. The thermally weakest link in polyurethane copolymers is the urethane bond, which starts to dissociate at around 200 °C. Three mechanisms of decompositions of urethane bonds have been suggested and the reactions may proceed simultaneously: dissociation to the original polyol and isocyanate, formation of a primary amine, an alkene, and carbon dioxide, and formation of a secondary amine and carbon dioxide.[37]

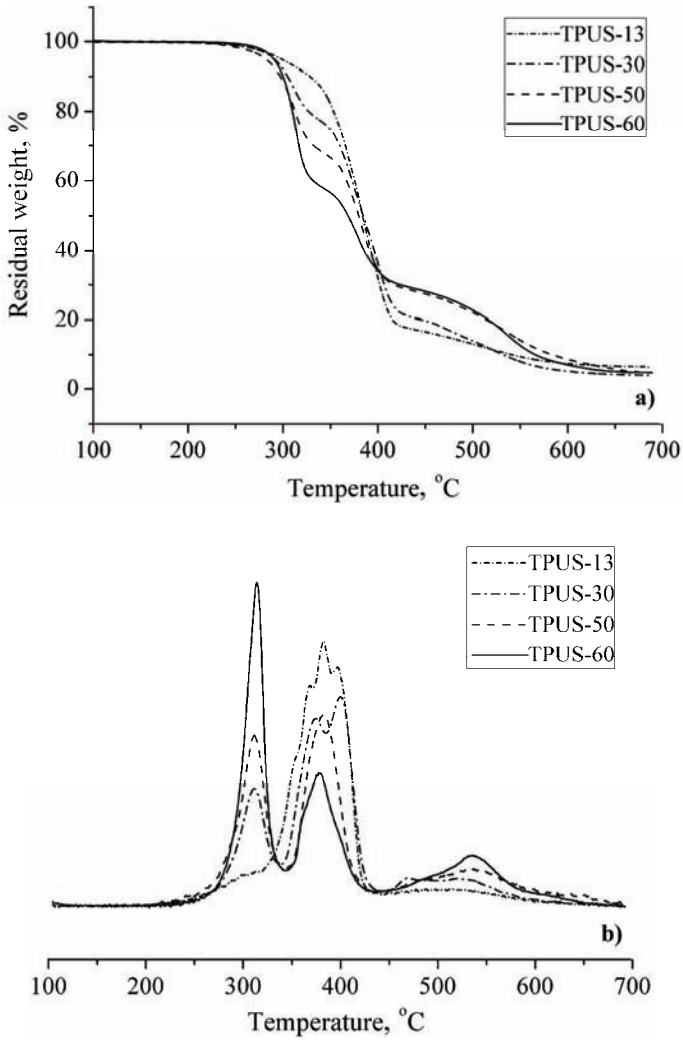

Fig. 6. TG and DTG curves for the polyurethane copolymers recorded at a heating rate of 10 °C under a nitrogen atmosphere.

The shapes of the weight loss curves of all the synthesized TPUSs were similar and overall differences in thermal stability appeared when the hard segment content increased. The thermal degradation of the synthesized TPUSs was a three-step process under a nitrogen atmosphere (Fig. 6b). The thermal degradation of the copolymers commenced *via* the decomposition of the urethane bonds, followed by degradation of the soft segments. Further decomposition in the region between 500 and 600 °C correlates with the aromatic content in the polyurethanes.[37,38] The obtained results indicated that TPUSs based on PCL-PDMS-

-PCL are sufficiently stable to be melt processed, for example, by injection molding and extrusion.

Table II. Thermal stability of the synthesized TPUSs under a nitrogen atmosphere

Sample	$t_{5\%}$ °C	$t_{50\%}$ °C	$t_{90\%}$ °C	t_{max} °C	Residual weight at 600 °C, %
TPUS-9	316	391	536	319/379/397/514	6.8
TPUS-13	306	391	548	310/376/391/515	7.6
TPUS-17	298	384	–	316/375/395/490	10.7
TPUS-21	301	394	538	316/374/399/525	6.8
TPUS-30	298	391	538	317/379/404/519	5.4
TPUS-40	286	386	555	313/383/538	6.3
TPUS-50	283	381	585	314/382/538	8.7
TPUS-60	281	367	555	318/382/538	4.8
α,*ω*-dihydroxy-(PCL-PDMS-PCL)	258	364	520	280/345/397/490	7.4

The residual weights of the TPUS samples at 600 °C ranged from 4.8 to 10.7 % (Table II). The residual weight originated mainly from the "organic"-fraction (MDI-BD and PCL), while the poly(dimethylsiloxane) chains under a nitrogen atmosphere degraded by depolymerization, giving cyclosiloxanes as the degradation products.[39]

It could be concluded that introduction of siloxane prepolymer with terminal PCL sequences enhanced the thermal stability in comparison with TPUs based on poly(caprolactone)-*b*-poly(tetrahydrofuran)-*b*-poly(caprolactone) diol (PCL--PTHF-PCL).[40]

Morphological investigation of the TPUSs by SEM

The "air" surface of the obtained films was investigated by SEM to observe any possible superstructure. The SEM microphotographs of the synthesized TPUSs and the *α*,*ω*-dihydroxy-(PCL-PDMS-PCL) prepolymer are shown in Fig. 7. The SEM microphotograph of *α*,*ω*-dihydroxy-(PCL-PDMS-PCL) exhibited a spherulitic structure typical for a semicrystalline polymer. The SEM microphotographs of the polyurethane films displayed a distinct spherulitic-like structure. There was a significant difference in the morphology between the copolymers with 9–20 and 30–63 mass % hard segments. For this reason, microphotographs of TPUSs at different magnifications are shown in Fig. 7.

The polyurethane samples with a hard segment content below 30 mass % showed a spherulite-like structure that is believed to arise from the crystallization of the PCL segments only, which was also suggested by the WAXS results. The mean size of the PCL crystalline superstructures in the prepolymer was 125 μm, while in the polyurethanes with a hard segment content below 30 mass %, it was in the range 46 – 64 μm. With increasing hard segment content, an enhancement in the crystallinity of the hard domains was evidenced. Due to this, at hard seg-

ment contents above 30 mass %, the visible ball-like structure probably arose from crystallization of both hard and PCL segments, which could lead to spherulitic structures. The interconnection of the crystallites, visible in SEM the micrographs, was most likely the consequence of the increasing length of the hard MDI-BD segments (Fig. 7). The main size of these crystalline superstructures in the TPUSs with more than 30 mass % hard segment was in the range 1 – 14 μm. The lack of crystalline fibrilar growth in these structures might be due to non-uniformity of the hard segment lengths in the mentioned samples, thereby impeding longer range ordering, but this is only a supposition.[41]

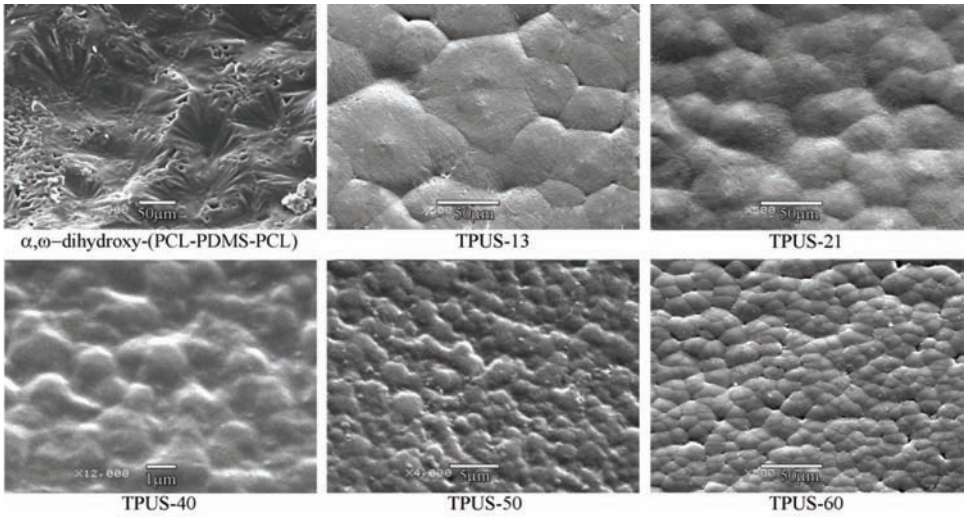

Fig. 7. SEM Microphotographs of the air surface of films of the polyurethanes and the *α*,*ω*-dihydroxy-(PCL-PDMS-PCL) prepolymer.

In addition, Fig. 8 shows the cross-sectional morphologies of polyurethane copolymers with different HS contents. In addition, it could be seen that the TPUSs show a unique structure with spherulitic-like structure in the longitudinal cross-section.[42] The average spherulite sizes in the TPUS copolymers were 2–4 μm. The spherulites of *α*,*ω*-dihydroxy-(PCL-PDMS-PCL) were 136 μm in size. The smaller size of the spherulites in the copolymer than in prepolymer can be explained by the introduction of the urethane block in polymer chains that restricts crystallization of the PCL-segments.

Water contact angle of the TPUSs

Special attention was focused on the wettability of the polyurethane surface, evaluated by water contact angle measurements (*WCA*). A water contact angle of 90° or more indicates a non-wetting surface. The relationship between the water contact angle and hard segment content is shown in Fig. 9, from which it can be seen

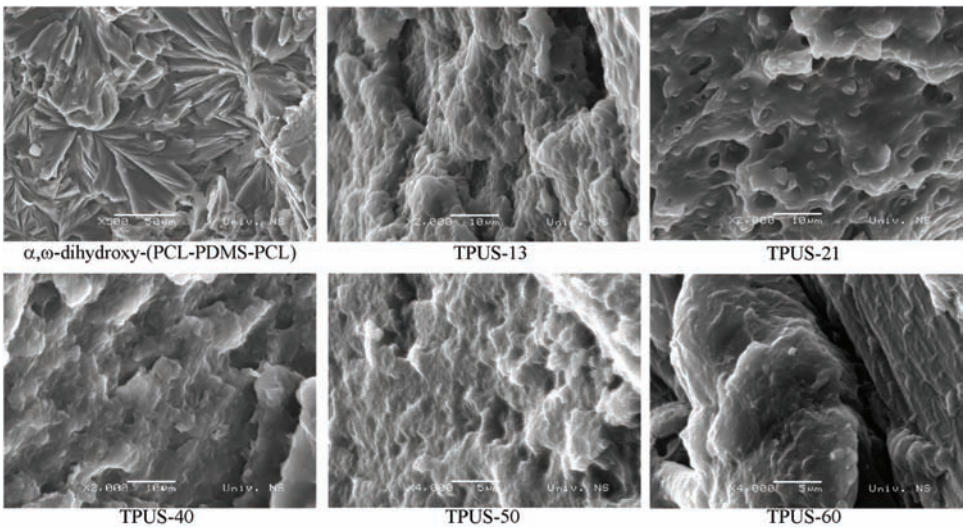

Fig. 8. SEM Microphotographs of the cross-section of films of the polyurethanes and the *α*,*ω*-dihydroxy-(PCL-PDMS-PCL) prepolymer.

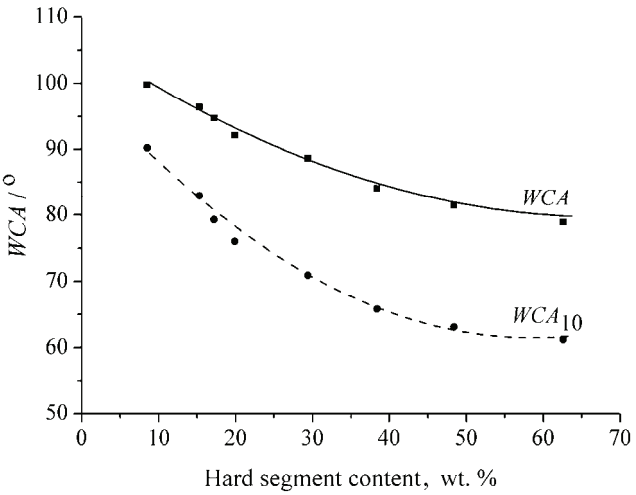

Fig. 9. Static water contact angle (*WCA*) and sorption rate (WCA_{10}) of the polyurethanes *vs.* hard segment content determined by ^{1}H-NMR spectroscopy.

that the value of the *WCA* for the TPUSs increased from 78.9 to 99.8° with increasing content of PDMS in the copolymers. The wettability of the copolymers decreased, *i.e.*, the hydrophobicity increased, with increasing weight fraction of PDMS. The water absorption rates of the TPUS samples, WCA_{10}, were measured after 10 min of the deposition of the water drop on the sample surface (Fig. 9), indicating that polyurethanes with higher HS contents absorbed the water drop more rapidly, decreasing their original values by 9.6 for TPUS-9 and 17.7 for TPUS-60. Thus, the polyurethanes with higher PDMS contents are more hydro-

phobic. The obtained results may be ascribed to the migration tendency of PDMS to the surface of the TPUSs, caused by the very low surface energy of PDMS.[26] The water contact angles for the TPUS-40, TPUS-50 and TPUS-60 samples were comparable with the contact angles of TPUs used in commercial implantable devices (75–80°) and culture grade polystyrene (80–85°).[43]

Water absorption of the TPUSs

Water uptake for the TPUS samples in PBS at 37 °C as a function of time is shown in Fig. 10. The obtained results showed that water absorption increased slightly with increasing immersion times. The water uptake of the TPUS samples after 24 h was between 1.42 and 2.90 %, while it was 1.50 % for the prepolymer. The value of the water uptake for the TPUSs increased with decreasing content of PDMS in the copolymers. This occurred because PDMS in copolymer formed a hydrophobic surface, which caused the reduction in the water uptake of TPUSs. All the synthesized TPUSs absorbed water. However, in comparison with polyurethanes based on more hydrophilic polyols reported by other authors,[44] the synthesized TPUSs were considered rather hydrophobic due to the hydrophobic nature of the PDMS and poly(ε-caprolactone). Therefore, polyurethanes based on PDMS with its potent water resistant properties demonstrated a great promise for use as medical implant.[11]

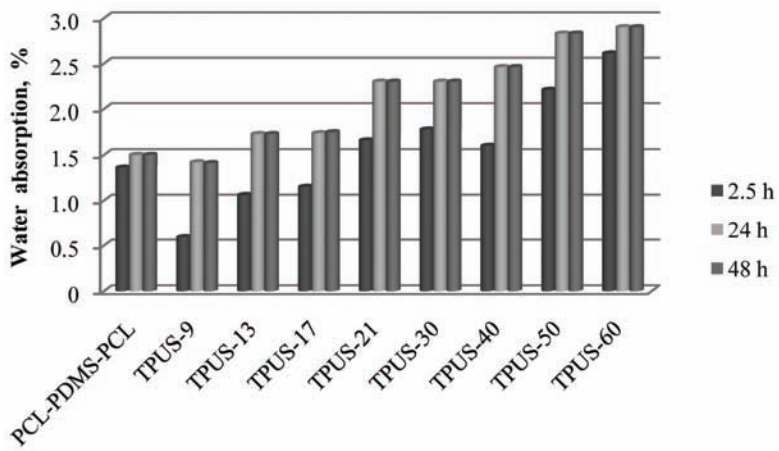

Fig. 10. Water absorption in dependence of the immersion time of the synthesized polyurethanes and α,ω-dihydroxy-(PCL-PDMS-PCL) prepolymer.

CONCLUSIONS

In order to investigate the influence of the hard segment length, *i.e.*, the average degree of polymerization, L_n, (MDI-BD) on the properties of TPUSs, novel thermoplastic siloxane–urethane copolymers based on biocompatible PCL--PDMS-PCL as soft segments with varying contents of hard segments were syn-

thesized. The weight fractions of the hard segments in the TPUS copolymers were in the range from 9 to 63 mass % and the average degree of polymerization of the hard segments varied between 1.2 and 14.4 MDI-BD units and was lower compared to the statistically calculated values. The increase in the HS degree of polymerization with hard segment content indicated that the chain-extension step in the synthesis of TPUSs was successful. The degree of crystallinity calculated from WAXS data was in the range from 17 to 40 %. The TPUS series represents a class of crystalline-crystalline block copolymers that consist of crystallizable hard and soft segments. Due to the increase in the degree of polymerization of the hard MDI-BD segments, the degree of crystallinity of the HS increased. It was found that an average number between 3.8 and 14.4 repeating MDI-BD units were effective segment lengths for a crystalline hard segment to be formed. As the HS content increased, there was a marked decrease in SS crystallinity. SEM images confirmed the presence of a spherulitic morphology, which arises from the crystallization of the hard segments and/or PCL segments depending on the content of the hard segments. The surface of the copolymers became more hydrophobic with increasing weight fraction of PDMS. The obtained results indicated that TPUSs based on soft PCL-PDMS-PCL segments are sufficiently stable to be melt processed, for example, by injection molding and extrusion. The synthesized TPUSs thus combine chemical, thermal, surface and morphological properties that might be employed in future biomedical applications.

Acknowledgement. This work was financially supported by the Ministry of Education and Science of the Republic of Serbia (Project No. 172062).

ИЗВОД

УТИЦАЈ САДРЖАЈА ТВРДОГ СЕГМЕНТА НА СВОЈСТВА НОВИХ УРЕТАН-СИЛОКСАНСКИХ КОПОЛИМЕРА НА БАЗИ ПОЛИ(*ε*-КАПРОЛАКТОН)-*b*-ПОЛИ(ДИМЕТИЛСИЛОКСАН)-*b*-ПОЛИ(*ε*-КАПРОЛАКТОНА)

МАРИЈА В. ПЕРГАЛ[1], ВЕСНА В. АНТИЋ[2], САЊА ОСТОЈИЋ[3], МИЛЕНА МАРИНОВИЋ-ЦИНЦОВИЋ[4] и ЈАСНА ЋОНЛАГИЋ[5]

[1]Центар за хемију, Институт за хемију, технологију и металургију, Универзитет у Београду, Студентски трг 12–16, Београд, [2]Пољопривредни факултет, Универзитет у Београду, Немањина 6, Београд, [3]Институт за општу и физичку хемију, Студентски трг 12–16, Београд, [4]Институт за нуклеарне науке Винча, п.пр. 522, Београд и [5]Технолошко–металушки факултет, Универзитет у Београду, Карнегијева 4, Београд

У овом раду приказана је структура и нека својства серије нових термопластичних уретан–силоксанских кополимера (TPUSs) на бази *α*,*ω*-дихидрокси-[поли(*ε*-капролактон)-*b*-поли(диметилсилоксан)-*b*поли(*ε*-капролактон)] триблок кополимера (*α*,*ω*-дихидрокси-PCL-PDMS-PCL), 4,4'-метилендифенилдиизоцијаната (MDI) и 1,4-бутандиола (BD). Испитан је утицај садржаја уретанског тврдог сегмента (9–63 мас. %) и његове дужине, тј. степена полимеризације, изражене преко броја MDI-BD остатака, на својства сегментираних TPUSs. Структура, састав и степен полимеризације тврдог сегмента су испитани помоћу ^{1}H- и квантитативне ^{13}C-NMR спектроскопије. Степен кристалиничности кополимера је одређен методом дифракције X-зрака на великим угловима (WAXS). Површинска својства кополимера су

испитана одређивањем контактних углова са водом и мерењем апсорпције воде. У серији кополимера дужина тврдог сегмента изражена преко броја понављајућих MDI-BD јединица је варирана од 1,2 до 14,4. Утврђено је да тврди сегменти са 3,8 до 14,4 понављајућих MDI-BD јединица ефикасно кристалишу, што је резултовало у повећању степена микрофазне сепарације кополимера. SEM анализа је показала присуство сферулитне структуре у кополимерним филмовима, која највероватније потиче од кристализације тврдих и/или PCL сегмената, зависно од садржаја тврдих сегмената. Хидрофобност површине кополимера је расла са повећањем масеног удела PDMS-а у одговарајућем узорку. Синтетисани полиуретани на бази PCL-PDMS-PCL показују повећање термичке стабилности са повећањем садржаја меких PDMS сегмената, што је потврђено порастом почетне температуре деградације, одређене TG анализом.

(Примљено 7. марта, ревидирано 8. априла 2011)

REFERENCES

1. S. Gogolewski, *Colloid Polym. Sci.* **267** (1989) 757
2. S. L. Cooper, J. C. West, R. W. Seymour, in *Encyclopedia of Polymer Science and Technology*, H. F. Mark, N. M. Bikales, Eds., Wiley, New York, 1976, p. 521–543
3. A. J. Müller, M. L. Arnal, V. Balsamo, in *Progress in Understanding of Polymer Crystallization*, G. Reither, G. R. Strobl, Eds., Springer Verlag, Berlin, 2007, p. 229–257
4. R. V. Castillo, A. J. Müller, *Prog. Polym. Sci.* **34** (2009) 516
5. M. A. Hood, B. Wang, J. M. Sands, J. J. La Scala, F. L. Beyer, C. Y. Li, *Polymer* **51** (2010) 2191
6. R. W. Hergenrother, Y. Xue-Hai, S. L. Cooper, *Biomaterials* **15** (1994) 635
7. D. J. Martin, G. F. Meijs, P. A. Gunatillake, S. P. Yozghatlian, G. M. Renwick, *J. Appl. Polym. Sci.* **71** (1999) 937
8. E. Briganti, P. Losi, A. Raffi, M. Scoccianti, A. Munaò, G. Soldani, *J. Mater. Sci. - Mater. Med.* **17** (2006) 259
9. A. Simmons, J. Hyvarinen, L. Poole-Warren, *Biomaterials* **27** (2006) 4484
10. İ. Yilgör, J. McGrath, *Adv. Polym Sci.* **86** (1988) 1
11. N. Roohpour, J. Wasikiewicz, D. Paul, P. Vadgama, I. Rehman, *J. Mater. Sci. Mater. Med.* **20** (2009) 1803
12. T. A. Speckhard, S. L. Cooper, *Rubber Chem. Technol.* **59** (1986) 405
13. E. Yilgor, I. Yilgor, *Polym. Prepr. (Am. Chem. Soc., Div. Polym. Chem.)* **39** (1998) 465
14. P. A. Gunatillake, G. F. Meijs, S. J. McCarthy, R. Adhikari, *J. Appl. Polym. Sci.* **76** (2000) 2026
15. J. P. Sheth, E. Yilgor, B. Erenturk, H. Ozhalici, I. Yilgor, G. L. Wilkes, *Polymer* **46** (2005) 8185
16. R. Hernandez, J. Weksler, A. Padsalgikar, T. Choi, E. Angelo, J. S. Lin, L.-C. Xu, C. A. Siedlecki, J. Runt, *Macromolecules* **41** (2008) 9767
17. T. Choi, J. Weksler, A. Padsalgikar, J. Runt, *Polymer* **50** (2009) 2320
18. J. P. Sheth, A. Aneja, G. L. Wilkes, E. Yilgor, G. E. Atilla, I. Yilgor, F. L. Beyer, *Polymer* **45** (2004) 6919
19. D. J. Martin, G. F. Meijs, P. A. Gunatillake, S. J. McCarthy, G. M. Renwick, *J. Appl. Polym. Sci.* **64** (1997) 803
20. D. De, R. J. Gaymans, *Macromol. Mater. Eng.* **293** (2008) 228
21. E. M. Maafi, F. Malek, L. Tighzert, *J. Appl. Polym. Sci.* **115** (2010) 3651
22. M. F. Barreiro, R. C. S. Dias, M. R. N. Costa, *Macromolecules* **27** (1994) 7650

23. N. Luo, D.-N. Wang, S.-K. Ying, *J. Polym. Sci. Part A: Polym. Chem.* **34** (1996) 2157
24. A. M. de Ilarduya, E. Carvalho, A. Alla, S. Muñoz-Guerra, *Macromolecules* **43** (2010) 3990
25. M. V. Pergal, V. V. Antic, M. N. Govedarica, D. Godjevac, S. Ostojic, J. Djonlagic, *J. Appl. Polym. Sci*. **122** (2011) 2715
26. M. A. Childs, D. D. Matlock, J. R. Dorgan, T. R. Ohno, *Biomacromolecules* **2** (2001) 526
27. N. Kayaman-Apohan, O. Karal-Yilmaz, K. Baysal, B. M. Baysal, *Polymer* **4**2 (2001) 4109
28. Z. Xu, S. Zheng, *Polymer* **48** (2007) 6134
29. A. Marand, J. Dahlin, D. Karlsson, G. Skarping, M. Dalene, *J. Environ. Monit*. **6** (2004) 606
30. L. H. Peebles, *Macromolecules* **9** (1976) 58
31. C. Lefèvre, D. Villers, M. H. J. Koch, C. David, *Polymer* **42** (2001) 8769
32. J. R. Quay, Z. Sun, J. Blackwell, R. M. Briber, E. L. Thomas, *Polymer* **31** (1990) 1003
33. B. Bogdanov, V. Toncheva, E. Schacht, L. Finelli, B. Sarti, M. Scandola, *Polymer* **40** (1999) 3171
34. F. Li, J. Hou, W. Zhu, X. Zhang, M. Xu, X. Luo, D. Ma, B. K. Kim, *J. Appl. Polym. Sci*. **62** (1996) 631
35. J. Kloss, M. Munaro, G. P. D. Souza, J. V. Gulmine, S. H. Wang, S. Zawadzki, L. Akcelrud, *J. Polym. Sci., A* **40** (2002) 4117
36. S. Mondal, J. L. Hu, *Polym. Eng. Sci*. **48** (2008) 233
37. F. S. Chuang, W. C. Tsen, Y. C. Shu, *Polym. Degrad. Stabil*. **84** (2004) 69
38. T. Hentschel, H. Münstedt, *Polymer* **42** (2001) 3195
39. P. R. Dvornic, R. W. Lenz, *High Temperature Siloxane Elastomers*, Hüthing & Wepf, Heidelberg, Germany, 1990
40. L. Rueda-Larraz, B. F. d'Arlas, A. Tercjak, A. Ribes, I. Mondragon, A. Eceiza, *Eur. Polym. J*. **45** (2009) 2096
41. Y. Xu, Z. Petrovic, S. Das, G. L. Wilkes, *Polymer* **49** (2008) 4248
42. J. Guan, K. L. Fujimoto, M. S. Sacks, W. R. Wagner, *Biomaterials* **26** (2005) 3961
43. H. Li, J. Chang, A. Cao, J. Wang, *Macromol. Biosci*. **5** (2005) 433
44. J. Guan, W. R. Wagner, *Biomacromolecules* **6** (2005) 2833.

Journal of the Serbian Chemical Society
JSCS-info@shd.org.rs • www.shd.org.rs/JSCS
J. Serb. Chem. Soc. 76 (12) 1725–1737 (2011)
JSCS–4242
UDC 639.42+546.47/.49+546.56+
546.815:504.42(262)(497.16)
Original scientific paper

Trace elements concentrations (Zn, Cu, Pb, Cd, As and Hg) in the Mediterranean mussel (*Mytilus galloprovincialis*) and evaluation of mussel quality and possible human health risk from cultivated and wild sites of the southeastern Adriatic Sea, Montenegro

SLAVKA STANKOVIĆ[1]*, MIHAJLO JOVIĆ[2], RAŠA MILANOV[3] and DANIJELA JOKSIMOVIĆ[4]

[1]*Faculty of Technology and Metallurgy, Karnegijeva 4, University of Belgrade, 11000 Belgrade,* [2]*Institute of Nuclear Science Vinča, University of Belgrade, 11000 Belgrade,* [3]*Ministry of Health, Sector for Sanitary Control, Omladinskih brigada 1, 11070 Belgrade, Serbia and* [4]*Institute of Marine Biology, University of Montenegro, 85330 Kotor, Dobrota bb, Montenegro*

(Received 20 April, revised 18 June 2011)

Abstract: The Mediterranean mussel *Mytilus galloprovincialis* (L.) was collected from the fall 2005 to the winter 2009 from the six sites on the Montenegrin coastline. Two wild samples were collected from the open sea coastline, and two cultivated and two wild were from the Boka Kotorska Bay. The mussels soft tissue was analyzed for zinc, copper, lead, cadmium, arsenic and total mercury. Concentrations of these metals, in mg kg^{-1} dry weight, ranged from 135–210 for Zn, 6.2–14.5 for Cu, 4.0–11.5 for Pb, 1.7–2.1 for Cd, 5.8––12.4 for As and 0.1–0.5 for Hg. The metals were found to be present in the samples at different levels, but not in concentrations higher than maximum residual levels prescribed by the European Union (EU) and US Food and Drug Administration (USFDA) regulations for seafood. This indicates that the consumption of wild or cultivated mussels from the studied area is safe in moderate quantities.

Keywords: *M. galloprovincialis*; trace elements; mussel quality; health risks; Montenegro; Adriatic.

INTRODUCTION

With the increase in consumption of seafood in recent years,[1,2] marine mussels have become commercially more important seafood species worldwide.[3] Among these, the Mediterranean mussel *Mytilus galloprovincialis* (L.) is widely

* Corresponding author. E-mail: slavka@tmf.bg.ac.rs
doi: 10.2298/JSC110420095S

distributed in the coastal waters of the eastern Atlantic–Mediterranean region and is mainly cultivated in the northwestern coastal waters of Spain and the northern shores of the Mediterranean Sea.[4] More recently, production of this mussel has been reported on the shores of the southern Mediterranean countries and on the Adriatic coast. Until recently, the main seafood product on the Montenegrin market was fish, but currently, the demand for nutrition sources such as mussels and other shellfish, has increased.[5]

The mussel *M. galloprovincialis* is a native species of this area and there are some indications that this bivalve was cultivated a hundred years ago. Cultivation of mussels in Montenegro is a family-run business and all farms are located in the Boka Kotorska Bay where the hydrological, physical and biological conditions are suitable for the type of rearing used on these farms. There is no modern mechanization on the farms and almost all the procedures are performed manually, which results in a long production cycle and low productivity. During the period 2003–2007, the average annual production of mussels in Montenegro was 150 t,[5] which is very small in comparison with the largest producers China (600,000 t year^{-1}) and Spain (200,000 t year^{-1}).[4] The farmed mussels are sold mostly to restaurants, hotels and on the local market stalls and small quantities of mussels are exported to neighboring countries, primarily to Serbia. Although the economic value of the aquaculture sector is currently very low, significant potential for the production and export of mussels, *M. galloprovincialis*, has been identified.[5]

Mussels are an important source of Ca and Fe, some vitamins such as niacin and thiamine, and are a good source of protein for humans.[6] Even though mussels are an excellent source of nutrients, they can potentially be toxic because certain metals, such as Pb, Cd, As and Hg, can accumulate in their soft tissue over time making them detrimental to human health.[7–10] As the natural habitats of *M. galloprovincialis* (L.) are usually close to estuaries, they are exposed to contaminants from land-based activities, as well as to sea based ones, making them an excellent heavy metal biomonitoring agent.[11] Conveniently, *M. galloprovincialis* (L.) are sedentary, long-lived, and easily identifiable and sampled organisms. They are fairly abundant and available throughout the year, reasonably tolerant to environmental change and pollution, and they have good net accumulation capacities.[4,11] Due to the propensity of *M. galloprovincialis* (L.) to accumulate metals and other contaminants in their soft tissue[12–16] and shells,[17] mussels have actively been used as a biomonitoring agent, as the determination of contaminant levels in mussel species provides a means of assessing the possible toxicant risk to public health.[4,8,18,19] Regular consumers of bivalve mollusks in Europe were found to have higher dietary exposures to Cd, up to 4.6 μg kg^{-1} body weight (b.w.).[20] Human exposure to Pb is mainly *via* food and water. On average, Pb dietary exposure ranges from 0.36 to 1.24, up to 2.43 μg kg^{-1}

b.w. per day for large mussels consumers in Europe.[21] The accepted tolerable weekly intakes of trace elements *via* the food change over time; concentrations of trace elements which were thought to be safe were later found to be harmful.[22,23]

Since trace elements are non-biodegradable chemicals which cannot be metabolized and do not break down into harmless forms,[24] the measurement of their concentration in mussel soft tissue intended for human consumption has become increasingly significant. Accumulation of toxic metals to above permissible limits in *M. galloprovincialis* (L.) would certainly create a notorious food image from the public health point of view, as it is well known that chronic exposure to trace elements is associated with disease,[25] as well as other health problems.[26]

All elements are toxic above some threshold bioavailable level, but Hg, Cd, As and Pb are particularly toxic[4,20–23] for animals and humans. Zn and Cu are two of the essential trace elements for both and zinc toxicity is rare and in addition, this element appears to have a protective effect against toxicities of cadmium and lead.[8]

In this study, the concentration levels of essential elements, Zn and Cu, and toxic ones, *i.e.*, Pb, Cd, As and total Hg, were determined in the soft tissue of *M. galloprovincialis* collected from natural (wild) and cultivation farms of the southeastern Adriatic – Montenegrin coast. The aim was to investigate whether the concentrations of these metals were within the permissible limits and the mussels thereby acceptable for human consumption.

EXPERIMENTAL

Sampling, storage and sample preparation

The sampling sites are shown in Fig. 1. Sampling was conducted between the fall 2005 and winter 2009. Wild mussels were collected from four locations (two from the open sea and two in the enclosed Boka Kotorska Bay) and cultivated mussels from two farms in the Bay. Mussels of similar shell length (the approximate age of the cultivated mussels was one and half years and the wild ones having the same shell length were assumed to be of the same age) were collected at each sampling site (Table I), placed in plastic bags with sea water and transported to the laboratory. After washing with distilled water, the size and weight of the samples were determined before dissection making sure that there were no significant differences regarding the size and weight of the samples among sites and within seasons ($p < 0.05$). The average water content in the soft tissues varied between 80.3 % (spring–fall) and 87.7 % (winter). Mussels were dissected by removing the byssus and shell and composite samples of mussel tissue were rinsed with de-ionized water, freeze-dried and homogenized using a mill. About 25–30 mussels from each sampling site were selected, pulverized and analyzed for the trace elements.

Analysis of trace elements

Preparation of mussel soft tissue (approximately 0.5 g) for trace metal analysis was performed as follows: the soft tissue was digested with a mixture of concentrated HNO_3 (65 % Merck, Suprapur) and H_2O_2 (30 % Merck, Suprapur) in a Microwave Digestion System (CEM. CORPORATION, MDS-2100). Prior to microwave decomposition, samples with added reagents were allowed to digest at room temperature in loosely capped Teflon beakers

for at least 1 h. Digested samples were diluted to 25 ml with deionized water containing 1.0 % HNO_3.

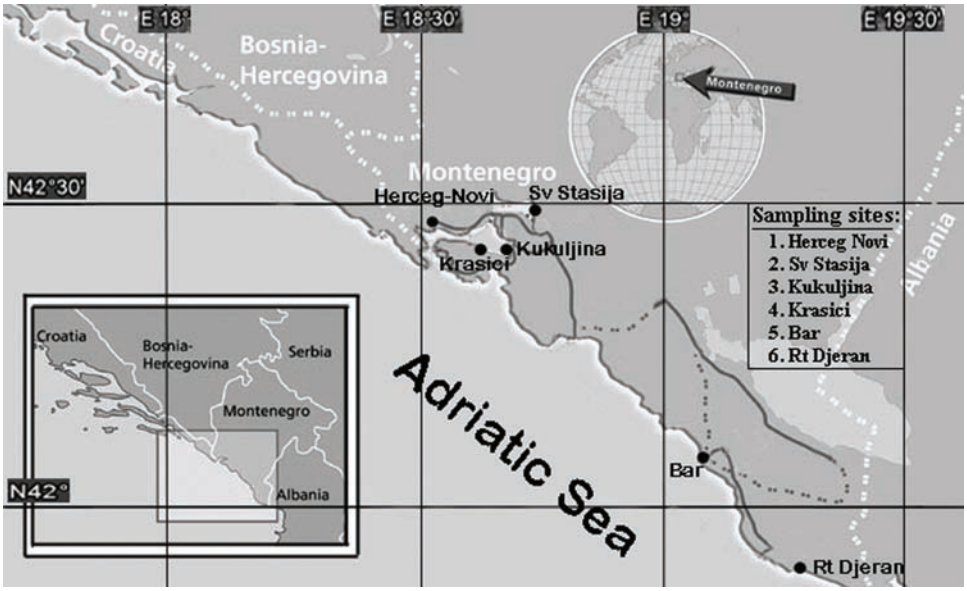

Fig. 1. Sampling sites of the Mediterranean mussel *M. galloprovincialis* from the southeastern Adriatic Sea, Montenegro.

TABLE I. Sampling locations and shell length of the Mediterranean mussel *M. galloprovincialis* collected from the SE Adriatic coast, Montenegro (Nos. follow those indicated in Fig. 1)

No.	Location	Sampling date	Sample nature	*N*	Shell length, mm
1	Herceg Novi, in Boka Kotorska Bay	19 Sep. 2005	Wild	25	71.3 (68.6–78.8)
		23 May 2006			70.3 (65.3–74.6)
		24 Sep.2006			74.8 (62.3–79.7)
		16 May 2007			69.4 (63.9–74.5)
		21 Sep. 2007			72.3 (66.8–76.3)
		04 Feb. 2008			68.7 (64.0–72.2)
		23 Jun 2008			70.9 (68.0–75.6)
		06 Oct. 2008			74.5 (67.8–79.2)
		09 Feb. 2009			70.2 (67.4–73.9)
2	Sveta Stasija, in Boka Kotorska Bay	19 Sep. 2005	Wild	25	73.6 (68.9–80.3)
		23 May 2006			72.0 (67.5–79.5)
		24 Sep.2006			72.5 (66.8–78.0)
		16 May 2007			70.8 (63.9–75.4)
		21 Sep. 2007			71.9 (65.6–76.9)
		04 Feb. 2008			67.1 (60.4–72.5)
		23 Jun 2008			68.5 (64.3–73.7)
		06 Oct. 2008			72.6 (61.0–81.9)
		09 Feb. 2009			68.0 (56.9–71.3)

TABLE I. Continued

No.	Location	Sampling date	Sample nature	*N*	Shell length, mm
3	Kukuljina, in Boka Kotorska Bay	21 Sep.2007	Cultured	27	64.8 (56.9–71.6)
		04 Feb.2008			62.4 (53.4–69.8)
		23 Jun 2008			63.7 (54.6–70.1)
		06 Oct.2008			67.1 (59.5–72.5)
		09 Feb. 2009			62.9 (52.1–71.4)
4	Krašići, in Boka Kotorska Bay	21 Sep. 2007	Cultured	25	66.9 (59.1–72.0)
		04 Feb. 2008			63.6 (55.9–70.7)
		23 Jun 2008			64.9 (56.0–71.9)
		06 Oct. 2008			68.0 (61.3–73.4)
		09 Feb. 2009			63.1 (56.8–68.9)
5	Bar, open coastal area	19 Sep. 2005	Wild	30	62.8 (53.8–69.6)
		23 May 2006			61.7 (53.0–66.9)
		24 Sep. 2006			63.1 (55.3–70.2)
		16 May 2007			61.4 (52.7–68.2)
6	Rt. Djeran, open coastal area	19 Sep. 2005	Wild	30	63.5 (54.4–72.5)
		23 May 2006			61.7 (53.4–70.3)
		24 Sep. 2006			63.1 (56.2–71.8)
		16 May 2007			60.9 (54.5–69.1)

The Zn and Cu concentrations were determined using flame atomic absorption spectrometry (Perkin-Elmer, AAnalyst 200) with an air–acetylene flame. Analyses of Pb and Cd were performed using graphite furnace atomic absorption spectrometry (Perkin-Elmer, 4100ZL, with Zeeman background correction). Hydride generation and cold vapor techniques were used for the analyses of As and Hg (Perkin-Elmer, AAnalyst 200). Each reported value is the average of five determinations. All results were measured in mg kg^{-1} of sample dry weight (dw). The accuracy of the applied analytical procedure for the determination of trace elements in mussels was tested using SRM 2976 (Mussel homogenate, NIST) certified reference material. To avoid possible contamination, all employed glassware and equipment were acid-washed. To check for contamination, procedural blanks were analyzed after every five samples. Quality control samples, made from standard solutions of Zn, Cu, Pb, Cd, As and total Hg, were analyzed after every five samples to check for element recovery, and these percentages were 98.5 for Zn, 106 for Cu, 94.3 for Pb, 110.9 for Cd, 92.1 for As and 103.8 for total Hg. The limits of detection (*LOD* / mg kg^{-1}) and standard errors of the mean for each element were: Zn, 0.09 and 11.4; Cu, 0.05 and 1.32; Pb, 0.02 and 1.06; Cd, 0.02 and 0.07, As, 0.05 and 1.01 and Hg, 0.05 and 0.06, respectively.

The concentrations of the investigated elements according to dry weight were converted into those based on wet weight by calculating the ratio between the dry and wet weight for each sample in each season. The mean and range of the minimal and maximal values of the studied elements related to dry and wet weight (mg kg^{-1}) are presented in Table II.

In this study, the provisional tolerable weekly intake (*PTWI*) values were used for the calculation of the metal concentration levels of concern associated with the consumption of wild and cultivated mussel from the study area. As there is no data on the average national rate of shellfish consumption (RSC) in Montenegro,[27] the *PTWI* values were employed as standards for calculating the metal concentration levels of concern associated with possible amounts of mussel consumed. According to the FAO/WHO,[28] *PTWI* (μg kg^{-1} of body weight

per week) is the term used by the JECFA (Joint FAO/WHO Expert Committee on Food Additives) to define the level of intake by an adult, whereby the assumed weight of an adult is 60 kg, of an accumulative contaminant which can be ingested without appreciable health risk over a lifetime. The average weekly intake per person for adults (in mg, 60 kg body weight) was estimated to be: 420 for Zn, 30 for Cu, 1.5 for Pb, 0.42 for Cd, 0.9 for As and 0.3 for Hg, according to the FAO/WHO.[28]

TABLE II. Concentrations (mg kg^{-1}) of Hg, Cd, Pb, As, Cu and Zn in the whole soft tissues of *M. galloprovincialis* collected from the Montenegrin coastal area, southeastern Adriatic Sea (Nos. follow those indicated in Fig. 1)

No.	Nature	Weight basis	Hg	Cd	Pb	As	Cu	Zn
1	Wild	Dry	0.51 (0.1–1.0)	2.14 (1.0–3.2)	6.40 (3.0–10.0)	12.4 (5.6–17.8)	6.54 (3.7–11.5)	205.8 (103–433)
		Wet	0.10 (0.02–0.17)	0.350 (0.19–0.59)	1.06 (0.5–1.7)	2.00 (0.9–2.9)	1.08 (0.6–1.9)	33.90 (17.0–71.5)
2	Wild	Dry	0.30 (0.07–0.95)	1.90 (1.20–3.20)	6.50 (1.5–12.2)	7.80 (1.9–24.8)	6.20 (3.7–8.9)	135.5 (60–255)
		Wet	0.050 (0.01–0.15)	0.310 (0.20–0.60)	1.08 (0.25–1.73)	1.30 (0.3–4.1)	1.02 (0.6–1.5)	22.40 (9.9–42.0)
3	Cultured	Dry	0.39 (0.18–0.79)	1.94 (1.2–3.22)	5.20 (2.0–7.5)	5.97 (2.6–10.0)	7.17 (4.5–13.7)	186.2 (126–325)
		Wet	0.060 (0.03–0.13)	0.320 (0.20–0.53)	0.860 (0.33–1.24)	0.990 (0.4–1.7)	1.18 (0.7–2.3)	30.70 (20.8–54.0)
4	Cultured	Dry	0.44 (0.25–0.76)	1.83 (1.2–2.8)	4.00 (1.5–7.5)	7.97 (2.5–13.0)	7.35 (3.7–13.2)	180.8 (101–309)
		Wet	0.080 (0.04–0.12)	0.300 (0.20–0.46)	0.660 (0.24–1.24)	1.30 (0.4–2.1)	1.21 (0.6–2.2)	29.80 (16.7–51.0)
5	Wild	Dry	0.49 (0.25–1.06)	2.13 (1.0–3.5)	11.5 (8.5–15.8)	5.80 (2.7–8.0)	14.5 (12.6–17.0)	205.9 (101–300)
		Wet	0.090 (0.04–0.17)	0.350 (0.17–0.58)	1.70 (1.4–2.4)	0.960 (0.45–1.30)	2.40 (2.1–2.9)	34.00 (17.0–49.5)
6	Wild	Dry	0.11 (0.08–0.14)	1.70 (1.0–2.3)	5.78 (1.30–7.86)	9.67 (4.2–20.5)	10.5 (7.5–12.4)	210.0 (118–345)
		Wet	0.020 (0.01–0.02)	0.290 (0.16–0.38)	0.950 (0.21–1.30)	1.60 (0.7–3.4)	1.80 (1.3–2.0)	34.60 (19.5–57.0)

RESULTS AND DISCUSSION

In the present study, six trace elements were analyzed in wild and cultivated mussels: zinc, copper, total arsenic, lead, cadmium and total mercury. The mean, and minimal and maximal range concentrations of the investigated metals of five replicates found in the soft tissues of *M. galloprovincialis* from six sites in the reported period are given in Table II. In general, the concentrations of the investigated elements found in the soft tissues of *M. galloprovincialis* sampled from different locations and periods from the Montenegrin coastal area showed that Zn was the element present in the highest mean levels 135 to 210 mg kg^{-1} dw (22.4–

–34.6 mg kg^{-1} ww), followed by Cu in the range from 6.2 to 14.5 mg kg^{-1} dw (1.0–2.4 mg kg^{-1} ww), total As from 5.8 to 12.4 mg kg^{-1} dw (1.0–2.0 mg kg^{-1} ww), Pb from 4.0 to 11.5 mg kg^{-1} dw (0.7–1.7 mg kg^{-1} ww), Cd from 1.7 to 2.1 mg kg^{-1} dw (0.30–0.35 mg kg^{-1} ww) and total Hg from 0.11 to 0.51 mg kg^{-1} dw (0.02–0.1 mg kg^{-1} ww) (Table II).

In order to compare the heavy metal concentrations with the legal limits regulated by law, the dry weight concentrations of the metals were converted into wet weight concentrations. As in other countries, Montenegrin law[29] defines legal limits for the permissible concentrations of trace elements in shellfish (Table III). In comparison with the permissible limits set by the Montenegrin Food Regulation[29] for total Hg (1.0 mg kg^{-1} ww), Cd (1.0 mg kg^{-1} ww), Pb (1.0 mg kg^{-1} ww), total As (4.0 mg kg^{-1} ww), Cu (30.0 mg kg^{-1} ww) and Zn (100 mg kg^{-1} ww), all the mean and range values (mg kg^{-1} ww) of these metals from all locations were lower than the limits, except for Pb (Table III). In the present study, the Pb mean concentrations in wild mussels (*M. galloprovincialis*) from locations Herceg Novi and Sveta Stasija (1.1 mg kg^{-1} ww) were the same as the Montenegrin limit, but from the location Bar (1.7 mg kg^{-1} ww), they were higher than the Montenegrin limit for Pb. At the locations where mussels were cultivated, Krasici (0.7 mg kg^{-1} ww) and Kukuljina (0.9 mg kg^{-1} ww), the Pb mean values in the investigated mussels were below the Pb limit set by the Montenegrin Food Regulation.[29] The EC[30] and USFDA[31] have permissible limits for Pb set at higher values than the Montenegrin Food Regulation[29] law, *i.e.* at 1.5 mg kg^{-1} ww and 1.7 mg kg^{-1} ww, respectively. The mean Pb concentration in the investigated samples from the Bar location was above the EC limit,[30] but the same as the USFDA limit,[31] Table III. In this study mercury was not detected in 10 % of the investigated samples and total mercury concentrations below the regulatory limits were found in the remaining samples. Total Hg concentrations in the edible mussel soft tissues ranged from 0.02 to 0.10 mg kg^{-1} ww, as given in Table II. The total Hg limit allowed in the European Union, regulated by the European Commission, is 0.5 mg kg^{-1} ww, except for some species for which it is 1.0 mg kg^{-1} ww.[30] In Montenegro, the total Hg limit, regulated by the Montenegrin Food Regulation law, is 1.0 mg kg^{-1} ww as given in Table III. The mean concentrations of Hg (0.02–0.10 mg kg^{-1} ww) and Cd (0.3–0.4 mg kg^{-1} ww) were below the legal limits regulated by the presented regulations,[29–31] and the mean As concentrations (1.0–2.0 mg kg^{-1} ww) were also below the legal limits[29,31] in the all investigated samples, Tables II and III.

Zn is one of the essential trace elements for both animals and humans. Nevertheless, the consumption of too much Zn is harmful. Zn is required for the synthesis of enzymes and proteins.[26,32] Zn toxicity is rare and Zn appears to have a protective effect against the toxicities of cadmium and lead.[8] The Zn–Cd ratio

is very important as the toxicity and storage of Cd are greatly elevated with Zn deficiency.[8]

TABLE III. Guidelines for the concentrations of trace elements (mg kg^{-1}) based on wet weight for food safety set by different countries

Origin	Hg	Cd	Pb	As	Cu	Zn
Permissible limits by Montenegrin Food regulation (2002)[29]	1.0	1.0	1.0	4.0	30	100
EU (2006)[30], Comm. Regulation (EC), No. 188/2006	0.5	1.0	1.50	–	–	–
USFDA (2007)[31], Food and Drug Administration of the United States	1.0	4.0	1.70	86	–	–

The Zn content in the collected samples ranged from 135–210 mg kg^{-1} dw or 22.4–34.6 mg kg^{-1} ww, with lower mean levels in the cultivated samples. The Joint Expert Committee of the FAO/WHO[28] established a provisional tolerable weekly intake (*PTWI*) for Zn of 7 mg kg^{-1} per week, *i.e.*, 420 mg per person per week. According to the present study, the concentrations of Zn in the wild and cultivated mussels in the investigated period were more then ten times below the toxic limits of 420 mg per person per week.[28]

Cu is another essential metal which is contained in several enzymes[32] and is necessary for the synthesis of hemoglobin.[10] Cu-containing proteins play an important role in animal biology, including dioxygen transport or activation, electron transfer and reduction of nitrogen oxides.[32] The mean concentrations of Cu found in the collected samples ranged from 6.2–14.5 mg kg^{-1} dw (1.0–2.4 mg kg^{-1} ww), with the highest concentrations found in the wild *M. galloprovincialis* from the Bar site, 12.6–17.2 mg kg^{-1} dw (2.1–2.9 mg kg^{-1} ww). The concentrations of Cu in the wild and cultivated mussels in the investigated period were more than one order of magnitude below the toxic limits of 30 mg per person per week.[28]

Some types of seafood contain up to 10 times of more As than other foods and people who consume large amounts of seafood may, therefore, ingest significant amounts of As.[4,23] As occurs naturally in the environment, in both organic and inorganic forms.[23,33] Inorganic As is more toxic than organic As.[33] The symptoms and signs of chronic As poisoning include pigmented skin, anemia and paralysis.[8] As in seafood is primarily present in organic forms.[8] This study gives the results for the total (inorganic and organic) concentrations of As. The JECFA recently re-evaluated As and the Committee withdrew the previous *PTWI* value of 15 μg kg^{-1} body weight set for inorganic As,[23,34] since a lower value of 0.3 μg kg^{-1} body weight (bw) per day was found to increase lung cancer.[23,34] The JECFA noted that more accurate information on the content of inorganic As in foods is required to improve assessments of dietary exposures of inorganic As species.[34] However, the majority of As in seafood is present in the organic ar-

senobetaine (AB), less toxic, water-soluble form,[33,34] which is considered non--hazardous and totally safe for human consumption.[34] The percentages of inorganic As in seafood are 1–5 %, while in mussels,[4] they are 1.9–6.5 %, but the toxic inorganic fraction of As increased with increasing content of total As.[34] Nevertheless, seafood also contributes substantially to dietary As, which is one of the trace elements of concern in relation to food safety.[34] No value of As intake is reported in this study because the As determined refers to the total As (Table II).

Pb is known to cause both acute and chronic adverse effects in the hematopoietic, nervous, gastrointestinal and renal systems.[4] Absorbed Pb is bound to erythrocytes in the blood and initially distributed to the liver, kidney and heart, where it preferentially binds to cell membranes and mitochondria, causes anemia due to a decrease in the hemoglobin levels leading to organ damage, but Pb is not carcinogenic.[4,21] The *PTWI* value for Pb is 1.5 mg person^{-1} week^{-1}.[28] The mean Pb content, in the all the collected mussel samples ranged from 0.7–1.7 mg kg^{-1} ww. Calculating the *PTWI* value for Pb in relation to the highest Pb level at the Harbor Bar, 1.7 mg kg^{-1} ww, the consumption of 880 g of fresh mussels on a weekly basis would reaching 1.5 mg person^{-1} week^{-1} for Pb, which is definitely feasible for large mussel consumers.[35] The absorption of Pb from ingested food greatly depends on the levels of other elements present in the diet, such as Ca, Fe and Zn. It was shown that dietary deficiencies in these essential elements enhance Pb absorption.[35]

Cd is an element that occurs naturally at low levels in the environment, and food represents the major source of Cd exposure.[4,20] Cd is found in marine waters mostly in the dissolved form, distributed in the marine environment at low concentrations and mussels accumulate Cd effectively[4,20] and may act as a poison to humans.[36] Under chronic Cd exposure of humans, Cd can inhibit the development of bone softening due to decalcification, a characteristic of ltai-itai disease.[36] The mean concentrations of Cd found in the analyzed mussel samples ranged from 0.3–0.4 mg kg^{-1} ww in the investigated period at all locations. With regards to the mean Cd concentrations, large mussel consumers would reach the permitted level of 0.42 mg per person per week for Cd by eating 1.2–1.4 kg per week of fresh mussels. In cultivated mussel samples from the Boka Kotorska Bay, from the farms Krasici and Kukuljina, the maximum Cd content was found to be 0.50 mg kg^{-1} ww (Table II), and according to the *PTWI* value, the safe weekly intake of cultivated mussels from these farms is estimated to be below 790–910 g of fresh mussels per week for a 60-kg adult.

Hg is one of the most closely scrutinized pollutants because of its effect on marine organisms and its potential hazard to human health. Methyl-mercury, formed in aquatic sediments through bacterial methylation of organic mercury, is a toxic compound which affects the kidneys and the central nervous system.[4,7] The joint FAO/WHO Expert Committee on Food Additives[28] established a pro-

visional tolerable weekly intake of 0.3 mg of total Hg, of which no more than 200 µg should be present as methyl mercury.[28] This amount equates weekly to 5 µg of total Hg per kg body weight and 3.3 µg of methyl-mercury per kg body weight.[28] However, as there is insufficient data on mussel consumption for Montenegro,[27] consumer exposure to Hg was assessed based on the highest mean value of Hg concentration found in mussels from two of the investigated samples, 0.20 mg kg^{-1} ww at the wild sites Herceg Novi in the Bay and Bar (a sea port in the open coastal area of Montenegro), which were compared with the *PTWI* value for Hg. Based on this data, a weekly consumption of 2.0 kg ww of mussel is sufficient to reach the *PTWI* limit for Hg (5 µg kg^{-1} body weight per day), which is an amount that may result in a risky daily intake of Hg if the exposure is long-term. In all others samples, including the cultivated ones from Krasici and Kukuljina, a weekly consumption of more than 2.5 kg ww of fresh mussels would be necessary to attain the *PTWI* limit for Hg.

In view of the *PTWI* limits estimated for the consumption of Mediterranean mussel from the Montenegrin coastline, in terms of Zn, Cu, Pb, Cd, As and Hg, consumption based on Cd would be the limiting factor for mussels as a food from the Bay farms, such as Krašići and Kukuljina, in terms of large consumers and coastal residents. A weekly consumption of 800–900 g of fresh cultivated mussels, or wild mussels from the location Bar, is sufficient to reach the Cd and Pb *PTWI* limits, which is the amount that may result in a risky weekly intake of Cd and Pb if the exposure is long-term.

A comparison of the data obtained in this study with those previously reported indicates that the levels of trace elements found in *M. galloprovincialis* are comparable to those reported for other areas of the Adriatic and Mediterranean regions[11] (Table IV).

TABLE IV. A comparison of reported concentrations (mg kg^{-1}) of Hg, Cd, Pb, As, Cu and Zn in the whole soft tissue of *M. galloprovincialis* from regional studies with the present results (WB: weight basis)

Location	WB	Hg	Cd	Pb	As	Cu	Zn	Ref.
NW Mediterranean	Dry	0.87	0.4–5.9	2.7–117	11.9–39.3	0.5–28.8	97–644	37
The Bay of Piran, N. Adriatic	Dry	0.28–1.3	2.9–8.3	–	11.9–39.3	6.5–7.6	102–108	38
Lim Chanel, Croatia	Dry	–	1.0	1.37	–	11.5	149	39
Eastern Adriatic coast, Croatia	Dry	–	0.7–1.7	1.2–8.3	–	4.2–17.7	109–189	40
Krka river estuary, Adriatic	Dry	–	0.8–2.3	0.5–4.1	–	4.6–7.7	124–269	41
Portugal southern coast	Dry		1.2–3.8	–	–	4.3–7.2	165–545	42

TABLE IV. Continued

Location	WB	Hg	Cd	Pb	As	Cu	Zn	Ref.
Black Sea, Romania	Dry	0.026–0.03	0.96–1.74	–	–	6.6–8.3	108–190	16
NW Mediterranean	Dry	0.18–0.96	1.13–1.82	1.07–1.43	–	–	–	43
E Adriatic, in Mali Ston Bay Croatia	Dry	0.15	0.4–2.4	0.24–3.7	–	2.0–11	49–418	18
Gulf of Gemlik, SE Marmara Sea, Turkey	Dry	–	2.4	0.5	–	5.5	196	44
Montenegro, SE Adriatic (6 sites)	Dry	0.10–0.50	1.7–2.1	4.0–11.5	5.8–12.4	6.2–14.5	135–210	This study

However, the values obtained for trace elements, *i.e.*, Hg, Cd, Pb and As, in the mussels from the enclosed Boka Kotorska Bay are similar to the average values found in more urbanized areas of the Adriatic and Mediterranean coast. Only the wild samples collected from the site close to the Port Bar had higher levels of the investigated trace elements. The concentrations of trace elements in mussels from the southeastern Adriatic coast of Montenegro could be attributed to anthropogenic and/or natural metal sources affecting their habitats.

CONCLUSIONS

All concentrations of the investigated element (Zn, Cu, Pb, Cd, As and Hg) found in the edible tissue of cultivated mussels from farms in the Boka Kotorska Bay, expressed on a wet weight basis, where lower than the maximum permissible levels for fresh mussels regulated by EU and USFDA laws, implying that their consumption is not harmful for humans. In addition, the results of an evaluation of the risks to human health associated with the consumption of mussels containing trace elements suggest that there is no health risk for people who consume mussels from this part of the Adriatic in moderation, *i.e.*, the consumption of 500 g of fresh mussels on a weekly basis or approximately 26 kg per person per year would not be risky in the long term.

A comparison of the results obtained in this work with already published values for this kind of mussel on the Adriatic and Mediterranean coasts shows that the values obtained herein fall in the range of values most commonly found in low to moderately polluted areas of the Mediterranean and Adriatic Sea. This means that the ecosystem of the Montenegrin coastal area and its Boka Kotorska Bay are not seriously polluted with the investigated trace elements.

Acknowledgements. This research was financed by the Ministry of Science and Technological Development of the Republic of Serbia, contract No. III43009 and EAR, contract No. 04SER02/05/007.

ИЗВОД

КОНЦЕНТРАЦИЈЕ ТРАГОВА ЕЛЕМЕНАТА (Zn, Cu, Pb, Cd, As И Hg) У УЗГАЈАНОЈ И ДИВЉОЈ МЕДИТЕРАНСКОЈ ШКОЉКИ (*M. Galloprovincialis)* УЗОРКОВАНОЈ НА ЛОКАЦИЈАМА ЈУГОИСТОЧНОГ ЈАДРАНА, ЦРНА ГОРА: ЕВАЛУАЦИЈА КВАЛИТЕТА И УТИЦАЈ НА ЧОВЕКОВО ЗДРАВЉЕ

СЛАВКА СТАНКОВИЋ[1], МИХАЈЛО ЈОВИЋ[2], РАША МИЛАНОВ[3] и ДАНИЈЕЛА ЈОКСИМОВИЋ[4]

[1]Технолошко–металуршки факултет, Универзитет у Београду, Карнегијева 4, 11000 Београд, [2]Институт за нуклеарне науке Винча, Универзитет у Београду, 11 000 Београд, [3]Министарство здравља, санитарна контрола, Омладинских бригада 1, 11070 Београ и [4]Институт за биологију мора, Универзитет Црне Горе, Доброта бб, 85330 Котор, Црна Гора

Медитеранска шкољка *Mytilus galloprovincialis* (L), или дагња, узоркована је од јесени 2005. до зиме 2009. године са шест локација црногорског приобаља. Узорковање је вршено на четири локације у Бококоторском заливу, два узорка са узгајалишта шкољки и два са дивљих станишта, и два преостала узорка дивљих шкољки била су са обале на отвореном мору. Мека ткива дагњи анализирана су на цинк, бакар, олово, кадмијум, арсен и укупну живу. Концентрације ових метала кретале су се у опсегу од 135,5–210,0 за Zn; 6,2–14,5 за Cu; 4,0––11,5 за Pb; 1,7–2,1 за Cd; 5,8–12.4 за As и 0,11–0,51 за Hg, изражено у mg kg^{-1} суве масе. Утврђено је да метали у испитиваним узорцима шкољки нису били изнад максимално дозвољених концентрација које су прописане законима Европске Уније и америчке агенције за храну и лекове (USFDA) за шкољке које се користе у исхрани. Ово указује на то да је конзумирање гајених или дивљих дагњи са црногорског приобаља безбедно у умереним количинама.

(Примљено 20 .априла, ревидирано 18. јуна 2011)

REFERENCES

1. N. Kalogeropoulos, N. K. Andrikopoulos, M. Hassapidou, *J. Sci. Food Agric*. **84** (2004) 1750
2. M. Perugini, P. Visciano, A. Giammarino, M. Manera, W. Di Nardo, M. Amorena, *Chemosphere* **66** (2007) 1904
3. J. W. Farrington, A. C. Davis, B. W. Tripp, D. K. Phelps, W. B. Galloway, *ASTM Spec. Tech. Publ.* **940** (1987) 125
4. S. Stanković, M. Jović, A. R. Stankovic, L. Katsikas, in *Environmental Chemistry for a Sustainable World*, Vol. 2, E. Lichtfouse, J. Schwarzbauer, D. Robert, Eds, Springer, Dordrecht, p. 313
5. *FAO/WHO*, *National Aquaculture Sector Overview*, *Montenegro (2007b)*, http:// //www.fao.org/fishery/countrysector/naso_montenegro/en
6. C. K. Yap, A. Ismail, S. G. Tan, *Food Chem.* **84** (2004) 569
7. T. W. Clarkson, *Environ. Health Perspect.* **110** (2002) 11
8. P. Sivaperumal, T. V. Sankar, P. G. Viswanathan Nair, *Food Chem.* **102** (2007) 612
9. V. K. Mubiana, R. Blust, *Mar. Environ. Res.* **63** (2007) 219
10. D. Joksimović, I. Tomić, A. R. Stanković, M. Jović, S. Stanković, *Food Chem.* **127** (2011) 632
11. M. Jović, A. R. Stanković, L. Slavković Beskoski, I. Tomić, S. Degetto, S. Stanković, *J. Serb. Chem. Soc.* **76** (2011) 933
12. D. J. H. Phillips, *Mar. Biol.* **37** (1976) 56
13. D. J. H. Phillips, *Mar. Biol.* **38** (1976) 71

14. E. D. Goldberg, V. T. Bowen, J. W. Farrington, *Environ. Conserv.* **5** (1978) 101
15. M. Roméo, P. Hoarau, G. Garello, M. Gnassia-Barelli, J. P. Girard, *Environ. Poll.* **122** (2003) 369
16. M. Roméo, C. Frasila, M. Gnassia-Barelli, G. Damiens, D. Micu, G. Mustata, *Water Res.* **39** (2005) 596
17. T. Kanduc, D. Medakovic, B. Hamer, *Isot. Environ. Health Stud.* **47** (2011) 42
18. Z. Kljaković-Gašpić, I. Ujević, T. Zvonarić, A. Barić, *Acta Adriat.* **48** (2007) 73
19. M. Türkmen, M. Ciminli, *Food Chem.* **103** (2007) 670
20. *EFSA Journal* 980 (2009), No. EFSA-Q-2007-138
21. *EFSA Journal* (2010) 8(4): 1570, doi:10.2903/j.efsa.2010.1570
22. A. L.H. Whyte, G. R. Hook, G. E. Greening, E. Gibbs-Smith, J. P. A. Gardner, *Sci. Total Environ* **407** (2009) 4348
23. L. Dahl, M. Molin, H. Amlund, M. H. Meltzer, K. Julshamn, J. Alexander, J. J. Sloth, (2010) *Food Chem.* **123** (2010) 720
24. D. Kromhout, E. B. Bosschieter, C. C. De Lezenne, *New England J. Med.* **312** (1985) 1205
25. J. M. Gorell, C. C. Johnson, B. A. Rybicki, E. L. Peterson, G. X. Korthsa, G. G. Brown, R. J. Richardson. *Neurology* **48** (1997) 650
26. A. S. Prasad, *Gastroenterol*ogy **12** (1983) 713
27. *FAO, GFCM Studies and Reviews*, Rome, No. 88 (2010) 1, http://www.fao.org/ /docrep/013/i1696e/i1696e.pdf
28. *FAO/WHO Internet Edition*, ILSI Press, Washington, DC, 2004, http://jecfa.ilsi.org
29. *Montenegrin Food Regulation*, *SRJ Official Gazette* **5** (2002) 67 (in Serbian)
30. *Commission Regulation*, *Official J. Eu. Union* **188** (2006)
31. *US FDA/CFSAN & ISSC, Guidance Documents*, Ch. II, 2007, p. 1
32. F. Firdaus, K. Fatma, A. U. Khan, M. Shakir, *J. Serb. Chem. Soc.* **74** (2009) 939
33. M. Simonič, *J. Serb. Chem. Soc.* **74** (2009) 85
34. *EFSA Panel on Contaminants in the Food Chain (CONTAM), EFSA Journal* **8** (2010) 1706
35. A.R. Goyer, *Am. J. Clin. Nutr.* **61** (1995) 646S
36. K. Eto, *Neuropath.* **20** (2000) S14
37. S. W. Fowler, B. Oregioni, *Mar. Poll. Bull.* **7** (1976) 26
38. L. Kosta, V. Ravnik, A. R. Byrne, *J. Radioanal. Nucl. Chem.* **44** (1978) 317
39. D. Martinčić, H. W. Nurnberg, M. Stoeppler, M. Branica, *Mar. Biol.* **81** (1984) 177
40. D. Martinčić, Z. Kwokal, M. Branica, M. Stoeppler, *Mar. Chem.* **22** (1987) 207
41. D. Martinčić, Z. Kwokal, Z. Peharec, D. Margus, M. Branica, *Sci. Total Environ.* **119** (1992) 211
42. M. J. Bebianno, L. M. Machado, *Mar. Poll. Bull.* **34** (1997) 666
43. C. Lafabrie, G. Pergent R. Kantin C. Pergent-Martini, J. L. Gonzalez, *Chemosphere* **68** (2007) 2033
44. S. Ünlü, S. Topçuoğlu, B. Alpar, Ç. Kirbaşoğlu, Z. Y. Yilmaz, *Environ. Monit. Assess.* **144** (2008) 169.

Journal of the Serbian Chemical Society
JSCS-info@shd.org.rs • www.shd.org.rs/JSCS
J. Serb. Chem. Soc. 76 (12) 1739 (2011)

Erratum (printed version only)

Issue No. 11 (2011), Vol. 76:
– page 1555, below Fig. 2, Fig. 3 should be inserted:

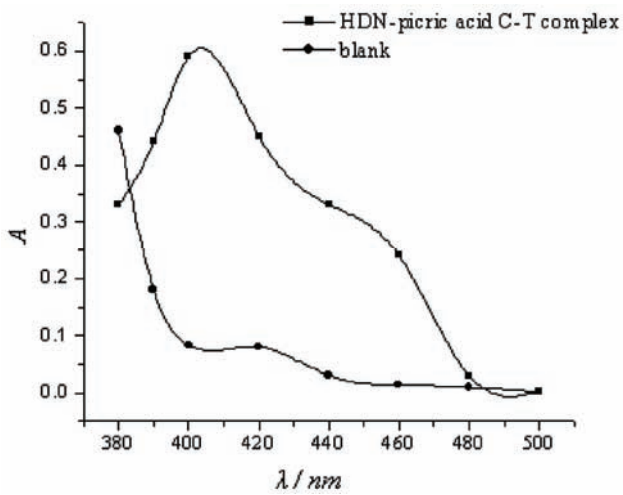

Fig. 3. Absorption spectra of the HDN–picric acid C-T complex (32 μg mL^{-1} HDN) and the reagent blank.

Journal of the Serbian Chemical Society
JSCS@tmf.bg.ac.rs • www.shd.org.rs/JSCS
J. Serb. Chem. Soc. 76 (12) 1741–1752 (2011)

Contents of Volume 76

NUMBER 1

NUMBER 4

Organic Chemistry

Biochemistry and Biotechnology

Inorganic Chemistry

Theoretical Chemistry

Electrochemistry

NUMBER 5

NUMBER 8

NUMBER 9

NUMBER 10

NUMBER 11

Journal of the Serbian Chemical Society
JSCS-info@shd.org.rs • www.shd.org.rs/JSCS
J. Serb. Chem. Soc. 76 (12) 1753–1760 (2011)

Author Index

Subject Index of Vol. **76** and *List of Referees* in the year *2011* are given at the Internet address of the Journal of the Serbian Chemical Society (http:// //www.shd.org.rs/jscs/).

End of Volume 76.

Journal of the Serbian Chemical Society
JSCS-info@shd.org.rs • www.shd.org.rs/JSCS
Volume *76* (2011)

Subject index